Investigating the role of phosphorylation in the regulation of Diacylglycerol Lipase / activity

Singh, Praveen

Awarding institution:
King's College London

Investigating the role of phosphorylation in the regulation of Diacylglycerol Lipase α/β activity

A thesis for the degree of Doctor of Philosophy

Praveen K Singh

Wolfson Centre for Age-Related Diseases

King's College London

Abstract

Diacylglycerol Lipase α (DAGLα) and β (DAGLβ) hydrolyse diacylglycerol (DAG) to produce 2-arachidonoylglycerol (2-AG), the main endogenous ligand for the cannabinoid receptors 1 (CB1) and 2 (CB2). Anatomical and pharmacological studies, complimented by knockout models, of these enzymes have implicated them in CB1/2 mediated processes such as axonal growth and guidance during development and neurogenesis and synaptic signalling in the adult. Despite considerable knowledge about the functions of these enzymes, little is known about their regulation.

To start to address this, we used bioinformatics tools to generate a model of the catalytic domain of the DAGLs which revealed a regulatory loop (putative lid) shielding the catalytic site of these enzymes, similar to other lipases like hormone sensitive lipase (HSL). A phospho-map of the DAGLs generated by collating phosphoproteomic data revealed several phosphorylation sites that were well placed to regulate an 'open' and 'closed' confirmation of the lid, thereby regulating substrate access to the active site. We developed a cellular assay monitoring DAGL dependent CB1 activation as well as surrogate substrate assays to directly monitor the catalytic activity of the DAGLs. Assay results revealed that the kinases PKA and PKC enhanced DAGL dependent CB1 signalling. However these kinases did not affect DAGL activity against the surrogate substrates; this might be explained by the surrogate substrates having access to the active site irrespective of the position of the regulatory loop. The catalytic domains of the DAGLs were purified using a baculovirus expression system and in the case of DAGLβ we were able to demonstrate using *in vitro* phosphorylation and phosphoproteomic studies that PKA and PKC can directly phosphorylate the regulatory loop of this enzyme. A phospho-specific antibody against one of these sites (S570) was generated and validated and conditions were identified that could up and down regulate phosphorylation at this site in cells.

In summary, the first structure/function model for the DAGLs is reported here together with considerable evidence for direct phosphorylation of the catalytic domain being a key regulatory mechanism.

Acknowledgements

I would like to thank Prof Pat Doherty for the opportunity to pursue this PhD and for his supervision and guidance throughout the process.

I am grateful to Dr Fiona Howell for being an ever present source of support, encouragement, and advice during the PhD. I greatly appreciate Dr Gareth William's advice and input towards the project from which I have learnt very much. I would like to thank Martina Sonego and Rachel Lane for all their help and support in the lab in getting through some hectic times. I would also like to thank past and present members of the Doherty lab - Dr Emma Williams, Zhou Ya, Dr Melina Reisenberg, Dr Madeleine Oudin and Sean Menezes as well as the Lalli lab - Dr Kasia Falenta and Dr Sangeetha Gajendra for their professional and personal support on a daily basis over the last four years. Thank you also to Brenda Williams, John Chesson, Carl Hobbs, Dr Umut Cagin, Dr Amelie Avet-Rochex, Ariana Gatt and Olivia Duncan for your help and support during the PhD. I would also like to acknowledge the help provided by Dr Roberto Steiner, Laura Fin, Dr Stefano Pernigo and Dr Louise Saul towards the purification work of the project and Steve Lynham for an insight into the world of mass spectrometry.

Finally, I am grateful for my family's support over the past 4 years that not only motivated me to set out on this journey but was also a constant source of motivation throughout the process.

Contributors

All studies described within the thesis were conducted by me with the following exceptions.

In Chapter 3 - the fold topologies of the lipases (Figure 3.3) were generated in collaboration with Dr Gareth Williams

In Chapter 4 - the Tango assays were performed in collaboration with Dr Emma Williams/Rachel Lane. The Western blot for Figure 4.14 was performed by Rachel Lane

In Chapter 5 - the DiFMUO assays for Figure 5.13A and B and Figure 5.16B were performed by Rachel Lane

In Chapter 6 - Mass spectrometry experiments and analysis were performed by Steven Lynham (Centre of Excellence for Mass Spectrometry, Proteomics Facility, Denmark Hill, KCL)

Table of contents

List of figures

Chapter 1

Chapter 3

Chapter 4

Chapter 6

List of tables

Abbreviations

2-AG	2-arachidonylglycerol
AA	arachidonic acid
ABH4	alpha/beta hydrolase 4
ABHD	alpha/beta hydrolase domain
AEA	anandamide
AKT	protein kinase B
ambic	ammonium bicarbonate
ALK	anaplastic lymphoma kinase
AMPK	5' adenosine monophosphate-activated protein kinase
APC	anaphase promoting complex
ATM	ataxia telangiectasia mutated kinase
ATP	adenosine-5'-triphosphate
BCA	bicinchoninic acid
Beta-ARK	beta-adrenergic-receptor kinase
BSA	bovine serum albumin
Ca^{2+}	calcium
cAMP	cyclic adenosine monophosphate
CAM	cell adhesion molecule
CamKII	calmodulin dependent protein kinase II
Ca-RER	calcium assisted receptor-driven endocannabinoid release
CB	cannabinoid
CB1	cannabinoid receptor 1
CB2	cannabinoid receptor 2
CD	catalytic domain
CDC2	cell division cycle protein 2 homolog
CDK	cyclin-dependent kinase
cDNA	complementary deoxyribonucleic acid
CK1	casein kinase 1
CK2	casein kinase 2
CNS	central nervous system
cPLA2	cytosolic phospholipase A2
C-terminus	carboxyl terminus

DAG	diacylglycerol
DAGL	diacylglycerol lipase
D-box	destruction Box
DHPG	dihydroxyphenylglycine
DiFMUO	6, 8-difluoro-4-methylumbelliferyl-octanoate
dlPAG	dorsolateral periaqueductal gray
DMEM	dulbecco's modified eagle medium
DMSO	dimethyl sulfoxide
DNA-PK	DNA-dependent protein kinase
DRG	dorsal root ganglion
DSE	depolarisation-induced suppression of excitation
DSI	depolarisation-induced suppression of inhibition
DTT	dithiothreitol
E	embryonic day
eCB	endocannabinoid
E. coli	*Escherichia coli*
eEPSC	evoked excitatory postsynaptic current
EGF	epidermal growth factor
EGFR	epidermal growth factor receptor
EPSC	excitatory postsynaptic current
ERK	extracellular-signal-regulated kinase
ELISA	enzyme-linked immunosorbent assay
FAAH	fatty acid amide hydrolase
FAC	final assay concentration
FCS	foetal calf serum
FGF	fibroblast growth factor
FGFR	fibroblast growth factor receptor
FMRP	fragile X mental retardation protein
FRET	fluorescence resonance energy transfer
GABA	γ aminobutyric acid
GDE1	glycerophosphodiesterase 1
GFP	green fluorescent protein
GL	gastric lipase
GPCR	g-protein coupled receptor

GPCRK1	g-protein coupled receptor kinase 1
GPR55	g-protein coupled receptor 55
GRASP65	Golgi reassembly stacking protein of 65 kDa
GSK-3	glycogen synthase kinase 3
GST	glutathione S-tranferase
GTP	guanosine triphosphate
H1-HK	growth-associated H1 histone kinase
HEK	human embryonic kidney
HSL	hormone sensitive lipase
IL	interleukin
IPSC	inhibitory postsynaptic current
IP	immunoprecipitation
IVP	*in vitro phosphorylation*
JAK2	janus kinase 2
kDa	kilo Dalton
KO	knockout
LB	Luria-Bertani
LPS	lipopolysaccharide
LPA	lysophosphatidic acid
LPI	lysophosphatidylinositol
MAG	monoacylglycerol
MAGL	monoacylglycerol lipase
MAPKAPK2	mitogen activated protein kinase-activated protein kinase 2
mGluR	metabotropic glutamate receptor
MPTP	1-methyl-4-phenyl-1,2,3,6-tetrahydropyridine
mRNA	messenger ribonucleic acid
MS	mass spectrometry
NAE	N-acyl ethanolamine
NAPE	N-acyl phosphatidylethanolamine
NAPE-PLD	N-acyl phosphatidylethanolamine hydrolysing phospholipase D
NAT	N-acyltransferase
N-cadherin	neural-cadherin
NCAM	neural CAM

NMDA	N-methyl-D-aspartate
NP	neural progenitor
NSC	neural stem cell
N-terminal	amino terminus
OD	optical density
PA	phosphatidic acid
pAb	phosphorylation-specific antibody
PBS	phosphate buffered saline
PBST	PBS with 0.1% Tween20
PC	phosphatidylcholine
PCR	polymerase chain reaction
PDGF	platelet derived growth factor
PDK	pyruvate dehydrogenase kinase
PGD2	prostaglandin D2
PE	phosphatidylethanolamine
PGE2	prostaglandin E2
phospho-site	phosphorylation site
PI	phosphatidylinositol
PI3-K	phosphatidylinositide 3-kinase
PKA	protein kinase A/cAMP dependent protein kinase
PKC	protein kinase C
PL	pancreatic lipase
PLA1	phospholipase A1
PLA2	phospholipase A2
PLC	phospholipase C
PLD	phospholipase D
PNPB	4-Nitrophenyl butyrate
PSD	post synaptic density
PTPN22	protein tyrosine phosphatase 22
Rfu	relative fluorescence units
RL	regulatory loop
RT-PCR	reverse transcriptase PCR
SDS	sodium dodecyl sulfate
SDS-PAGE	sodium dodecyl sulfate polyacrylamide gel electrophoresis

Sf9 cells	*Spodoptera frugiperda* 9 cells
SGZ	subgranular zone
sIPSC	spontaneous inhibitory postsynaptic current
SVZ	subventricular zone
TGL4	triacylglycerol lipase 4
THC	Δ9–tetrahydrocannabinol
THL	tetrahydrolipstatin
TM	transmembrane
TNF	tumor necrosis factor

Chapter 1 : Introduction

1.1 From cannabis to the endocannabinoid (eCB) system

'Cannabis' has been used for recreational and medicinal purposes for centuries dating back to as early as 2700 BC (Russo et al., 2008). However, it wasn't until the 1960s that Gaoni and Mechoulam successfully isolated and synthesized the major 'psychoactive' ingredient of cannabis, Δ9–tetrahydrocannabinol (THC), one of the major milestones in cannabis research (Mechoulam and Gaoni, 1965). Besides its psychotropic affects, THC is associated with a range of pharmacological effects including analgesia and anti-inflammation. It took several years of research aided by the development of radio-labelled THC probes to determine that the actions of THC were receptor driven, culminating in the cloning and identification of the cannabinoid receptor 1 (CB1) from a rat brain cDNA library (Matsuda et al., 1990). Shortly after, Munro et al. reported the cloning of the cannabinoid receptor 2 (CB2) from a leukemic cell line (Munro et al., 1993). The cannabinoid receptors are G-protein coupled receptors (GPCRs) and have been shown to regulate a range of cellular processes by their downstream signalling pathways. Inhibition/activation of adenylate cyclase (resulting in an increase/decrease in cyclic AMP and protein kinase A (PKA) signalling), activation of phosphatidylinositide 3-kinase/protein kinase B (PI3-kinase/AKT) signalling and regulation of calcium and potassium ion channels are some of the main responses elicited by the cannabinoid receptors linking them to a diverse range of cellular processes (Bosier et al., 2010). The CB1 and CB2 receptors share 44% overall identity, CB1 is predominantly expressed in the nervous system whereas CB2 is predominantly expressed in the immune system (Sugiura et al., 2006).

Identification of CB1 and CB2 as molecular targets for THC initiated the hunt for their endogenous ligands (eCBs). Cannabimimetic probes were crucial in the discovery of the cannabinoid receptors. These probes (often radiolabelled), like CP 55,940 were modelled on THC and then manipulated to achieve greater potency (Herkenham et al., 1990; Xie et al., 1996). They were identified as cannabimimetic based on their ability to bind to

cannabinoid receptors and to trigger cannabinoid like behavioural symptoms (hypoactivity, hypothermia, catalepsy and analgesia) and physiological responses (increase/decrease in cellular cAMP and calcium levels) (Martin et al., 1991; Fride and Mechoulam, 1993; Howlett, 1995). Cannabimimetic probes also proved valuable in the discovery of the two most well studied eCBs - N-arachidonoylethanolamine, also called anandamide (AEA) (Devane et al., 1992), and 2-arachidonylglycerol (2-AG) (Mechoulam et al., 1995; Sugiura et al., 1995) (Figure 1.1).

Devane et al. tested the ability of fractionated organic solvent extracts from porcine brains to displace a radiolabelled cannabinoid probe (HU-243) from rat synaptosomal membranes which enabled them to isolate and identify the first putative eCB AEA. AEA also demonstrated cannabimimetic properties in a mouse isolated vas deferens twitch assay (Devane et al., 1992). Mechoulam et al. isolated 2-AG from canine guts and demonstrated binding of 2-AG to the membranes of cells overexpressing CB1 and CB2 receptors. They also demonstrated the ability of 2-AG to cause THC like responses *in vivo* in mice (Mechoulam et al., 1995) and in the same year Sugiura et al. reported the ability of 2-AG to displace the radioactive cannabinoid probe CP 55,940 from cannabionid receptors in rat brain synaptosomes (Sugiura et al., 1995).

Subsequently a number of other candidate eCBs like virodhamine (Porter et al., 2002) and noladin ether (Hanus et al., 2001) have been discovered based on their structural relationship with AEA and 2-AG and their ability to bind and activate the cannabinoid receptors, however their physiological relevance as eCBs has yet to be determined and some of them are present at very low levels (Figure 1.1). Similarly, other putative cannabinoid receptors have been identified based on their ability to bind CB1/2 ligands (Baker et al., 2006; Ryberg et al., 2007). For example GPR55 is a GPCR activated by l-α-lysophosphatidylinositol (LPI) and although GPR55 can indeed interact with certain CB1/2 drugs, any physiological relevance for this has yet to be reported (Oka et al., 2010; Anavi-Goffer et al., 2012).

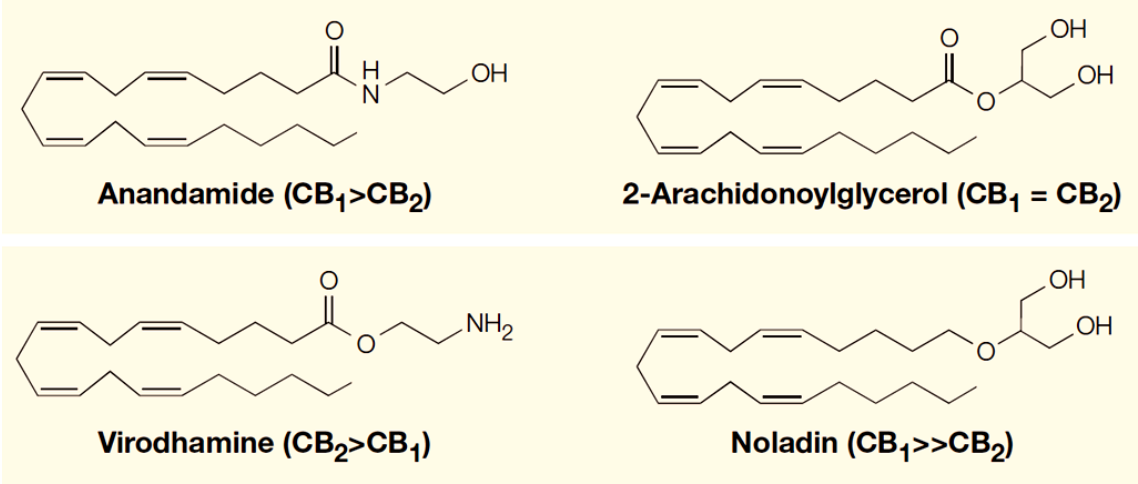

Figure 1.1. Structure of the eCBs

Structures of the two most well studied endocannabionids – Anandamide (AEA) and 2-Arachidonoylglycerol (2-AG) and two putative endocannabionids Virodhamine and Noladin are presented above. Anandamide and Noladin exhibit greater affinity towards CB1 when compared to CB2. 2-AG exhibits similar affinity towards both cannabinoid receptors. Virodhamine on the other hand exhibits greater affinity towards CB2 versus the CB1 receptor (Adapted from (Di Marzo et al., 2004).

The umbrella term - the eCB system is generally used to collectively describe the two most well studied eCBs (AEA and 2-AG), their target receptors (CB1 and CB2), as well as the enzymes involved in their synthesis and degradation which will be discussed in the next section.

1.2 Synthesis and degradation of the eCBs AEA and 2-AG

Following the discovery that AEA and 2-AG can bind and activate the cannabinoid receptors, several groups focussed on identifying pathways involved in their synthesis and degradation in order to establish physiological roles for these molecules. As this thesis is focussed on the major 2-AG synthesising enzymes DAGLα and DAGLβ, this section will briefly discuss AEA synthesis and degradation before a more detailed report on 2-AG metabolism.

1.2.1 AEA synthesis and degradation

AEA belongs to a class of lipids called N-acyl ethanolamines (NAE). Multiple synthetic pathways have been described for AEA as discussed below (Figure 1.2). Di Marzo et al. used [3H]ethanolamine labeled cultured neurons to demonstrate ionomycin stimulated AEA synthesis. They also identified the presence of an AEA precursor N-arachidonyl phosphatidylethanolamine in neurons which could be hydrolyzed to AEA using rat homogenates, presumably due to an endogenous phosphodiesterase (Di Marzo et al., 1994). This calcium stimulated AEA synthesis is believed to involve 2 steps, first calcium activates a transacylase (yet to be identified) which catalyses the formation of N-acyl phosphatidylethanolamine (NAPE) using phosphatidylethanolamine (PE) and phosphatidylcholine (PC), followed by the hydrolysis of NAPE to AEA by a phosphodiesterase (Figure 1.2A).

Okamoto et al. cloned the phosphodiesterase - NAPE-specific phospholipase D (NAPE-PLD) which could indeed convert NAPE to AEA. This enzyme is expressed in various organs in mice, including the brain (Okamoto et al., 2004), and very soon established itself as the likely synthetic enzyme for AEA synthesis (Ligresti et al., 2005).

Figure 1.2. Putative pathways involved in AEA synthesis and the primary pathway involved in AEA degradation

A. An unidentified N-acyl transacylase (NAT) is believed to catalyse the formation of N-acyl phosphatidylethanolamine (NAPE) using phosphatidylethanolamine (PE) and phosphatidylcholine (PC). NAPE can then be hydrolysed to anandamide (AEA) by a NAPE-specific phospholipase D (NAPE-PLD).

B. The serine hydrolase α/β-hydrolase 4 (ABH4) can deacylate both NAPE to lyso-NAPE and then lyso-NAPE to glycero-NAPE. Glycerophosphodiesterase 1 (GDE1) can then convert glycero-NAPE to AEA. Rat tissues also contain lysoPLD activity that can convert lyso-NAPE to AEA.

C. A third pathway involved in the lipopolysaccharide (LPS) stimulated synthesis of AEA in macrophages involves an unidentified phospholipase C (PLC) converting NAPE to phospho-AEA and then phosphatases including protein tyrosine phosphatase 22 (PTPN22) that convert phospho-AEA to AEA.

D. Fatty acid amide hydrolase (FAAH) hydrolyses AEA to arachidonic acid (AA) and ethanolamine.

(Adapted from (Deutsch et al., 2002; Placzek et al., 2008).

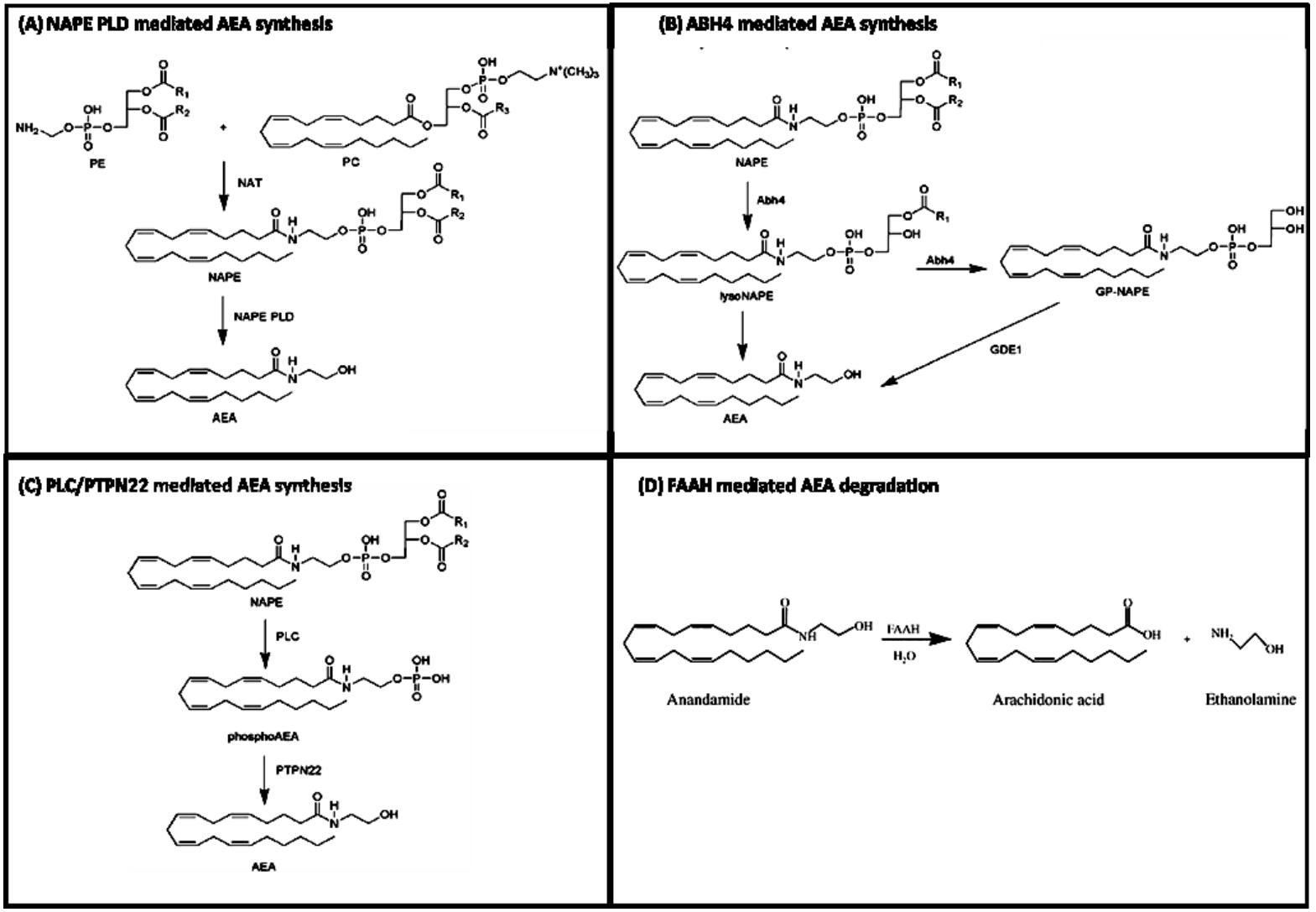
(A) NAPE PLD mediated AEA synthesis
PE
PC
NAT
NAPE
NAPE PLD
AEA
(B) ABH4 mediated AEA synthesis
NAPE
Abh4
lysoNAPE
Abh4
GP-NAPE
GDE1
AEA
(C) PLC/PTPN22 mediated AEA synthesis
NAPE
PLC
phosphoAEA
PTPN22
AEA
(D) FAAH mediated AEA degradation
FAAH
H2O
Anandamide
Arachidonic acid
Ethanolamine

Surprisingly however, no differences in AEA levels were observed in the brains of NAPE-PLD wild type and knockout (KO) mice (Leung et al., 2006). Brain homogenates did however have significantly lower activity in assays converting NAPE to AEA. These assays contained high concentrations of calcium, surprisingly the calcium independent 'NAPE-PLD' activity observed in knockout brains were almost equivalent to wild type controls revealing an alternative pathway for AEA synthesis.

The NAPE-PLD KO data suggested that multiple pathways may exist for AEA synthesis, with the potential to compensate for each other. Subsequently, at least two other pathways involved in the synthesis of AEA have been reported (Figure 1.2B and 1.2C). Simon et al. reported that a significant amount of NAPE-PLD independent AEA synthesis could be blocked by a serine hydrolase inhibitor methoxy arachidonyl fluorophosphonate (MAFP) and also demonstrated using mouse brain tissues *in vitro* that this AEA synthesis occurred via the conversion of lyso-NAPE to AEA. Furthermore EDTA blocked the conversion of lyso-NAPE to AEA and resulted in the accumulation of the intermediate glycero-NAPE (Simon and Cravatt, 2006). Subsequently, this was also demonstrated *ex vivo* (Simon and Cravatt, 2008). This led to the cloning and identification of the serine hydrolase α/β-hydrolase 4 (ABH4) which can deacylate both NAPE to lyso-NAPE and then lyso-NAPE to glycero-NAPE (Simon and Cravatt, 2006). The EDTA sensitive conversion of glycero-NAPE to AEA was attributed to a metal dependent phosphodiesterase - the integral membrane enzyme glycerophosphodiesterase 1 (GDE1) (Simon and Cravatt, 2008) (Figure 1.2B). Both ABH4 and GDE1 were found to be expressed in various tissues including the brain, however, neither GDE1 KO mice nor GDE1-NAPE-PLD double KO mice showed a significant decrease in AEA levels in the brain compared to wild type controls (Simon and Cravatt, 2010). Additionally, rat brain tissues have been shown to contain lysoPLD activity than can generate AEA from lyso-NAPE (Sun et al., 2004).

A third pathway involved in the LPS stimulated synthesis of AEA in macrophages has also been described involving an unidentified

phospholipase C (PLC) and phosphatases including protein tyrosine phosphatase 22 (PTPN22) (Liu et al., 2006) (Figure 1.2C).

The AEA synthesis pathways have generally been identified by the presence of putative AEA precursor/intermediate molecules in tissues coupled with the identification of some of the endogenous enzymes capable of producing AEA from these precursors *in vitro*. Knock-out studies so far have failed to identify a 'bulk' pathway for AEA synthesis suggesting that different pathways can work in a co-operative and compensatory manner to maintain AEA levels in tissues. Development of pharmacological tools specifically targeting the various enzymes as well as cloning the as of yet unidentified enzymes involved in AEA synthesis will help shed further light on pathways contributing to tissue/cell specific AEA levels. This would also help in understanding the contribution of these pathways towards the regulation of basal levels and increased 'on demand' (e.g. calcium or LPS stimulated) production of AEA.

On the other hand the primary enzyme involved in AEA degradation has been well characterized (Figure 1.2D). Cravatt et al. isolated and then cloned fatty acid amide hydrolase (FAAH) from rat liver membranes and then demonstrated its ability to hydrolyze AEA *in vitro*. FAAH was found to be expressed in a range of tissues and was especially abundant in the liver and brain (Cravatt et al., 1996). Most notably FAAH KO mice displayed a 15-fold increase in brain AEA levels (Cravatt et al., 2001).

Despite the fact that AEA has shown cannabimimetic activities *in vitro* and *in vivo*, certain questions with regards to its role as an 'eCB' still remain unanswered. AEA has been shown to act only as a partial CB1 and CB2 agonist but shown to be a full/partial agonist (tissue-dependent) for other receptors like vanilloid receptors (Burkey et al., 1997; Sugiura et al., 1999; Zygmunt et al., 1999; Sugiura et al., 2000b; Ross, 2003). The development of pharmacological tools to disrupt AEA synthesis *in vivo* coupled with a better understanding of its synthetic pathways will help shed light on its role as an eCB.

In contrast to AEA, 2-AG is a full agonist of both the CB1 and CB2 receptors and also the most abundant eCB in the brain leading to the argument that 2-AG is indeed the 'true' eCB (Table 1.1) (Sugiura et al., 1999). Several factors have enabled a detailed inspection of the role of 2-AG as an eCB. A better understanding of 2-AG synthesis and degradation/metabolic pathway in the brain has been pivotal to this and is discussed in the next section.

1.2.2 2-AG synthesis and degradation

2-AG as the name suggests consists of a glycerol molecule with an arachidonoyl group present at the sn-2 position. Prior to the discovery of 2-AG as an eCB, this molecule was primarily studied as a substrate for arachidonic acid (AA) synthesis (Chau and Tai, 1981; Prescott and Majerus, 1983). This section will first discuss early reports into 2-AG synthesis in the context of AA synthesis followed by more recent reports focusing on 2-AG synthesis as an eCB (Sugiura et al., 2006).

1.2.2.1 2-AG as an intermediate for AA synthesis

During the 1970s and 1980s, 2-AG was primarily studied as an intermediate in the synthesis of AA where AA subsequently served as an inflammatory mediator through a range of pathways. This AA synthesis pathway involves PLC activity that can release DAG (more specifically 1-stearoyl-2-arachidonoyl-sn-glycerol) from phospholipids, followed by sn-1 specific DAGL activity to form the monoacylglycerol (MAG) 2-AG and subsequently the release of AA from 2-AG by a MAG lipase activity (MAGL) (Figure 1.3).

In one of the earlier studies, Rittenhouse-Simons observed the rapid but transient accumulation of a DAG in thrombin activated platelets (Rittenhouse-Simmons, 1979). The study used [3H]AA labelled platelets to show that phosphatidylinositol (PI) was the likely precursor of DAG and demonstrated *in vitro* that platelets indeed possessed endogenous PLC activity that could hydrolyse PI to DAG. A separate study went on to demonstrate thrombin (and the calcium ionophore A23187) treatment of human platelets resulted in rapid depletion of PI, with a corresponding rise in free inositol, providing further evidence that PI is the likely source of the DAG (Bell and Majerus, 1980).

Table 1.1. 2-AG is present at several fold higher levels than AEA in the brain

Brain region	AEA (pmol/g)	2-AG (nmol/g)	Fold diff (2-AG/AEA)
Medulla	44.9 ± 5.9	10.5 ± 0.2	234
Cortex	13.6 ± 2.8	4.3 ± 2.4	316
Limbic forebrain	28.1 ± 19.8	10 ± 5.1	356
Brainstem	87.0 ± 45.1	14.0 ± 7.1	161
Striatum	51.5 ± 24.4	10.7 ± 0.3	208
Hippocampus	45.8 ± 2.6	12.6 ± 1.8	275
Diencephalon	10.2 ± 2.3	2.0 ± 0.1	196
Cerebellum	14.8 ± 7.0	3.5 ± 2.4	237
Mesencephalon	30.2 ± 17.7	4.0 ± 2.6	133

Lipids were extracted from rat (10-12 weeks old) brains using chloroform-methanol. Deuterium-8 labelled 2-AG and AEA standards were added to the extracts. 2-AG and AEA were then purified using silica gel column chromatography and normal-phase high pressure liquid chromatography (NP-HPLC) and measured using gas chromatography-electron impact mass spectrometry, relative to the standards. (Adapted from (Bisogno et al., 1999b).

Figure 1.3. Pathways involved in 2-AG synthesis and the primary pathway involved in 2-AG degradation

Several pathways have been described for 2-AG synthesis. Sequential actions of phospholipase C (PLC) and then diacylglycerol lipase (DAGL) catalyse the conversion of phospholipids to diacylglycerol (DAG) and then to 2-AG. DAG hydrolysis to 2-AG by DAGLα and DAGLβ has been identified as the major pathway for 2-AG synthesis in the nervous system and liver. Other putative pathways involved in 2-AG synthesis have also been described. 2-arachidonoyl lysophosphatidic acid (2-arachidonoyl LPA) is present in rat brains and can be converted to 2-AG using brain homogenates (presumably via a phosphatase). Phospholipase A1 (PLA1) activity that can convert phospholipids (PI) to lysophospholipids (LPI) and membrane lyso-PLC (LPI-PLC) activity capable of converting the lysophospholipid to 2-AG have been described. The major 2-AG degradation pathway involves the hydrolysis of 2-AG to arachidonic acid (AA) and glycerol by monoacylglycerol lipase (MAGL). (Adapted from (Nakane et al., 2002).

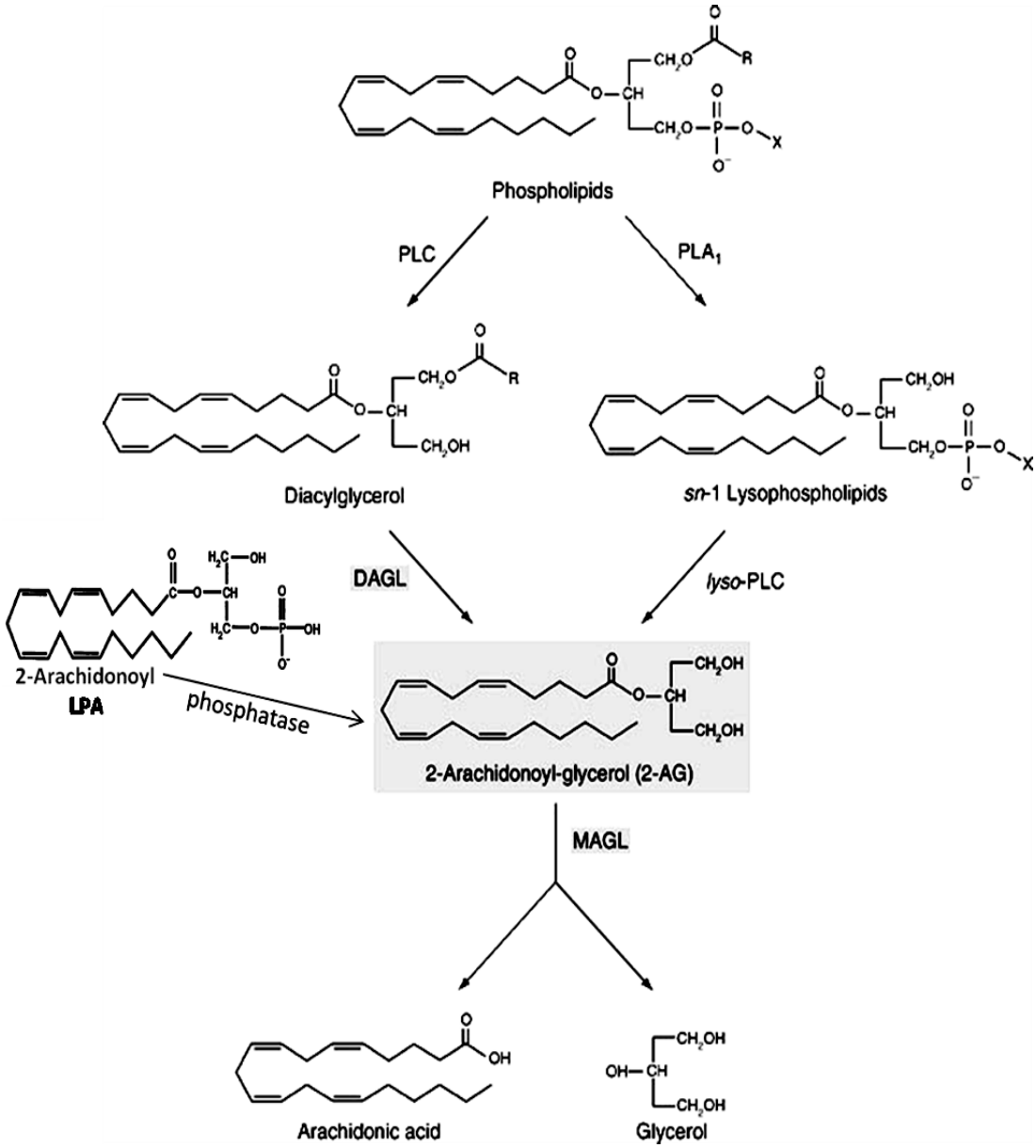
Phospholipids
PLC
PLA1
Diacylglycerol
sn-1 Lysophospholipids
DAGL
lyso-PLC
2-Arachidonoyl
LPA
phosphatase
2-Arachidonoyl-glycerol (2-AG)
MAGL
Arachidonic acid
Glycerol

Bell et al. identified the accumulated DAG as 1-stearoyl-2-arachidonoyl-sn-glycerol and demonstrated that platelet membrane fractions possessed lipase(s) activity capable of releasing the arachidonoyl group *in vitro* (Bell et al., 1979). As they observed an increase in AA (did not observe 2-AG) following thrombin stimulation in platelets they hypothesised that a DAGL directly released AA from the sn-2 position of the DAG. Chau et al. used DAG radiolabelled at either the sn-1 or sn-2 position to demonstrate that DAGL activity in platelet microsomes preferentially hydrolysed 1-stearoyl-2-arachidonoyl-sn-glycerol at the sn-1 position, generating 2-AG, with an optimum pH of 3.5. They also demonstrated the presence of MAGL activity in the microsomes that released AA from 2-AG, with a more alkaline optimum pH (Chau and Tai, 1981). In a separate study, Okazaki et al. demonstrated that microsomal fractions from human decidua vera tissue contained both DAGL and MAGL activity. The DAGL cleaved at the sn-1 position, with a preference for an arachidonoyl group in the sn-2 position (compared to oleoyl). The MAGL preferentially cleaved 2-AG (compared to 2-oleoyl-sn-glycerol), and both lipase activities showed differential cellular fractionation profiles (Okazaki et al., 1981). These were indeed important studies in demonstrating the stereo-specificity of the endogenous DAGL activity (for the sn-1 position) and the presence of a separate MAGL activity that was capable of releasing AA from 2-AG.

Prescott and Majerus went on to report the transient accumulation of not only the DAG, but 2-AG as well, in thrombin stimulated platelets indicating that the DAGL-MAGL activity was physiologically relevant (Prescott and Majerus, 1983). Similar to previous studies, they also demonstrated *in vitro* that the DAGL activity preferentially cleaved DAG at the sn-1 position with an arachidonate group present at the sn-2 position. Importantly, they were able to separate the endogenous platelet MAGL activity from the DAGL activity using ion exchange chromatography. Platelet DAGL activity was also shown to be inhibited by RHC-80267 *in vitro*, and this pivotal study has led to the widespread use of this small molecule as a relatively selective DAGL inhibitor (Sutherland and Amin, 1982).

Further studies went on to confirm the presence of the distinct DAGL and MAGL activity in other cells and tissues. Heparin sepharose affinity chromatography was successfully used to separate MAGL and DAGL activities from bovine brain (Farooqui et al., 1984). Human neutrophil extracts were shown to possess DAGL and MAGL activity by using synthetic substrates, these activities were stimulated by the calcium ionophore A23187 (Balsinde et al., 1991). Radio-labelling studies of Swiss 3T3 cells, a fibroblast cell line, were used to demonstrate an increase of 2-AG production and release following platelet-derived growth factor (PDGF) treatment (Hasegawa-Sasaki, 1985).

The peptide bradykinin which is known to increase intracellular calcium levels was found to transiently increase DAG (2-fold) and MAG (3-fold) levels which preceded a 3-fold increase in AA levels in [3H]AA labelled rat dorsal root ganglion (DRG) neurons implicating a DAGL and MAGL in calcium stimulated AA release. Increases in inositol phosphates (1, 2 and 3) were also observed indicating PLC as a likely source of the DAG. The AA increase was significantly reduced by calcium channel blockers and chelators but not by a PLA2 inhibitor (at concentrations up to 20μM). Similarly, the calcium ionophore A23187 caused an increase in DAG (7-fold), 2-AG (1.7-fold) and AA (27-fold) in DRG neurons (Gammon et al., 1989). In a subsequent study, the same group used [3H]AA and [14C]stearic acid labelled DRG neurons to demonstrate that bradykinin preferentially increased the level of the DAG 1-stearoyl-2-arachidonoyl-sn-diacylglycerol which is then hydrolysed to 2-AG and subsequently AA. Additionally, bradykinin stimulated AA formation was inhibited by the DAGL inhibitor RHC-80267 (Allen et al., 1992).

Indeed, several lines of evidence strongly indicated the presence of a DAGL that was capable of hydrolysing DAG to 2-AG with 2-AG acting as an intermediate in AA synthesis. It wasn't until 2-AG was identified as an eCB in 1995 (Mechoulam et al., 1995; Sugiura et al., 1995) that it was considered as a signalling molecule in its own right, which raised further interest towards understanding its metabolic pathways in the nervous system.

1.2.2.2 2-AG synthesis in the nervous synthesis (as an eCB)

In the late 1990s numerous studies reporting the presence and abundance of 2-AG in the nervous system were published. Stella et al. reported that 2-AG levels in rat brains were 170 times higher than AEA (Stella et al., 1997). Kondo et al. also reported that 2-AG levels in rat brains were higher when compared to other tissues including the liver, spleen, lung, and kidney (Kondo et al., 1998). Bisogno et al., measured 2-AG levels in 9 different brain regions (including the hippocampus and cerebellum) and found it to be ~150 to 300-fold more abundant than AEA (Bisogno et al., 1999b) (Table 1.1). Other groups too detected 2-AG in the nervous system including rat retinal tissue (Straiker et al., 1999), spinal cord, and the DRG (Huang et al., 1999).

These reports establishing 2-AG as the most abundant eCB were accompanied by efforts to identify pathways involved in its synthesis. Two studies published in 1997 were the first reports describing 2-AG synthesis as an eCB. Stella et al. found that electrically stimulating hippocampal slices resulted in a 4-fold increase (calcium-dependent) in 2-AG suggesting that neural activity could stimulate 2-AG synthesis. They also observed a calcium dependent increase in 2-AG levels in [14C]AA labelled cultured neurons, this was blocked by a PI specific PLC inhibitor as well as the DAGL inhibitor RHC-80267 implicating a PLC-DAGL pathway in the production of 2-AG in the hippocampus (Stella et al., 1997). Bisogno et al. pre-labelled a mouse neuroblastoma cell line (a neuronal cell model) with [^{3}H]AA to demonstrate ionomycin stimulated 2-AG synthesis. They also observed potential DAGL and MAGL activity in homogenates using synthetic substrates. Importantly, these cells express the CB1 receptor and ~20% of the (ionomycin stimulated) 2-AG was found in the media, possibly so that it could fulfil its role as an eCB (Bisogno et al., 1997). The ionomycin stimulated 2-AG levels was blocked by the DAGL inhibitor RHC-80267 (which also caused an increase in DAG levels) but not by 4 different PLC inhibitors. Furthermore, they observed a corresponding decrease in phosphatidic acid (PA) levels with increases in 2-AG levels following ionomycin stimulation. The ionomycin stimulated 2-AG levels was also blocked by two PA-phosphohydrolase inhibitors and enhanced by pre-treating the cells with PLD (Bisogno et al., 1999a).

These results collectively implicated a PA-DAG pathway in 2-AG synthesis in neuroblastoma cells. A similar pathway involved in 2-AG synthesis has also been described in a microglial cell line (Carrier et al., 2004).

2-AG synthesis in a range of cells/tissues in response to numerous stimuli has since been reported. Endothelin 1 (endothelin A receptor and calcium dependent) and ionomycin stimulated 2-AG production (5-fold) in primary mouse astrocyte cultures (Walter and Stella, 2003). ATP enhanced 2-AG levels via $P2X_7$ receptors in a calcium, PI-PLC, and DAGL dependent manner in astrocytes (Walter et al., 2004). Additionally, MAGL inhibitors enhanced the ATP stimulated 2-AG levels, once again implicating the PLC-DAGL-MAGL pathway in 2-AG metabolism in astrocytes and microglia (Walter et al., 2004; Witting et al., 2004). The link between $P2X_7$ activation and 2-AG synthesis is not surprising as both are involved in the production of key inflammatory molecules like TNF-α (Lister et al., 2007; Hsu et al., 2012).

Kondo et al. reported evidence for calcium independent 2-AG synthesis pathway(s) in the brain. They found that 2-AG production in rat brain homogenates was greatly enhanced after 5 min treatment with $CaCl_2$ (~6-fold) but a 2-fold increase in 2-AG levels was also observed in the presence of a calcium chelator, implying the presence of calcium independent pathways for 2-AG synthesis (Kondo et al., 1998). Ethanol (~1.7-fold), ionomycin (~2-fold) and glutamate (~1.6-fold) have also been found to increase 2-AG levels in primary cultures of cerebellar granular neurons (CGNs) (Basavarajappa et al., 2000).

Neurotransmitters too can enhance 2-AG levels. Sugiura et al. reported ~5-fold increase in brain 2-AG levels of rats that were first treated intra-peritoneally with picrotoxinin. Picrotoxinin can cause sustained stimulation of excitatory neurons by interfering with transmission of the inhibitory neurotransmitter - γ-Aminobutyric acid (GABA) (Sugiura et al., 2000a). In primary cortical neuron cultures, the neurotransmitter glutamate and NMDA enhanced 2-AG levels (~3-fold) in a calcium dependent manner, this effect was blocked by the NMDA receptor antagonist (MK801) (Stella and Piomelli,

2001). Interestingly, an earlier study had reported that glutamate or NMDA elevated DAGL activity in primary mouse neuronal cultures, this was inhibited by the NMDA receptor antagonists dextrorphan and MK-801 (Farooqui et al., 1993).

Most of the studies mentioned above and in the previous section implicated DAGL activity in 2-AG synthesis in the nervous system as well as in other cell types including neutrophils and platelets. Several groups attempted to purify and characterise the enzyme(s) responsible for the DAGL activity. As mentioned earlier, Farooqui et al. were able to separate MAGL and DAGL activity found in a solubilised microsomal fraction from bovine brain. They found that the DAGL activity bound to heparin sepharose, whereas the MAGL activity did not bind (Farooqui et al., 1984). They went on to demonstrate that the DAGL activity was enriched in plasma membrane and microsomal fractions, could be solubilised by Triton X-100 and inhibited by the DAGL inhibitor RHC-80267. Interestingly, the plasma membrane and microsomal activities showed some differences. Microsomal DAGL activity was stimulated by Triton X-100 and $CaCl_2$ whereas plasma membrane DAGL activity was unaffected by $CaCl_2$, and inhibited by Triton X-100. Whether these activities represented two distinct enzymes was unclear due to the crude nature of the fractions (Farooqui et al., 1986). The same group managed to subsequently purify DAGL from bovine brain microsomes and plasma membrane using a multiple column chromatographic procedure (Farooqui et al., 1989). The enzymes had apparent molecular weights of 27kDa (microsomal) and 52kDa (plasma membrane) as determined by SDS-PAGE. An antibody raised against the microsomal enzyme cross-reacted with the plasma membrane enzyme indicating they could be related isoforms, isoenzymes or that the 27kDa protein was a degradation product of the 52kDa protein (Farooqui et al., 1989). In a follow up study, the microsomal enzyme displayed a preference for 1-2-sn-DAG over 1-3-sn-DAG and stearate over palmitate at the sn-1 position. It was also directly activated by PKA but not $MgCl_2$ or $CaCl_2$ (Rosenberger et al., 2007). Efforts to purify DAGL extended beyond the brain. Lee et al. partially purified DAGL from bovine aorta and found it to be potently inhibited by a selective lipase

inhibitor tetrahydrolipstatin (THL) (Lee et al., 1995). Moriyama et al. also managed to purify DAGL from human platelets with an apparent molecular weight of 33kDa and its activity was inhibited by RHC-80267 (Moriyama et al., 1999).

However, despite considerable headway in the partial characterisation of the biochemical/enzymatic properties of one or more DAGL activities in the 1980s and 1990s, the molecular identity of these enzymes was not resolved. It was not until almost a decade after the discovery of 2-AG as a putative eCB, that the enzymes largely responsible for its synthesis were cloned.

1.2.2.3 Discovery of the elusive Diacylglycerol Lipases

Our group was interested in the role cell adhesion molecules (CAMs) like NCAM, N-cadherin, and L1 play in regulating axonal growth and guidance during development and found that several of these molecules regulated growth cone motility by signalling through the fibroblast growth factor receptor (FGFR) resulting in calcium influx through N and L-type calcium channels that was necessary and sufficient to drive the axonal growth response. Pivotal experiments included the use of dominant negative FGFR expression studies to show that NCAM, N-cadherin and L1 promoted neurite outgrowth in PC12 cells as well as in cerebral neurons via a FGFR-PLCγ pathway (Saffell et al., 1997). A considerable body of evidence from several groups supported this “CAM/FGFR hypothesis” and extended it to a pathogenic role in the migration of some cancer cells (Nieman et al., 1999; Cavallaro et al., 2001; Suyama et al., 2002); however it remained unclear as to how activation of PLCγ was coupled to calcium influx into growth cones. Important insights, including the observation that a DAGL inhibitor (RHC-80267) could block at a step downstream from the activated FGFR, but upstream from calcium influx, led to the hypothesis that direct cross-talk between the FGFR and cannabinoid receptors might mediate the response (Williams et al., 1994b; Williams et al., 1994a). In support, the CB1 receptor was shown to be expressed in growth cones of cerebellar neurons and the CB1 receptor antagonists AM251 and AM281 (but not a CB2 receptor antagonist) were found to inhibit FGF2 and N-cadherin stimulated neurite

outgrowth in primary cerebellar neuron cultures. Similarly, CB1 agonists stimulated neurite outgrowth, a response that was also blocked by N and L-type calcium channel antagonists (Williams et al., 2003). In addition to this, FGF, NCAM, N-cadherin and L1 stimulated neurite outgrowth was inhibited by the DAGL inhibitor RHC-80267 (Williams et al., 1994b; Williams et al., 1994a), and FGF, but not WIN55,2122-2 (CB1 agonist) stimulated neurite outgrowth was blocked by another DAGL inhibitor THL (Bisogno et al., 2003). These results collectively revealed that FGFR stimulated neurite outgrowth signalled through the eCB system via a PLCγ-DAGL-CB1 pathway (Williams et al., 2003).

In order to identify the elusive DAGL, our group used the sequence of a fungal enzyme with both MAGL/DAGL activity to probe mammalian genome sequences which identified two distantly related enzymes that were subsequently shown to be specific DAGLs and named - diacylglycerol lipase α (DAGLα) and β (DAGLβ) (Bisogno et al., 2003). COS-7 cells overexpressing these enzymes showed 3-fold greater activity against 1-stearoyl-2-arachidonoy-sn-glycerol when compared to untransfected cells. This activity was inhibited by the DAGL inhibitors RHC-80267 and THL thus verifying the catalytic activities of these enzymes. When tested against a range of radio-labelled DAGs as substrates, these enzymes showed selectivity for the sn-1 position. Besides demonstrating DAGL catalytic activity *in vitro*, expression of these enzymes resulted in increased total 2-AG levels (cells + media) in the transfected cells (Bisogno et al., 2003). Similarly, overexpressing DAGLα in Neuoro-2A cells resulted in an increase in 2-AG and stearic acid and a decrease in 1-stearoyl-2-arachidonoyl-sn-glycerol, whereas knocking down DAGLα caused a decrease in 2-AG and stearic acid and an increase in 1-stearoyl-2-arachidonoyl-sn-glycerol levels (Jung et al., 2007). These results indeed demonstrated that DAGLα and DAGLβ were capable of hydrolysing DAG to 2-AG *in vitro* and in cells. Moreover, immunohistochemistry showed the enzymes to be expressed in the right place at the right time to mediate the well established function for an eCB synthesising enzyme in retrograde synaptic transmission and the emerging role in axonal growth and guidance. More specifically, DAGLα was

shown to be present in developing axonal tracts, but to become restricted to dendrites in the adult brain (Bisogno et al., 2003). These results will be discussed in more detail later.

RT-PCR and gene expression profiling showed that DAGLα expression was particularly high in the central nervous system and pancreas (Bisogno et al., 2003) which correlates well with this enzymes role in synaptic signalling in the brain (Gao et al., 2010) and the involvement of DAGL activity in pancreatic amylase secretion (Hou et al., 1997). DAGLβ was also expressed in the nervous system, but expression levels were particularly high in macrophages and microglia which correlates well with its recently established role in inflammation (Bisogno et al., 2003; Gao et al., 2010; Hsu et al., 2012). *In situ* hybridisation studies in the adult mouse brain revealed that DAGLα expression was highest in the hippocampus (in pyramidal cells but not in non-pyramidal cells), cerebellar cortex (Purkinje cells but not in granule cells) and dentate granule cells. Moderate expression was also observed in the cerebral cortex, olfactory bulb and thalamus (Figure 1.4A). DAGLβ expression levels were high in the cerebral cortex, cerebellar cortex (especially granular layer), olfactory bulb and dentate gyrus and low in the thalamus and hippocampal pyramidal cells (Figure 1.4B) (Yoshida et al., 2006). Additionally, numerous immunohistochemistry studies using different antibodies further characterised the expression of the DAGLs in the brain (Bisogno et al., 2003; Yoshida et al., 2006; Berghuis et al., 2007; Mulder et al., 2008).

These studies collectively demonstrated that the DAGLs were expressed in the brain, were catalytically capable of hydrolysing DAG to 2-AG and contributed towards cellular 2-AG levels in cells. In the last decade (since the DAGLs were cloned), a flurry of pharmacological and anatomical studies have revealed the importance of the DAGLs in eCB signalling. A range of DAGL dependent CB1/2 processes like axonal growth and guidance, synaptic signalling and adult neurogenesis have been identified and characterised (these will be discussed in more detail in later sections).

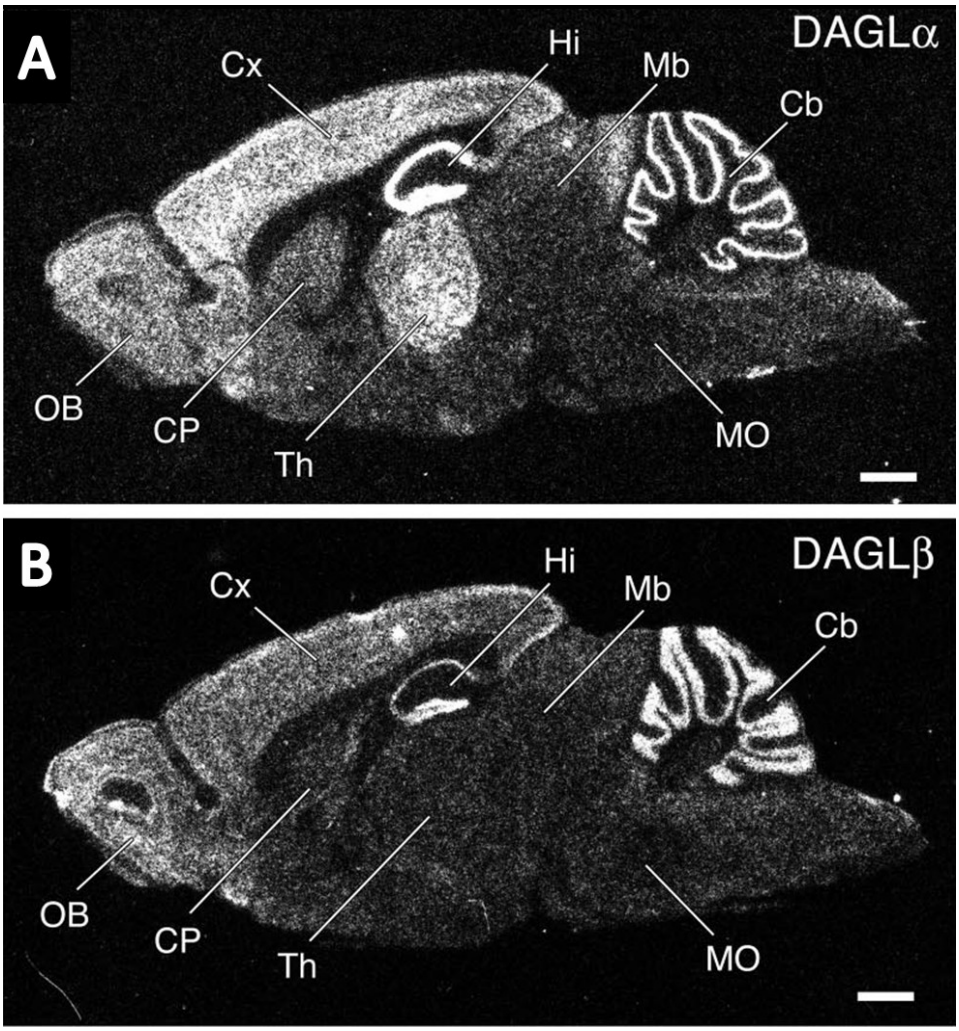

Figure 1.4. DAGLα and β *in situ* hybridization studies in the adult mouse

In situ hybridisation studies in the adult mouse brain revealed that both DAGLα and DAGLβ are expressed in the adult mouse brain. DAGLα expression was highest in the hippocampus (Hi) (in pyramidal but not in non-pyramidal cells), cerebellar (Cb) cortex (Purkinje cells but not in granule cells) and dentate granule cells. Moderate expression was also observed in the cerebral cortex (Cx), olfactory bulb (OB) and thalamus (Th) (A). DAGLβ expression levels were high in the cerebral cortex (Cx), cerebellar (Cb) cortex (especially granular layer), olfactory bulb (OB) and dentate gyrus and low in the thalamus (Th) and hippocampal (Hi) pyramidal cells. (Adapted from (Yoshida et al., 2006)**.** (Cb, cerebellum; CP, Caudate–putamen; Cx, cerebral cortex; Hi, hippocampus; Mb, midbrain; MO, medulla oblongata; OB, olfactory bulb; Th, thalamus). Scale bar 1mm.

Besides the DAGL pathway, other pathways involved in 2-AG synthesis have also been described (Figure 1.3). Nakane et al. detected 2-arachidonoyl lysophosphatidic acid (2-arachidonoyl LPA) in rat brains and also demonstrated that brain homogenates could convert 2-arachidonoyl LPA to 2-AG (presumably via a phosphatase) (Nakane et al., 2002). Ueda et al. showed that rat brain extracts contained an EDTA insensitive PI-PLA1 activity (converting PI to LPI) and a membrane LPI-PLC activity (converting LPI to 2-AG) using synthetic substrates (Ueda et al., 1993; Tsutsumi et al., 1994). These multiple (potential) pathways involved in 2-AG synthesis could introduce significant redundancy in 2-AG synthesis, as was observed for AEA where knockout studies failed to reduce AEA levels.

However, in 2010, two independent studies detailing knockout studies of the DAGLs in mice were important breakthroughs in establishing the DAGLs as major contributors to 2-AG levels in various tissues as well as establishing them as key mediators of eCB signalling (Gao et al., 2010; Tanimura et al., 2010). A remarkable 80% reduction of 2-AG levels was observed in the brains and spinal cord of adult DAGLα KO mice establishing this enzyme as the major 2-AG synthesising enzyme in the nervous system. A 50% reduction in 2-AG levels was observed in the brains of adult DAGLβ KO mice with no significant reduction in the spinal cord detected. On the other hand a 90% reduction in 2-AG levels was observed in the liver of the DAGLβ KO mice, compared to a 60% reduction in the DAGLα KO mice (Figure 1.5).

The differences in the reduction of 2-AG levels observed in various tissues obtained from the DAGLα and DAGLβ knockout studies suggest that the individual contribution of the DAGL isoforms towards 2-AG levels is different depending on the tissue. Furthermore these enzymes appear to maintain tissue 2-AG levels in a cooperative and compensatory manner. A much unexpected observation made in the DAGL KO animals was the parallel reductions in AA and 2-AG in some tissues, most notably in the brains of DAGLα KO mice and the liver of DAGLβ KO mice (Figure 1.5), this will be discussed in more detail later.

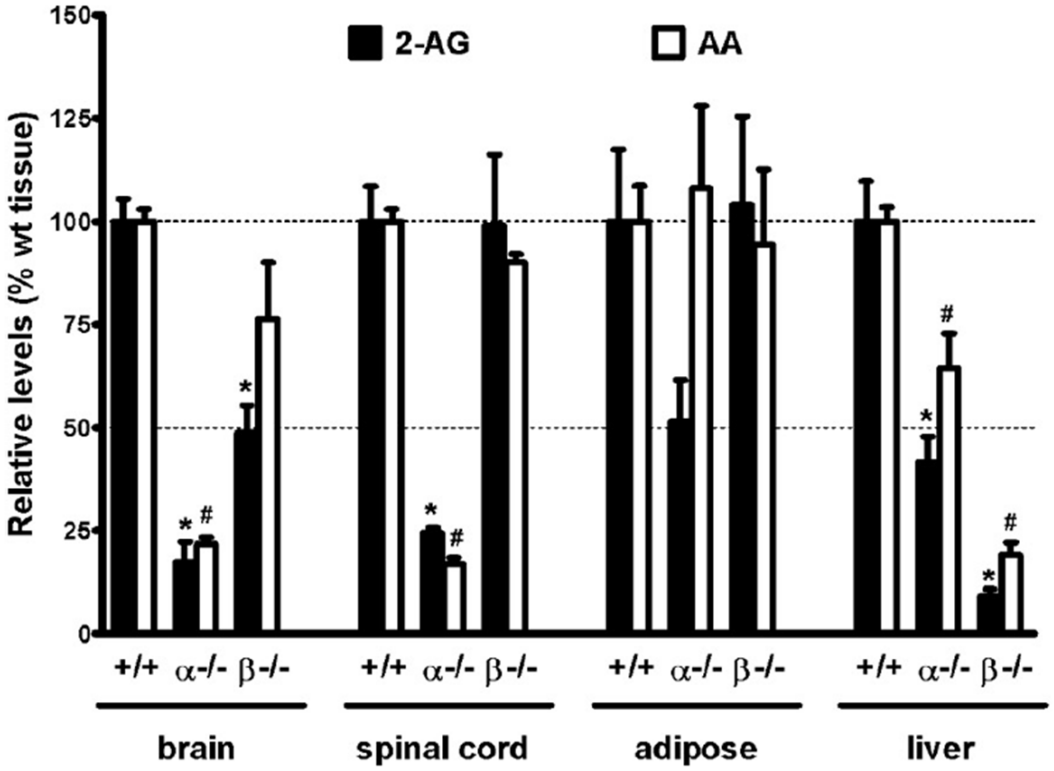

Figure 1.5. Reduction of 2-AG (and AA) levels in DAGL KO mice

Reduction of 2-AG levels in the brain, spinal cord, liver, and adipose tissue of the DAGL KO mice was measured relative to wild type tissue. An 80% reduction of 2-AG levels was observed in the brains and spinal cord of adult DAGLα KO mice. A 50% reduction in 2-AG levels was observed in the brains of adult DAGLβ KO mice with no significant reduction in the spinal cord detected. A 90% reduction in 2-AG levels was observed in the liver of the DAGLβ KO mice, compared to a 60% reduction in the DAGLα KO mice. In adipose tissue, a 50% reduction in 2-AG levels was observed in the DAGLα KO mice, no significant reduction was detected in the DAGLβ KO mice. Reduction in AA levels in the KO tissues compared to wild type tissues is also shown. (Adapted from (Gao et al., 2010).

The DAGL knockout studies therefore identified the DAGLs as the major 2-AG synthesising enzymes, especially in the brain and liver. Similarly, a MAGL was found to be the key 2-AG hydrolysing enzyme in the brain. Dinh et al. cloned MAGL from a rat brain cDNA library and found it to be widely expressed in the brain. HeLa cell extracts overexpressing MAGL contained increased 2-AG (but not AEA) hydrolase activity and MAGL overexpression in rat primary cortical neurons resulted in reduced accumulation of 2-AG following NMDA+carbachol stimulation (Dinh et al., 2002). In addition to this, inhibiting or genetically deleting MAGL increases 2-AG levels by 5 to 30-fold (Long et al., 2009; Schlosburg et al., 2010; Piro et al., 2012). Although other enzymes like FAAH, alpha/beta hydrolase domain 6 (ABHD6) and ABHD12 can indeed hydrolyse 2-AG, ~85% of the 2-AG hydrolysing activity in the brain has been attributed to MAGL (Blankman et al., 2007).

Pharmacological studies have since shown that this enzyme can limit 2-AG and CB1 mediated synaptic signalling (Makara et al., 2005; Szabo et al., 2006; Hashimotodani et al., 2007c; Pan et al., 2009; Straiker et al., 2009) making it a key regulator of DAGL signalling.

1.3 Physiological roles of the DAGLs

In the last decade, since the DAGLs were cloned, numerous studies have revealed their importance in eCB signalling. The DAGL inhibitors THL and RHC-80267, often but not always used alone, have been important tools in attributing various functions to the DAGLs. Hoover et al. evaluated the selectivity of these inhibitors by competitive activity based protein profiling (ABPP) (Hoover et al., 2008).

As part of this study they evaluated the ability of THL and RHC-80267 to prevent binding of a generic serine hydrolase active site probe (fluorophosphonate) to its targets (which include the DAGLs) in a complex proteome (brain). They discovered that both inhibitors bound to other serine hydrolases. Crucially however, the overlap of their 'non-specific' targets was very small (2) (Hoover et al., 2008). Therefore, observations made using both these inhibitors, especially in conjunction with other tools (CB1/2 agonists/antagonists) can be taken as convincing evidence for a DAGL

dependent CB1/2 process. These pharmacological studies have been supported by elegant anatomical studies of the eCB system enabling a detailed inspection into the localisation of the DAGLs (especially DAGLα) relative to the cannabinoid receptors and MAGL. However, it was the knockout studies that ultimately provided the most critical evidence to truly establish the DAGLs as key mediators of eCB signalling. The physiological roles of the DAGLs are discussed below.

1.3.1 Axonal growth, guidance, fasciculation and target selection

The detrimental effect pre-natal exposure of cannabis can have on neurodevelopment of the offspring is well documented (reviewed in (Keimpema et al., 2011). In this context, CB1 receptor expression has been detected in the human foetal brain (Wang et al., 2003), suggesting a role of eCB signalling in neurodevelopment. It was therefore not surprising to find that DAGL dependent eCB signalling plays important roles during development, namely in axonal growth and guidance and this is discussed below.

The CB1 receptor is expressed in the first born neurons of both the central and peripheral nervous system (Begbie et al., 2004). During development, both the CB1 receptor and DAGLα/β are found to be expressed in axons and growth cones of developing neurons, in close proximity to each other (Berghuis et al., 2007; Mulder et al., 2008; Wu et al., 2010) therefore implying an autocrine role for them in axonal development.

Pharmacological and/or genetic disruption of the CB1 receptor has indeed been shown to impair various axonal processes *in vivo and in vitro*. CB1 KO mice display abnormal axonal fasciculation and path-finding (Mulder et al., 2008; Wu et al., 2010). For example, CB1 receptor deletion specifically in cortical GABAergic neurons results in impaired target selection *in vivo* (Berghuis et al., 2007). Genetic and pharmacological disruption of the CB1 receptor causes abnormal axonal growth and fasciculation in pyramidal neurons of mice during late stage development and at birth (Mulder et al., 2008). Similar detrimental effects of CB1 receptor deletion have been reported in corticothalamic and thalamocortical projections (Wu et al., 2010).

Additionally, Watson et al. used pharmacological studies in chick embryos, along with knock-down studies in zebra fish embryos, to demonstrate the requirement of the CB1 receptor for axonal growth and fasciculation. For example, treating chick embryos with the CB1 antagonist AM251 perturbed directionality of axonal growth in various CNS ganglia (Watson et al., 2008).

Further studies have implicated DAGLα/β in these processes. Pharmacological studies *in vitro* have shown that DAGL mediated CB1 receptor signalling can regulate neurite outgrowth. CB1 agonists can stimulate neurite outgrowth in cerebellar neuron cultures as a model, an effect that was not only inhibited by CB1 antagonists, but also by the DAGL inhibitor THL as well as N/L type calcium channel antagonists (Bisogno et al., 2003; Williams et al., 2003). Similarly, FGFR stimulated neurite outgrowth in these cultures are blocked by CB1 antagonists, the DAGL inhibitor RHC-80267 as well as a PLCγ inhibitor (Williams et al., 1994b; Williams et al., 1994a; Saffell et al., 1997; Williams et al., 2003). These results collectively revealed that FGFR stimulated neurite outgrowth signalled through the eCB system via a - PLCγ-DAGL-CB1 receptor pathway. In addition to this, retinoic acid (RA) treatment of Neuro-2A cells causes an increase in DAGLα and DAGLβ expression (and 2-AG) levels and also stimulates neurite outgrowth. Blocking 2-AG degradation, treating these cells with a stable 2-AG analogue, or overexpressing the DAGLs stimulated neurite outgrowth in these cells. Similarly, knocking down the DAGLs (individually or both) inhibited the RA stimulated neurite outgrowth (Jung et al., 2011). Interestingly, a CB1 antagonist blocked neurite outgrowth in these cells when overexpressing DAGLα but not DAGLβ. These findings have helped to explain a much earlier observation that was made before 2-AG was established as a cannabinoid receptor ligand. In these earlier studies, the DAGL inhibitor RHC-80267 inhibited FGFR mediated axonal growth in rat retinal ganglion cell cultures (from E13.5) and perturbed the directionality of axonal growth towards the optic fissure in retinal whole-mounts (Brittis et al., 1996). RHC-80267 also inhibited FGFR mediated neurite outgrowth in *Xenopus* retinal neuron cultures and inhibited axonal growth rate of retinal ganglion cells *in vivo*, shortened retinotectal projections were also observed (Lom et al., 1998).

These pharmacological studies have been further supported by anatomical studies demonstrating that the DAGLs are well placed to regulate CB1 signalling in axons during development. For example, immunohistochemistry studies in chick embryos have detected expression of the DAGLs in the vicinity of the CB1 receptors in developing axons (Watson et al., 2008). In mice, during development, the DAGLs are found to be expressed in axonal tracts (Bisogno et al., 2003). More specific reports have demonstrated that DAGLα is expressed in the axon shafts and growth cones of pyramidal neurons in close proximity to CB1 receptors (Mulder et al., 2008), therefore enabling autocrine 2-AG signalling to regulate CB1 signalling. On the other hand paracrine 2-AG signalling between thalamocortical (DAGLβ) and corticothalamic (CB1) axons (in close proximity) has been also been implicated in axonal development (Wu et al., 2010).

The pharmacological, genetic, and anatomical studies detailed above demonstrate the importance of DAGL dependent eCB signalling in axonal development. As mentioned briefly above, immunohistochemistry studies reveal a shift in the expression patterns of DAGLα/β from the axons during development to the dendrites in the adult brain that may correlate with a shift in function towards synaptic signalling as discussed in the next section (Bisogno et al., 2003).

1.3.2 Synaptic signalling

The restricted expression of the DAGLs to dendritic spines and the CB1 receptor to pre-synaptic terminals in the adult brain clearly points to a role for eCB signalling in the regulation of synaptic function (Oudin et al., 2011a). In this context, early reports suggested that cannabinoids could regulate neurotransmitter release, revealing a potential physiological role for the eCBs (Gill et al., 1970; Roth, 1978).

During the 1990's retrograde signalling at synapses became a well accepted phenomenon. This referred to the release of 'a messenger' from the depolarized post-synaptic site which then acts on the pre-synaptic terminal to suppress further neurotransmitter release (e.g. the inhibitory GABA and the excitatory glutamate), thus providing an elegant mechanism to regulate

synaptic strength and plasticity (Alger, 2012). The generation of CB1 antibodies in the late 1990's began to shed light on the localisation of this receptor in the adult brain. The CB1 receptor was found to be located to the soma of 5 day old hippocampal neurons but shifted to neurites in 4 week old cultures (Twitchell et al., 1997) . In adult rat brains, CB1 was localised to the pre-synaptic terminals of cerebellar granular and basket neurons which form synaptic contacts on dendritic spines on the Purkinje cells (Egertova et al., 1998). Similarly, CB1 was found to be localised in pre-synaptic terminals of hippocampal CCK positive basket neurons (Katona et al., 1999). Subsequently other immunohistochemistry studies supported by knockout studies have indeed confirmed that CB1 receptors are predominantly expressed in pre-synaptic terminals throughout the adult brain and spinal cord, including that of the hippocampus and cerebellum (Katona et al., 2006; Kawamura et al., 2006). The CB1 receptor was therefore well placed to modulate transmitter release, possibly in response a retrograde messenger.

Besides its localisation, pharmacological studies have demonstrated that CB1 activation can inhibit neurotransmitter release (e.g. GABA, Glutamate, acetylcholine) in cultured neurons as well as from slices from various parts of the brain including the hippocampus, cerebellum and the cerebral cortex (reviewed in (Schlicker and Kathmann, 2001). For example, Cadogan et al. demonstrated that AEA and the CB1 agonist CP 55940 could inhibit dopamine release in electrically stimulated rat striatal slices, this was mostly reversed by the CB1 antagonist SR 141716 (Cadogan et al., 1997). The CB1 agonist WIN 55,212-2 also inhibited electrically evoked GABA and acetylcholine release from human hippocampal slices, this was once again reversed by SR 141716A (Katona et al., 2000).

Further pharmacological studies coupled with electrophysiology demonstrated the role of the CB1 receptor as not only a modulator of neurotransmitter release but also of synaptic transmission itself. Evoked excitatory postsynaptic current (eEPSC) and spontaneous inhibitory postsynaptic currents (sIPSCs) in Purkinje cells of cerebellar slices were inhibited by the CB1 agonist WIN 55212-2, an effect blocked by the CB1 antagonist SR 141716 (Takahashi and Linden, 2000).

If an endogenous messenger could mediate pre-synaptic CB1 dependent inhibition of EPSCs or IPSCs then depolarization-induced suppression of inhibition/excitation (DSI/E) should not only be blocked by CB1 antagonists, but also occluded by CB1 agonists i.e. the effect of the retrograde messenger will not be observed as the CB1 receptors are pharmacologically activated prior to the depolarisation step. In 2001, several papers used this approach to implicate eCBs as the retrograde messenger that affect CB1 mediated suppression of neurotransmitter release. In Purkinje cells of cerebellar slices, the CB1 antagonist AM251 blocked DSI whereas the CB1 agonist WIN 55212-2 occluded DSI (Kreitzer and Regehr, 2001b). This strongly indicated that DSI was mediated by the action of an endogenous CB1 agonist that acted on CB1 receptors (in response to depolarisation of the post synaptic cell). Similarly, AM251 blocked and WIN 55212-2 occluded DSE in Purkinje cells (Kreitzer and Regehr, 2001a). This phenomenon was not restricted to the cerebellum, in pyramidal neurons of hippocampal slices, the CB1 antagonists AM251 and SR141716 blocked DSI, and this was once again occluded by WIN 55212-2 (Wilson and Nicoll, 2001). DSE and DSI were shown to be mediated via calcium influx in the depolarised post-synaptic cell (Kreitzer and Regehr, 2001a; Brenowitz and Regehr, 2003; Rancz and Hausser, 2006).

In 2001, two additional studies reported a different mechanism (independent of depolarisation) of eCB release from the post-synaptic cell as a retrograde messenger involving the activation of post-synaptic receptors (receptor driven eCB release - RER). Activation of type 1 metabotropic glutamate receptors (mGluR) in Purkinje cells was found to inhibit neurotransmitter release from excitatory climbing fibers in a CB1 dependent manner. This mechanism did not rely on a calcium influx in the post synaptic cell (Maejima et al., 2001). Additionally, in hippocampal slices, activation of type 1 mGluRs was found to enhance DSI and this was blocked by CB1 and mGluRs antagonists. Furthermore, both DSI and type 1 mGluRs dependent inhibition of IPSCs were absent in CB1 KO mice (Varma et al., 2001).

Therefore, CB1 receptors were well placed (pre-synaptically) to act as a target for a retrograde messenger and their modulation could indeed regulate

neurotransmitter release and synaptic transmission. Being the most abundant eCB in the brain, 2-AG is an obvious candidate to act as the retrograde messenger. Following the cloning of DAGLs in 2003, immunohistochemical studies in various parts of the brain have found DAGLα to be located post-synaptically in the adult brain and excluded from the pre-synapse. Bisogno et al. reported that the DAGLs were absent from axons in the adult mouse brain but present in dendrites (Bisogno et al., 2003). Using electron microscopy Yoshida et al. carried out extensive DAGLα localisation studies in the adult mouse brain and found them predominantly localised to post-synaptic dendritic spines in both cerebellar and hippocampal neurons (Yoshida et al., 2006). Similarly DAGLα was located to the dendrites in medium spiny neurons of the striatum while CB1 was predominantly located at axon terminals (Uchigashima et al., 2007). Katona et al. also used electron microscopy to demonstrate that at hippocampal glutamatergic synapses, DAGLα was localised at the plasma membrane of dendritic spines, in compliment to the CB1 receptor which was localised at pre-synaptic axonal terminals (Katona et al., 2006). DAGLα is therefore perfectly placed to respond to post-synaptic depolarisation and synthesise 2-AG as a retrograde messenger.

Pharmacological studies using DAGL inhibitors provided further evidence to support the role of DAGLα/β in retrograde synaptic signalling. A recently developed and relatively specific DAGL inhibitor OMDM-188 (Ortar et al., 2008) can block various forms of retrograde signalling including DSI in hippocampal slices and cultures as well as in striatal and cerebellar slices. OMDM-188 also blocked DSE in cerebellar slices and IPSC suppression induced by mGluR1/5 agonist DHPG in hippocampal neuron cultures (Hashimotodani et al., 2013). Similarly, THL can block DSI and DSE in mouse cerebellar slices, DSI in the rat cerebellum and DSI in rat hippocampal neuron cultures (Szabo et al., 2006; Hashimotodani et al., 2008).

However, conflicting evidence using the DAGL inhibitors have been reported (reviewed in (Min et al., 2010a). For example, one study reported that none of the three DAGL inhibitors - OMDM-188, RHC-80267 or THL inhibited DSI

in hippocampal slices (Min et al., 2010b). Differences in the methods of drug application coupled with the lipophilic nature of these inhibitors may explain the conflicting results obtained using the DAGL inhibitors. The knockout models of the DAGLs were therefore crucial tools for critically testing the role of the DAGLs in retrograde signalling, and for determining if DAGLα and or DAGLβ were required for this.

Two independent studies indeed reported the loss of eCB mediated retrograde signalling at synapses (hippocampus, cerebellum, and striatum) in DAGLα KO mice. This coupled with the significant reduction in 2-AG levels in the brains of the DAGLα KO animals demonstrated that DAGLα mediated production of 2-AG was the key pathway involved in retrograde signalling at synapses in the brain (Tanimura et al., 2010 and Gao et al., 2010). These studies also demonstrated that DAGLα and not DAGLβ was the key mediator of this function as no defects in retrograde signalling were observed in the DAGLβ KO mice.

Several aspects of DAGL dependent 2-AG release at synapses are still poorly understood. Mechanisms behind 2-AG release and its retrograde transport at the synapse are yet to be addressed. The increase in 2-AG production within the post-synaptic cell is mediated via a calcium influx and/or via the activation of post synaptic receptors (e.g. mGluR5) by neurotransmitters (reviewed in (Hashimotodani et al., 2007a). Type1 mGluRs can activate PLCβ thereby increasing DAG levels (Figure 1.6) (Hashimotodani et al., 2007b). The calcium influx may also cause an increase in 2-AG levels via PLCβ dependent and independent pathways (Hashimotodani et al., 2007a) (Figure 1.6). Increasing substrate (DAG) levels via PLCβ would indeed increase DAGL activity and 2-AG levels. However, other mechanisms affecting the DAGLs (localisation, activation) may also occur in response to the calcium influx or receptor activation. A recent report found increased DAGL activity in DHPG (mGluR5 agonist) treated synaptoneurosomes compared to untreated controls (Jung et al., 2012).

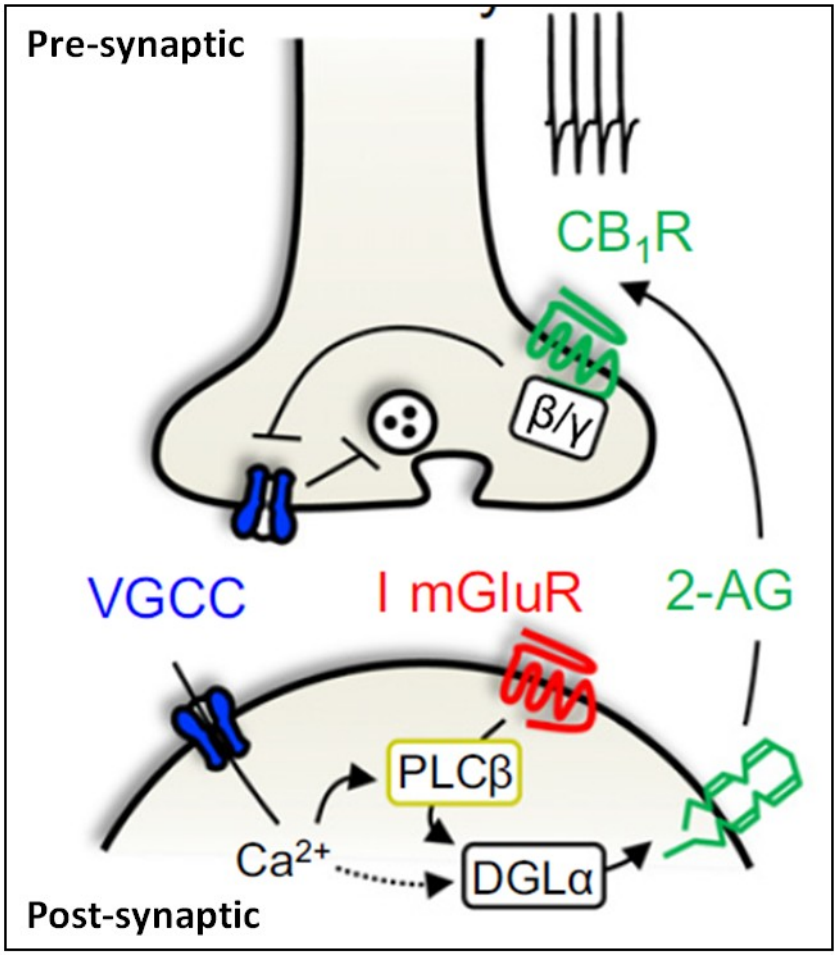

Figure 1.6. General molecular mechanism behind 2-AG retrograde signalling

Depolarisation of the post-synaptic cell causes an influx of calcium via voltage-gated calcium channels (VGCC). The influx in calcium stimulates DAGLα dependent 2-AG production and release via PLCβ dependent and independent (unknown) pathways. Similarly, activation of postsynaptic group I metabotropic glutamate receptors (I mGluRs) activates PLCβ resulting in increased DAGLα dependent 2-AG production and release which is referred to as receptor driven eCB release (RER). Calcium influx and RER can work co-operatively to enhance retrograde signalling via PLCβ and is referred to as calcium assisted RER (Ca-RER). The released 2-AG targets presynaptic CB1 where its β/γ subunits probably couple to VGCC to suppress neurotransmitter release.(Adapted from (Castillo et al., 2012).

Another study has demonstrated a role for calcium/calmodulin-dependent protein kinase IIa (CamKIIa) in the regulation of DAGL activity. In this study, enhanced DSE was observed in striatal slices from mice expressing mutated CamKIIa, which has reduced activity (Shonesy et al., 2013). These effects were also seen using a CamKIIa inhibitory peptide. Furthermore, striatal DAGLα and 2-AG levels were enhanced in the CamKIIa mice versus wild type mice. They also demonstrated that phosphorylation of DAGLα (but not DAGLβ) by CamKIIa inhibits its activity *in vitro*. The calcium influx in the post-synaptic cells could therefore activate CamKIIa which in turn could inhibit the activity of DAGLα thereby modulating/fine tuning retrograde signalling.

Further studies focussing on the DAGLα at the synapses may indeed reveal other mechanisms for its regulation.

1.3.3 Neurogenesis

Neurogenesis in the adult mammalian brain occurs in two niches - the subventricular zone (SVZ) of the lateral ventricle and the subgranular zone (SGZ) in the dentate gyrus (DG) of the hippocampus, via proliferation and differentiation of neural progenitor/stem cells (NP/NSC). The newly generated neurons in the SVZ migrate via the rostral migratory stream (RMS) to the olfactory bulb (OB) where they integrate. In the adult hippocampus, the NSCs form dentate granules cells that then integrate into the local circuitry (reviewed in (Ming and Song, 2011).

Expression profiles of the DAGLs and CB1/2 receptors support a role for DAGL dependent cannabinoid signalling in adult neurogenesis. The CB1 receptor is expressed in the rat dentate gyrus (Morales and Backman, 2002) and SVZ (Xapelli et al., 2013). High expression of DAGLα and DAGLβ are also seen in the SVZ (Goncalves et al., 2008) and in the DG (Yoshida et al., 2006). Several studies have confirmed the expression of CB1 receptors in NP/NSCs *in vivo* (Jin et al., 2004; Jiang et al., 2005; Aguado et al., 2006) and in cultures (Aguado et al., 2005; Aguado et al., 2006; Molina-Holgado et al., 2007; Rubio-Araiz et al., 2008; Xapelli et al., 2013). Similarly CB2 receptors are expressed in NP/NSCs *in vivo* and in cultures (Palazuelos et al., 2006; Molina-Holgado et al., 2007; Rubio-Araiz et al., 2008). In further support of

the expression profiles, CB1 and CB2 agonists have been found to promote proliferation/neurogenesis in NP/NSC cultures, and this effect has generally been reversed by antagonists and absent in CB1 and CB2 KO mice (Aguado et al., 2005; Palazuelos et al., 2006; Molina-Holgado et al., 2007; Rubio-Araiz et al., 2008).

CB1 and CB2 antagonism can also block basal proliferation in these cultures indicating a role for eCBs in NP/NSC proliferation (Molina-Holgado et al., 2007). Expression of DAGLα in NP/NSC cultures has been detected (Molina-Holgado et al., 2007) and 2-AG levels in NP/NSC cultures have been reported to be 100 times higher than AEA (Aguado et al., 2005) indicating that the DAGLs are likely candidates to mediate the neurogenic effects of the cannabinoid receptors. Further evidence supporting the role of DAGLα/β and the cannabinoid receptors in adult neurogenesis has been provided by *in vivo* studies in animal models.

In the hippocampus, a 50% reduction in adult neurogenesis has been observed in the DG of adult CB1 KO mice. (Jin et al., 2004). Additionally, a CB2 agonist caused increased proliferation in the DG, this effect was not seen in CB2 KO mice which also showed decreased proliferation compared to wild type controls (Palazuelos et al., 2006). Similarly, a significant reduction in proliferation (~20-30%) was observed in the hippocampus of adult DAGLα and DAGLβ KO mice compared to wild type controls, implying a role for both these enzymes in hippocampal neurogenesis (Gao et al., 2010). The results above indicate that DAGLα and DAGLβ as well as CB1 and CB2 play a role in neurogenesis in the adult hippocampus.

Similar studies implicating the DAGLs and CB1/2 signalling in neurogenesis in the adult SVZ have also been presented. A 50% decrease in neurogenesis in the SVZ of adult CB1 KO mice has been reported (Jin et al., 2004). However, CB1 antagonist treatment did not affect neurogenesis in the SVZ in adult mice (Goncalves et al., 2008). The reduction of neurogenesis in the CB1 KO may therefore be a developmental defect. On the other hand, CB2 agonists caused an increase and CB2 antagonists caused a decrease in neurogenesis in the SVZ of adult mice. Proliferating cells in the SVZ of the

adult mice (including neuroblasts) express high levels of DAGLα and a reduction in SVZ neurogenesis was observed in adult mice treated with DAGL inhibitors (Goncalves et al., 2008). In adult DAGLα KO mice, a 50% reduction in proliferation coupled with a 50% reduction in neuroblasts was observed in the SVZ when compared to wild type controls, demonstrating reduced neurogenesis in the KO animals (Gao et al., 2010). No significant reduction in proliferation was observed in the SVZ of DAGLβ KO mice. The results above implicate the involvement of a DAGLα-CB2 pathway in neurogenesis in the adult SVZ.

The DAGLs and cannabinoid receptors have also been implicated in the differentiation of oligodendrocyte progenitor cells (Gomez et al., 2010; Gomez et al., 2011) and in the migration of neuroblasts from the SVZ to the OB (Oudin et al., 2011b).

Collectively these results demonstrate a role for the DAGLs and the cannabinoid receptors in adult neurogenesis in both the hippocampus and SVZ.

1.3.4 Eicosanoid signalling - a non-cannabinoid role for the DAGLs

One of the most unpredicted outcomes of the genetic deletion of the DAGLs in mice was the impact this had on AA levels where parallel reductions between 2-AG and AA levels were observed (Figure 1.5). PLA2 was generally believed to be the primary enzyme involved in AA synthesis, it was therefore very surprising when no reduction in AA levels in the brain were observed in cPLA2 KO mice. (Rosenberger et al., 2003). The ~80% reduction of AA (and 2-AG) levels in the brains of DAGLα KO mice provided strong evidence that the DAGL-MAGL pathway was the principle source of AA in the brain (Gao et al., 2010). This indicated a role beyond eCB signalling for the DAGL-MAGL signalling axis where the DAGLs may also generate 2-AG as a substrate for MAGL rather than as an eCB. As part of this model - the hydrolysis of 2-AG by MAGL would have the direct function of generating AA per se as opposed to terminating the action of 2-AG at eCB receptors. This pathway would serve to maintain the steady state levels of

AA and also serve as a responsive pathway to generate signalling pools of AA in inflammatory states.

In further support of this model, MAGL inhibition *in vivo*, resulted in an increase in 2-AG levels coupled with a complimentary decrease in AA levels in mouse brain, spinal cord, liver, spleen, and lung (Nomura et al., 2008a; Nomura et al., 2008b). In the brain, treatment with the MAGL inhibitor JZL184 brought about relatively large increases (8 to 20-fold) in 2-AG levels (Long et al., 2009). These increases seem particularly high to support a notion that 2-AG hydrolysis by MAGL is predominantly carried out to terminate eCB signalling. Similarly, MAGL KO mice brains contain 5 to 10-fold greater 2-AG levels than wild type mice, which is coupled with not only a 5-fold decrease in AA but also with a decrease in levels of eicosanoids like prostaglandin E2 (PGE2), PGD2 and thromboxane B2 (TXB2) (Schlosburg et al., 2010; Piro et al., 2012). AA derived eicosanoids are involved in various physiological and pathological processes including inflammation (reviewed in (Harizi et al., 2008) and include prostaglandins, leukotrienes and lipoxins.

In a separate study, inhibiting MAGL or knocking it out increased brain levels of 2-AG by about 5-fold and reduced AA and PGE2 (basal and LPS stimulated) levels 3 to 5-fold. MAGL inhibition also reduced LPS stimulated inflammatory cytokine levels (IL1α, IL1β, IL6 and TNFα) by ~4 to 8-fold (in a CB1/2 independent manner) as well as LPS-induced microglial activation (Nomura et al., 2011). Furthermore MAGL inhibition in cPLA2 KO mice revealed that cPLA2 made a much smaller contribution towards LPS stimulated PG synthesis compared to MAGL. Firstly, in the brain, cPLA2 KO mice did not show any reduction in basal AA levels compared to a 5 to 10-fold reduction in MAGL KO mice or following MAGL inhibition. Secondly, only a 20% reduction in LPS stimulated AA levels was observed in the cPLA2 KO mice when compared to a 3 to 5-fold reduction in MAGL KO mice or following MAGL inhibition. In addition to this, studies in other tissues comparing MAGL and cPLA2 KO mice revealed that MAGL was mainly responsible for regulating basal and LPS stimulated levels of AA, PGE2 and PGD2 in the liver and lung whereas cPLA2 played a more prominent role in the gut and spleen. (Nomura et al., 2011).

The knockout studies of the DAGLs demonstrating reduced 2-AG and AA levels coupled with MAGL KO studies which show an increase in 2-AG levels and a decrease in AA levels demonstrate the importance of the DAGL-MAGL axis in maintaining AA levels *in vivo*. The corresponding reduction of eicosanoids linked to decreases in AA and increases in 2-AG levels following pharmacological or genetic disruption of MAGL further confirms that the AA generated by 2-AG hydrolysis is not simply a by-product. This is further supported by a recent report where a reduction in 2-AG (~3 to 5-fold), AA (~2 to 3-fold) and the eicosanoids PGE2 and PGD2 (~2 to 5-fold) was observed in macrophages derived from DAGLβ KO mice or following the selective inhibition (*in vivo*) of DAGLβ in wild type macrophages (Hsu et al., 2012). Similarly, a reduction in the LPS stimulated levels of various eicosanoids and cytokines was also reported in primary macrophage cultures from DAGLβ KO mice or from wild type macrophages treated with selective DAGLβ inhibitors (Hsu et al., 2012). The DAGLs may therefore be interesting drug targets for inflammation.

1.4 A pathological and therapeutic perspective on the DAGLs

The role of the DAGLs as key eCB signalling mediators as well as potential inflammatory mediators has implicated them in various diseases linked to the nervous system.

Dorsolateral periaqueductal gray (dlPAG) is a region in the brain involved in nociceptive signalling. mGLuR5 and DAGLα (post-synaptically) and CB1 (pre-synaptically) are expressed in this region. mGLuR5 antagonism in this brain region reduces stress antinociception. On the other hand activation of mGLuR5 in this brain region enhances stress antinociception, an effect blocked by a mGLuR5 antagonist as well as a CB1 antagonist. DAGL inhibition and DAGLα knock-down, specifically targeted in this region also suppressed stress antinociception. Collectively these results implicate a role for DAGL mediated synaptic signalling (receptor driven eCB release and retrograde signalling) towards stress antinociception (Gregg et al., 2012).

Fragile X syndrome (causes autism, mental retardation) is caused by the failure to express Fragile X mental retardation protein (FMRP). FMRP plays

an important role in the transport of various mRNA to the synapses (Sidorov et al., 2013). A recent report has demonstrated a role for FMRP in the transport and precise localisation of DAGLα mRNA at the synapse (Jung et al., 2012). In addition to this, genetic deletion of FMRP disrupted mGluR5 signalling at the synapses, an effect that was overcome by blocking 2-AG hydrolysis. Furthermore blocking 2-AG hydrolysis in FMRP KO mice restored behavioural deficits caused by the deletion of the gene. Pharmacological tools to activate DAGLα may therefore hold therapeutic potential towards treating certain aspects of Fragile X syndrome.

The role of the DAGL-MAGL pathway in AA and thereby eicosanoids production in the brain has also implicated them in neurodegenerative diseases. For example, elevated brain levels of AA and eicosanoids like PGE2, PGD2 and TXB2 are observed in an Alzheimer's disease mouse model (PS1/APP^{+}) (Piro et al., 2012). Genetic deletion of MAGL in this model increased 2-AG levels and reduced AA and eicosanoid levels by approximately 5 to 10-fold. MAGL ablation was also found to reduce microglia and astrocyte activation, inflammatory cytokine levels as well as amyloid plaques (4-fold). Similarly, the MAGL inhibitor JZL184 was found to increase 2-AG levels and reduce AA, eicosanoid and inflammatory cytokine levels (independent of CB1/2 receptors) *in vivo*, in this model (Piro et al., 2012). In a separate study, in a model for Parkinson's disease, MAGL deletion or inhibition prevented MPTP (the neurotoxin 1-methyl-4-phenyl-1,2,3,6-tetrahydropyridine) induced increases in AA, PGE2 and PGD2 as well as neuronal loss in the brain, in a CB1/2 independent manner (Nomura et al., 2011). The studies above have focussed on the disruption of MAGL activity to prevent neuroinflammation. Similar studies on the DAGLs to evaluate their therapeutic potential in neuroinflammation models would be interesting, especially considering the dramatic reduction of AA levels in DAGL KO mice (Gao et al., 2010). Additionally, the role of the DAGLs in neurogenesis may hold therapeutic potential in counteracting the effects of neuronal loss in neurodegenerative diseases and brain injury.

The pathological roles of the DAGLs extend beyond the brain. Considering, the large reduction of 2-AG and AA levels observed in the liver of DAGLβ KO

mice (Figure 1.5), it is not surprising that eCB signalling has been implicated in liver disease. Increased CB1 expression, DAGLβ expression and 2-AG levels were observed in the liver of mice following ethanol feeding and has been linked to alcohol induced hepatic steatosis (Jeong et al., 2008). In addition to this, a reduction in ethanol induced hepatic steatosis and inflammation was observed in CB1 KO (global or hepatocyte specific) mice or in wild type mice treated with a CB1 antagonist. This was found to be mediated by hepatocyte CB1 receptors (Jeong et al., 2008; Trebicka et al., 2011). The increases in DAGLβ (but not DAGLα or MAGL) expression and 2-AG (but not AEA) levels in the liver following ethanol feeding were localised to hepatic stellate cells (Jeong et al., 2008). Collectively these results implicate paracrine 2-AG signalling in the pathogenesis of hepatic alcohol induced steatosis (Bataller and Gao, 2012). Similar results have also implicated CB1 in the pathogenesis of high fat diet induced hepatic steatosis (Osei-Hyiaman et al., 2008). Examining the effects of alcohol and high fat diet on hepatic steatosis using the DAGLβ KO mice will help assess the therapeutic potential of DAGLβ in treating these conditions.

Additionally, MAGL deletion or inhibition enhanced 2-AG levels, reduced AA and eicosanoid levels, reduced hepatic neutrophil infiltration and reduced levels of inflammatory, liver damage and cell death markers *in vivo* following hepatic ischemia/reperfusion-induced tissue injury (Cao et al., 2013). This MAGL inhibition mediated reduction in liver disease biomarkers was complimented by a CB1 antagonist or CB1 ablation but partially reversed by CB2 antagonism or ablation. This suggests that the hepatoprotective affects of the MAGL inhibitor are partially mediated by cannabinoid signalling via the CB2 but not CB1 receptor and partially by inhibition of eicosanoid production. In this context, CB2 activation has been linked with a down regulation of inflammation and associated injuries in a number of diseases (Pacher and Mechoulam, 2011). On the other hand, as mentioned above, CB1 activation is linked with the pathogenesis of alcohol and high fat diet induced liver disease (Jeong et al., 2008; Osei-Hyiaman et al., 2008). Further studies exploring the link between DAGLα/β, CB1/2 and the production of inflammatory mediators in different cell types will help establish the relative

contribution of cannabinoid and non cannabinoid 2-AG signalling in inflammatory responses, which in turn will help devise therapeutic strategies to target MAGL, DAGLα/β and CB1/2 in order to treat inflammatory diseases.

The cannabinoid receptors have been long standing targets for drug discovery (reviewed in (Pertwee, 2012; Skaper and Di Marzo, 2012; Pacher and Kunos, 2013). Three CB1/2 agonists are currently used in clinic. Marinol contains THC, the active ingredient of cannabis and is used as an appetite stimulant and to suppress chemotherapy side effects like nausea. Cesamet contains a synthetic THC analogue and is also used to suppress chemotherapy side effects like nausea. Sativex is a 50/50 mix of THC and the other major cannabis constituent cannabidiol (less psychoactive). Sativex is used to treat neuropathic pain and spasticity related to multiple sclerosis (Pacher and Kunos, 2013). Despite these successes, there have also been several failures too, most notably in the case of the small molecule CB1 antagonist Rimonabant. Rimonabant was approved for the treatment of obesity; however, it later had to be withdrawn due to unwanted side-effects which included depression and suicidal thoughts (Moreira and Crippa, 2009).

As key regulators of eCB signalling, the DAGLs provide alternative targets to modulate CB1/2 receptor activity. DAGLα and DAGLβ demonstrate different tissue specific contributions towards 2-AG (and AA) levels and hence targeting them individually could prove to be therapeutically attractive and achievable. DAGLα is responsible for most of the 2-AG in the brain whereas DAGLβ is responsible for most of the 2-AG in the liver. Theoretically, one could exploit the impermeability of the blood brain barrier to prevent DAGLβ inhibitors causing unwanted neurological side effects. A DAGLβ selective inhibitor (50 times more potent against DAGLβ than DAGLα) has recently been developed (Hsu et al., 2012), this provides encouraging signs that differences in these enzymes can be exploited by medicinal chemistry.

Understanding how the DAGLs are regulated, which may include both overlapping and distinct mechanism for these enzymes will help further our understanding of these enzymes and eCB signalling and support longer term studies to evaluate their therapeutic potential as drug targets.

1.5 Aims and objectives

At the start of this project, two studies characterising DAGL KO mice were published, driving home the important physiological roles these enzymes played in processes like neurogenesis and synaptic signalling (Gao et al., 2010; Tanimura et al., 2010). Indeed, a combination of pharmacological, anatomical and knockout studies have recognized the DAGLs as major regulators of eCB signalling, however, very little is known about how these enzymes are regulated.

Several studies have reported increases in DAGL dependent 2-AG signalling in response to a range of stimuli, including calcium and FGF (Williams et al., 2003; Aguado et al., 2005; Sugiura et al., 2006). These increases in 2-AG signalling and hence DAGL activity can partially, on occasions be explained by increased substrate availability due to the associated increase in activity of PLCβ/γ. Enhanced 2-AG release from a pre-formed pool could also play a role in enhancing 2-AG signalling, however several reports have measured increased 2-AG levels in response to various stimuli, strongly suggesting that activation mechanisms of the major 2-AG synthesising enzymes - DAGLα and β do exist.

Phosphorylation is one of the most common mechanisms involved in the modulation of enzymatic activity, including that of several lipases like the hormone sensitive lipase (HSL). Therefore, in order to further our understanding of how the DAGLs are regulated, we decided to investigate the potential role of phosphorylation in the regulation of DAGL activity.

The specific aims of the thesis were:-

(1) To use bioinformatics and related tools to develop a working model for DAGL regulation

(2) To develop a cellular assay to measure DAGL-dependent eCB signalling to test the requirement of kinases for calcium stimulated responses.

(3) To evaluate the use of surrogate substrates to directly measure DAGL activity in membranes and intact cells

(4) To purify the catalytic domain of DAGLs in an active state to determine phosphorylation sites (phospho-sites) in direct kinase assays

(5) To develop phospho-specific antibodies to the DAGLs

Chapter 2 : Materials and Methods

2.1 General solutions, constructs, primers, antibodies and drugs

All reagents were purchased from Sigma or Fisher Scientific unless otherwise stated.

Lysis buffer

50mM Tris pH 8.0, 150mM NaCl, 10mM MgCl2, 2mM CaCl2, 5% glycerol, 1% Triton X-100, 1mM Na_3VO_4, 10mM NaF, 1mM PMSF and 1x 'Complete protease inhibitors' (Roche).

Mowiol mounting solution

17% (w/v) Mowiol 4-88 (Calbiochem), 33% (v/v) glycerine in PBS.

4% paraformaldehyde

4% (w/v) paraformaldehyde in PBS, pH 7.4.

Phosphate buffered saline (PBS)

1 PBS tablet (Oxoid) in 100ml water to give KCl (0.20g/l); KH_2PO_4 (0.20g/l); NaCl (8g/l); Na_2HPO_4 (1.15g/l).

PBST

0.1% Tween20 in PBS.

5x SDS protein loading buffer

0.4M Tris pH 6.8, 10% SDS, 40% glycerol, 0.2M DTT, 0.1% bromophenol blue.

SDS-running buffer

25mM Tris, 200mM glycine, 0.1% SDS.

Transfer buffer

25mM Tris, 200mM glycine, 20% methanol.

Trypsin-EDTA

1.25mg/ml trypsin, 0.5mM EDTA, pH 8.0 in PBS.

SDS-polyacrylamide gels

Reagent	**10% gel**	**7.5% gel**	**5% stacking gel**
30% acrylamide/Bis (National Diagnostics)	3.3ml	2.5ml	1.67ml
1M Tris, pH 8.8	3.7ml	3.7ml	-
1M Tris, pH 6.8	-	-	1.25ml
10% SDS	100µl	100µl	100µl
H_2O	2.38ml	3.63ml	6.91ml
TEMED	6.6µl	6.6µl	20µl
10% ammonium persulphate	66µl	66µl	50µl

SDS-polyacrylamide gels - Phos-tag

Reagent	7.5% gel	5% stacking gel
30% acrylamide/Bis (National Diagnostics)	2.33ml	1.67ml
1.5M Tris, pH 8.8	1.75ml	-
1M Tris, pH 6.8	-	1.25ml
10% SDS	70µl	100µl
H_2O	2.52ml	6.91ml
TEMED	20µl	20µl
10% ammonium persulphate	100µl	50µl
5mM Phos-tag	98µl	-
10mM $MnCl_2$	98µl	-

DNA vectors and constructs

Construct	Vector	Source	Details
DAGLα-V5-6His(C)	pCDNA3.1D/V5-His-Topo	Made by Dr Fiona Howell	Used as a template for other constructs
DAGLα 229-687–6His-Tev(N)	pENTR	Dr Louise Saul	Used to generate GST-DAGLα CD construct
Human DAGLβ	pBluescriptR	Source bioscience	Mutation corrected by SDM (K545T) then used as a template for other constructs,
	pDONOR207	Invitrogen	Used as a shuttle vector for gateway cloning
	pCDNA-DEST47	Invitrogen	Used to generate DAGLβ-GFP construct
	pCDNA6.2/V5-DEST	Invitrogen	Used to generate DAGLα/β-V5 constructs which were in turn used to generate cell lines V5α11 and V5β4

	pDEST20	Invitrogen	Used to generate GST-DAGL catalytic domain constructs

Primers

All primers were ordered from either Sigma or Invitrogen.

Primers to correct K545 mutation to T545 in the human DAGLβ pBluescriptR (Image clone 4830264) construct

Forward	CAACAACTTGCCCACGGAGCTGGACGG
Reverse	CCGTCCAGCTCCGTGGGCAAGTTGTTG

Primers to generate full length human DAGLα pENTR construct (no stop codon)

Forward	GGGGACAAGTTTGTACAAAAAAGCAGGCTTCACCATGCCC GGGATCGTGGTGTTCC
Reverse	GGGGACCACTTTGTACAAGAAAGCTGGGTGGCGTGCTGAG ATGACCAGCTC

Primers to generate full length human DAGLβ pENTR construct (no stop codon)

Forward	GGGGACAAGTTTGTACAAAAAAGCAGGCTTCACCATGCCGG GGATGGTACTCTTCG
Reverse	GGGGACCACTTTGTACAAGAAAGCTGGGTGGGCCACGTCCA CACTGG

Primers to generate DAGLβ 228-672 pENTR construct

Forward	GGGGACAAGTTTGTACAAAAAAGCAGGCTTCACAGATCTG GTGCCCAGC
Reverse	GGGGACCACTTTGTACAAGAAAGCTGGGTGTCAGGCCACG TCCACACTGG

Cell lines

Cell line	Source	Culture media
Tango (CB1) U2OS	Osteosarcoma	McCoy's 5A modified 10% FCS
COS-7	Monkey kidney	DMEM 10% FCS
Sf9	*S. frugipera* (insect cells)	Sf900 II SFM

Primary antibodies

Antibody	Company	Species	Application	Dilution
β-actin	Abcam	Rabbit	Western	1/500
DAGLα	Dr.M. Watanabe	Rabbit	Western	1/1000
DAGLβ*	Eurogentec	Rabbit	Western	1/1000
DAGLβ phospho-S570**	Eurogentec	Rabbit	Western	1/500
GFP	Invitrogen	Rabbit	Western	1/1000
GFP	Invitrogen	Rabbit	ICC	1/1000
GRASP65	Abcam	Rabbit	ICC	1/5000
GST	Millipore	Rabbit	Western	1/1000
V5	Invitrogen	Mouse	Western	1/1000
V5	Invitrogen	Mouse	ICC	1/1000
Hoechst 3342 (blue)	Invitrogen		ICC	1/10,000

* rabbit antibody raised and purified against DAGLβ epitope SSDSPLDSPTKYPLT

** rabbit antibody raised and purified against modified DAGLβ epitope LTRW(phospho)SPAYSFSSD

Secondary antibodies

Antibody	Company	Species	Application	Dilution
AlexaFluor 488	Invitrogen	mouse	ICC	1/2000
AlexaFluor 488	Invitrogen	rabbit	ICC	1/2000
AlexaFluor 594	Invitrogen	rabbit	ICC	1/2000
HRP-conjugated	Vector Lab.	mouse	Western	1/3000
HRP-conjugated	Vector Lab.	rabbit	Western	1/3000
IR-Dye 680	Licor	mouse	Western	1/5000
IR-Dye 800	Licor	rabbit	Western	1/5000

Drugs

Drug	Supplier
8-MA-cAMP	Sigma
ACEA	Tocris
AM251	Tocris
Forskolin	Sigma
Go6976	Millipore
H89	Sigma
Ionomycin	Invitrogen
JZL184	Tocris
OMDM-188	Dr Vincenzo Di Marzo
RHC-80267	Tocris
THL	Tocris

2.2 Bioinformatics (homology modelling/phosphorylation related predictions)

Primary sequence alignments were performed using Clustal Omega (http://www.ebi.ac.uk/Tools/msa/clustalo/). Secondary structure predictions were performed using NetSurfP (http://genome.cbs.dtu.dk/services/NetSurfP/). DAGL phospho-maps were compiled by collating data from PhosphositePlus (http://www.phosphosite.org). Prediction of phosphorylation sites (phospho-sites) were performed using DISPHOS (http://www.dabi.temple.edu/disphos/) and NetPhos 2.0 (http://www.cbs.dtu.dk/services/NetPhos/). Prediction of kinases potentially responsible for phosphorylating the DAGLs was carried out using a phospho-motif finder (http://www.hprd.org/PhosphoMotif_finder).

2.3 Molecular biology

Human DAGLα-V5 (pCDNA6.2/V5-DEST)

The full length human DAGLα gene was first amplified from the DAGLα-V5-6His(C) construct mentioned in the table above. The gene was amplified by PCR with flanking attB1 and attB2 sites at the 5' and 3' ends respectively and with no stop codon, using the primers mentioned above. PCR was carried out using Pfu ultra polymerase (Stratagene). The reaction mix (50µl) contained 5µl 10X Pfu reaction buffer, 0.4µl 100mM deoxyribonucleotide triphosphate mix, 1µl template (200ng/µl), 1µl each of forward and reverse primer (100µM stock), 1µl Pfu ultra polymerase, 2µl DMSO and 38.6µl water. PCR was performed as follows: denaturing at 95ºC for 2 minutes followed by 30 cycles each consisting of 95ºC for 30sec, 65ºC for 30sec and 72ºC for 3 minutes 30 sec, then a final extension time of 72°C for 10 minutes. The PCR products were analysed by agarose (1%) gel electrophoresis using TAE buffer and 1µg/ml ethidium bromide.

The PCR product detected at the expected size was gel extracted (Qiagen kit) and then cloned into the gateway shuttle vector pDONOR207 using the BP clonase II kit (Invitrogen) as follows - 150ng PCR product, 150ng pDONOR207 and 2µl BP clonase II mix in a total reaction volume of 10µl

were incubated at 25°C for 1 hour and then treated with 1µl Proteinase K for 10 minutes at 37°C. 5µl of the reaction was then transformed into Top10 chemically competent *E. coli* cells (Invitrogen) and plated on LB gentamicin (12.5µg/ml) agar plates. The plates were incubated overnight at 37°C. At least 2 of the colonies obtained were then grown in 5ml LB gentamicin cultures and the plasmid DNA was extracted (Qiagen miniprep kit).

Sequence of the construct (DAGLα pENTR) was then confirmed by DNA sequencing (Beckman Coulter genomics) and used as part of a gateway LR clonase II (Invitrogen) reaction to shuttle the gene into the pCDNA6.2/V5-DEST vector as follows. 150ng of the DAGLα pENTR construct, 150ng of pCDNA6.2/V5-DEST and 2µl LR clonase II mix in a total reaction volume of 10µl were incubated at 25°C for 1 hour and then treated with 1µl Proteinase K for 10 minutes at 37°C. 5µl of the reaction was then transformed into Top10 chemically competent *E. coli* cells and plated on LB ampicillin (100µg/ml). The plates were incubated overnight at 37°C. At least 2 colonies obtained were then grown in 5ml cultures and the plasmid DNA was extracted (Qiagen Miniprep kit). Sequence of the construct (human DAGLα-V5) was then confirmed by DNA sequencing (Beckman Coulter genomics).

Correction of the K545 mutation to T545 in the human DAGLβ pBluescriptR (Image clone 4830264) construct

A K545 mutation detected in the DAGLβ image clone was corrected to T545 by site directed mutagenesis using the QuikChange II XL kit (Agilent) using the primers mentioned above. PCR (50µl) was carried out using the following settings - 95°C 1min, 18 cycles each consisting of 95°C for 50sec, 60°C for 50sec, 68°C for 10min, and then a final step of 68°C for 10min. The PCR reaction was then treated with 1µl Dpn1 for 1 hour at 37°C and after which 5µl of the reaction was transformed into Top10 chemically competent *E. coli* cells and plated on LB ampicillin (100µg/ml). The plates were incubated overnight at 37°C. At least 2 colonies obtained were then grown in 5ml cultures and the plasmid DNA was extracted (Qiagen Miniprep kit). The corrected sequence was then confirmed by DNA sequencing (Beckman

Coulter genomics). This enabled the expression of DAGLα with a C-terminus V5 tag using mammalian expression systems.

Human DAGLβ-V5 (pCDNA6.2/V5-DEST)

The full length human DAGLβ gene was first amplified from the DAGLβ pBluescriptR (corrected) construct mentioned above. The gene was amplified by PCR with flanking attB1 and attB2 sites at the 5' and 3' ends respectively and with no stop codon as described for the human DAGLα-V5 construct. DAGLβ pENTR and subsequently DAGLβ-V5 were generated as described for DAGLα-V5. This enabled the expression of DAGLβ with a C-terminus V5 tag using mammalian expression systems.

Human DAGLβ-GFP (pCDNA-DEST47)

The DAGLβ pENTR construct generated above was used to shuttle DAGLβ into pCDNA-DEST47 using the LR clonase II kit (Invitrogen) as described for the DAGLα-V5 construct. This enabled the expression of DAGLβ with a C-terminus GFP tag using mammalian expression systems.

GST-6His-Tev-DAGLα 229-687 (pDEST20)

6His-Tev-DAGLα 229-687 (catalytic domain) pENTR construct was used to shuttle 6His-Tev-DAGLα 229-687 into pDEST20 using the LR clonase II kit (Invitrogen) as described for the DAGLα-V5 construct. This enabled expression of the DAGLα catalytic domain (CD) with an N-terminus GST-6His-Tev tag using the baculovirus expression system.

GST-DAGLβ 228-672 (pDEST20)

DAGLβ 228-672 (catalytic domain) was first amplified from the DAGLβ pBluescriptR (corrected) construct using the primers mentioned above. The gene was amplified by PCR with flanking attB1 and attB2 sites at the 5' and 3' ends respectively (with a stop codon) as described for the human DAGLα-V5 construct. DAGLβ 228-672 pENTR was generated as described for DAGLα. Subsequently the DAGLβ 228-672 gene was shuttled into pDEST20 using the LR clonase II kit (Invitrogen), as described for the DAGLα-V5

construct. This enabled expression of the DAGLβ catalytic domain with an N-terminus GST tag using the baculovirus expression system.

2.4 Cell culture

The Tango-CB1 (referred to as Tango cells) cells were cultured at 37°C and 5% CO_2 in McCoy's 5A modified media with the following supplements - 10% FCS (unless otherwise stated), 0.1mM non essential amino acids, 25mM HEPES (pH 7.3), 1mM sodium pyruvate, 100U/ml penicillin, 100µg/ml streptomycin, 200µg/ml zeocin, 50µg/ml hygromycin and 100µg/ml geneticin (Invitrogen). The V5α11 and V5β4 cell lines described below were cultured in the same media as the Tango cells, supplemented with the antibiotic blasticidin. The COS-7 cells were grown in Dulbecco's Modified Eagle Media (DMEM) containing 10% FCS.

2.5 Tango assay

All the reagents for the Tango-CB1 (Tango) assay were obtained from Invitrogen. 20,000 Tango cells/well were seeded in a 96-well black clear bottom plate (Costar) in a total volume of 120 µl Freestyle assay media or McCoy's 5A media supplemented with 1% FCS as indicated. The cells were cultured overnight and then treated with the drugs as indicated. Generally, the treatments were diluted from higher concentrations to 5x stocks in the indicated media and 30µl was added to the appropriate wells. The plate was then incubated for the indicated times at 37°C before 30µl of 6x substrate mix (Invitrogen) was added to the wells. Following this, the plate was incubated in the dark at room temperature for 2 hours. CB1 activation was then measured and quantified as a ratio of the fluorescence signal in the blue channel (excitation 409nm, emission 460nm) and the FRET signal in the green channel (excitation 409nm, emission 530nm) using the FlexStation (Molecular Devices). The FRET signal is generated by the intact substrate whereas the fluorescence signal corresponds to the cleaved substrate (cleaved by β-lactamase). In some cases the data is presented as a percentage of the maximum values obtained using the CB1 agonist ACEA (1µM).

2.6 Transfections

Transfections of the Tango or COS-7 cells with the DAGLα/β constructs were carried out in 6 well dishes (~90% confluent) using the Lipofectamine 2000 transfection reagent (Invitrogen). Prior to the transfections, where appropriate, the media was replaced with antibiotic free media. For the transfections, 4µg plasmid DNA was incubated with 150µl Opti-MEM media for 5 minutes. At the same time 10µl Lipofectamine 2000 was incubated with 150µl Opti-MEM media for 5 minutes. These were then pooled and incubated for 20 minutes. Following this, the transfection mix was added to the cells, which were then incubated for 5 hours at 37°C. The media was subsequently changed and the cells were cultured overnight. At this point, 24 hours post transfection, cells were generally trypsinised and seeded into 24 well plates for ICC (described below) or in 6 well plates/10cm dishes for lysis and Western blotting analysis. Cells were generally fixed or lysed 48 hours post transfection.

2.7 Immunocytochemistry

10,000 cells per well were seeded onto 13mm poly-lysine coated coverslips and cultured overnight after which they were fixed in 4% paraformaldehyde for 30 minutes at room temperature. The fixed cells were washed three times with PBS and then permeabilised with 0.2% Triton X-100/PBS for 10 minutes. The permeabilised cells were washed three times with PBS before blocking with 1% BSA/PBS (block solution) for 30 minutes. The cells were then incubated with the primary antibodies (diluted in block solution) for 1 hour at room temperature or overnight at 4^{o}C. Following that, cells were washed with PBS before the addition of the appropriate goat anti-mouse/rabbit AlexaFluor 488/594 secondary antibodies diluted in block solution. This was incubated for a further hour before a final three washes with PBS. In some instances cells were also stained with the nuclear stain Hoechst 33258 which was used at a dilution of 1:10,000 (in block solution) along with the secondary antibodies. After the final wash, the coverslips were mounted in Mowiol onto microscope slides. Images of the immunostained

cells were collected using the Carl Zeiss LSM 710 microscope and the Carl Zeiss Zen software (version 1.0.1.0).

2.8 Generation of the stable cell lines

Tango cells were transfected with either DAGLα-V5 or DAGLβ-V5 (pCDNA6.2/V5-DEST) DNA. 24 hours post transfection, the cells were trypsinised and seeded at low densities and then cells stably expressing the DAGLα or DAGLβ-V5 genes were selected by continuous growth in blasticidin. Individual colonies obtained were picked and transferred to single wells of a 24 well plate and cultured. Colonies (clones) were screened for expression by Western blotting and ICC to determine the stable expression of the gene and the clonal nature of the cultures. Based on this the V5α11 and V5β4 cell lines were chosen for further experiments.

2.9 Mammalian cell lysis and protein assay

Cell lysis

Cells were lysed in a standard lysis buffer (50mM Tris-HCl pH 8.0, 150mM NaCl, 10mM $MgCl_2$, 1% Triton-X-100, 5% glycerol, 10mM NaF, 1mM PMSF, 1mM Na_3VO_4 and 1x complete protease inhibitor cocktail (Roche Applied Science) as follows. Media from the cells was first aspirated and the cells were washed with PBS. The cells were then scraped in an appropriate volume of lysis buffer (6 well dish - 100-200µl/well, 10cm dish - 0.5-1ml). The cell suspensions were incubated at 4°C for 30 minutes using an end-over-end rotator. After the 30 minute incubation, the cell lysates were clarified by centrifugation at 11,000g for 10 minutes and the supernatants were collected for further analysis.

Protein assay

Protein concentrations of the clarified lysates were determined using the Pierce BCA Protein assay kit (Thermo Scientific) in a 96-well flat clear bottom plate. The volume of BSA standards and samples (serially diluted) was 20µl. 200µl of BCA protein detection was added to the standards and samples. The plate was then incubated for 20 minutes at 37°C. Following that, the

absorbance was measured at 562nm using a Spectramax plate reader (Molecular Devices). A standard curve was generated using BSA (5 to 250µg/ml) and the concentration of the lysates was determined using an appropriate dilution.

2.10 Membrane preparation, cellular fractionation and protein assay

Membrane preparation

Media from cells cultured in 10cm dishes was aspirated and the cells were washed using PBS. The cells were then scraped in 1ml (per dish) of the following lysis buffer - 20mM HEPES pH7.0, 2mM DTT, 0.25M sucrose, 10mM NaF, 1mM Na_3VO_4 and 1x 'Complete' protease inhibitor (Roche) and then homogenised on ice using a Polytron (PT 1200 E) homogeniser (three ~7sec bursts at the maximum setting with 30sec interval in between). The homogenates were then subjected to centrifugation at 100,000g for 30 minutes at 4°C. The supernatants obtained were discarded and the pellets (membrane enriched fraction) were resuspended in 200µl of lysis buffer, with the sucrose excluded, using the Polytron homogeniser. This membrane resuspension was then aliquoted (generally 20µl) and stored at -80°C.

Cellular fractionation

For the cellular fractionation experiments, cells were homogenised as described above and then subjected to centrifugation for 30 minutes at 1,000, 19,000 or 100,000g. The supernatants and pellets (resuspended as described for the membranes above) were then aliquoted (generally 20µl) and stored at -80°C.

Protein assay

Protein concentration of the membranes and fractions was determined using the Coomassie (Bradford) Protein Assay Kit (Thermo Scientific) in a 96-well flat clear bottom plate. The volume of BSA standards and samples (serially diluted) was 20µl. 200µl of the Coomassie assay reagent was added to the standards and samples. The plate was then incubated for 10 minutes at room temperature. The absorbance was then measured at 595nm using a

Spectramax plate reader (Molecular Devices). A standard curve was generated using BSA (5 to 250µg/ml) and the concentrations of the membranes/fractions were determined using an appropriate dilution.

2.11 Phosphatase treatment of membranes

100µg V5α11 or Tango membranes were incubated with 50 units of calf intestinal phosphatase (NEB) at 37ºC for 60 minutes in 1x NEBuffer and a total reaction volume of 500µl.

2.12 Western blotting

Sample preparation and SDS-PAGE

Samples were diluted using water and 5x SDS protein loading buffer to a concentration of 1µg/µl and then denatured by boiling for 5 minutes. Typically, 20µg of the denatured samples were loaded on the gels and then resolved at a setting of 100 volts for ~2 hours using the SDS-running buffer, till the dye front exited the gel.

Transfer

The resolved proteins on the gel were transferred to a nitrocellulose membrane (GE healthcare) using the transfer buffer either for 1 hour at 100 volts (4°C) or overnight at 20 volts (room temperature).

Blocking, primary and secondary antibody incubations

Membranes were typically blocked for 1 hour at room temperature in PBS 5% milk and then incubated overnight at 4°C with the primary antibody (diluted in PBST 2% milk). The membranes were then washed in PBST (4 times, 10 minutes each) and then incubated for 1 hour at room temperature with the secondary antibody (diluted in PBST 2% milk). Following this, the membranes were washed in PBST (4 times, 10 minutes each) and then PBS (1 time for 10 minutes).

Detection and quantification

The proteins on the membranes were either detected using Enhanced Chemiluminescence (ECL) or ECL Plus reagents (GE Healthcare) and X-ray film (GRI) or using the Odyssey imaging system (LI-COR). The membranes visualised using ECL were quantified using the ImageJ software whereas the membranes visualised using the Odyssey system were quantified using the Odyssey software. Typically the band of interest was normalised to a loading control (β-actin or tag like GST or V5) and then effects of treatments were quantified relative to an untreated normalised control.

2.13 Coomassie stained SDS-PAGE

For Coomassie staining, samples were resolved by SDS-PAGE as described above. The gels were then incubated with Coomassie stain (1g Coomassie brilliant blue R-250, 50ml acetic acid, 500ml methanol, 450ml water) for 20 minutes at room temperature on a shaker. The stain was then discarded and the gels were incubated in destaining solution (10% acetic acid, 20% methanol) for 90 minutes. The destaining solution was changed every 30 minutes. Following this, the gels were stored in water.

2.14 PNPB activity assay

Membrane assay

Membranes were typically diluted to 4x the final assay concentration (FAC) using 50mM HEPES pH 7.5, 5% DMSO (assay buffer) and then 50µl/well was dispensed in a 96-well clear polypropylene plate (normally 3 replicate wells). 50µl of the drug (4x FAC) or assay buffer was added to the membranes which were then incubated for 5 minutes at room temperature. The substrate PNPB (Sigma) was diluted to 40x FAC using DMSO and then to 2x FAC using 50mM HEPES pH 7.5. 100µl of the diluted substrate was added to each well and the OD_{400} was measured every 12 seconds for 30 minutes using a Spectramax plate reader (Molecular devices). Typically, the total assay volume was 200µl containing 12.5µg/ml membranes, 250µM PNPB, and 5% DMSO. The reactions rates were generally calculated over the first 10 minutes using 3 replicate wells.

Live cell assay

Cells were seeded at a density of 40,000/well of 96-well plates in Freestyle media (Invitrogen) and maintained overnight. Prior to assaying, the media was discarded and the cells were washed with 50mM HEPES pH 7.5 (assay buffer). 100µl of drugs (2x FAC) or assay buffer was then added to the wells following which the plate was incubated for 5 minutes or for the indicated times. PNPB was diluted to 100x FAC in DMSO and then to 2x FAC in assay buffer. 100µl was then added to each well and the activity was measured as described for the membrane assay (6 replicate wells). Typically, the total assay volume was 200µl containing 500µM PNPB, and 1% DMSO.

2.15 DiFMUO activity assay

Membrane assay

Membranes were typically diluted to 4x the final assay concentration (FAC) using 50mM MES pH 6.5, 5% DMSO (assay buffer) and then 50µl was dispensed in each well of a 96-well clear polypropylene plates (normally 3 replicate wells). 50µl of the drug (4x FAC) or assay buffer was added to the membranes which were then incubated for 5 minutes at room temperature. The substrate DiFMUO (Invitrogen) was diluted to 40x FAC using DMSO and then to 2x FAC using 50mM MES pH 6.5. 100µl of the diluted substrate was added to each well and the fluorescence (excitation 360nm, emission 450nm) was measured every 30 seconds for 30 minutes using the FlexStation (Molecular devices). Typically, the total assay volume was 200µl containing 12.5µg/ml membranes, 10µM DiFMUO, and 5% DMSO. The reactions rates were generally calculated over the first 10 minutes using 3 replicate wells.

Live cell assay

Cells were seeded at a density of 40,000/well of 96-well plates in Freestyle media (Invitrogen) and maintained overnight. Prior to assaying, the media was discarded and the cells were washed with 50mM MES pH 6.5 (assay buffer). 100µl of drugs (2x FAC) or assay buffer was then added to the wells following which the plate was incubated for 5 minutes or for the indicated times. DiFMUO was diluted to 100x FAC in DMSO and then to 2x FAC in assay buffer. 100µl was then added to each well and the activity was

measured as described for the membrane assay (6 replicate wells). Typically, the total assay volume was 200µl containing 10µM DiFMUO, and 1% DMSO.

2.16 EnzCheK activity assay

Membranes were typically diluted to 4x FAC using 50 mM HEPES pH 7.5, 10% DMSO (assay buffer) and then 25µl was dispensed in each well of a 96-well clear polypropylene plate (normally 3 replicate wells). 25µl of the drug (4x FAC) or assay buffer was added to the membranes which were then incubated for 5 minutes at room temperature. The substrate EnzCheK (Invitrogen) was diluted to 20x FAC using DMSO and then to 2x FAC using 50mM HEPES pH 7.5. 50µl of the diluted substrate was added to each well and the fluorescence (excitation 480nm, emission 540nm) was measured every 48 seconds for 10 minutes using the FlexStation. Typically, the total assay volume was 100µl containing 12.5µg/ml membranes, 2µM EnzChek, and 10% DMSO. The reactions rates were generally calculated over the first 2 minutes using 3 replicate wells.

2.17 Baculovirus generation and expression

SF-900 II SFM media (Invitrogen) was used to culture the Sf9 (*Spodoptera frugiperda*) insect cells unless otherwise stated.

Baculovirus generation

Recombinant baculoviruses (P1) were generated and amplified using Sf9 cells and the GST-DAGL CD pENTR constructs following the Bac-to-Bac system (Invitrogen). Briefly - 50µl DH10Bac competent cells (Invitrogen) were transformed with 5µl of the plasmid DNA and selected on LB Agar plates containing 50µg/ml kanamycin, 7µg/ml gentamicin,10µg/ml tetracycline, X-gal, and IPTG. White colonies obtained were restreaked to confirm the selection (blue/white). The selected clones were then grown in 5ml LB 50µg/ml kanamycin, 7µg/ml gentamicin, and 10µg/ml tetracycline, overnight at 37°C. The bacmid DNA was extracted from the cells and used to transfect Sf9 cells in 6-well plates using Cellfectin and Grace's insect media (Invitrogen). The media was changed to SF-900 II SFM media 5 hours post

transfection. The media containing the P1 viruses was collected 4-5 days post transfection and stored in the presence of 5% FCS in the dark at 4°C.

In order to amplify the virus, 200mls Sf9 cells at a density of 1.2 x 10^6 cells/ml in 1L Erlenmeyer flasks were infected with 500µl of P1/2 virus and incubated in a shaker at 27.5°C (110rpm) for 4-5 days (or until viability <80%). The P2/3 virus (supernatant) was then collected by centrifugation (3,000g for 10 minutes). The cell count at time of harvest was generally ~3 x 10^6 cells/ml with a viability of 60-70%, as determined by the trypan blue exclusion method. The viruses were stored in the dark at 4°C in the presence of 5% FCS.

Expression

For expression, 10ml P2/3 virus was added to 200ml Sf9 cells at a density of 2 x 10^6 cells/ml (in 1L Erlenmeyer flask). The cells were cultured for 48 hours (27.5°C and 110rpm) and then harvested by centrifugation at 3000g. Cell count at the time of harvest was generally ~3-4 x 10e6/ml (~75% viable).

2.18 Purification of the GST tagged DAGL catalytic domains

Lysis

3 x 10^9 cells were resuspended (0.5 x 10^8 cells/ml) in lysis buffer (50mM Tris, 150mM NaCl, 2mM DTT, 1% Triton-X-100, pH 7.8) by vortexing and then lysed by dounce homogenisation (10 strokes). Lysates were incubated in the cold room on a roller for 2 hours. The lysates were then centrifuged at 75,000g for 60 minutes and the supernatant was collected.

GST affinity purification

GST purifications were performed using glutathione sepharose 4B beads (GE healthcare). 1ml of settled beads were equilibrated in lysis buffer and then incubated with the lysates in the cold room on a roller for 30 minutes. The beads were then collected using a plastic drip column. The collected beads were washed with 20 column volume wash buffer (50mM Tris, 150mM NaCl, 2mM DTT, 0.05% Triton-X-100, pH 7.8) and then 0.5ml elution fractions were collected using the elution buffer (50mM Tris, 150mM NaCl,

2mM DTT, 0.05% Triton-X-100, 50mM glutathione, pH 7.8). The elutions obtained were analysed by Coomassie stained SDS-PAGE and typically elutions 2-5 were stored at -80°C and used for the gel filtration chromatography.

Gel filtration purification of the GST affinity purified DAGL catalytic domains

The purification buffer used for the gel filtration chromatography was 50mM Tris, 150mM NaCl, 2mM DTT, 0.05% Triton-X-100, pH 7.8. Gel filtrations purifications were performed using an Akta prime (GE healthcare) at a flow rate of 1ml/minute using either the HiLoad 13/300 Superdex 200 GL or the HiLoad 16/600 Superdex 200 pg column (GE healthcare).

The 13/300 column was equilibrated in 1 column volume of purification buffer after which 0.5ml of the GST elution (~0.5mg) was loaded and 1ml fractions were collected. Fractions correspoding to peaks in the chromatogram (A280) were analysed by Coomassie stained SDS-PAGE (20µl sample). The native molecular weights of the proteins in the fraction were determined using a chromatogram of protein standards provided by the manufacturer (GE healthcare). The purification using the 16/600 column was performed as above except 2ml (~2mg) of the GST elutions were used and 1.5ml fractions were collected.

2.19 *In vitro* phosphorylation and Phos-tag analysis

Kinase treatment

0.5-1µM of GST-MBP (Millipore) or GST-DAGLα/β catalytic domain (purified by GST affinity and gel filtration) were incubated with varying concentrations of either PKA (Promega) or PKC (Invitrogen) in IVP buffer (50mM Tris, 0.05% Triton-X-100, 2mM DTT pH 7.8, 2.4mM ATP and 240mM $MgCl_2$) for 1 hour at 30ºC. Temperature, incubation times, and kinase concentrations were varied in some experiments. Typical reaction volumes were 24µl. Following the set incubation times, 6µl of 5x SDS protein loading buffer was added and the samples were boiled for 5 minutes. The denatured samples were analysed by Phos-tag Western blotting analysis as described below.

Phos-tag Western blotting analysis

SDS-PAGE gels containing 70μM Phos-tag (Alpha laboratories) and 140μM $MnCl_2$ were prepared and used as part of Western blotting analyses as described above with the following variation. After the samples were resolved by SDS-PAGE, the gels were incubated in transfer buffer + 1mM EDTA for 10 minutes and then in transfer buffer for 10 minutes prior to the transfer.

2.20 Phospho-mapping

Tryptic digestion

Bands of interest (~5μg of GST-DAGL CD) were excised from Coomassie stained gels and washed with 100mM ammonium bicarbonate (ambic) for 5 minutes. Following this, the gel pieces were dehydrated with acetonitrile, dried, and then rehydrated with 10mM DTT (made up in 100mM ambic) at 56°C for 30 minutes. The DTT solution was then discarded and the gel pieces were once again dehydrated with acetonitrile, dried, and then incubated with 55mM iodoacetamide (made up in 100mM ambic) for 20 minutes in the dark, at room temperature. The supernatant was then discarded and the gel pieces were washed twice with 100mM ambic after which they were dehydrated with acetonitrile and then dried again. Following this, the gel pieces were rehydrated in a minimal volume (enough to immerse and rehydrate) of trypsin (13ng/ml in 50mM ambic) for 20 minutes at 4°C. Unabsorbed trypsin was removed and the gel pieces were submerged in 50mM ambic and incubated at 37°C for 2 hours and then overnight at room temperature.

Peptide extraction

The supernatant from the gel pieces above was collected after which the gel pieces were washed with a minimal volume of 50mM ambic (enough to immerse the gel pieces) for 5 minutes at 37°C, the supernatant was collected and pooled with the initial supernatant. The gel pieces were then dehydrated using acetonitrile for 10 minutes at 37°C and the supernatant was once again collected and pooled. The wash and dehydration steps were repeated. The

pooled supernatants containing the peptide extract were dried down and stored at -80^{o}C.

Mass spectrometry analysis

The peptide extracts above were resuspended in 20µl 50mM ambic and 10µl was used for mass spectrometry analysis. Chromatographic separations were first performed using an EASY NanoLC system (ThermoFisherScientific, UK). Peptides were resolved by reversed phase chromatography on a 75µm C18 EASY column using a three step linear gradient of acetonitrile (5-40%, 40-95%, 95-5%) in 0.1% formic acid. The gradient was delivered to elute the peptides at a flow rate of 300 nL/min over 60 min. The eluate was ionised by electrospray ionisation using an Orbitrap Velos Pro (ThermoFisher Scientific), running the Xcaliber software v.2.1.0 SP1.1160, with the following parameters: 50 minute acquisition; Top 20 CID (collision induced dissociation) method; Normalised collision energy - 35v; Activation Q - 0.250; Activation Time - 10ms; Lock Mass - m/z 445.120024; MS Scan width - m/z 400-2000; MS/MS Scan width - m/z 100-2000, 30 sec dynamic exclusion). The MS/MS analyses were conducted using collision energy profiles that were chosen based on the mass-to-charge ratio (*m/z*) and the charge state of the peptide.

The mass spectral data was processed into peak lists using Proteome Discoverer v1.3 (v. 1.3.0.339). The peak list was searched against the Uniprot database (www.uniprot.org) using Mascot software v2.2 (www.matrixscience.com) with the following parameters: Precursor ion mass tolerance 10ppm; Fragment ion mass tolerance 0.8Da; Tryptic digest with up to three missed cleavages; Variable modifications: Acetyl (Protein N-term), Carbamidomethylation (C), Oxidation (M) & Phosphorylation (S, T & Y); Target FDR 0.01 (Strict) – 0.05 (Relaxed). Any identified phosphorylation sites (phospho-sites) were then manually verified.

Chapter 3 (Results 1): Regulation of DAGL activity - A bioinformatics perspective

3.1 Introduction

The first reports of the isolation and partial biochemical characterisation of DAGL activity were made almost 30 years ago (Farooqui et al., 1984, 1986). However, to date very little, if anything, is known about how these enzymes are regulated. In the last decade, since the DAGLs were cloned, several studies have established key physiological roles for these enzymes in processes like axonal growth and guidance, synaptic signalling and adult neurogenesis (Reisenberg et al., 2012). More recent studies have also focussed on their roles in diseases e.g. Fragile X syndrome and pain (Gregg et al., 2012; Jung et al., 2012) and on their therapeutic potential (Hsu et al., 2012), which has raised further interest in the mechanisms regulating these enzymes.

There is a considerable body of evidence describing the structure and function of molecules that are structurally related to the DAGLs, and a very large and generally untapped amount of data in public databases describing phospho-peptides that have been identified based on proteomic type studies. Likewise, there are now numerous computational tools that can predict phospho-sites, and indeed the kinases that might act upon them (Blom et al., 1999; Iakoucheva et al., 2004; Amanchy et al., 2007). In this chapter I use structural homology and bioinformatics to build a working model that provides a template for determining the mechanisms that regulate DAGL activity. However, before that I will briefly outline some evidence that points to mechanisms that are likely to regulate DAGL activity.

Several fold differences between basal and stimulated 2-AG levels have been reported (e.g. (Sugiura et al., 2000a; Aguado et al., 2005), raising the possibility that intra-molecular mechanisms to activate the DAGLs may exist. In the absence of a crystal structure for either DAGLα or DAGLβ, I have used a homology modelling approach to identify the key sites in the enzymes that most probably regulate function. In brief, secondary sequence alignments of

the mammalian DAGLs with the fungal DAGL whose crystal structure has been solved (Yamaguchi et al., 1991; Derewenda et al., 1994) revealed a large insert in the catalytic domain between the β strands 7 and 8. On comparison with other lipases (HSL and PL), this insert is well placed to act like a 'lid', preventing substrate access to the catalytic site. The activity of several lipases is modulated by phosphorylation; for example, in the case of HSL, the opening and closing of the lid is regulated by phosphorylation (Holm, 2003). In order to therefore explore the potential role of phosphorylation in the regulation of DAGL activity I searched phospho-peptide databases and identified candidate regulatory phospho-sites within the DAGL sequence. 30 sites for DAGLα and 12 sites for DAGLβ were identified of which 9 and 12 were located within the catalytic domain. I have mapped these sites onto a structural model of the enzymes to identify the ones that are most likely to regulate substrate access to the catalytic site. Finally, I have used additional bioinformatics tools (DISPHOS, NetPhos2.0), to assess the likelihood of these sites being genuine phospho-sites as well as to identify candidate kinases responsible for these phosphorylation events.

3.2 Results

3.2.1 Primary, secondary and domain structure of the DAGLs

DAGLα and DAGLβ both consist of a 4 transmembrane domain towards the N-terminus followed by an intracellular catalytic domain as represented by the overall domain structure of the DAGLs in Figure 3.1 (Bisogno et al., 2003). Additionally, DAGLα contains a tail region at the C-terminus that is absent in DAGLβ (Figure 3.1). The predicted and apparent (by SDS-PAGE) molecular weight of the 1042 amino acid long DAGLα is ~120kDa and the 672 amino acid long DAGLβ is ~70kDa (Bisogno et al., 2003). DAGLα and DAGLβ amino acid sequences are highly conserved between human and mouse: 97% identity for DAGLα and 79% for DAGLβ (Bisogno et al., 2003). Additionally, the amino acid sequences of the human DAGLs display an overall 35% homology, which is even higher in the catalytic domain (Gareth Williams unpublished data).

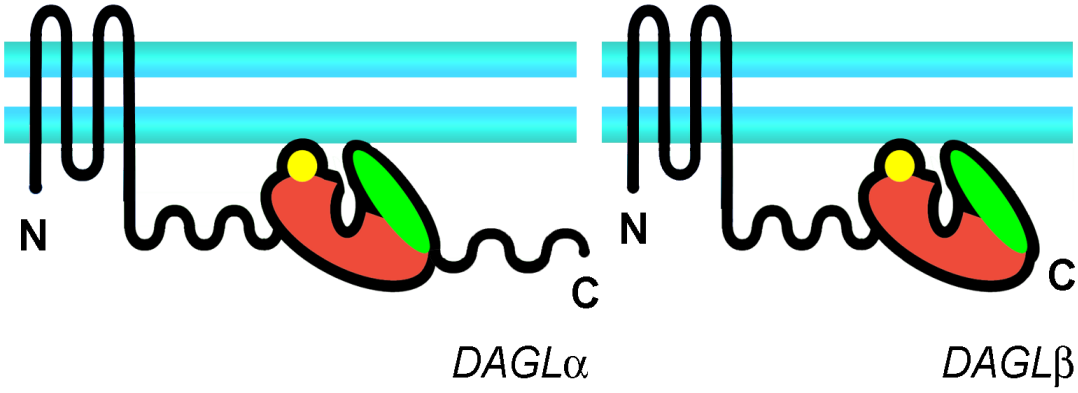

Figure 3.1. Domain structure of mammalian DAGLα and DAGLβ

The DAGLs consist of an N terminal transmembrane domain, followed by a catalytic domain (red). DAGLα consists of a tail at the C-terminus which is absent in DAGLβ. Secondary structure alignments with other lipases indicate the presence of two inserts in the catalytic domain, a cysteine rich insert (yellow), and a putative lid (green). The cysteine rich insert may act as a palmitoylation site that could help localise the enzyme to specific membrane microdomains. The putative lid may regulate the activity of the enzyme by preventing substrate access to the catalytic site. (Adapted from (Reisenberg et al., 2012).

Structurally, the DAGLs belong to the alpha/beta hydrolase fold family, a large group of structurally related but catalytically diverse enzymes that include lipases, peptidases and esterases (Holmquist, 2000). They consist of a mostly parallel beta sheet composed of eight beta strands which are generally linked by alpha helices but also by loops. They all possess a nucleophile-acid-His catalytic triad (Ser, Asp and His in the case of the DAGLs) (Figure 3.2, highlighted in red). The nucleophile is located within a Gly-X-Nucleophile-X-Gly consensus sequence (Gly-His-Ser-Leu-Gly for the DAGLs, Figure 3.2, boxed), referred to as the nucleophile elbow, which plays an important role in presenting the nucleophile to the substrate (Nardini and Dijkstra, 1999). The catalytic triad and nucleophile elbow sequence are conserved between both human and mouse DAGLα/β as highlighted in the primary sequence alignment in Figure 3.2. The catalytic triad of the DAGLs have been experimentally verified in our lab and by others (Bisogno et al., 2003; Pedicord et al., 2011).

The ability of the alpha/beta hydrolase domain (ABHD) fold to accommodate structural insertions between the β strands contributes to the functional diversity observed in this family. For example, in the case of lipases, a commonly found insert is a lid like structure that covers and regulates substrate access to the catalytic site (Nardini and Dijkstra, 1999). Our group exploited sequence information of a fungal MAGL/DAGL from *P. camembertii* to clone the vertebrate DAGLs and the crystal structure of this minimal fold DAGL has been solved (Derewenda et al., 1994). In order to gain structural insights into the DAGLs, we generated secondary structure alignments of the DAGLs and the fungal lipase. This identified 2 key features - a cysteine rich insert (highlighted in yellow in Figure 3.1 and Figure 3.2) and a putative lid (highlighted in green in Figure 3.1 and Figure 3.2). These are discussed below.

3.2.2 The Cysteine rich insert

Secondary structure alignments of the DAGLs with *P. camembertii* revealed that DAGLα and DAGLβ sequences contain a 20-24 amino acid long

Figure 3.2. Multiple sequence alignment of the catalytic domain sequences of human and mouse DAGLβ and DAGLα

Multiple sequence alignment was performed using CLUSTAL 2.1. The catalytic triad (Ser, Asp and His) are highlighted in red. The serine containing nucleophile elbow is annotated with a box. The cysteine rich insert and putative lid are highlighted in yellow and green respectively. A highly conserved signature motif is highlighted in blue.

Alignment of DAGLs highlighting key structural features

```
hDAGLβ          TDLVPSDIAAGLALLHQQQDNIR------NNQEPAQVVCHAPGSSQEADLDAELEN---- 277
mDAGLβ          TDLVPSDIAAGFTLLHQQQDNIS------HSREPPEVVTHTPGQPQETELDAEVEN---- 277
hDAGLα          LDIVPSDIIAGLVLLRQRQRAKRNAVLDEANNDILAFLSGMPVTRNTKYLDLKNSQEMLR 288
mDAGLα          LDIVPSDIIAGLVLLRQRQRAKRNAVLDEANNDILAFLSGMPVTRNTKYLDLKNSHEMLR 288
                 *:***** **:.**:*:*           ..:   .:   *   :   ** : .:

hDAGLβ          ---CHHYMQFAAAAYGWPLYIYRNPLTGLCRIGGDC----CRSRTTDYDLVGGDQLNCH- 329
mDAGLβ          ---CHHYMPFAAAAYGWPLYIYRNPFTGLCRIGGDC----CRARDIEYDAVEGDQHNCH- 329
hDAGLα          YKEVCYYMLFALAAYGWPMYLMRKPACGLCQLARSCSCCLCPARPRFAPGVTIEEDNCCG 348
mDAGLα          YKEVCYYMLFALAAYGWPMYLMRKPTCGLCQLARSCSCCLCPARPRFAPGVTIEEDNCCG 348
                     :** ** ******:*: *:*  ***::. .*    * :*      *  :: **

hDAGLβ          -----FGSILHTTGLQYRDFIHVSFHDKVYELPFLVALDHRKESVVVAVRGTMSLQDVLT 384
mDAGLβ          -----FASILKTTGLQYRDFIHISFHDKVYELPFIVVLDHRKESVVVAVRGTMSLQDVLT 384
hDAGLα          CNAIAIRRHFLDENMTAVDIVYTSCHDAVYETPFYVAVDHDKKKVVISIRGTLSPKDALT 408
mDAGLα          CNAIAIRRHFLDENMTAVDIVYTSCHDAVYETPFYVAVDHDKKKVVISIRGTLSPKDALT 408
                     :   :   .:   *::: * ** *** ** *.:** *:.**:::***:* :*.**

hDAGLβ          DLSAESEVLDVECEVQDRLAHKGISQAARYVYQRLINDGILSQAFSIAP-----EYRLVI 439
mDAGLβ          DLSAESETLELGIELQDCVAHKGIAQAARYIHRRLVNDGILSQAFSVAP-----EYQLVL 439
hDAGLα          DLTGDAERLPVEGHHGTWLGHKGMVLSAEYIKKKLEQEMVLSQAFGRDLGRGTKHYGLIV 468
mDAGLα          DLTGDAERLPVEGHRGTWLGHKGMVLSAEYIKKKLEQEMVLSQAFGRDLGRGTKHYGLIV 468
                **:.::* * :  .    :.***:  :*.*: ::* :: :*****.        .* *::

hDAGLβ          VGHSLGGGAAALLATMLRAAYPQVRCYAFSPPRGLWSKALQEYSQSFIVSLVLGKDVIPR 499
mDAGLβ          VGHSLGAGAAALLAIMLRGAYPQVRAYAFSPPRGLLSKSLYEYSKDFVVSLILGMDVIPR 499
hDAGLα          VGHSLGAGTAAILSFLLRPQYPTLKCFAYSPPGGLLSEDAMEYSKEFVTAVVLGKDLVPR 528
mDAGLα          VGHSLGAGTAAILSFLLRPQYPTLKCFAYSPPGGLLSEDAMEYSKEFVTAVVLGKDLVPR 528
                ******.*:**:*: :**  ** ::.:*:*** ** *:   ***:.*:.:::** *::**

hDAGLβ          LSVTNLEDLKRRILRVVAHCNKPKYKILLHGLWYELFGGNPNNLPTELDGGDQEVLTQPL 559
mDAGLβ          LSVTNMEDLKRRILRVIANCNKPKYKILLHGCWYGLFGGSPDNFPTELDEGTQGALTQPL 559
hDAGLα          IGLSQLEGFRRQLLDVLQRSTKPKWRIIVG--------------------ATKCIPKSEL 568
mDAGLα          IGLSQLEGFRRQLLDVLQRSTKPKWRIIVG--------------------ATKCIPKSEL 568
                :.::::*.::*::* *: ...***::*::                      . :   .. *

hDAGLβ          LGEQSLLTRWSPAYSFSSDSPLDSSP-KYPPLYPPGRIIHLQEEGASGRFGCCS--AAHY 616
mDAGLβ          LGEQTLLTRYSPGY-CSSDSPLDSPT-KYPTLYPPGRIIHLEEEGGSGRFGCCS--AAQY 615
hDAGLα          P-EEVEVTTLASTRLWTHPSDLTIALSASTPLYPPGRIIHVVHNHPAEQCCCCEQEEPTY 627
mDAGLα          PEDQVEVTTLASTRLWTHPSDLTIALSASTPLYPPGRIIHVVHNHPAEQCCCCEQEEPTY 628
                  ::  :*  :.    :  * *  .    ..*********: .:  : :  **.   . *

hDAGLβ          SAKWSHEAEFSKILIGPKMLTDHMPDILMRALDSVVSDR----AACVSCPAQGVSSVDVA 672
mDAGLβ          RARWAHEAEFSKILIGPKMLIDHMPDVMIRALDRVLADR----TACVSCPGQGGSSVP-- 669
hDAGLα          FAIWGDNKAFNEVIISPAMLHEHLPYVVMEGLNKVLENYNKGKTALLSAAKVMVSPTEVD 687
mDAGLα          FAIWGDNKAFNEVIISPAMLHEHLPYVVMEGLNKVLENYNKGKTALLSAAKVMVSPTEVD 688
                 * *..:  *.:::*.* ** :*:* ::::..*: *: :     :* :*..    *..
```

Cysteine rich insert
Signature motif
Lid
Catalytic triad
GXSXG motif

CLUSTAL 2.1 multiple sequence alignment

cysteine rich insert within the catalytic domain, between the first two alpha helices. (Figure 3.1 and Figure 3.2). It is tempting to speculate that this insert contains palmitoylation sites. Palmitoylation is a reversible post-translational modification of cysteine residues which occurs by the attachment of a palmitic acid via a thioester linkage (Aicart-Ramos et al., 2011) and regulates subcellular trafficking of proteins (Canobbio et al., 2008). This insert could potentially regulate DAGL activity by affecting its localisation at the membrane relative to its substrate and down-stream receptors (CB1/2).

3.2.3 The DAGLs contain a putative lid like insert

As mentioned earlier, a common structural feature among lipases is a lid like structure that is inserted between β strands of the canonical ABHD fold. The lid is responsible for the 'interfacial activation' phenomenon, commonly observed with these enzymes. Interfacial activation refers to the displacement of the lid and increased activity when the lipase comes in contact with a lipid phase (Nardini and Dijkstra, 1999; Holmquist, 2000). The lid can simply act as a physical barrier preventing substrate access e.g. gastric lipase (GL) (Canaan et al., 1999), but displacement of the lid can also lead to a structural rearrangement of the active site rendering the enzyme active, as in the case of pancreatic lipase (PL) (van Tilbeurgh et al., 1993). Presumably, the activity of the DAGLs is regulated by similar mechanisms.

The size of the lid can vary amongst lipases. In the case of human PL, a 24 amino acid α-helical surface loop shields the active site (Figure 3.3) (Winkler et al., 1990). In the case of human GL, a large cap domain (124 amino acids) is present between the canonical β strands 6 and 7 and is made up of 8 helices, turns and random coils (Miled et al., 2003). In the case of hormone sensitive lipase (HSL), an even larger ~150 amino acid insert between the canonical β strands 6 and 7, often referred to as the regulatory domain or regulatory module, is well placed to function as the lid (Lampidonis et al., 2011) (Figure 3.3).

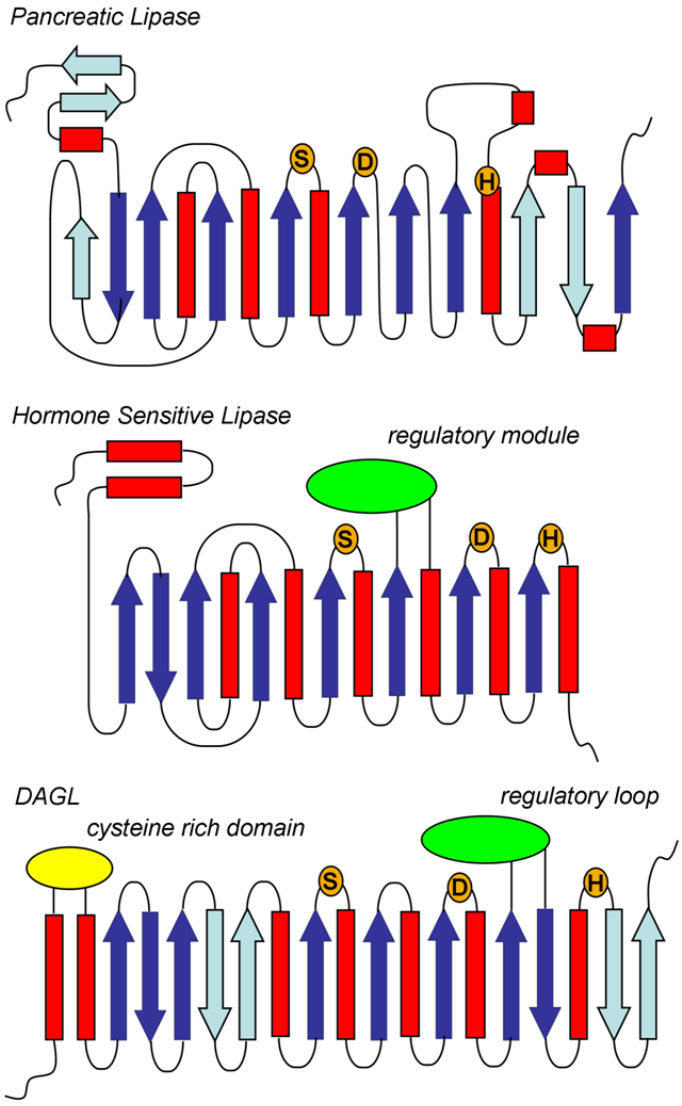

Figure 3.3. Fold topologies of the catalytic domain of the DAGLs relative to other lipases

PL, HSL and DAGL are members of the ABHD fold family and consist of a core eight stranded beta sheet (dark blue) which are connected by α helices (red), β strands (blue, canonical in dark blue) and loops. The catalytic triad consisting of a Ser, Asp and His are highlighted in orange. The lid of PL is present after the core β strand 7. The lid region of HSL (green) is a more pronounced insert present between core β strand 6 and 7. In the case of the DAGLs, a putative lid referred to as the regulatory loop (RL) (green) is present between core β strands 7 and 8. An additional cysteine rich insert is present towards the N-terminus of the DAGL catalytic domain that may act as a site for palmitoylation. (Adapted from (Reisenberg et al., 2012).

The catalytic domains of the DAGLs contain a 50-60 amino acid insert of unknown structure between the β strands 7 and 8 (highlighted in green in Figure 3.1, Figure 3.2 and Figure 3.3). This insert is encoded by a single exon (Reisenberg et al., 2012), appears to be membrane proximal (discussed further down) and is well positioned to act as a lid, shielding the catalytic site (Figure 3.3). This insert is smaller than the ~150 amino acid regulatory domain of HSL and larger than the ~25 amino acid lid of PL, and is henceforth referred to as the regulatory loop (RL). One of the most striking features of the loop is a highly conserved short peptide sequence 'LYPPGRIIH' (highlighted in dark blue in Figure 3.2). This polyproline 'signature motif' is not only conserved amongst human DAGLα and β but also conserved between mammalian, invertebrate, and plant DAGLs (data not shown).

The highly conserved nature of this sequence could implicate it as a binding site for an interaction partner; however this would also require the interacting partner to be conserved across the species. It is therefore more likely that this sequence is involved in an intra-molecular interaction which could stabilise the open/closed conformation of the enzyme.

3.2.4 Phosphorylation of the DAGLs

The relatively large RL in the DAGLs provides a potential regulatory mechanism given that lid displacement could directly determine an 'open' and 'closed' conformation, and thereby regulate activation of the DAGLs. In this context, the activity of several lipases is regulated by phosphorylation at specific sites e.g. PLC-γ (Gresset et al., 2010), TGL4 (Kurat et al., 2009) and HSL (Lampidonis et al., 2011). HSL is probably the most studied lipase in terms of its phosphorylation. The activity of HSL is regulated by PKA *in vitro* and in cells (Lampidonis et al., 2011). PKA can phosphorylate HSL directly at 3 different sites and can cause ~2-fold increase in activity *in vitro* (Holm et al., 1994; Anthonsen et al., 1998). In addition to this, PKA dependent phosphorylation of HSL in cells results in translocation of HSL to lipid droplets (Brasaemle et al., 2000). Interestingly, all the PKA phospho-sites in the HSL sequence are located in the regulatory domain and *in vitro*

phosphorylation by PKA increases the hydrophobic surface area of the protein, presumably due to displacement of the regulatory domain (Krintel et al., 2009; Lampidonis et al., 2011). This has led to a model, where in cells, in response to certain stimuli, phosphorylation of HSL by PKA displaces its lid to expose its hydrophobic core which results in increased interaction with the lipid droplets (Lampidonis et al., 2011).

3.2.4.1 The DAGL phospho-map

'PhosphositePlus' from Cell Signalling Technology (CST) is a curated web resource of experimentally observed phospho-sites identified from published sources as well as from previously unpublished data generated at CST. This resource can be used to identify DAGL derived phospho-peptides and I have used this to generate the first comprehensive DAGLα/β phospho-maps (Figure 3.4). The phospho-sites highlighted in the primary sequence are presented in Figure 3.5. A total of 30 sites for DAGLα and 12 sites for DAGLβ have been identified of which 9 (2 in the RL) and 12 (8 in the RL) were located within the catalytic domain. The tail region of DAGLα was particularly heavily phosphorylated (20 sites). In the case of DAGLβ, a short stretch of 15 amino acids located in the RL was found to be heavily phosphorylated (8 sites). This region is poorly conserved between DAGLα and DAGLβ and no phospho-sites in this region of DAGLα have been identified. However, this could simply be because these phospho-sites have not been detected yet, especially considering 5 of the 15 amino acids are serine/threonines (Figure 3.5). Overall, 7 of the sites are conserved between the DAGLs but only 1 conserved site (S402/S378) was reported in both DAGLα and DAGLβ (Figure 3.5).

3.2.4.2 Note of caution towards false positives and false negatives

With the exception of one study (Shonesy et al., 2013), all the studies identifying DAGL derived phospho-peptides were performed using complex cellular or tissue extracts, including U2OS and Jurkat T cell lines, synaptosomes and brain tissues (Table 3.1 and Table 3.2). When simply identifying proteins in a complex sample, data from multiple peptides are normally available to confirm the identity of a protein.

Figure 3.4. The DAGLα/β phospho-map

Experimentally observed phospho-sites of the DAGLs are annotated above. The numbering is according to the human enzyme. The regions highlighted are - transmembrane domain (yellow), catalytic domain (blue), regulatory loop (green) and the signature motif (red).

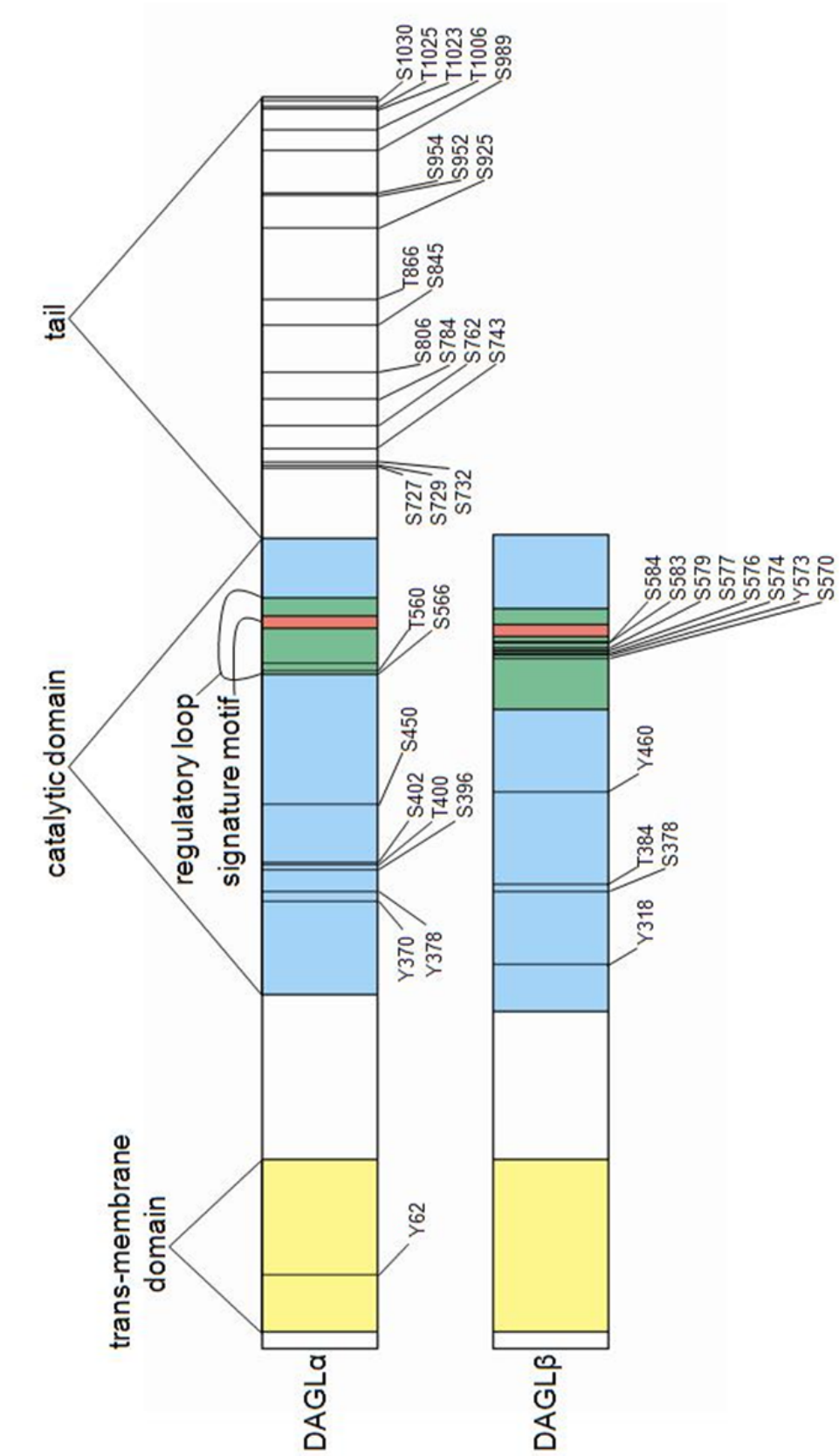
tail
catalytic domain
regulatory loop
signature motif
trans-membrane domain
DAGLα
DAGLβ
S1030
T1025
T1023
T1006
S989
S954
S952
S925
T866
S845
S806
S784
S762
S743
S727
S729
S732
T560
S566
S450
S402
T400
S396
Y370
Y378
Y62
S584
S583
S579
S577
S576
S574
Y573
S570
Y460
T384
S378
Y318

Figure 3.5. DAGL phospho-sites highlighted in the catalytic domain sequences of human and mouse DAGLβ and DAGLα

Multiple sequence alignment was performed using CLUSTAL 2.1. Experimentally identified phospho-sites in the DAGL catalytic domain are annotated as follows - phospho-sites identified in mouse/human DAGLα - pink, mouse/human DAGLβ - blue, phospho-sites identified in both DAGLα and DAGLβ - grey. The catalytic triad (Ser, Asp and His) are highlighted in red. The serine containing nucleophile elbow is also annotated with a box. The cysteine rich insert and regulatory loop are highlighted in yellow and green respectively. The signature motif is highlighted in blue.

Alignment of DAGLs highlighting key structural features and identified phosphosites

```
hDAGLβ          TDLVPSDIAAGLALLHQQQDNIR------NNQEPAQVVCHAPGSSQEADLDAELEN---- 277
mDAGLβ          TDLVPSDIAAGFTLLHQQQDNIS------HSREPPEVVTHTPGQPQETELDAEVEN---- 277
hDAGLα          LDIVPSDIIAGLVLLRQRQRAKRNAVLDEANNDILAFLSGMPVTRNTKYLDLKNSQEMLR 288
mDAGLα          LDIVPSDIIAGLVLLRQRQRAKRNAVLDEANNDILAFLSGMPVTRNTKYLDLKNSHEMLR 288
                 *:***** **:.**:*:*           ..:   .:   *   :   ** : .:

hDAGLβ          ---CHHYMQFAAAAYGWPLYIYRNPLTGLCRIGGDC----CRSRTTDYDLVGGDQLNCH- 329
mDAGLβ          ---CHHYMPFAAAAYGWPLYIYRNPFTGLCRIGGDC----CRARDIEYDAVEGDQHNCH- 329
hDAGLα          YKEVCYYMLFALAAYGWPMYLMRKPACGLCQLARSCSCCLCPARPRFAPGVTIEEDNCCG 348
mDAGLα          YKEVCYYMLFALAAYGWPMYLMRKPTCGLCQLARSCSCCLCPARPRFAPGVTIEEDNCCG 348
                     :** ** ******:*: *:*  ***::. .*    * :*      *  :: **

hDAGLβ          -----FGSILHTTGLQYRDFIHVSFHDKVYELPFLVALDHRKESVVVAVRGTMSLQDVLT 384
mDAGLβ          -----FASILKTTGLQYRDFIHISFHDKVYELPFIVVLDHRKESVVVAVRGTMSLQDVLT 384
hDAGLα          CNAIAIRRHFLDENMTAVDIVYTSCHDAVYETPFYVAVDHDKKKVVISIRGTLSPKDALT 408
mDAGLα          CNAIAIRRHFLDENMTAVDIVYTSCHDAVYETPFYVAVDHDKKKVVISIRGTLSPKDALT 408
                     :   :   .:   *::: * ** *** ** *.:** *:.**::***:* :*.**

hDAGLβ          DLSAESEVLDVECEVQDRLAHKGISQAARYVYQRLINDGILSQAFSIAP-----EYRLVI 439
mDAGLβ          DLSAESETLELGIELQDCVAHKGIAQAARYIHRRLVNDGILSQAFSVAP-----EYQLVL 439
hDAGLα          DLTGDAERLPVEGHHGTWLGHKGMVLSAEYIKKKLEQEMVLSQAFGRDLGRGTKHYGLIV 468
mDAGLα          DLTGDAERLPVEGHRGTWLGHKGMVLSAEYIKKKLEQEMVLSQAFGRDLGRGTKHYGLIV 468
                **:.::* * :  .    :.***:  :*.*: ::* :: :*****.        .* *::

hDAGLβ          VGHSLGGGAAALLATMLRAAYPQVRCYAFSPPRGLWSKALQEYSQSFIVSLVLGKDVIPR 499
mDAGLβ          VGHSLGAGAAALLAIMLRGAYPQVRAYAFSPPRGLLSKSLYEYSKDFVVSLILGMDVIPR 499
hDAGLα          VGHSLGAGTAAILSFLLRPQYPTLKCFAYSPPGGLLSEDAMEYSKEFVTAVVLGKDLVPR 528
mDAGLα          VGHSLGAGTAAILSFLLRPQYPTLKCFAYSPPGGLLSEDAMEYSKEFVTAVVLGKDLVPR 528
                ******.*:**:*: :**  ** ::.:*:*** ** *:   ***:.*:.:::** *::**

hDAGLβ          LSVTNLEDLKRRILRVVAHCNKPKYKILLHGLWYELFGGNPNNLPTELDGGDQEVLTQPL 559
mDAGLβ          LSVTNMEDLKRRILRVIANCNKPKYKILLHGCWYGLFGGSPDNFPTELDEGTQGALTQPL 559
hDAGLα          IGLSQLEGFRRQLLDVLQRSTKPKWRIIVG-------------------ATKCIPKSEL 568
mDAGLα          IGLSQLEGFRRQLLDVLQRSTKPKWRIIVG-------------------ATKCIPKSEL 568
                :.::::*.::*::* *: ...***::*::                     . :   .. *

hDAGLβ          LGEQSLLTRWSPAYSFSSDSPLDSSP-KYPPLYPPGRIIHLQEEGASGRFGCCS--AAHY 616
mDAGLβ          LGEQTLLTRYSPGY-CSSDSPLDSPT-KYPTLYPPGRIIHLEEEGGSGRFGCCS--AAQY 615
hDAGLα          P-EEVEVTTLASTRLWTHPSDLTIALSASTPLYPPGRIIHVVHNHPAEQCCCCEQEEPTY 627
mDAGLα          PEDQVEVTTLASTRLWTHPSDLTIALSASTPLYPPGRIIHVVHNHPAEQCCCCEQEEPTY 628
                  ::  :*  :.    :  * *  .    ..*********: .:  : :  **.   . *

hDAGLβ          SAKWSHEAEFSKILIGPKMLTDRMPDILMRALDSVVSDR----AACVSCPAQGVSSVDVA 672
mDAGLβ          RARWAHEAEFSKILIGPKMLIDRMPDVMIRALDRVLADR----TACVSCPGQGGSSVP-- 669
hDAGLα          FAIWGDNKAFNEVIISPAMLHERLPYVVMEGLNKVLENYNKGKTALLSAAKVMVSPTEVD 687
mDAGLα          FAIWGDNKAFNEVIISPAMLHERLPYVVMEGLNKVLENYNKGKTALLSAAKVMVSPTEVD 688
                 * *..:  *.:::*.* ** :*:* ::::..*: *: :     :* :*..    *..
```

Phospho-sites identified in mouse/human DAGLα
Phospho-sites identified in mouse/human DAGLβ
Phospho-sites identified in both DAGLα and β
Cysteine rich insert
Signature motif
Regulatory loop
Catalytic triad
GXSXG motif

CLUSTAL 2.1 multiple sequence alignment

Table 3.1. Summary of DAGLα phospho-sites

DAGLα site	TM/CD/ RL/Tail	CST reports	Published	Cell/Tissue type	Reference
Y62	TM	0	1	Non small cell lung cancer cell line/tumours	(Rikova et al., 2007)
Y370	CD	0	1	Non small cell lung cancer cell line/tumours	(Rikova et al., 2007)
Y378*	CD	0	1	Non small cell lung cancer cell line/tumours	(Rikova et al., 2007)
S396	CD	1	0	Neuroendocrine tumor	
T400*	CD	1	0	Neuroendocrine tumor	
S402*	CD	1	0	Neuroendocrine tumor	
T411	CD	0	1	HEK293T (over-expressed)	(Shonesy et al., 2013)
S450*	CD	0	1		(Hsu et al., 2011)
T560	RL	9	0	Jurkat T cell (8), K562 (myelogenous leukaemia) cell line	
S566	RL	1	0	Jurkat T cell	
S725	Tail	0	1	HEK293T (over-expressed)	(Shonesy et al., 2013)
S727	Tail	0	2	HEK293T (over-expressed), Brain	(Munton et al., 2007; Shonesy et al., 2013)
S729	Tail	0	1	Brown fat, Kidney	(Huttlin et al., 2010)
S732	Tail	0	3	Brown fat Kidney Synaptosomes PSD	(Trinidad et al., 2006; Huttlin et al., 2010; Trinidad et al., 2012)
S743	Tail	0	8	HEK293T (over expressed) Brain (3) Synapse (2) PSD	(Trinidad et al., 2006; Trinidad et al., 2008; Huttlin et al., 2010; Wisniewski et al., 2010; Goswami et al., 2012; Trinidad et al., 2012; Shiromizu et al., 2013; Shonesy et al., 2013)
S762	Tail	1	0	Brain	
S782	Tail	0	1	HEK293T (over expressed)	(Shonesy et al., 2013)
S784	Tail	0	2	Brain Synapse	(Huttlin et al., 2010; Trinidad et al., 2012)
S806	Tail	0	5	Brain (2)	(Trinidad et al.,

				Synapse HeLa	2008; Chen et al., 2009; Huttlin et al., 2010; Wisniewski et al., 2010; Shiromizu et al., 2013)
S808	Tail	0	1	HEK293T (over expressed)	(Shonesy et al., 2013)
S845	Tail	0	2	HEK293T (over expressed) Brain	(Wisniewski et al., 2010; Shonesy et al., 2013)
T866	Tail	0	2	HEK293T (over expressed) Brain	(Huttlin et al., 2010; Shonesy et al., 2013)
S925	Tail	0	1	Brain	(Wisniewski et al., 2010)
S952	Tail	0	2	Brain (2)	(Huttlin et al., 2010; Wisniewski et al., 2010)
S954	Tail	0	1	Brain	(Wisniewski et al., 2010)
S989	Tail	1	0	Brain	
T1006	Tail	1	0	Brain	
T1023	Tail	2	3	HEK293T (over expressed) Brain (3)	(Huttlin et al., 2010; Shiromizu et al., 2013; Shonesy et al., 2013)
T1025	Tail	0	1	Brain	(Huttlin et al., 2010)
S1030	Tail	4	5	HEK293T (over expressed) Brain (6) Synapse	(Huttlin et al., 2010; Wisniewski et al., 2010; Trinidad et al., 2012; Shiromizu et al., 2013; Shonesy et al., 2013)

* conserved in DAGLβ

(TM - transmembrane domain, CD - catalytic domain, RL - regulatory loop)

Table 3.2. Summary of DAGLβ phospho-sites

DAGLβ site	TM/CD/ RL/Tail	CST reports	Published	Cell/Tissue type	Reference
Y318	CD	3	0	Jurkat cells	
S378*	CD	0	1	Human embryonic stem cells	(Brill et al., 2009)
T384*	CD	0	1	Human embryonic stem cells	(Brill et al., 2009)
Y460*	CD	1	0	PC12	
S570	RL	0	3	HeLa (2) Jurkat T Cell,	(Daub et al., 2008; Mayya et al., 2009; Olsen et al., 2010)
Y573	RL	0	1		(Wang et al., 2006)
S574	RL	17	1	breast cancer liver cancer (4) lung cancer (9) skin cancer (2) Jurkat T cell K562 cell	(Mayya et al., 2009)
S576	RL	3	0	Lung cancer Skin cancer	
S577	RL	0	3	Brain (2) Jurkat T cell	(Mayya et al., 2009; Tweedie-Cullen et al., 2009; Huttlin et al., 2010)
S579*	RL	0	5	HeLa KG1 AML cells U2OS Brain (2)	(Huttlin et al., 2010; Olsen et al., 2010; Raijmakers et al., 2010; Wisniewski et al., 2010; Weber et al., 2012)
S583/4**	RL	0	5	Brain (3) synaptosomes HeLa	(Dephoure et al., 2008; Tweedie-Cullen et al., 2009; Huttlin et al., 2010; Wisniewski et al., 2010; Trinidad et al., 2012)

* Conserved in DAGLα
* *Alignment of these sites to mouse DAGLβ is ambiguous

(TM - transmembrane domain, CD - catalytic domain, RL - regulatory loop)

On the other hand identifying a phospho-site from a complex sample can often rely on a single peptide. The peptide maybe poorly ionisable and present in low abundance which can result in poor quality mass spec data and result in false negatives. On the other hand, lowering the stringency criteria of phospho-peptide identification to minimise false negatives can in turn introduce false positives (Alcolea et al., 2009). If we were to only consider DAGL phospho-sites identified in at least two separate studies then the number of identified sites for DAGLα is reduced from 30 to 11. If the criteria is set to a minimum of three studies the number drops to 6 (Table 3.1). For DAGLβ, 12 sites have been identified at least once, 7 at least twice and all 7 have actually been identified at least three times (Table 3.2).

As the CST studies have not been published yet, if one was to overlook those then 22 DAGLα sites have been identified at least once, 10 sites at least twice and 5 sites at least 3 times. For DAGLβ 8 sites have been identified at least once, 4 at least twice and all 4 have actually been identified at least three times respectively. Therefore if one was to place a minimal requirement of 3 independent published studies to consider a phospho-site as genuine, then the total number of 'genuine' phospho-sites identified for the DAGLs drops from 42 to 9 (5 sites for DAGLα, all in the tail and 4 sites for DAGLβ, all in the regulatory loop).

3.2.5 Prediction of phospho-sites based on sequence and structure

The substrate for the DAGLs, DAG, is generally found integrated in the membrane (Goni and Alonso, 1999). The DAGLs are likely to use their transmembrane domains coupled with mechanisms like palmitoylation to sub localise them at membranes, close to the substrate, and orient themselves in a manner that facilitates sequestration of the substrate from the membrane to the catalytic site. The regulatory loop (lid) is on the same face as the active site, and therefore likely to be membrane and substrate proximal, which would facilitate interfacial activation. Phospho-sites that are membrane proximal are more likely to regulate catalytic activity when compared to sites that are buried or located on the cytoplasm facing surface of these enzymes. A model of the catalytic domains of DAGLα and DAGLβ using structural and

sequence information of the *P. camembertii* fungal DAGL was constructed to determine the location of the numerous phosphorylated residues (Figure 3.6) (Yamaguchi et al., 1991; Derewenda et al., 1994) . The membrane proximal surface was identified based on the orientation of the catalytic triad (red) that would need to be membrane proximal in order to hydrolyze DAG. Based on the location of the identified phospho-sites in the catalytic domain model, 7 out of 9 of the DAGLα sites and 11 of the 12 DAGLβ sites were located on the membrane proximal surface (substrate facing). These sites are therefore potential candidates to regulate the opened and closed conformation of these enzymes (Figure 3.6, Table 3.3 and Table 3.4).

Studies indicate that phosphorylation often occurs at sites within disordered/unstructured sequences, therefore disordered regions have a higher frequency of phospho-sites compared to ordered regions (Iakoucheva et al., 2004). Phosphorylation can promote structure in disordered region or disorder in a structured region, thus affecting inter/intramolecular changes (Johnson and Lewis, 2001). DISPHOS is an online resource that uses protein disorder information to predict phospho-sites (~80% accuracy against known sites) (Iakoucheva et al., 2004). The DAGL sequences were probed using DISPHOS to gain further information on DAGL phospho-sites. Amongst the identified phospho-sites all the DAGLβ residues in the regulatory loop (7/7) were predicted to be phosphorylated (Table 3.4), none of the corresponding residues in the DAGLα sequence were predicted to be phosphorylated (data not shown).

None of the other identified phospho-sites in the DAGLβ catalytic domain and none of the identified phospho-sites in the DAGLα catalytic domain were predicted as phospho-sites. Most of the residues in the DAGLα tail (16/20) were predicted to be phospho-sites by DISPHOS (Table 3.3 and Table 3.4). These results provided further evidence to support the fact that some of the phospho-sites in the RL of DAGLβ and in the tail of DAGLα are genuine phospho-sites.

Figure 3.6. 3D model of the catalytic domains of DAGLα and DAGLβ

A model of the catalytic sites of DAGLα (A) and DAGLβ (B) was generated using structural and sequence information of a fungal mono and diacylglycerol lipase from *P. camembertii.* The membrane proximal surface is adjudged based on the orientation of the catalytic triad (red) that need to be membrane proximal in order to hydrolyze DAG. Several phospho-sites identified in the catalytic domain of the DAGLs were found to be located on the membrane proximal surface of the enzyme. These sites are deemed more likely to regulate catalytic activity of these enzymes when compared to sites that maybe buried or located on the cytoplasmic facing surface and are represented in yellow (residues highlighted in grey are unlikely to be membrane proximal). The residues highlighted with black text were identified by mass spectrometry studies, the residues highlighted in with green text are conserved between DAGLα and DAGLβ but were identified in the other isoenzyme. (green insert - cysteine rich region, blue insert - regulatory loop (RL), white arrows - β strands, blue arrows - canonical β strands, cylinders - α helix).

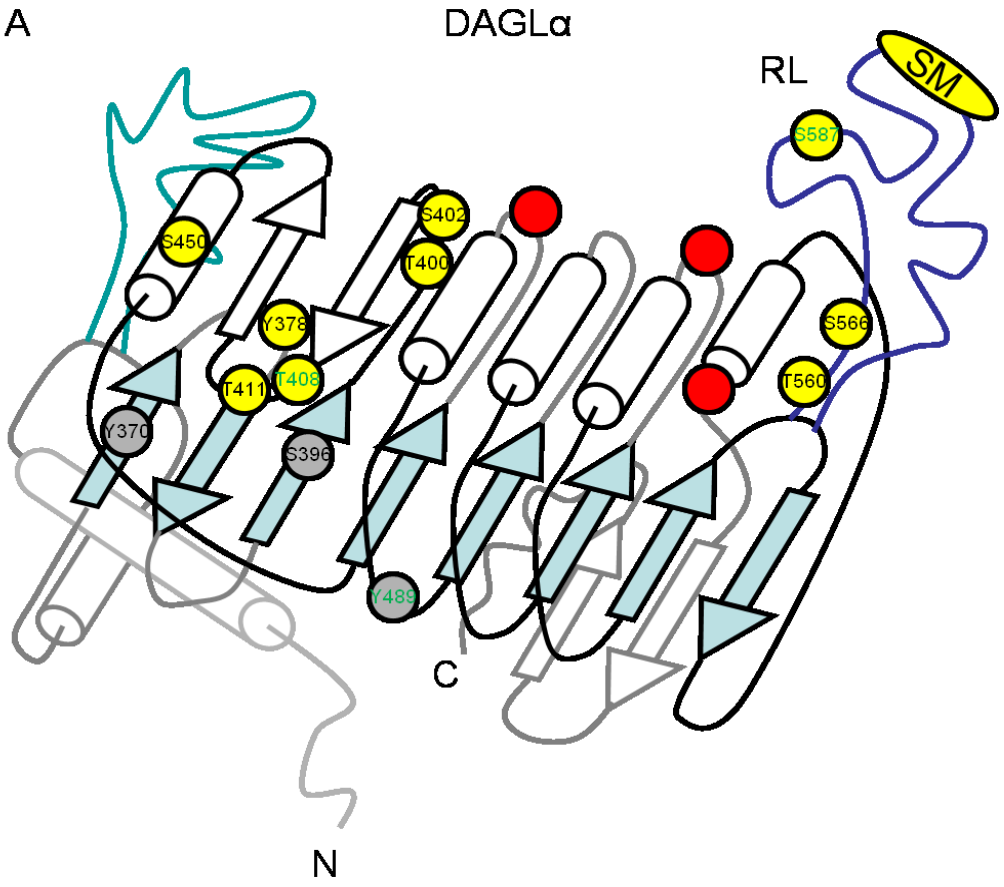
A
DAGLα
RL
SM
S587
S402
S450
T400
Y378
S566
T411
T408
T560
Y370
S396
Y489
C
N

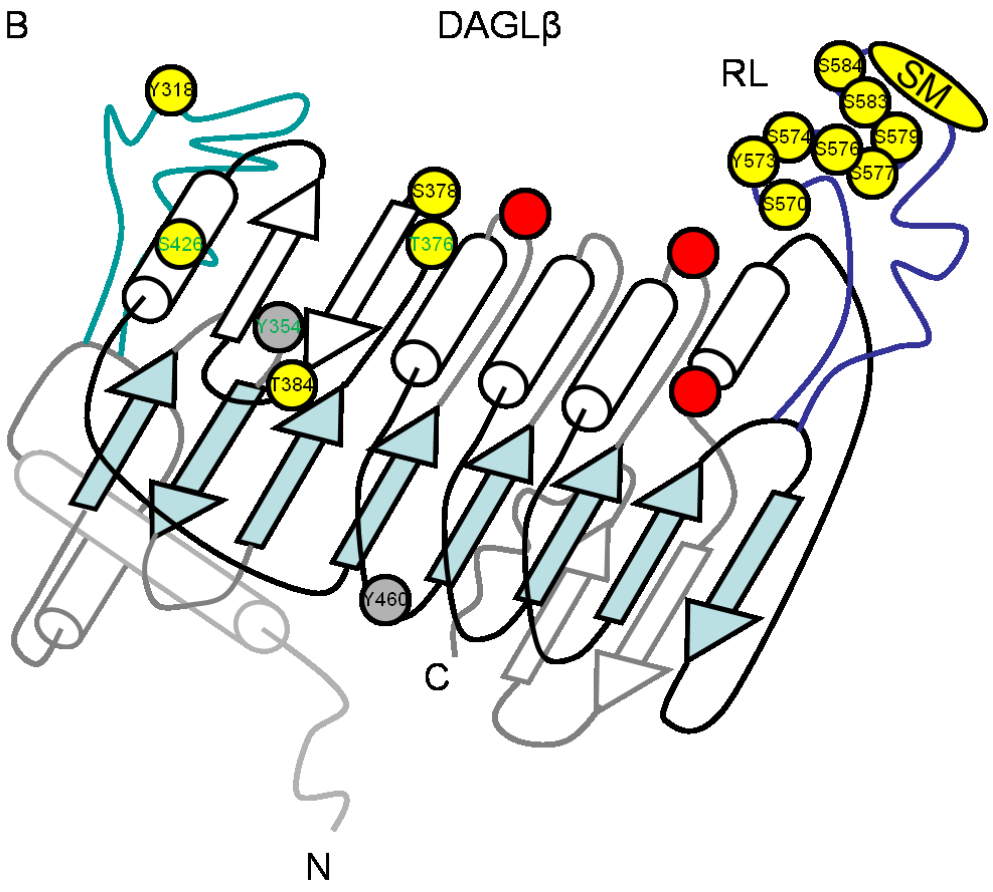
B
DAGLβ
RL
SM
Y318
S584
S583
S574
S579
S576
Y573
S577
S570
S378
S426
T376
Y354
T384
Y460
C
N

Table 3.3. Summary of phosphorylation related predictions for human DAGLα

DAGLα site	TM CD RL Tail	CST/ Published reports	DIS PHOS	Netphos 2	Membrane proximal	Predicted kinase
Y62	TM	0/1				
Y370	CD	0/1				ALK, Src
Y378	CD	0/1			Yes	ALK, Src
S396	CD	1/0		Yes		PKA, PKC, CK1, GPCRK1, MAPKAPK2
T400	CD	1/0		Yes	Yes	MAPKAPK2 PKA, PKC
S402	CD	0/1		Yes	Yes	PKA, PKC,CK2, GSK3, ERK1, ERK2, CDK5, GPCRK1, PDK, H1-HK
T408	*CD*				*Yes*	*PKA, CK1*
T411	CD	1/0			Yes	
S450	CD	0/1			Yes	ATM, DNA-PK
Y489	*CD*					*JAK2*
T560	RL	9/0			Yes	GPCRK1
S566	RL	1/0		Yes	Yes	GPCRK1
S587	*RL*				*Yes*	*AMPK, DNA-PK, CK2*
S725	Tail	0/1	Yes	Yes		MAPKAPK2 CK2
S727	Tail	0/2	Yes	Yes		AMPK, CamKII, PKA, PKC, DNA-PK, ATM, CK2
S729	Tail	0/1	Yes	Yes		AKT, PKA, GPCRK1, CK1
S732	**Tail**	**0/3**	**Yes**	**Yes**		**CK2**
S743	**Tail**	**0/8**	**Yes**	**Yes**		**CamKII, PKA, PKC, GSK3, ERK1, ERK2, CDK5, GPCRK1**
S762	Tail	1/0				
S782	Tail	0/1	Yes	Yes		Beta-ARK, GPCRK1, PDK, CK2,

						MAPKAPK2
S784	Tail	0/2	Yes	Yes		CK1, CK2, GSK3,
S806	**Tail**	**0/5**	**Yes**	**Yes**		**MAPKAPK2, PKA, PKC, GSK3, ERK1, ERK2, CDK5, CK2**
S808	Tail	0/1	Yes			AMPK, DNA-PK
S845	Tail	0/2	Yes			Beta-ARK, CK2
T866	Tail	0/2	Yes	Yes		CDC2, H1-HK, CDK, GSK3, ERK1, ERK2
S925	Tail	0/1				Beta-ARK ,GPCRK1, MAPKAPK2, GSK3, CK1, CK2
S952	Tail	0/2	Yes	Yes		GSK3, ERK1, ERK2, CDK5, H1-HK, CK2
S954	Tail	0/1	Yes	Yes		PKA, PKC, DNA-PK, ATM, CK2
S989	Tail	1/0	Yes	Yes		GSK3, ERK1, ERK2, CDK5
T1006	Tail	1/0				DNA-PK, GPCRK1, CK1, CK2
T1023	**Tail**	**2/3**	**Yes**	**Yes**		**CamKII, GSK3, ERK1, ERK2, CDK5**
T1025	Tail	0/1	Yes			DNA-PK
S1030	**Tail**	**4/5**		**Yes**		**GSK-3, ERK1, ERK2, CDK, CDC2, H1-HK**

Italics - included based on homology to a site detected in DAGLβ
Bold - identified in at least 3 published studies
(TM - transmembrane domain, CD - catalytic domain, RL - regulatory loop)

Table 3.4. Summary of phosphorylation related predictions for human DAGLβ

DAGLβ site	TM CD RL Tail	CST/ Published reports	DIS PHOS	NetPhos 2	Membrane proximal	Predicted kinase
Y318	CD	3/0		Yes	Yes	EGFR, Src, JAK2, ALK
Y354	*CD*					*ALK, Src*
T376	*CD*				*Yes*	*PKA, PKC*
S378	CD	0/1			Yes	AMPK, PDK, CK2
T384	CD	0/1			Yes	CK1, CK2, GPCRK1
S426	*CD*				*Yes*	*CK1, DNA-PK, GSK3, GPCRK1, ATM, MAPKAPK2*
Y460	CD	1/0				JAK2
S570	**RL**	**0/3**	**Yes**		**Yes**	**PKA, PKC, GSK3, ERK1, ERK2, CDK5, MAPKAPK2CK1**
Y573	RL	0/1	Yes	Yes	Yes	Src
S574	RL	17/1	Yes		Yes	CK1, CK2, MAPKAPK2
S576	RL	3/0	Yes		Yes	GPCRK1
S577	**RL**	**0/3**	**Yes**	**Yes**	**Yes**	**CK2**
S579	**RL**	**0/5**	**Yes**	**Yes**	**Yes**	**GSK3, ERK1, ERK2, CDK5, Beta-ARK, CK1, MAPKAPK2CK2, PDK**
S583/ S584*	**RL**	**0/5**	**Yes**	**Yes**	**Yes**	**MAPKAPK2 PKA, PKC, CK2, GA-H1K, ERK1, ERK2, GSK3, CDK5, GPCRK1**

Italics - included based on homology to a site detected in DAGLα
Bold - identified in at least 3 published studies
* Alignment of these sites to mouse DAGLβ is ambiguous
(TM - transmembrane domain, CD - catalytic domain, RL - regulatory loop)

Additionally, the DAGL sequences have been interogated using a neural-network based phosphorylation prediction tool, NetPhos 2.0, that uses sequence and structural data of reported phosphorylation events to predict phospho-sites (~70% accuracy against known sites) (Blom et al., 1999; Iakoucheva et al., 2004) (Table 3.3 and Table 3.4). In the catalytic domain, 4 out of 9 (1/2 in RL) for DAGLα and 5 out of 12 (4/8 in RL) for DAGLβ were predicted as phospho-sites. 14 out of 20 of the identified sites in the tail region of DAGLα were predicted as phospho-sites. Once again, these results provided further evidence to support the fact that some of the phospho-sites within the RL of DAGLβ and tail of DAGLα are genuine. Furthermore, even if more stringent criteria are applied where a phospho-site is only considered as genuine if it has been reported at least 3 times in the literature and is predicted as a phospho-site by DISPHOS/Netphos2.0, 5 DAGLα phospho-sites (all in the tail) and 4 DAGLβ phospho-sites (all in the RL) still remain.

Finally, a phospho-motif finder algorithm has been used to identify candidate kinases that may phosphorylate the above sites (Table 3.3 and Table 3.4) (Amanchy et al., 2007). Almost all the sites (39 out of 42) lay within well defined consensus phosphorylation motifs reinforcing the hypothesis that they likely represent regulatory sites.

3.3 Discussion and conclusions

The ability of the ABHD fold to accommodate structural insertions contributes to the diversity observed in this large family of enzymes (Holmquist, 2000) which includes the DAGLs. A homology modelling and bioinformatics led approach presented here has identified two potential inserts, within the DAGL catalytic domains, a cysteine rich insert, and a putative lid that we refer to as the regulatory loop.

The cysteine rich insert contains consensus palmitoylation sites and might therefore be a key regulatory motif. Palmitoylation is a reversible post-translational modification of cysteine residues which occurs by the attachment of a palmitic acid via a thioester linkage (Aicart-Ramos et al., 2011). Palmitoylation has been shown to regulate subcellular trafficking of proteins. For example, localisation of the small GTPase Rap2b to lipid rafts is

regulated by palmitoylation (Canobbio et al., 2008). Lipid rafts are membrane microdomains playing important roles in signal transduction and membrane transport. Interestingly DAG, 2-AG and DAGLα were found to be enriched in lipid rafts of a DRG cell line (Rimmerman et al., 2008). In order to investigate this further, I have searched a number of databases of palmitoylated proteins to determine if the DAGLs have been picked up in unbiased screens. This reveals three independent studies providing evidence for DAGL palmitoylation. Palmitoylated DAGLα has been detected in rat brain synaptosomes as well as in rat cortical neuron cultures (Kang et al., 2008). On the other hand palmitoylated DAGLβ has been identified in Jurkat cells (human T lymphocyte cell line) (Martin and Cravatt, 2009) and in a human prostate cancer cell line DU145 (Yang et al., 2010). Interestingly, the CB1 receptor can also be palmitoylated and there is increasing evidence towards its localisation to lipid rafts (Bari et al., 2005; Sarnataro et al., 2005; Oddi et al., 2012). Palmitoylation of the cysteine rich insert could therefore play a role in localising the DAGLs to lipid rafts in order to place them in close proximity to their substrate DAG and downstream cannabinoid receptor targets.

As mentioned earlier, a common structural feature among lipases is a lid like structure that is inserted between β strands of the canonical ABHD fold. The lid is responsible for the 'interfacial activation' phenomenon, commonly observed with these enzymes. Interfacial activation refers to the displacement of the lid and increased activity when the lipase comes in contact with a lipid phase (Nardini and Dijkstra, 1999; Holmquist, 2000).

In the case of human pancreatic lipase (PL), a 24 amino acid α-helical surface loop shields the active site (Winkler et al., 1990). The opening of the lid is facilitated by an interacting partner, Procolipase. Procolipase binds to a C-terminal domain of PL and can also bind lipids, thus facilitating PL-lipid interactions in a 'difficult' bile-salt rich environment (van Tilbeurgh et al., 1992). The opened PL lid also interacts with Procolipase, stabilising the opened-confirmation. The opening of the lid not only allows substrate access to the active site, but also causes conformational changes within the active site that renders it active (van Tilbeurgh et al., 1993).

In the case of human gastric lipase (GL), a large cap domain (124 amino acids) is present between the canonical β sheets 6 and 7 and is made up of 8 helices, turns and random coils (Miled et al., 2003). The cap domain can structurally prevent substrate access. Crystal structure of 'opened' GL revealed that displacement of a smaller lid composed of 3 helices (30 amino acids), within the cap domain is sufficient to reveal the catalytic site (Roussel et al., 2002). The remaining part of the cap domain (minus the lid) forms a hydrophobic region around the catalytic site and probably plays a role towards enhancing affinity for the substrate (Roussel et al., 1999; Roussel et al., 2002). The 'opened' crystal structure revealed that the displaced lid interacts with the N-terminus of the enzyme and that no major structural rearrangements within the catalytic site occurred when compared to the closed structure, suggesting that unlike PL, even when shielded by the lid, the catalytic site of GL is in the active confirmation.

Based on secondary structure predictions and alignments with other lipases we identified a 50-60 amino acid 'regulatory loop' (RL) in the DAGLs which is well placed to act as the lid and therefore regulate DAGL activity. A highly conserved polyproline 'signature motif' was identified in the RL of the DAGLs which is not only conserved amongst human DAGLα and β but also conserved between mammalian, invertebrate, and plant DAGLs. The highly conserved nature of this sequence could implicate it as a binding site for an interaction partner (e.g. PL-Procolipase); however this would also require the interacting partner to be conserved across the species. It is therefore more likely that this sequence is involved in an intra-molecular interaction which could stabilise the open/closed conformation of the enzyme (e.g. GL).

In addition to the signature motif we also identified several phospho-sites within the RL that may regulate the activity of the DAGLs. Phosphorylation is a reversible post-translational modification involving the transfer of a phosphate group from ATP to the hydroxyl groups of serine, threonine, and tyrosine residues. This can introduce conformational changes within a proteins structure, thus affecting a range of cellular processes. For instance, phosphorylation at specific sites can cause intra-molecular changes within an enzyme resulting in a change in activity (increase or decrease).

Phosphorylation can also block or promote protein-protein interactions which may affect their activity, localization, and stability (degradation) (Johnson and Lewis, 2001; Salazar and Hofer, 2009).

Activity of several lipases is regulated by phosphorylation e.g. TGL4, PLCγ, HSL (Kurat et al., 2009; Gresset et al., 2010; Lampidonis et al., 2011). As mentioned in the introduction, PLC-γ lies upstream of DAGL, generating DAG, in the FGFR pathway involved in axonal growth and guidance. Many tyrosine kinases directly phosphorylate PLC-γ isozymes to enhance their lipase activity (Gresset et al., 2010). The activities of most PLCs are inhibited by a disordered linker (X/Y linker) that inserts into the catalytic domain to prevent substrate access. Phosphorylation of the linker region of PLC-γ results in a large conformational change that releases this inhibition (Gresset et al., 2010).

HSL is probably the most studied lipase in terms of its phosphorylation. The activity of HSL is regulated by PKA *in vitro* and in cells via multiple mechanisms (Lampidonis et al., 2011). In adipocytes, activation of β-adrenergic receptors leads to a (sequential) increase in cAMP levels, PKA activity, HSL phosphorylation and lipolysis (Stralfors and Honnor, 1989; Anthonsen et al., 1998; Holm, 2003). On the other hand, insulin causes a reduction in cAMP levels, PKA activity, HSL phosphorylation, and lipolysis (Stralfors and Honnor, 1989; Eriksson et al., 1995). PKA can phosphorylate HSL directly at 3 different sites and phosphorylation by PKA *in vitro* can cause ~2-fold increase in HSL activity against lipid substrates (Holm et al., 1994; Anthonsen et al., 1998). In addition to this, PKA dependent phosphorylation of HSL in cells results in translocation of HSL to lipid droplets (Brasaemle et al., 2000). Interestingly, all the PKA phospho-sites in the HSL sequence are located within its regulatory domain (lid). *In vitro* phosphorylation by PKA not only increases the catalytic activity of HSL but also increases the hydrophobic surface area of the protein, presumably due to the displacement of the regulatory domain (Krintel et al., 2009; Lampidonis et al., 2011). This has led to a model, where in cells, in response to certain stimuli, phosphorylation of HSL at multiple sites by PKA results in the localisation of HSL to lipid droplets as well as displacement of the lid resulting

in increased lipolysis (Lampidonis et al., 2011). Additionally, phosphorylation of a lipid droplet binding protein, Perilipin A by PKA, has been shown to play an important role in regulating the HSL-lipid drop interaction (Sztalryd et al., 2003; Wang et al., 2009).

The phospho-map of the DAGLs in Figure 3.4 is a schematic of the experimentally identified DAGL phospho-sites. A total of 42 DAGL phospho-sites have been reported. Most of these sites have been identified by mass spectrometry analysis of complex samples (tissue/cell extracts), this can often result in false positives/negatives for phospho-sites in low abundance (Alcolea et al., 2009). However, several of these sites have been identified in two or more independent (published studies), and these sites are also predicted to be candidate phospho-sites based on prediction tools (DISPHOS, NetPhos2.0). These prediction tools have a 70-80% success rate in predicting experimentally verified phospho-sites (Iakoucheva et al., 2004). The DAGLs therefore appear to be phosphorylated at multiple sites which in turn are likely to regulate the DAGLs, possibly via multiple mechanisms (inter and intra-molecular interactions and localisation, as in the case of HSL).

Two regions in the DAGL sequences were especially found to be phosphorylated. In the case of DAGLβ, a short stretch of 15 amino acids located in the RL has 7 reported phospho-sites, 4 of which have been identified in at least three published studies. These sites (S570, S577, S579, S583/S584) were also predicted to be phosphorylated by NetPhos2.0 (structure/sequence based predictor) and/or DISPHOS (disorder based predictor). We therefore consider these sites as likely candidates to regulate the opened/closed conformation of the enzyme. It is tempting to speculate that these phospho-sites will be conserved amongst the DAGLs, however this region is poorly conserved between DAGLα and DAGLβ, and no phospho-sites in this region of DAGLα have been identified. In addition to that no sites within this region of DAGLα were predicted phospho-sites (DISPHOS/NetPhos2.0). Nevertheless, this does not completely rule out the identification of phospho-sites in this region in the future (5 of the 15 amino acids are serine/threonines). Overall, there were 2 sites identified in the RL of DAGLα, however neither of these sites were identified in published sources

and neither were predicted to be phosphorylated by DISPHOS (one of the sites predicted by NetPhos2.0) so it remains to be seen whether these are genuine phospho-sites. As of yet, we did not identify likely candidate phospho-sites within the RL of DAGLα, it remains to be seen whether this insert is not phosphorylated or the phospho-sites have yet to be identified.

Additional phospho-sites were identified within the catalytic domain of the DAGLs, however none of them have been reported more than once in published sources. Overall, 7 of the identified phospho- sites are conserved between the DAGLs but only 1 of these sites was identified in both DAGLα (S402) and DAGLβ (S378). This site is located within the catalytic domain but not the RL and is likely to be membrane proximal (based on the catalytic domain model). It is tempting to speculate that this phospho-site might represent a conserved regulatory mechanism amongst the DAGLs, however there is only one published report (DAGLβ) and one CST report (DAGLα) for this site and neither site was predicted as a phospho-site by DISPHOS (only the DAGLα site predicted by NetPhos2.0). The evidence supporting this site as a genuine phospho-site is therefore limiting.

The tail of DAGLα, which is absent in DAGLβ, contained multiple phospho-sites (20). 5 of these (S732, S743, S806, S1023, and S1030) have been reported in at least three published studies and were also predicted to be phospho-sites (DISPHOS/NetPhos 2.0) indicating these are genuine phospho-sites. In general, many of the DAGLα tail phospho-sites were identified in the brain (Huttlin et al., 2010; Wisniewski et al., 2010) and more specifically at synapses (Trinidad et al., 2006; Munton et al., 2007; Trinidad et al., 2008; Trinidad et al., 2012). As the localisation of DAGLα to the post synaptic dendritic spine is crucial for its role in synaptic signalling, these sites may play an important role in DAGLα localisation to the synaptic membrane. The tail is dispensable with regards to the catalytic activity of the enzyme indicating that it may not regulate catalytic activity (Pedicord et al., 2011). However, a recent study has demonstrated that phosphorylation in the tail region by CamKIIa inhibits DAGLα activity *in vitro* by ~50% (Shonesy et al., 2013). The mechanism behind this is unknown but may occur due to

increased intramolecular interactions between the tail and catalytic domain (or RL, therefore preventing the lid from opening) following phosphorylation.

We also used a phospho-motif finder to predict candidate kinases responsible for the DAGL phospho-sites. Almost all the sites (39 out of 42) lay within phospho-motifs, majority of which were present within multiple motifs (multiple candidate kinases). Amongst the phospho-sites that were identified in at least 3 published sources (5 in DAGLα (tail) and 5 in DAGLβ (RL)) kinases like PKA, PKC, ERK1, ERK2, GSK3 and CDK5 were frequently identified as candidate kinases (Table 3.3 and Table 3.4).

In conclusion, the DAGLs are likely to use their transmembrane domains, possibly coupled with mechanisms like palmitoylation to sub localise them at the membranes, close to their substrate DAG. This would enable them to orient themselves in a manner facilitating DAG-catalytic site interaction. This would also orient the regulatory loop (lid) towards the membrane which would facilitate inter-facial activation. Furthermore, numerous DAGL phospho-sites have been reported, at least some of which appear to be genuine. Based on structural analogy with HSL and the membrane proximity of some of these sites, phosphorylation of the DAGLs (especially DAGLβ) appears to be a likely mechanism to regulate the activity of these enzymes by regulating the opened and closed conformation of these enzymes.

Chapter 4 (Results 2): Investigating DAGL activation using the Tango assay

4.1 Introduction

Several stimuli like ionomycin and LPS increase 2-AG levels in cells and tissues, but it is not always clear as to whether this is a signalling pool of 2-AG (Bisogno et al., 1997; Stella et al., 1997; Varga et al., 1998; Di Marzo et al., 1999; Bisogno et al., 2003). Also, the mechanisms behind this are poorly understood. Besides monitoring physiological responses like DSI/DSE, studying DAGL activity generally relies on 2-AG quantification. This normally involves the treatment of cells/tissues with appropriate stimuli and/or drugs before extracting the lipids and quantifying 2-AG. Another approach involves testing DAGL activity in cellular/tissue extracts using synthetic DAG as a substrate and then once again by measuring the release of 2-AG (Bisogno et al., 2003; Jung et al., 2007). Quantification of 2-AG relies on mass spectrometry techniques (Balgoma et al., 2013) which requires an elaborate laboratory setup, specialised equipment and tends to be low throughput. Also, as hinted at above, it is unclear if the 2-AG measured in many studies is reflective of a signalling pool of the lipid, as opposed to a general metabolic pool.

The CB1-Tango assay is a recombinant cell based assay that can be used to measure CB1 activation via a reporter gene (β-lactamase) system (van der Lee et al., 2009). The cells were primarily developed to directly measure the activity of small molecule CB1 receptor agonists or antagonists. However, we reasoned that if the cells express the DAGLs, they might be adapted to provide a convenient format to study DAGL-dependent activation of CB1 receptors (Figure 4.1). The Tango cells are commercially available U2OS (human osteosarcoma cell line) cells that stably overexpress the human CB1 receptor. The CB1 receptor is a chimeric molecule that contains a TEV protease site and a Gal4-VP16 transcription factor towards the C terminus. This cell line also stably expresses a β-arrestin-TEV protease fusion protein and the β-lactamase reporter gene under the control of a UAS response element.

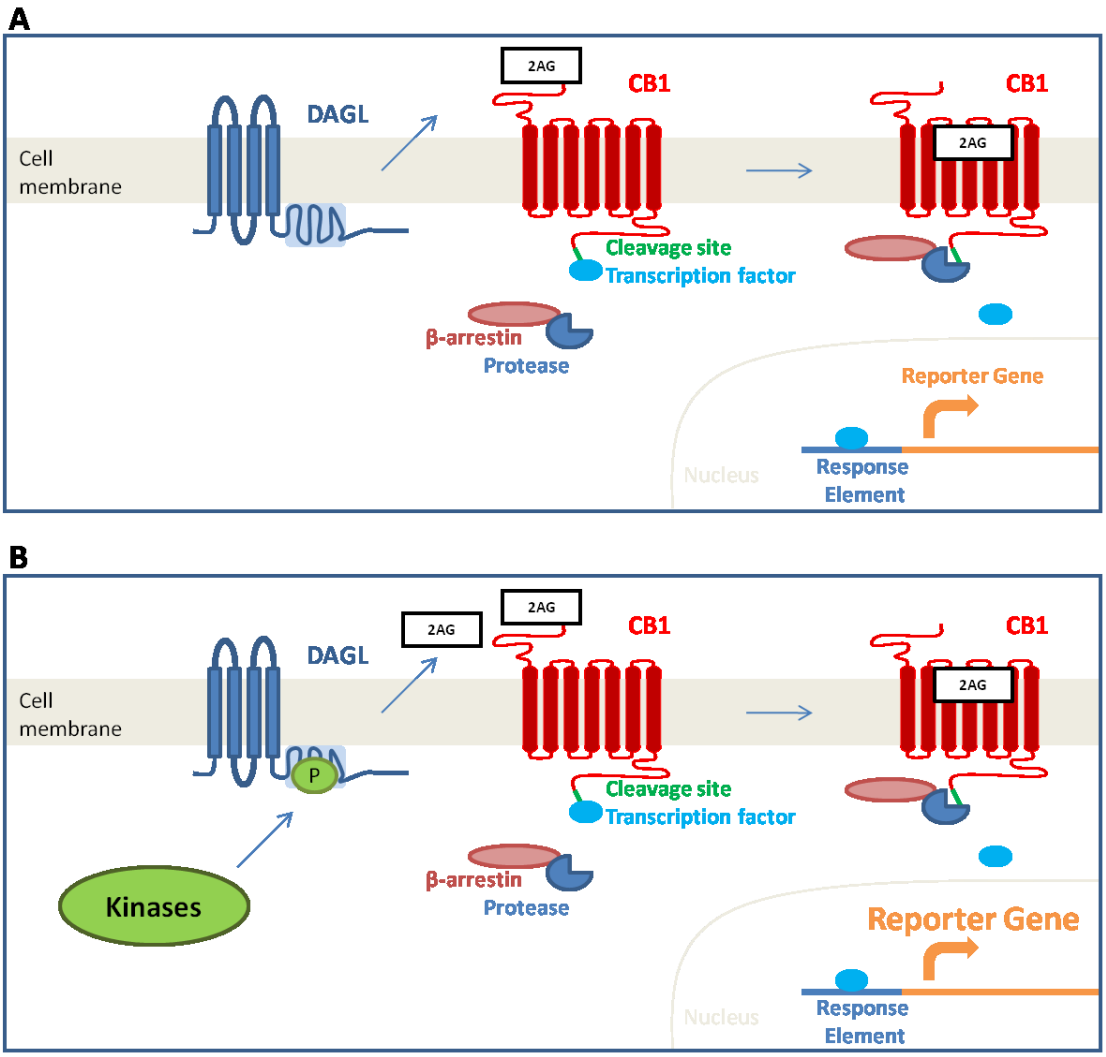

Figure 4.1. The Tango-CB1 cell-based assay monitoring CB1 activation as a potential tool to study DAGLα/β activity

2-AG produced by DAGLα/β in the Tango cell activates the recombinant CB1 receptor linked to a TEV protease site and a Gal4-VP16 transcription factor. CB1 activation results in the recruitment of TEV-protease tagged β-arrestin to the receptor. The TEV protease then cleaves the transcription factor which then binds to the UAS element upstream of a β-lactamase gene resulting in expression of this reporter gene (A). Activation of DAGLα/β activity by single or multiple kinases in response to stimuli would result in increased 2-AG levels and therefore increased CB1 activation and increased β-lactamase expression (B).

Ligand induced activation of CB1 results in the recruitment of the TEV protease tagged β-arrestin to the receptor. The TEV protease then cleaves the Gal4-VP16 transcription factor resulting in expression of the β-lactamase (reporter) gene. β-lactamase activity is then monitored using a FRET based substrate conversion assay (van der Lee et al., 2009).

In this chapter I will report on the successful adaptation of the Tango assay to monitor DAGL dependent CB1 activation. This enabled us to assess mechanisms regulating the activity of the DAGLs in a cellular context, with a primary focus on testing the hypothesis that DAGL activity is regulated by phosphorylation.

4.2 Results

4.2.1 The Tango assay can measure CB1 activation

The response of Tango cells towards a CB1 agonist ACEA was initially established as this would serve as a positive control throughout (10nM to 10μM). Preliminary experiments (conducted by others) identified optimal culture conditions that minimised non-specific background signals. In brief, Tango cells were plated onto 96-well plates and maintained overnight in the presence of 1% FCS in McCoy's 5A media. The cells were then treated for 4 hours with ACEA after which CB1 activation was measured using the β-lactamase FRET substrate. An ACEA dose dependent increase in CB1 activation was readily detected. Maximal CB1 activation was measured following 0.1-1μM ACEA treatments (Figure 4.2A). This confirmed that the cells were responsive to CB1 activation. The ability of a CB1 antagonist AM251 (10nM to 10μM) to block the ACEA (1μM) response was then confirmed. AM251 successfully prevented the ACEA response, with maximal inhibition measured using 1-10μM AM251 (Figure 4.2B). These results confirmed that the ACEA response observed in the Tango assay was CB1 specific and that the Tango assay could therefore successfully be used to measure CB1 activation.

Figure 4.2. The Tango assay can measure agonist mediated CB1 activation

Tango cells were seeded in 96-well plates and grown overnight in McCoy's 5A media 1% FCS. The cells were then treated for 4 hours with ACEA, AM251 or ACEA + AM251. CB1 activation was measured using the β-lactamase FRET substrate as a ratio of the fluorescence of the product (excitation 409 nm, emission 460 nm) and the FRET signal of the intact substrate (excitation 409 nm, emission 530 nm).

(A) Dose-response curve for ACEA in the Tango assay following 4 hour treatment of the Tango cells with the CB1 agonist ACEA (10nM to 10μM). Increased CB1 activation was observed with increasing concentrations of ACEA, maximal activation occurring between 0.1-1μM. (mean of 4 wells ±SEM)

(B) The CB1 antagonist AM251 blocks the ACEA response (1μM) in the Tango assay. Tango cells were treated for 4 hours with 1μM ACEA and increasing concentrations of AM251 (10nM to 10μM). AM251 concentration dependent inhibition of CB1 activation was observed, maximal inhibition was observed between (1μM to 10μM). This confirmed that the ACEA response detected in the Tango assay was CB1 specific (mean of 4 wells ±SEM).

A

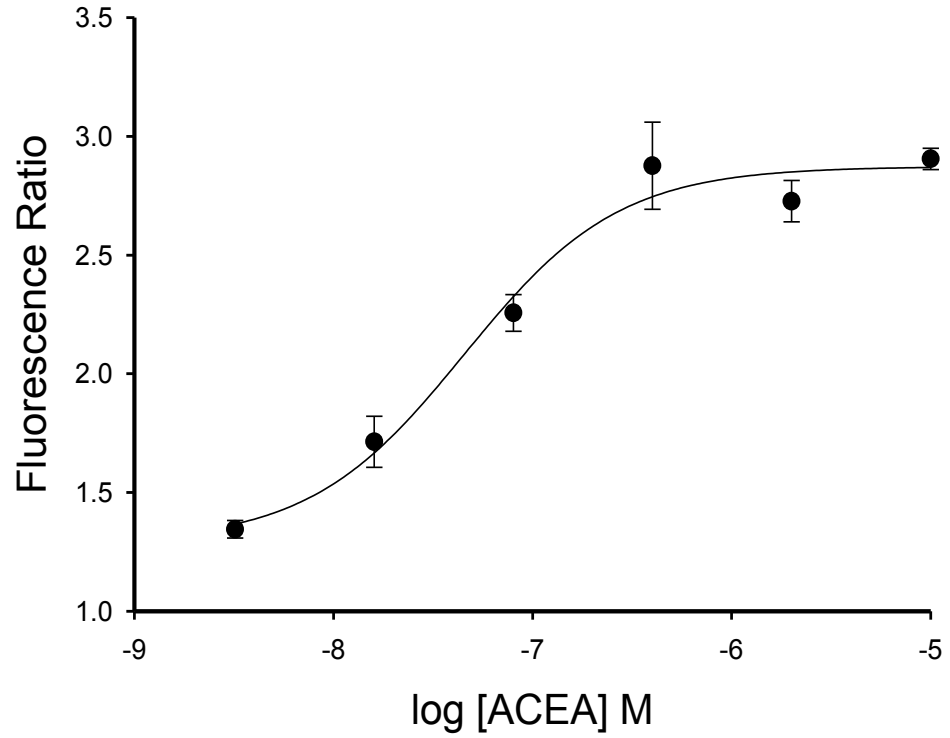
Fluorescence Ratio
3.5
3.0
2.5
2.0
1.5
1.0
-9
-8
-7
-6
-5
log [ACEA] M

B

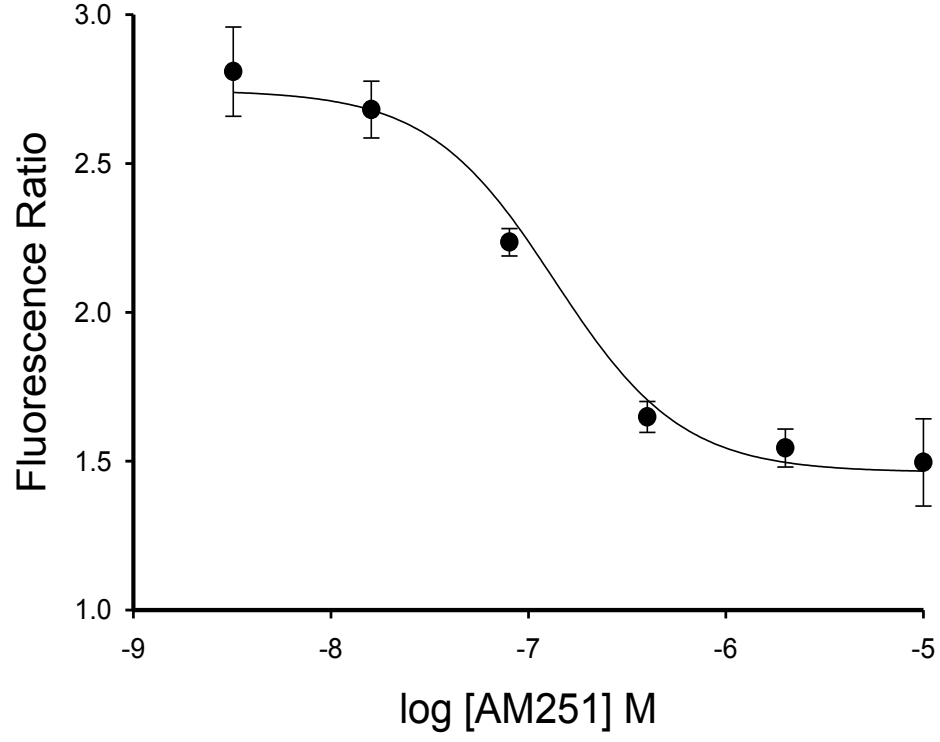
Fluorescence Ratio
3.0
2.5
2.0
1.5
1.0
-9
-8
-7
-6
-5
log [AM251] M

4.2.2 A basal eCB tone is detected in the Tango cells using the Tango assay

In order to determine if there was any basal endogenous eCB signalling in Tango cells cultured in the above conditions, cells were plated out and maintained in 1% FCS containing media as described above and then treated with the CB1 antagonist AM251 (5μM) for 4 hours. Results pooled from 6 independent experiments showed that this resulted in a relatively small negative response (~5% of the maximal ACEA response) indicating a low basal eCB tone (Figure 4.3). We next determined the effect of a dual MAGL and FAAH inhibitor JZL195 (100nM) in this model.

This compound stimulated a small but highly significant activation of the CB1 receptor; importantly this response was completely blocked by 5μM AM251 (Figure 4.3). This suggests that the Tango cells have a low basal turnover of an eCB, the activity of which is limited by MAGL and/or FAHH.

Having detected an eCB tone in the Tango cells using the Tango assay, Western blotting analysis was next used to check whether the Tango cells expressed 2-AG metabolising enzymes. Tango cell lysates were analysed by Western blotting using antibodies for the major 2-AG synthesising enzymes DAGLα and DAGLβ as well as the 2-AG hydrolysing enzymes MAGL and FAAH (Figure 4.4). Lysates obtained from the mouse neuronal stem cell line Cor1 were included as we have previously reported expression of these enzymes in this cell line (Goncalves et al., 2008). Firstly, DAGLα (115kDa) expression was detected in the Tango cells, albeit at lower levels than Cor1. A band potentially corresponding to DAGLβ (human) was also detected in the Tango lysates although the band was resolved at a lower molecular weight than the mouse DAGLβ detected in the Cor1 lysates, even though they share similar molecular weights (74kDa). However, a recombinant tagged (V5) version of human DAGLβ is also resolved at a lower molecular weight than mouse DAGLβ-V5 (Figure 4.10E) indicating that the band (~75kDa) detected in the Tango lysates is specific. These results indicate that DAGLα/β are expressed in the Tango cells and may therefore be responsible for the basal eCB tone detected in the Tango assay.

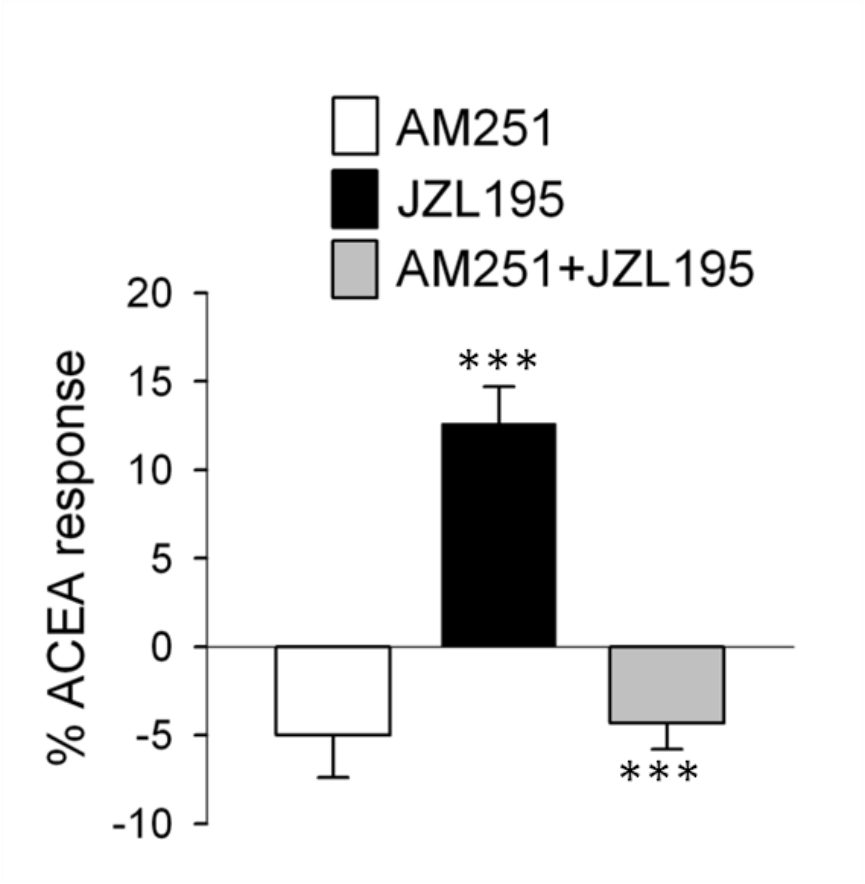

Figure 4.3. A basal eCB tone is detected in the Tango cells

Tango cells were seeded in 96-well plates and grown overnight in McCoy's 5A media supplemented with 1% FCS. The cells were then treated for 4 hours with various drugs as indicated and then CB1 activation was measured (generally in 6-8 replicate wells for each independent experiment) using the β-lactamase FRET substrate as a ratio of the fluorescence of the product (excitation 409 nm, emission 460 nm) and the FRET signal of the intact substrate (excitation 409 nm, emission 530 nm). Results are presented as a percentage of the maximal CB1 activation achieved using the CB1 agonist ACEA (1μM). (CB1 activation following treatment with 5μM AM251 n=6±SEM, 100nM JZL195 n=13±SEM, and both JZL195 and AM251 n=6±SEM are presented above). In each instance, n=the number of independent experiments. *** $p < 0.001$ (two tailed t-test) comparing AM251 to JZL195 and JZL195 to AM251+JZL195.

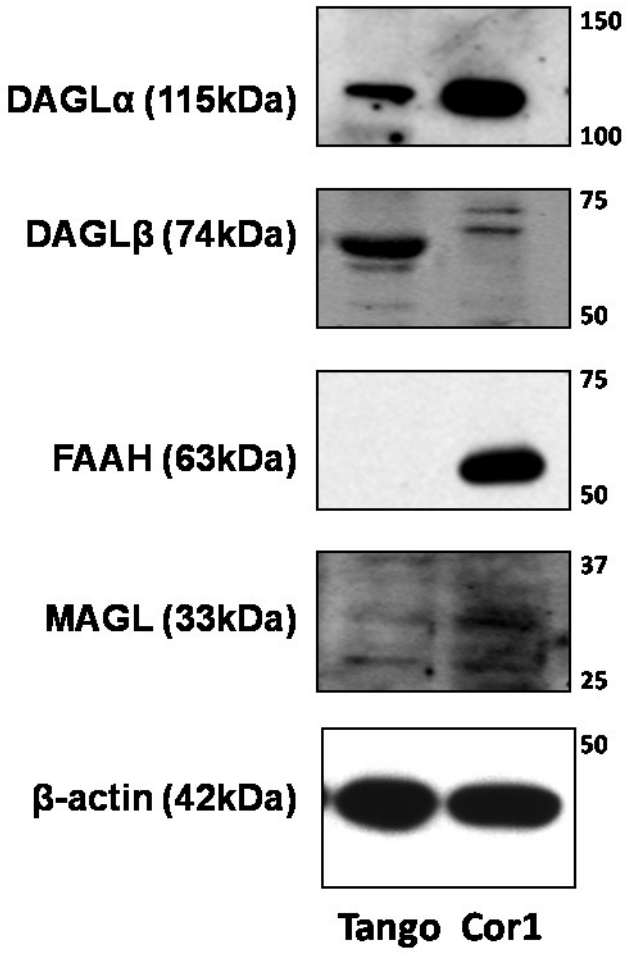

Figure 4.4. The Tango cells express 2-AG metabolising enzymes

20µg of lysates from Tango and Cor1 cells were analysed by Western blotting using DAGLα, DAGLβ, MAGL, and FAAH antibodies. The specificity of the DAGL antibodies has been established using samples from DAGL knockout animals (not shown). β-actin was also detected as a loading control. Cor1 lysate was included as a positive control.

We also detected expression of the 2-AG hydrolysing enzyme FAAH in the Cor1 cell lysates, however no FAAH (63kDa) was detected in the Tango lysates. Finally, a faint band at approximately the right size (~33kDa) was detected for MAGL in both the Tango and Cor1 lysates. Therefore MAGL is likely to limit the basal eCB signalling in the Tango cells, suggesting that 2-AG is the probable eCB responsible for this. In further experiments, JZL195 was included in all the treatments to prevent 2-AG hydrolysis.

4.2.3 Calcium stimulated DAGLα/β activity detected using the Tango assay

Treating cells with the calcium ionophore ionomycin increases 2-AG levels, in a DAGL dependent manner, in COS-7 cells (Bisogno et al., 2003). Furthermore, calcium influx in the post-synaptic cell is responsible for increased 2-AG signalling at the synapse (Hashimotodani et al., 2007a). We therefore tested the effects of ionomycin in the Tango assay. We treated the Tango cells grown in McCoy's media 1% FCS for 4 hours with different concentrations of ionomycin before measuring β-lactamase activity. Increasing concentrations of ionomycin (0.25 to 2μM) caused an increase in activity from ~10 to ~80% of the response stimulated by a maximally active concentration of ACEA (Figure 4.5).

In order to test whether the ionomycin response reflected DAGL-dependent CB1 signalling, Tango cells were treated with ionomycin (2μM) in the presence or absence of the standard CB1 antagonist (AM251) or THL (10μM) or OMDM-188 (2μM); two independent DAGL inhibitors. AM251 and the DAGL inhibitors fully blocked the ionomycin response (Figure 4.6). Importantly, THL and OMDM-188 did not have a significant effect on the ACEA response (95.8 ± 3.1% and 88.2 ± 2.1% of the maximal ACEA response, n=5), confirming that their effects were upstream of the CB1 receptor. Collectively these results implicate DAGLα/β activity in the ionomycin stimulated CB1 receptor activation. In order to confirm that the effects of ionomycin on DAGL activity were calcium mediated, we next tested the effects of exogenous calcium in the Tango assay.

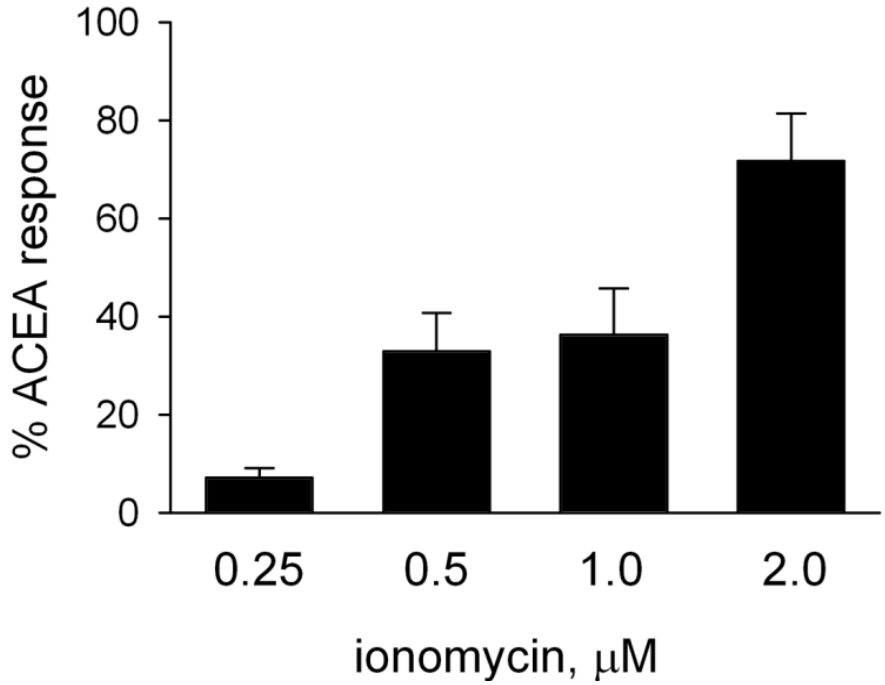

Figure 4.5. Ionomycin treatment of Tango cells activates CB1 in the Tango assay

Tango cells were seeded in 96-well plates and maintained overnight in McCoy's media supplemented with 1% FCS. The cells were then treated with different concentrations of ionomycin for 4 hours as indicated, in the presence of 100nM JZL195 to prevent 2-AG hydrolysis. CB1 activation was then measured using the β-lactamase-assay as previously described. Results are presented as a percentage of the maximal CB1 activation achieved using the CB1 agonist ACEA (1μM) (n=4-7 independent experiments and shown as the mean ±SEM).

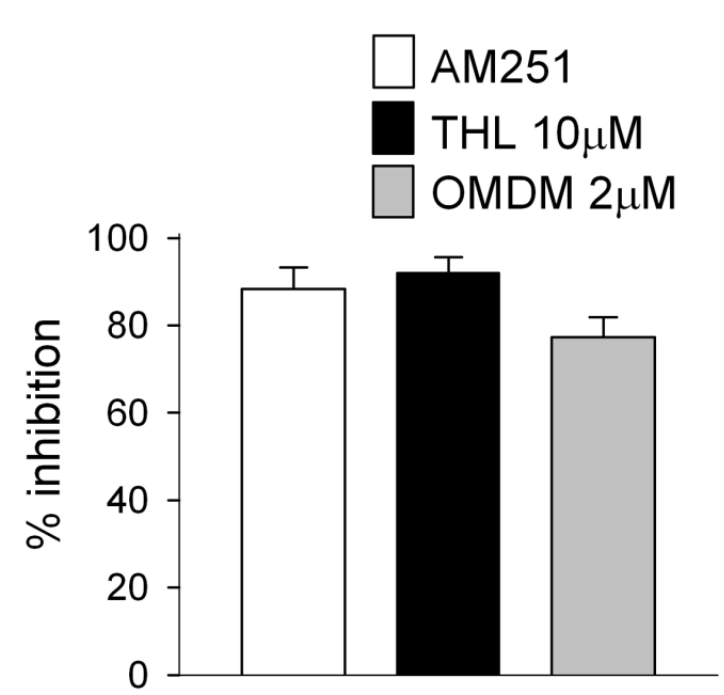

Figure 4.6. Ionomycin mediated CB1 activation in the Tango assay is DAGL dependent

Tango cells were seeded in 96-well plates and maintained overnight in McCoy's 5A media supplemented with 1% FCS. The cells were then treated with ionomycin (2μM) for 4 hours in the presence or absence of either AM251 (5μM), THL (10μM) or OMDM-188 (2μM). 100nM JZL195 was included in all the treatments to block 2-AG hydrolysis. CB1 activation was then measured using the β-lactamase-assay as previously described. Results are presented as a percentage inhibition of the ionomycin response (n=3-5 independent experiments and are shown as the mean ±SEM).

Tango cells were maintained overnight in a calcium and serum free media recommended for Tango cells (called Freestyle media) and then treated with 2mM $CaCl_2$ overnight. An increase in β-lactamase activity was apparent in the cultures treated with calcium containing media relative to control media, and this was a substantial response as it was ~70% of that seen with a maximally active concentration of ACEA (Figure 4.7). The $CaCl_2$ response was fully blocked by AM251 (5μM), confirming that it was CB1 receptor dependent and by THL (10μM) and RHC-80267 (10μM) demonstrating that it was DAGL dependent (Figure 4.7). A possible mechanism by which calcium could stimulate DAGL activity is phosphorylation. Increased calcium concentrations within the cell may activate single or multiple kinases that could directly or indirectly activate the DAGLs. As discussed in chapter 3, several phospho-sites have been identified in the DAGL sequences and some of these sites are well placed to activate the enzymes. Two of the kinases predicted to phosphorylate the DAGLs at these sites are PKA and PKC, both these kinases can be activated by calcium (Steinberg, 2008; Dunn et al., 2009). Pharmacological activators (Castagna et al., 1982; de Souza et al., 1983) and inhibitors (Chijiwa et al., 1990; Martiny-Baron et al., 1993) are also commercially available for these kinases. We therefore decided to test whether calcium mediated DAGL activation in the Tango assay was PKA and/or PKC dependent.

4.2.4 PKA and PKC mediated DAGLα/β activation in the Tango assay

In order to assess whether PKA or PKC played a role in the calcium dependent DAGL activation measured in the Tango assay, Tango cells (maintained in the absence of calcium and serum) were treated with $CaCl_2$ (2mM overnight) in the presence or absence of either the PKA inhibitor H89 (5μM) or the PKC inhibitor Go6976 (5μM). Both inhibitors largely blocked $CaCl_2$ dependent CB1 activation in the Tango assay (Figure 4.7) but did not have a significant effect on CB1 activation by the CB1 agonist ACEA (88.9 ± 6.6% and 110.6 ± 4.8% of the maximal ACEA response, n=3). This indicated that the calcium stimulated DAGL activity measured in the Tango assay was also PKA and PKC dependent.

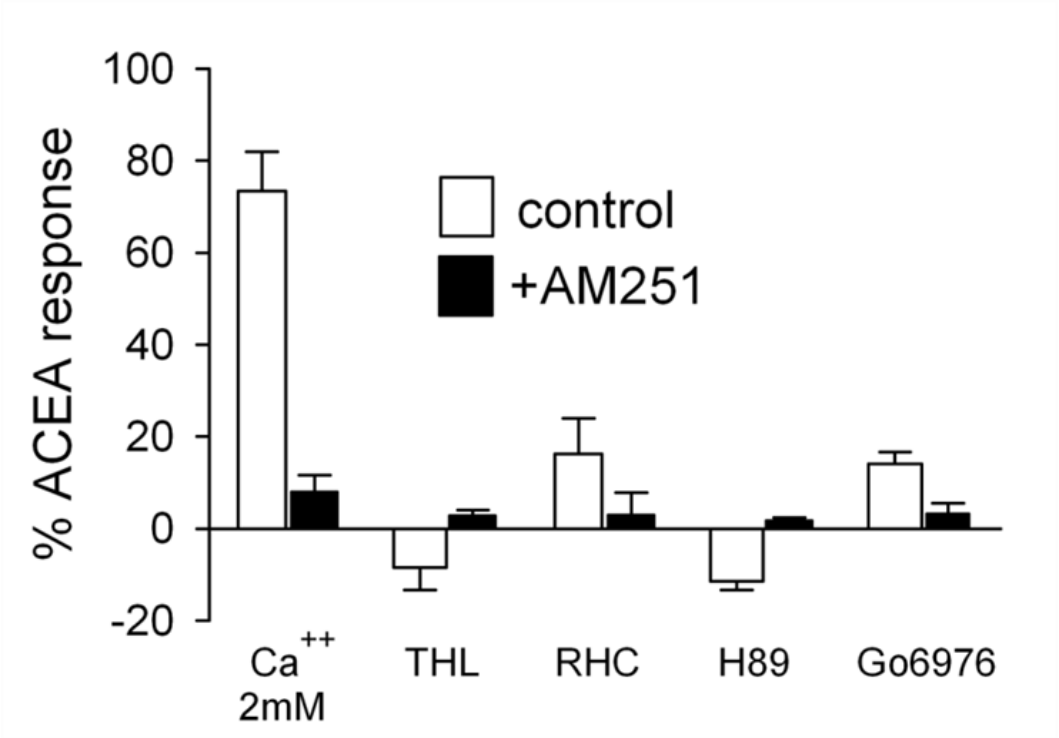

Figure 4.7. Calcium stimulated CB1 activation in the Tango assay is DAGL, PKA and PKC dependent

Tango cells were seeded in 96-well plates and grown overnight in the suppliers Freestyle media (see methods). The cells were then treated with $CaCl_2$ (2mM) overnight in the presence or absence of either the CB1 antagonist AM251 (5μM), the DAGL inhibitors THL (10μM) or RHC-80267 (10μM), the PKA inhibitor H89 (5μM) or the PKC inhibitor Go6976 (5μM). 100nM JZL195 was included in all the treatments to block 2-AG hydrolysis. CB1 activation was then measured using the β-lactamase-assay. Results are presented as a percentage of the maximal CB1 activation achieved using the CB1 agonist ACEA (1μM) in the assay (n=3 independent experiments and results show mean ±SEM).

We next tested the effects of PKA and PKC activators in the Tango assay. Tango cells were grown overnight in Freestyle media in the absence of added calcium or serum. The cells were then treated overnight with either the PKA activator forskolin (10μM) or the PKC activator PMA (25nM) in the presence or absence of either the CB1 antagonist AM251 (5μM) or the DAGL inhibitor THL (10μM). Both PKA and PKC activators stimulated a substantial β-lacatamase response that was ~50% of the maximal ACEA response (Figure 4.8). The effects of both activators were blocked by the CB1 antagonist AM251 confirming that it reflected CB1 receptor activation (Figure 4.8). Similarly the effects of both activators were also blocked by the DAGL inhibitor THL confirming that they were also DAGL dependent (Figure 4.8). These results demonstrate that PKA and PKC can activate DAGL-dependent eCB signalling in the Tango cells. Additionally, calcium stimulated DAGL activation in the Tango cells is dependent on PKA and PKC.

Collectively, the pharmacological studies above support the following model. Ionomycin, $CaCl_2$ and other pharmacological tools can activate PKA and PKC which in turn can activate DAGLα/β in the Tango cells. The activated DAGLs increase cellular 2-AG levels that results in an increase in CB1 activation which is detected in the Tango assay. The results above lead us to the next set of questions. Firstly, which DAGL is responsible for the PKA/PKC stimulated activity in the Tango assay, is it DAGLα, DAGLβ or indeed both? And secondly, how do PKA and PKC activate the DAGLs, is it via a direct (phosphorylation) or indirect mechanism?

In order to address these questions, a DAGLα/β gain of function approach was pursued using the Tango cells for the following reasons.

- at the time of carrying out these experiments, no inhibitors that could distinguish between DAGLα and DAGLβ were available, the potential gain of function observed in the Tango assay by expressing DAGLα or DAGLβ transgenes would enable us to study each enzyme individually.
- establishing and validating a gain of function DAGLα/β assay using the Tango cells would provide us with the 'proof of concept' that the Tango cells and assays could be used as a platform that would allow detailed structure/function studies on the DAGLs.

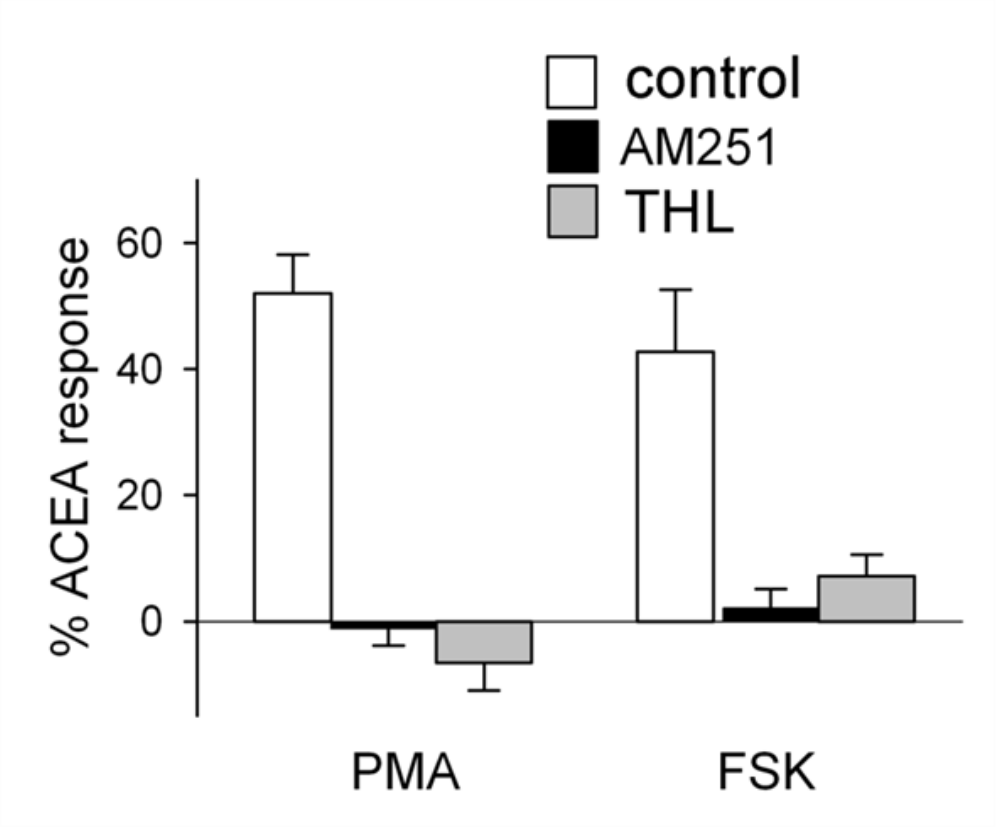

Figure 4.8. PKA and PKC activate DAGLα/β in the Tango assay

Tango cells were seeded in 96-well plates and grown overnight in Freestyle media in the absence of calcium and serum. The cells were then treated with the PKC activator PMA (25nM) or the PKA activator Forskolin (10μM) overnight in the presence or absence of either the CB1 antagonist AM251 (5μM) or the DAGL inhibitor THL (10μM). 100nM JZL195 was included in all the treatments to block 2-AG hydrolysis. CB1 activation was then measured using the β-lactamase-assay. Results are presented as a percentage of the maximal CB1 activation achieved using the CB1 agonist ACEA (1μM) in the assay (n=3 independent experiments and results show mean ±SEM).

This would enable us to test whether any of the DAGLα/β phospho-sites discussed in chapter 3 are involved in the PKA and PKC stimulated DAGL activity measured in the Tango assay.

4.2.5 Expression of DAGLα and DAGLβ transgenes in the Tango cells

In order to overexpress DAGLα/β in the Tango cells, human DAGLα and DAGLβ constructs were cloned into the vector pCDNA6.2/V5-DEST. This vector enabled expression of the DAGL transgenes with a C-terminus V5 tag and also contains an antibiotic selection gene blasticidin that is a suitable selection marker to make stable cell lines using the Tango cells. The DAGLα-V5 and DAGLβ-V5 constructs were transfected into COS-7 or Tango cells and expression was then tested by immunocytochemistry using fixed cells and Western blotting using lysates. COS-7 cells were used as a positive control as the DAGLs overexpressed in these cells are active, cause an increase in cellular 2-AG levels and localise to the membrane (Bisogno et al., 2003). Immunohistochemical analysis using a V5 antibody revealed that human DAGLα-V5 localised to the surface of both COS-7 and Tango cells (Figure 4.9A and B). Western blotting analysis using the V5 antibody confirmed that DAGLα-V5 was expressed at the predicted molecular weight (120kDa) in both of the cell types (Figure 4.9C).

Immunocytochemical studies using a V5 antibody also indicated that human DAGLβ-v5 was expressed on the surface of both COS-7 and Tango cells. However, a dense immunopositive (V5) region of staining close to the nucleus was also seen in both cell types (Figure 4.10A and B). To confirm that this was not an artefact of this specific construct, COS-7 and Tango cells were also transfected with a mouse DAGLβ-V5 construct that has been previously characterised in COS-7 cells (Bisogno et al., 2003). Immunocytochemical studies of mouse DAGLβ-V5 in the Tango and COS-7 cells using the V5 antibody revealed a similar expression profile to the human construct (Figure 4.10C and D). Expression was detected on the surface but was also concentrated in a region close to the nuclei. To ensure this was not an artefact of the V5 tag, a human DAGLβ-GFP construct was expressed in both cell types and similar results were obtained (Figure 4.11A and B).

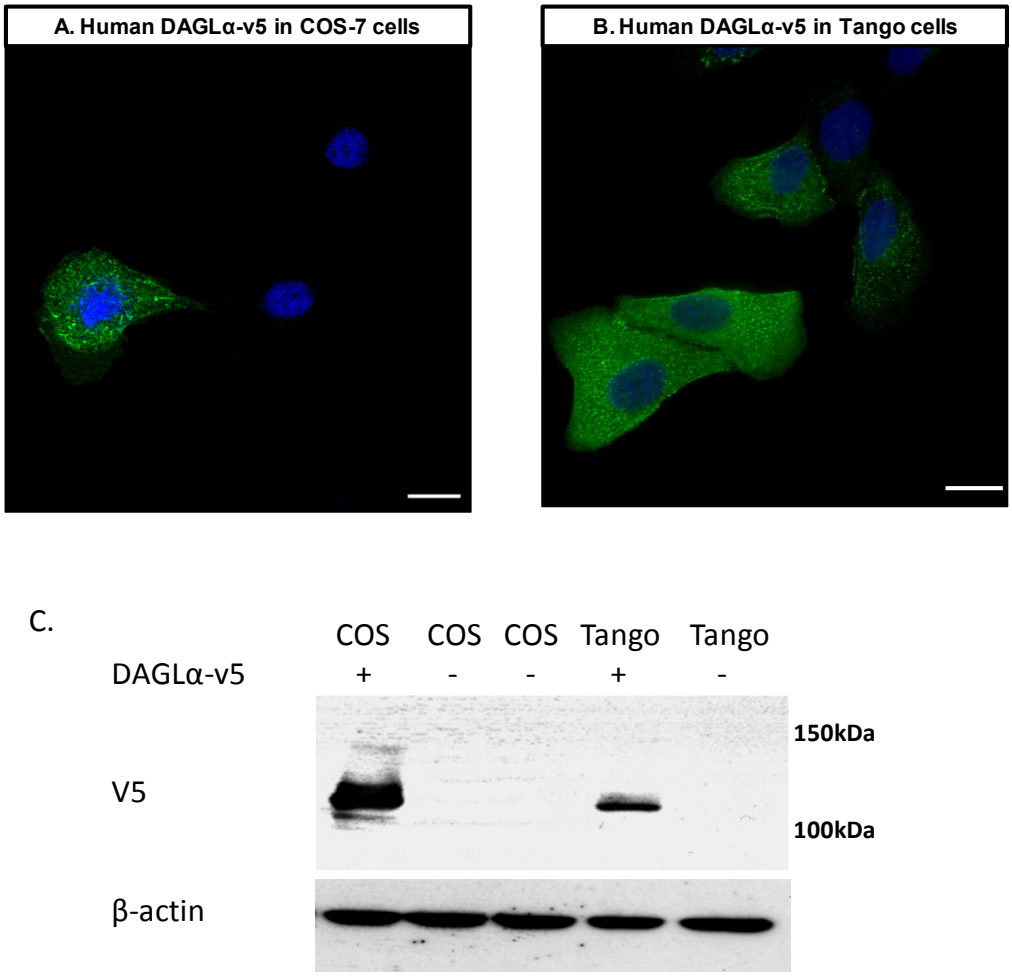

Figure 4.9. Human DAGLα-V5 is expressed at the predicted molecular weight and on the cell surface when transfected in Tango or COS-7 cells

Tango or COS-7 cells grown in 6-well plates were transfected with human DAGLα-V5 plasmid using lipofectamine 2000 and grown overnight. The transfected cells were then detached by trypsinization and seeded and grown overnight on poly-L-lysine coated coverslips or in a 10cm dish. Transfected cells grown on the coverslips were fixed and stained using a V5 antibody for immunocytochemical studies which revealed that DAGLα-V5 was expressed on the surface of both COS-7 (A) and Tango cells (B) (green - V5, blue - DAPI). The transfected cells grown in the 10cm dish were lysed and 20µg lysates were analysed by Western blotting using a V5 antibody which revealed that DAGLα-V5 is expressed at the predicted molecular weight (~120kDa) in Tango and COS-7 cells (C). Scale 20µm.

Figure 4.10. Human and mouse DAGLβ-V5 are expressed on the cell surface and in a peri-nuclear zone in both COS-7 and Tango cells

Tango or COS-7 cells grown in 6-well plates were transfected with human or mouse DAGLβ-V5 plasmid using lipofectamine 2000 and grown overnight. The transfected cells were then detached by trypsinization and seeded and grown overnight on poly-L-lysine coated coverslips or in a 10cm dish. Transfected cells grown on the coverslips were fixed and stained using a V5 antibody. Immunocytochemical studies revealed that both human and mouse DAGLβ-V5 were expressed on the surface as well as in a peri-nuclear zone in both COS-7 (A and C) and Tango cells (B and D) (green - V5, blue - DAPI). The transfected cells grown in the 10cm dish were lysed and 20µg lysates were analysed by Western blotting using a V5 antibody which revealed that both mouse and human DAGLβ-V5 are expressed close to their predicted molecular weight (~75kDa) in Tango and COS-7 cells (E). Scale 20µm.

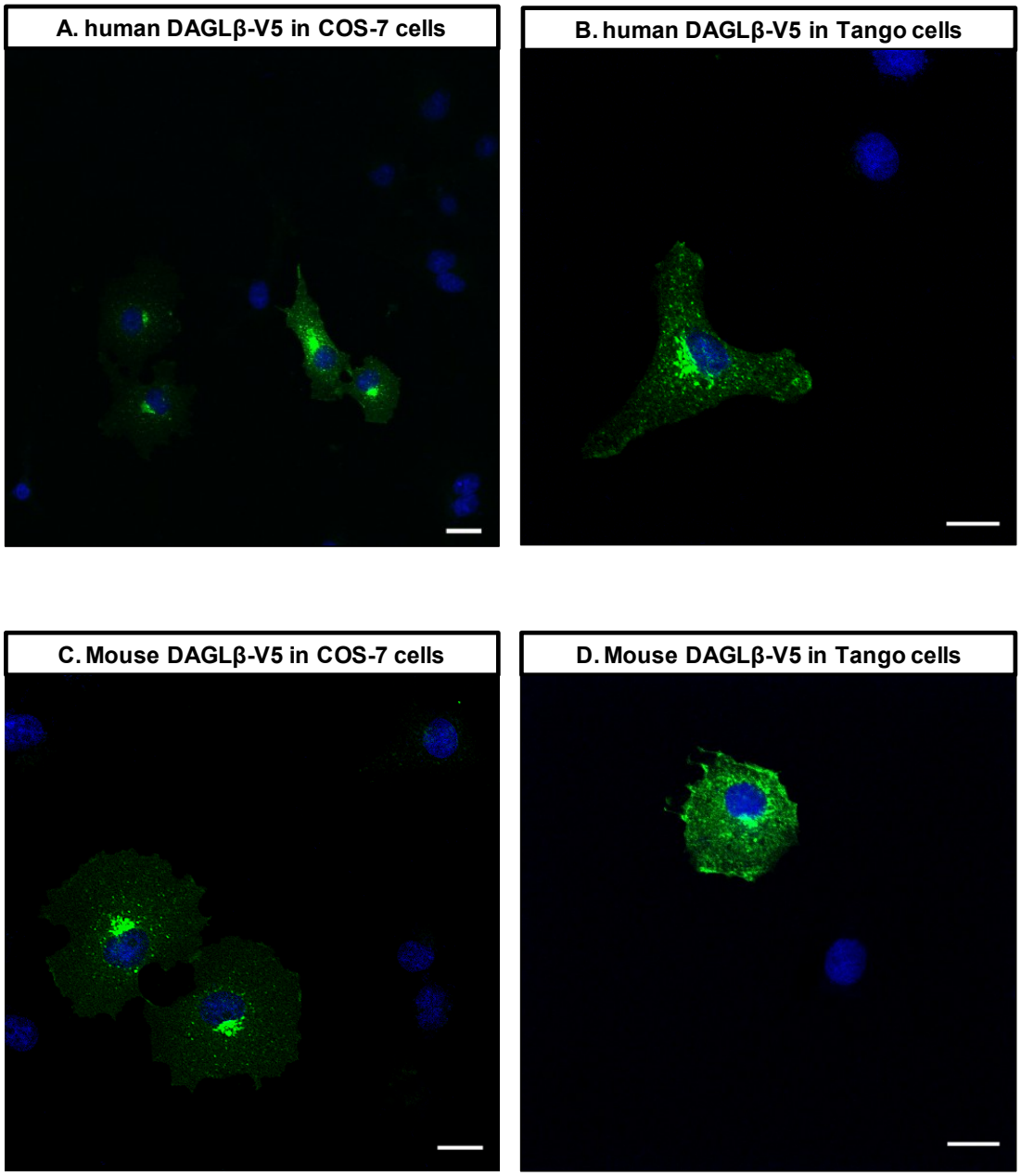
A. human DAGLβ-V5 in COS-7 cells
B. human DAGLβ-V5 in Tango cells
C. Mouse DAGLβ-V5 in COS-7 cells
D. Mouse DAGLβ-V5 in Tango cells

E

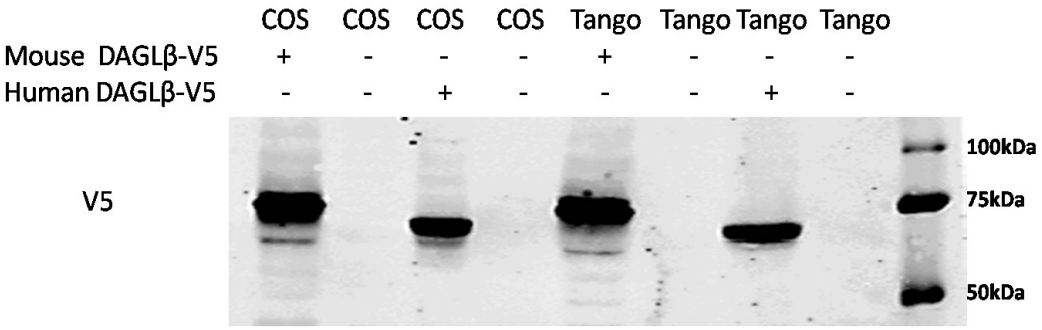
COS COS COS COS Tango Tango Tango Tango
Mouse DAGLβ-V5 + - - - + - - -
Human DAGLβ-V5 - - + - - - + -
V5
100kDa
75kDa
50kDa

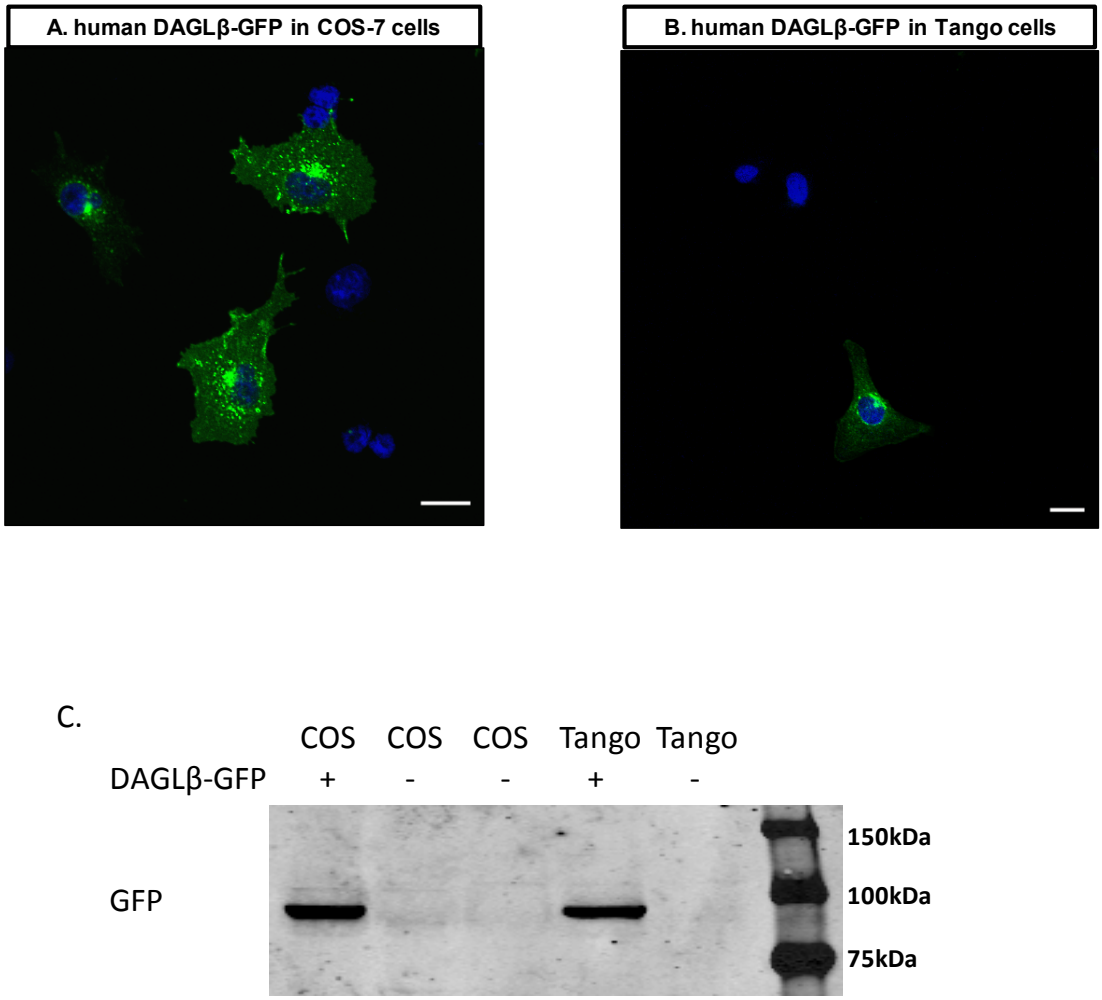

Figure 4.11. Human DAGLβ-GFP is expressed on the cell surface and in a peri-nuclear zone in both COS-7 and Tango cells

Tango or COS-7 cells grown in 6 well plates were transfected with human DAGLβ-GFP plasmid using lipofectamine 2000 and grown overnight. The transfected cells were then detached by trypsinization and seeded and grown overnight on poly-L-lysine coated coverslips or in a 10cm dish. Transfected cells grown on the coverslips were fixed and stained using a GFP antibody and used for immunocytochemical studies which revealed that human DAGLβ-GFP was expressed on the cell surface as well as in a peri-nuclear zone in both COS-7 (A) and Tango cells (B) (green - GFP, blue - DAPI). The transfected cells grown in the 10cm dish were lysed and 20µg lysates were analysed by Western blotting using a GFP antibody which revealed that human DAGLβ-GFP was expressed close to its predicted molecular weight (~100kDa) in Tango and COS-7 cells (C). Scale 20µm.

Western analysis using the V5 antibody confirmed that the human and mouse DAGLβ-V5 transgenes were expressed at a size close to their predicted molecular weights (~75kDa) in both Tango and COS-7 cells (Figure 4.10E). Similarly the DAGLβ-GFP transgene was expressed at a size close to its predicted molecular weight (~100kDa) when detected by Western blotting using a GFP antibody (Figure 4.11C).

The dense immunopositive region close to the nuclei was detected following the expression of human/mouse DAGLβ-V5 and human DAGLβ-GFP in both the Tango and COS-7 cells. This resembled immunocytochemical profiles observed in cells stained with Golgi markers (Houghton et al., 2012). In order to test whether the overexpressed DAGLβ was localised to the Golgi, COS-7 and Tango cells were transfected with the human DAGLβ-V5 plasmid. Immunocytochemical studies were then carried out using V5 and GRASP65 (a Golgi marker) antibodies. The overlap of immunopositivity using the antibodies confirmed that some of the DAGLβ expressed by the transgene (human DAGLβ-V5) co-localised with GRASP65, suggesting localisation to the Golgi (Figure 4.12).

4.2.6 Establishing cell lines stably expressing DAGLα-V5 and DAGLβ-V5

Having confirmed expression of DAGLα-V5 and DAGLβ-V5 using the pCDNA6.2/V5DEST vector by immunocytochemistry and Western blotting based on transient transfection paradigms, we used the blasticidin selection marker in these constructs to generate Tango cell lines stably expressing DAGLα-V5 or DAGLβ-V5, as described in the methods sections. The cell lines named V5α11 (stably expressing DAGLα-V5) and V5β4 (stably expressing DAGLβ-V5) were found to be clonal (after 10 passages) by immunocytochemical analyses (V5 antibody) (Figure 4.13A and B). Western blotting using lysates obtained from the V5α11 and V5β4 cell lines and a V5 antibody confirmed that DAGLα-V5 (~120kDa) and DAGLβ-V5 (~75kDa) in these cell lines were expressed at sizes close to their predicted molecular weights (Figure 4.13C and D).

Figure 4.12. Human DAGLβ-V5 colocalises with the Golgi marker GRASP65 in both Tango and COS-7 cells

Tango or COS-7 cells were grown on poly-L-lysine coverslips overnight and then transfected with human DAGLβ-V5 plasmid using lipofectamine 2000. Transfected cells were grown overnight and then fixed and stained using a V5 (green) and GRASP65 (red) antibody for immunocytochemical studies which revealed that human DAGLβ-V5 colocalised with the Golgi marker in both Tango and COS-7 cells (A). An image of an individual Tango cell demonstrating the colocalisation is also presented (B). (blue - DAPI). Scale 20μm.

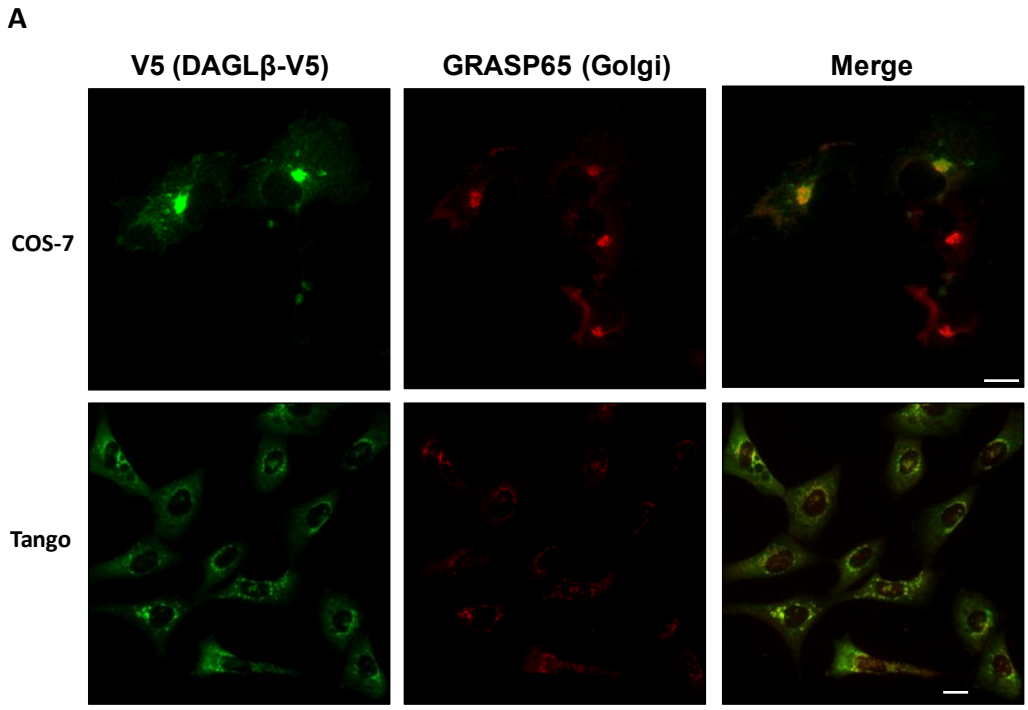
A
V5 (DAGLβ-V5)
GRASP65 (Golgi)
Merge
COS-7
Tango

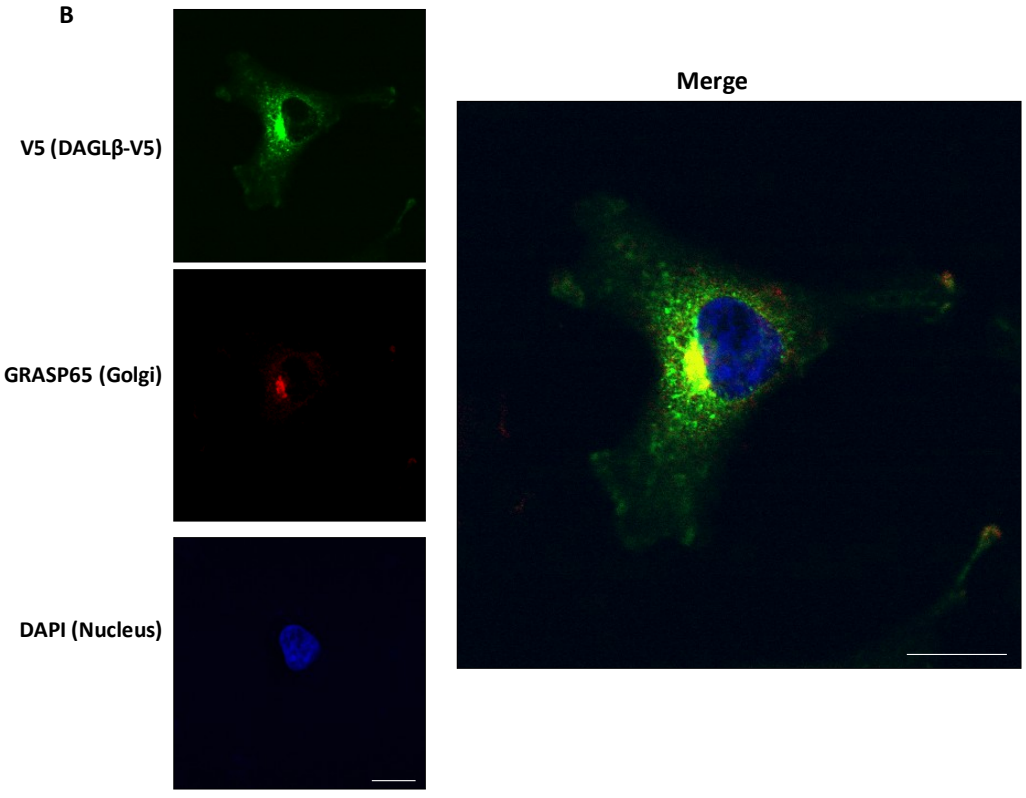
B
V5 (DAGLβ-V5)
GRASP65 (Golgi)
DAPI (Nucleus)
Merge

Figure 4.13. The cell lines V5α11 and V5β4 stably express human DAGLα-V5 and human DAGLβ-V5 respectively

Tango cells were transfected with either human DAGLα-V5 or human DAGLβ-V5 plasmids using lipofectamine 2000 and then grown in the presence of the selection marker blasticidin. Clones were selected, expanded, and screened (immunocytochemistry and Western blotting) for the stable expression of the DAGL genes. Two clones V5α11 and V5β4 were found to stably express human DAGLα-V5 and human DAGLβ-V5 respectively. Following ~10 passages V5α11 and V5β4 cells were grown on poly-L-lysine coverslips overnight and then fixed and stained. Immunocytochemical analyses were then performed using a V5 antibody which confirmed that the cell lines were clonal and that the cells expressed the genes stably, even after 10 passages (A and B) (green - V5, blue - DAPI). Parental Tango cells were used as a negative control. For Western blotting, V5α11 and V5β4 cells grown for ~10 passages were lysed and then 20μg of lysates were analysed by Western blotting using a V5 antibody. DAGLα-V5 (V5α11) and DAGLβ-V5 (V5β4) were expressed at sizes close to their predicted molecular weights (120kDa and 75kDa) in these cell lines (C and D). Lysates from parental Tango cells were used as a negative control. Scale 20μm.

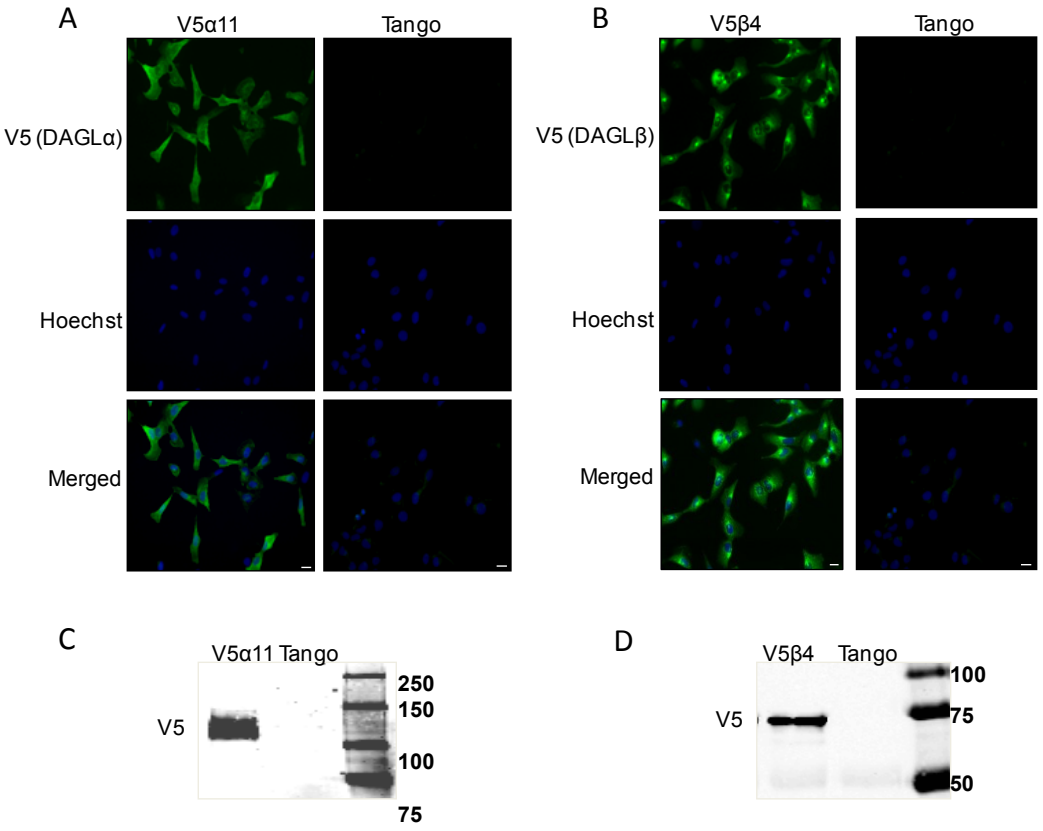
A
V5α11
Tango
V5 (DAGLα)
Hoechst
Merged
B
V5β4
Tango
V5 (DAGLβ)
Hoechst
Merged
C
V5α11 Tango
V5
250
150
100
75
D
V5β4
Tango
V5
100
75
50

In order to estimate the increase in levels of DAGLα in the V5α11 cell line relative to the parental Tango cells (endogenous DAGLα) we prepared membranes (to enrich DAGL) from both these cell lines. The DAGLs are enriched in membrane fractions as they are transmembrane proteins. 10μg of membranes were analysed by Western blotting using a DAGLα antibody. A band corresponding to endogenous DAGLα was detected in both sets of membranes (Figure 4.14A). A band at a slightly higher molecular weight than the endogenous DAGLα corresponding to DAGLα-V5 was only detected in the V5α11 membranes.

Quantification of the band intensities indicated that DAGLα expression levels were 5-fold greater in the V5α11 cells compared to the Tango cells (Figure 4.14B). This difference was predominantly due to DAGLα-V5 expression in the V5α11 cells. Similarly, membranes prepared from V5β4 and Tango cells were analysed by Western blotting using a DAGLβ antibody. Two bands close to the predicted molecular weight were detected in the Tango membranes (Figure 4.15A). It was unclear which of the two bands corresponded to endogenous DAGLβ. Similarly two bands were detected in the V5β4 membranes. The higher molecular weight band was more prominent compared to the corresponding band in the Tango membranes and was therefore identified as DAGLβ-V5 (Figure 4.15A). Quantification of the band intensities indicated that DAGLβ expression levels were either 4 or 5-fold greater in the V5β4 membranes compared to the Tango membranes, depending on whether the two putative endogenous DAGLβ bands were quantified collectively or individually (Figure 4.15B). We have therefore successfully generated clonal cell lines that appear to express DAGLα-V5 and DAGLβ-V5 at 4 to 5-fold greater levels than the endogenous genes.

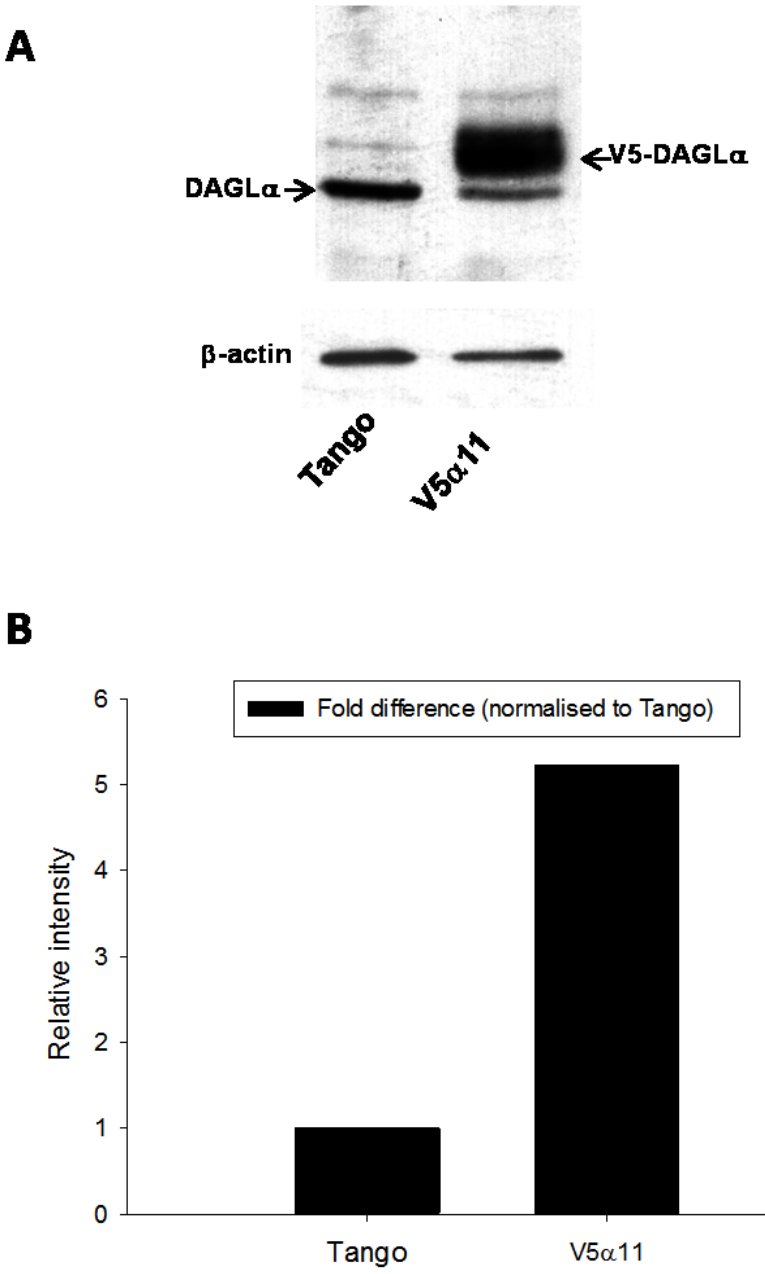

Figure 4.14. V5α11 express 5-fold more DAGLα than the parental Tango cells

Membranes (10μg) prepared from V5α11 and Tango cells were analysed by Western blotting using a DAGLα antibody that recognises an epitope present on both the endogenous and transfected enzyme (A). The intensities of the annotated bands were quantified using ImageJ. The intensity of the DAGLα bands (normalised to β-actin) detected in the V5α11 membranes relative to the DAGLα band detected in the Tango membranes is presented above (B).

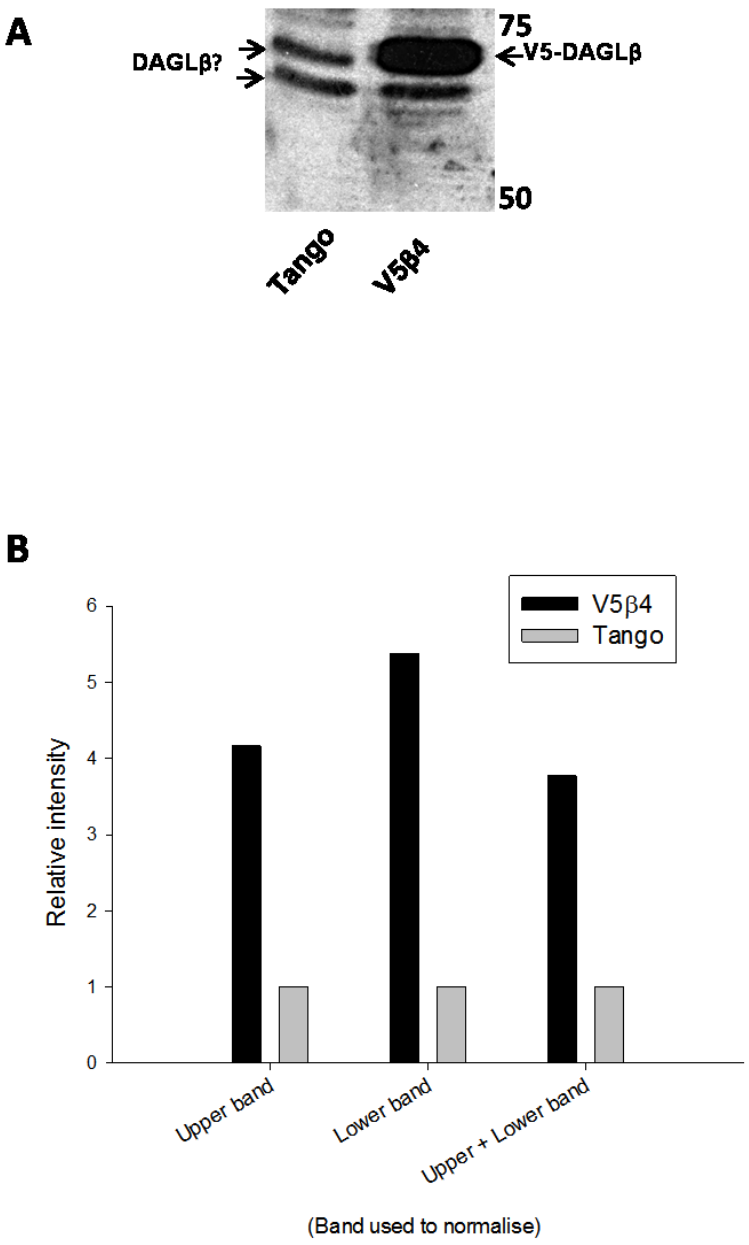

Figure 4.15. V5β4 express 4 to 5-fold more DAGLβ than the parental Tango cells

Membranes (10µg) prepared from V5β4 and Tango cells were analysed by Western blotting using a DAGLβ antibody that recognises an epitope present on both the endogenous and transfected enzyme (A). Two potential DAGLβ bands were detected at the predicted molecular weight (~73kDa). The intensities of the annotated bands were quantified using ImageJ. The intensity of the DAGLβ band(s) detected in the V5β4 membranes relative to the DAGLβ band(s) detected in the Tango membranes is presented above (B).

4.3 Discussion

The numerous reports on stimulus dependent increases in 2-AG levels and signalling in cells/tissues indicate that mechanisms to activate the major 2-AG synthesising enzymes DAGLα and DAGLβ exist (Sugiura et al., 2000a; Bisogno et al., 2003; Walter et al., 2004; Aguado et al., 2005; Sugiura et al., 2006). In the previous chapter we compiled a phospho-map of the DAGLs and proposed mechanisms by which these phospho-sites could regulate DAGL activity. In this chapter we adapted a cell based CB1 activation assay (Tango assay) (van der Lee et al., 2009) to study DAGL activation mechanisms. This assay provided a convenient 96-well microtitre assay to study DAGL-dependent CB1 signalling when compared to the traditional lower through-put mass spectrometry approaches (Bisogno et al., 2003; Jung et al., 2007; Pedicord et al., 2011; Balgoma et al., 2013).

We first confirmed that the Tango cells and assay were sensitive to a CB1 agonist and antagonist. We detected expression of DAGLα, DAGLβ, and the 2-AG hydrolysing enzyme MAGL (but not FAAH) in these cells by Western blotting analysis. Our expression data is further supported by 'The Human Protein Atlas' (www.proteinatlas.org), a project focussed on antibody-based proteomics to profile the human proteome. As part of this project mRNA analysis of several cell lines have been carried out and are publicly available at www.proteinatlas.org. In U2OS (Tango background) cells, expression of DAGLα has been classified as medium abundance, DAGLβ high, MAGL medium, and FAAH as low which agrees with our Western results.

Despite the presence of both DAGLs, there is little eCB tone in the Tango cells maintained in McCoy's media supplemented with 1% FCS. This could be due to a lack of substrate being available under these growth conditions, due to the enzymes being in a closed state that restricts substrate access to the catalytic domain, or possibly due to MAGL acting as a "gatekeeper" by hydrolysing 2-AG and thereby directly preventing CB1 receptor activation despite the presence of basal DAGL activity. Such a "gatekeeper" role has recently been identified in neurons – here MAGL is excluded from the growth cones to allow localised DAGL-dependent eCB signalling in this

compartment, but enriched in the axon to prevent this signalling (Keimpema et al., 2013). Interestingly, treatment of the Tango cells with JZL195, a potent MAGL inhibitor, led to a small but highly significant increase in β-lactamase activity that was CB1 dependent as determined by the use of AM251. This supports the hypothesis that MAGL has a general gate keeping role that extends to non-neuronal cells.

Interestingly, there was little if any evidence for an increase in eCB tone in the two cell lines that stably over express DAGLα and DAGLβ (data not shown as this was not a focus for this study). This clearly indicates that the lack of tone is not simply a consequence of low levels of enzyme expression, and again points to lack of substrate and/or the enzymes being in a closed state as a mechanism that can limit eCB signalling.

Having confirmed that the Tango cells express reasonable levels of endogenous DAGLα/β, we sought to determine if we could stimulate DAGL-dependent eCB signalling in the cells. Calcium stimulated 2-AG production has been widely reported (Bisogno et al., 2003; Aguado et al., 2005; Sugiura et al., 2006), presumably via DAGL dependent mechanisms. Here, two paradigms have been established that generate a robust DAGL-dependent CB1 response. The first involved treating cells maintained in McCoy's 1% FCS media with the calcium ionophore ionomycin for 4 hours. The second involves maintaining the cells in the manufacturers recommended Freestyle media overnight and then treating them overnight with Freestyle media supplemented with 2mM $CaCl_2$. Both resulted in very robust responses that did not fall far too short of the maximal response elicited by the CB1 agonist ACEA. We have therefore successfully adapted the Tango assay to measure a calcium stimulated DAGL-dependent eCB response.

At least 3 different mechanisms, individually or collectively could be responsible for the calcium stimulated DAGLα/β-dependent CB1 response in the Tango cells. Firstly, calcium mediated mechanisms could cause an increase in substrate (DAG) levels resulting in increased DAGL activity. This could potentially be mediated by the activation of a PLC enzyme in the cells (Gresset et al., 2010). However, we have as yet been unable to block the

response with a general PLC inhibitor (Emma Williams, unpublished observation).

Secondly, calcium could directly (or via calmodulin) interact with and activate the DAGLs as has been observed for other proteins (Rellos et al., 2010). The evidence for this is not clear. Calcium stimulated DAGL activity *in vitro* was observed with purified DAGL (activity) from some endogenous sources like bovine aorta (Lee and Severson, 1994) but not others like human platelets (Moriyama et al., 1999), brain plasma membrane (Farooqui et al., 1986), and brain microsomes (Rosenberger et al., 2007). Two separate studies using membranes overexpressing the DAGLs and synthetic DAG (as the substrate) in biochemical assays have shown an ~2-fold increase in DAGL activity in the presence of $CaCl_2$ (Bisogno et al., 2003; Pedicord et al., 2011). In the first study, Bisogno et al. observed significant increases in activity (~20% to 100%) at high (0.1 to 10mM) but not low (1 to 10μM) concentrations of $CaCl_2$. In the second study, Pedicord et al. observed ~2-fold increase in activity using high (5mM) concentrations of $CaCl_2$. Collectively, these results indicate that $CaCl_2$ can stimulate DAGL activity *in vitro*, however, due to the high concentrations required, one cannot rule out an effect on substrate solubility rather than a direct effect on the enzymes (Lee and Severson, 1994; Rosenberger et al., 2007). Our own results on this question, presented in later chapters, do not support the hypothesis for a direct activation of DAGL activity by calcium.

Another mechanism by which calcium could (indirectly) activate the DAGLs is by phosphorylation. Calcium stimulated kinases could potentially phosphorylate and activate the DAGLs. As discussed in chapter 3, several phospho-sites have been identified in the DAGL sequences and some of these sites are well placed to activate the enzymes by potentially regulating their open and closed conformation. Out of the 9 phospho-sites that appeared to be genuine (supported by at least three published studies), 4 were predicted to be phosphorylated by PKA and PKC.

The activity of DAGL purified from bovine brain microsomes was increased 3-fold when treated with PKA *in vitro* (Rosenberger et al., 2007). Similarly, PKA

treated bovine rod membranes showed ~70% increase in DAGL activity *in vitro* (Perez Roque et al., 1998). Vellani et al. observed ~3-fold increase in 2-AG levels when treating HEK293 cells with the PKC activator PMA, this was prevented by the PKC inhibitor RO318820 (Vellani et al., 2008). They observed similar effects with the PKA activator Forskolin and PKA inhibitor RpcAMPS. These increases in 2-AG are presumably mediated by one or both of the DAGLs. Increases in 2-AG levels in glucocorticoid stimulated hypothalamic slices was also shown to be PKA dependent (Malcher-Lopes et al., 2006). Collectively these studies coupled with the phospho-map/phospho-prediction results in chapter 3 made PKA and PKC attractive kinases to study in relation to DAGL activation. Furthermore, both these kinases can be activated by calcium (Steinberg, 2008; Dunn et al., 2009). Pharmacological activators (Castagna et al., 1982; de Souza et al., 1983) and inhibitors (Chijiwa et al., 1990; Martiny-Baron et al., 1993) are also commercially available for these kinases. We therefore decided to test whether calcium mediated DAGL activation in the Tango assay was PKA and/or PKC dependent. Both PKA and PKC inhibitors blocked calcium stimulated DAGL dependent CB1 activation in the Tango assay. Furthermore, PKA and PKC activators stimulated DAGL dependent eCB signalling in this assay providing evidence that these two kinases can activate the DAGLs. It was unclear whether DAGLα, DAGLβ or for that matter both were responsible for the PKA/C stimulated activity as the Tango cells express both DAGLα and DAGLβ. No inhibitors at the time were available to distinguish between DAGLα and DAGLβ activity and so we therefore pursued a DAGLα/β gain of function approach using the Tango cells.

We successfully expressed various DAGLα/β transgenes in the Tango cells and also successfully generated clonal cell lines expressing DAGLα-V5 (V5α11) or DAGLβ-V5 (V5β4) at 4 to 5-fold higher levels than the corresponding endogenous genes. As mentioned above, this resulted in little if any increase in basal eCB tone using the V5α11 and V5β4 cells in the Tango assay compared to the parental cells (data not shown). This could indicate that the majority of the DAGL in these cell lines was in the inactive

'closed' conformation, but the alternative possibility is that substrate availability is the limiting factor.

Under stimulated conditions (e.g. ionomycin) there was some evidence for a greater CB1 response in the cells that over expressed DAGLα, however, despite several optimisation experiments (time course and dose responses of ionomycin) the window of the response remained quite small (at best 2-fold) and was deemed to be insufficient to pursue detailed gain of function studies. Current work in the lab is therefore focussing on genetically deleting the native DAGL genes in the Tango cells. This, in theory, should provide us with a more suitable platform to perform gain of function studies using the DAGLs. Ultimately, this would enable us to screen DAGL mutants in the Tango assay in order to investigate the role of the phospho-sites detailed in the DAGL phospho-maps. We would be particularly interested in identifying phospho-sites responsible for PKA and PKC stimulated DAGL activity.

An interesting observation made while evaluating expression of the DAGLβ transgene was that a significant amount of DAGLβ was localised to the Golgi. The functional significance of this is unknown. The lack of good antibodies for DAGLβ has hindered immunocytochemical studies of the endogenous enzyme and so despite the fact that Golgi localisation of DAGLβ was observed using 3 different constructs in 2 different cell lines, we cannot rule out the fact that this might be an artefact of overexpressing the enzyme. However, besides our observations, another study suggests that this warrants further investigation. SPIED is an online resource that has collated publicly available gene expression data from many different platforms. SPIED enables one to identify genes whose expression are frequently up or down-regulated in conjunction with a gene of interest (Williams, 2012). For example, using this resource we determined that DAGLα expression correlates with the expression of synaptic proteins. DAGLα is responsible for retrograde signalling at synapses in the brain (Gao et al., 2010; Tanimura et al., 2010); therefore the fact that its expression is regulated with other synaptic proteins isn't surprising. When DAGLβ was queried using SPIED, its expression was found to be regulated along with Golgi proteins indicating the Golgi localisation observed in our results maybe physiologically relevant.

Current work to isolate the Golgi from various cell types in order to test for endogenous DAGLβ expression by Western blotting is ongoing in our lab, and our very recent development of an antibody that can be used to localise endogenous human DAGLβ in cells should help us resolve this question.

In conclusion, our results show that calcium stimulated DAGL-dependent eCB signalling in Tango cells requires PKA and PKC activity, and that agents that activate these kinases can directly stimulate DAGL dependent eCB signalling. Based on the results presented that identifies regulated phospho-sites in DAGLα and DAGLβ, and the above results, we postulated that direct phosphorylation of the DAGLs by PKA or PKC regulates their activity, and go on to explore this further in the next chapter.

Chapter 5 (Results 3): Investigating DAGL activity using surrogate substrates

As discussed in the previous chapters, phosphorylation of the DAGLs is a likely mechanism to regulate the activation of these enzymes. In order to understand the mechanism behind DAGL activation it is important to be able to directly monitor their catalytic activity. *In vitro* DAGL assays have traditionally involved the use of synthetic DAG as a substrate coupled with the measurement of 2-AG as the product (Bisogno et al., 2003; Jung et al., 2007). Measuring 2-AG is no trivial task involving mass spectrometry techniques with limited throughput (Balgoma et al., 2013).

Additional tools have been developed to monitor DAGL catalytic activity. For example generic probes including fluorophosphonate (FP) linked to either biotin or rhodamine have been developed that bind to catalytically active serine hydrolases including ABHDs (Liu et al., 1999; Kidd et al., 2001; Patricelli et al., 2001). These probes have been used to screen proteomes to identify novel serine hydrolases as well as to determine the specificity of various serine hydrolase inhibitors, as inhibitor binding competes with FP binding (Blankman et al., 2007; Hoover et al., 2008). Once the probe has bound to the target, the binding can be detected and measured using SDS-PAGE methodologies including Western blotting and in-gel fluorescence, or the targets can be enriched and then detected and measured by mass spectrometry. However this tool has certain limitations. Firstly, not all serine hydrolases are well recognised by this probe, including DAGLα (Ben Cravatt, personal communication). Secondly, although binding of these probes rely on the catalytic sites of their targets being in the active conformation, it is unclear whether they are able to distinguish between lipases in their opened and closed conformations. And thirdly, the SDS-PAGE or mass spectrometry dependent detection methods involved with these probes means they have limited throughput.

At least two recent reports have detailed the development of DAGL activity assays utilising surrogate substrates. Johnston et al. have developed FRET reporter substrates, which rely on DAGL activity to relieve internal quenching

in the reporters resulting in an increase in fluorescence (Johnston et al., 2012). A commercially available fluorogenic lipase substrate (EnzChek Lipase substrate) is based on the same principle (Basu et al., 2011). Pedicord et al. on the other hand used two commercially available substrates to develop 96-well plate microtitre assays to measure DAGL activity using membranes from cells overexpressing DAGLα (Pedicord et al., 2011).

The substrates used were either the chromogenic substrate 4-Nitrophenyl butyrate (PNPB) or the fluorogenic substrate 6,8-difluoro-4-methylumbelliferyl Octanoate (DiFMUO). These assays are cost effective, high throughput tools to study DAGL catalytic activity. In this chapter I will report on the successful adaptation of these assays to not only measure DAGL activity in membranes but to also measure activity in intact living cells. In this chapter I have confirmed that these substrates can be used in assays to identify DAGL inhibitors and confirm the overexpression of DAGL in both cell membranes and living cells. However, despite developing a range of different assays (membrane/cell based using PNPB/DiFMUO to measure DAGLα/β activity) we were unable to detect changes in DAGL activity with calcium or PKA and PKC activators suggesting that these surrogate substrates are unsuitable tools to study DAGL regulation. Potential explanations are discussed, and these include the possibility that the regulatory lid does not limit access of these substrates to the catalytic domain.

5.1 Results

5.1.1 DAGL substrates

The structure of the native substrate DAG, three surrogate substrates (PNPB, DiFMUO, and EnzChek), and the products formed following hydrolysis by the DAGL enzymes are shown in Figure 5.1. PNPB is a chromogenic substrate whereas DiFMUO and EnzChek are fluorescent substrates. Details describing a human DAGLβ membrane assay using the EnzChek substrate are publicly available at Pubchem Bioassay. Human DAGLα membrane assays using PNPB and DiFMUO have been published (Pedicord et al., 2011) and both these substrates were used to develop DAGL assays in this chapter.

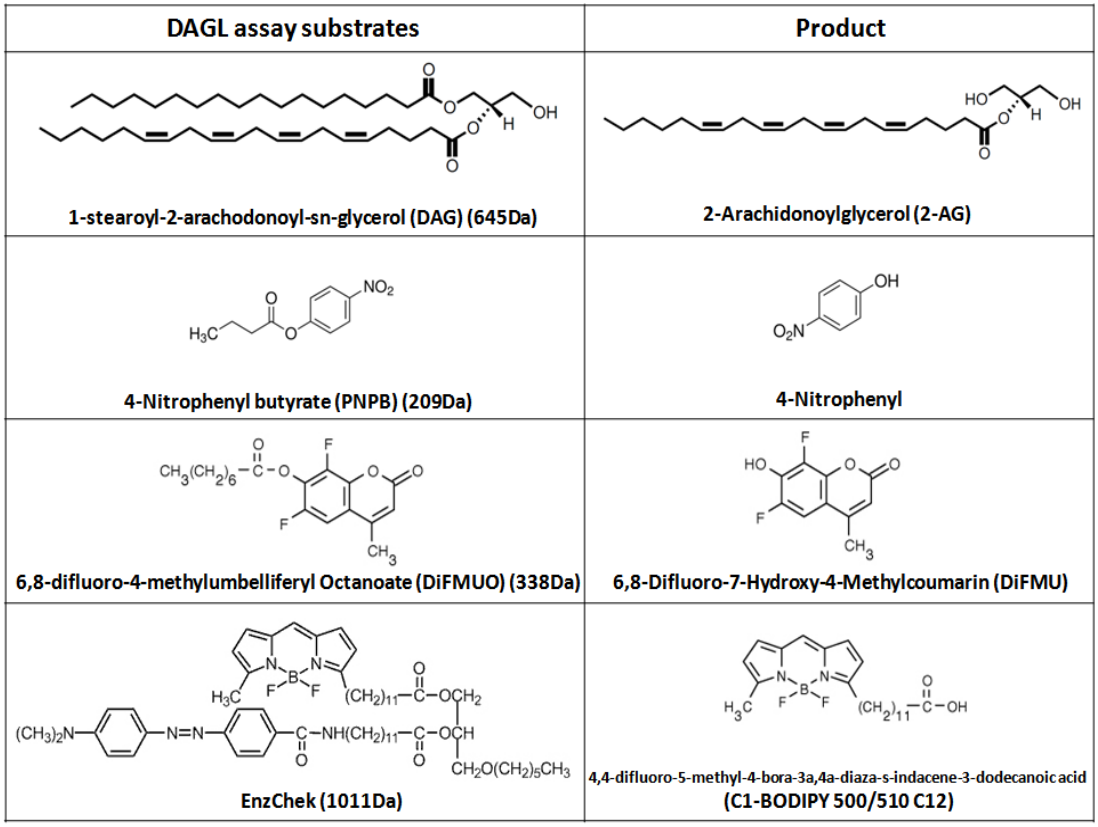

Figure 5.1. Native and surrogate DAGL substrates

The native (DAG) and surrogate (PNPB, DiFMUO, and EnzChek) substrates (molecular weights in brackets) of DAGL and the products generated following their hydrolysis by DAGL are presented above. PNPB is a chromogenic substrate, whereas DiFMUO and EnzChek are fluorogenic substrates.

5.1.2 Development of a DAGLα PNPB membrane assay

PNPB is a chromogenic substrate; its hydrolysis is measured by detecting the product 4-nitrophenyl at OD_{400}. In order to develop a DAGLα PNPB membrane assay, membranes were prepared from parental Tango and the DAGLα overexpressing V5α11 cells that had been in grown in McCoy's media supplemented with 10% FCS. Membranes were prepared by mechanically lysing the cells using a homogenizer and separating the membrane enriched fraction (pellet) from the soluble cytoplasmic proteins (supernatant) by centrifugation at 100,000g. The membrane enriched fraction was then resuspended in the membrane buffer (20mM HEPES pH 7.0, 2mM DTT) using a homogeniser and frozen in aliquots.

The activity of different concentrations of membranes was tested (1 to 50µg/ml) using 250µM PNPB as the substrate. Activity was determined by measuring the rate of product formation (ΔOD_{400}/min) over 10 minutes. Increasing activity was observed with increasing concentrations of both sets of membranes. The V5α11 membranes were more active (~6-fold) than the parental Tango membranes at all the concentrations tested (Figure 5.2A). This difference in activity is likely to be due to DAGLα as the V5α11 membranes are Tango cells overexpressing the human DAGLα-V5 transgene (~5-fold higher levels Figure 4.14). A membrane concentration of 12.5µg/ml was selected for further experiments as this was deemed to provide a good signal to background (no membranes) ratio and also provided a 6-fold window between the parental Tangos and V5α11 membranes. Additionally, the reaction progress curves for both sets of membranes at a concentration of 12.5µg/ml were found to be linear for up to 30 minutes (Figure 5.2B). Having established a suitable membrane concentration to use in the assay, activity of V5α11 and Tango membranes (12.5µg/ml) were tested with different concentrations of the PNPB substrate (125µM to 1mM) as described above. Increasing activity was observed with increasing substrate concentrations up to 500µM for both sets of membranes (Figure 5.3). Approximately 6-fold greater activity was measured between the V5α11 and the parental Tango membranes at all of the substrate concentrations tested.

Figure 5.2. Measuring DAGLα activity using the chromogenic substrate PNPB in membranes prepared from V5α11 Tango cell line or parental Tango cells

V5α11 and Tango cells were grown in McCoy's media supplemented with 10% FCS. The cells were lysed and membranes enriched as described in the methods section. The activity of different concentrations of V5α11 or Tango membranes, as indicated, were measured using PNPB (250μM) by measuring the OD_{400} every 12 seconds for 30 minutes. The reaction rates were calculated over 10 minutes and are presented above (mean of 3 wells ±SEM) (A). The OD_{400} values measured over 30 minutes using membranes at a concentration of 12.5μg/ml are also shown (B).

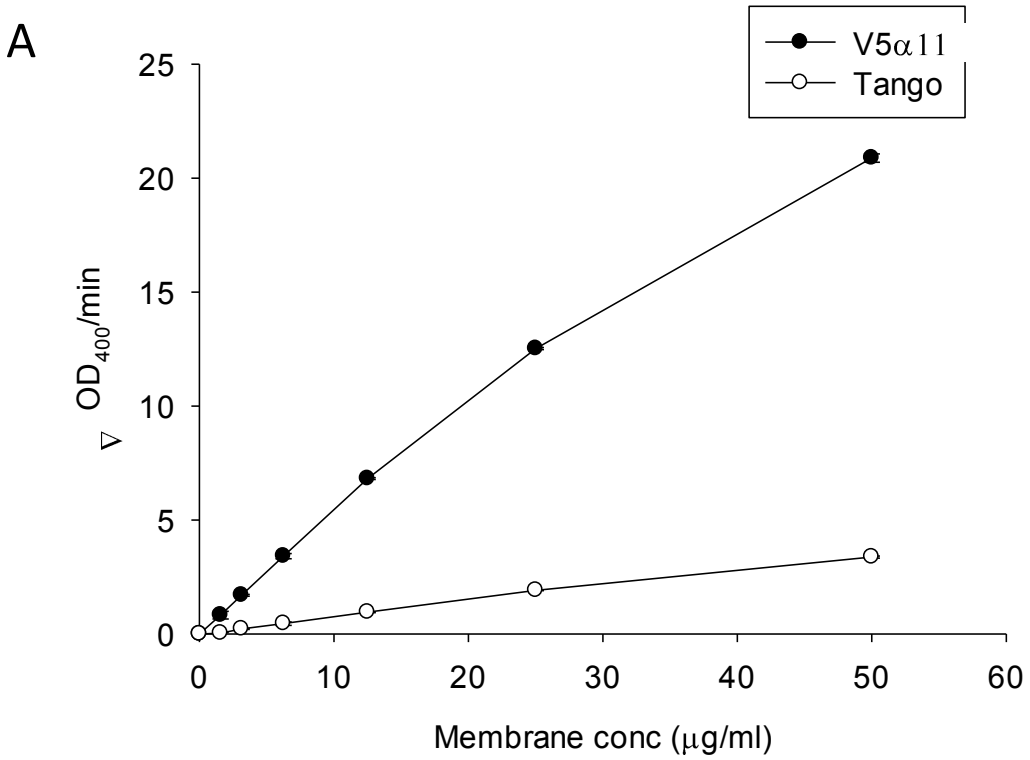
A
V5α11
Tango
25
20
15
10
5
0
V OD400/min
0
10
20
30
40
50
60
Membrane conc (μg/ml)

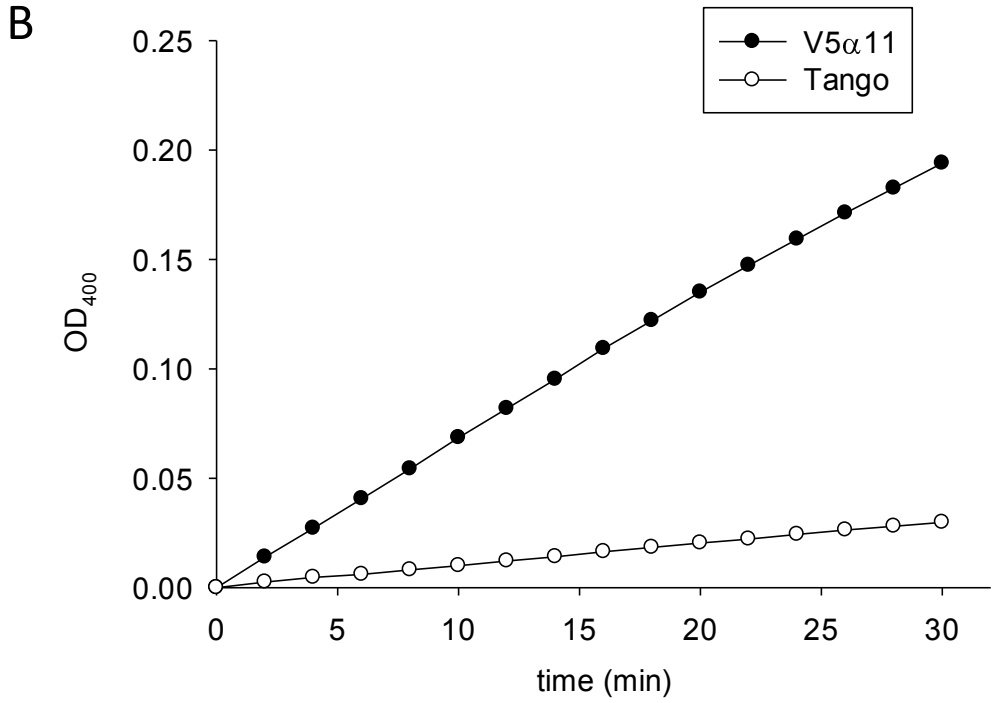
B
V5α11
Tango
0.25
0.20
0.15
0.10
0.05
0.00
OD400
0
5
10
15
20
25
30
time (min)

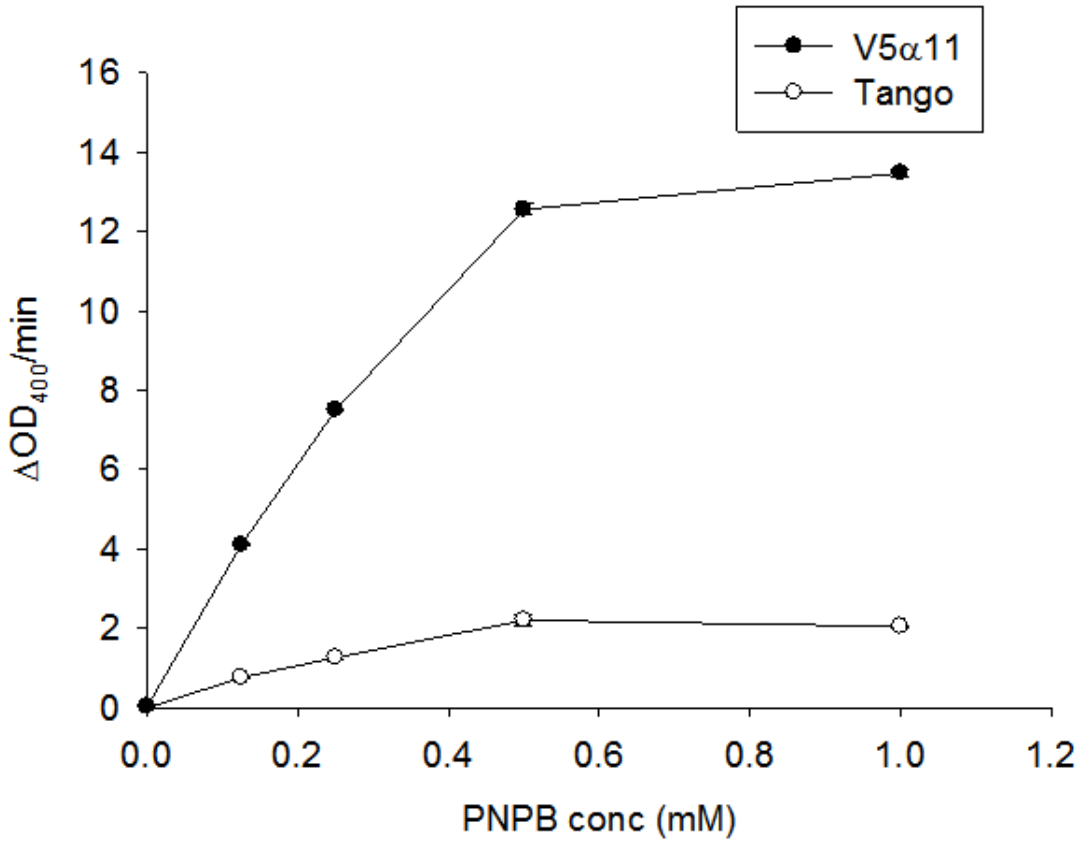

Figure 5.3. Substrate concentration response in the DAGLα PNPB membrane assay

The activity of V5α11 or Tango membranes (12.5µg/ml) prepared from cells grown in McCoy's media supplemented with 10% FCS were tested with different concentrations of PNPB as indicated. The OD_{400} was measured every 12 seconds for 30 minutes. The reaction rates were calculated over 10 minutes and are presented above (mean of 3 wells ±SEM).

Employing 500μM PNPB in the assay resulted in a higher background absorbance (in the absence of membranes) than expected (data not shown). This indicated that a concentration of 500μM was close to PNPB solubility limits which could introduce variability in the assay. Further experiments were therefore performed using 250μM PNPB as the substrate concentration, especially as this concentration provided the same signal window between V5α11 and parental Tango cells as 500μM.

The human DAGLα-V5 transgene which was stably transfected into the Tango cells was probably responsible for the difference in activity between the V5α11 and Tango membranes detected at various membrane and substrate concentrations. To verify this, cellular fractions were prepared which would enable a comparison of activity measured in the PNPB assay to DAGLα-V5 protein expression in the various fractions. In order to prepare the fractions, V5α11 and Tango cells were homogenised and then subjected to centrifugation at different speeds (1000, 19,000 and 100,000g) after which the supernatants and pellets were separated. The pellets were resuspended in membrane buffer and activities of both the supernatants and pellets (12.5μg/ml) were measured using 250μM PNPB. DAGLα-V5 protein was also detected in these fractions by Western blotting using a V5 antibody. The activity in the non-fractionated (total) homogenates obtained from the V5α11 cells was ~4-fold that of the parental Tango cells. This was surprising as we expected to see higher background (cytoplasmic) lipase activity in the total homogenates and therefore a lesser window between the activities measured in the two homogenates (Figure 5.4A). DAGLα-V5 activity was most enriched in the 19,000 and 100,000g pellets (6-fold more activity compared to the corresponding Tango fraction). Any difference in activity between the V5α11 and Tango fractions corresponded to the positive detection of DAGLα-V5 in the Western blots (Figure 5.4B). No DAGLα-V5 was detected in the V5α11 19,000 and 100,000g supernatants indicating that DAGLα-V5 was localised to the membrane.

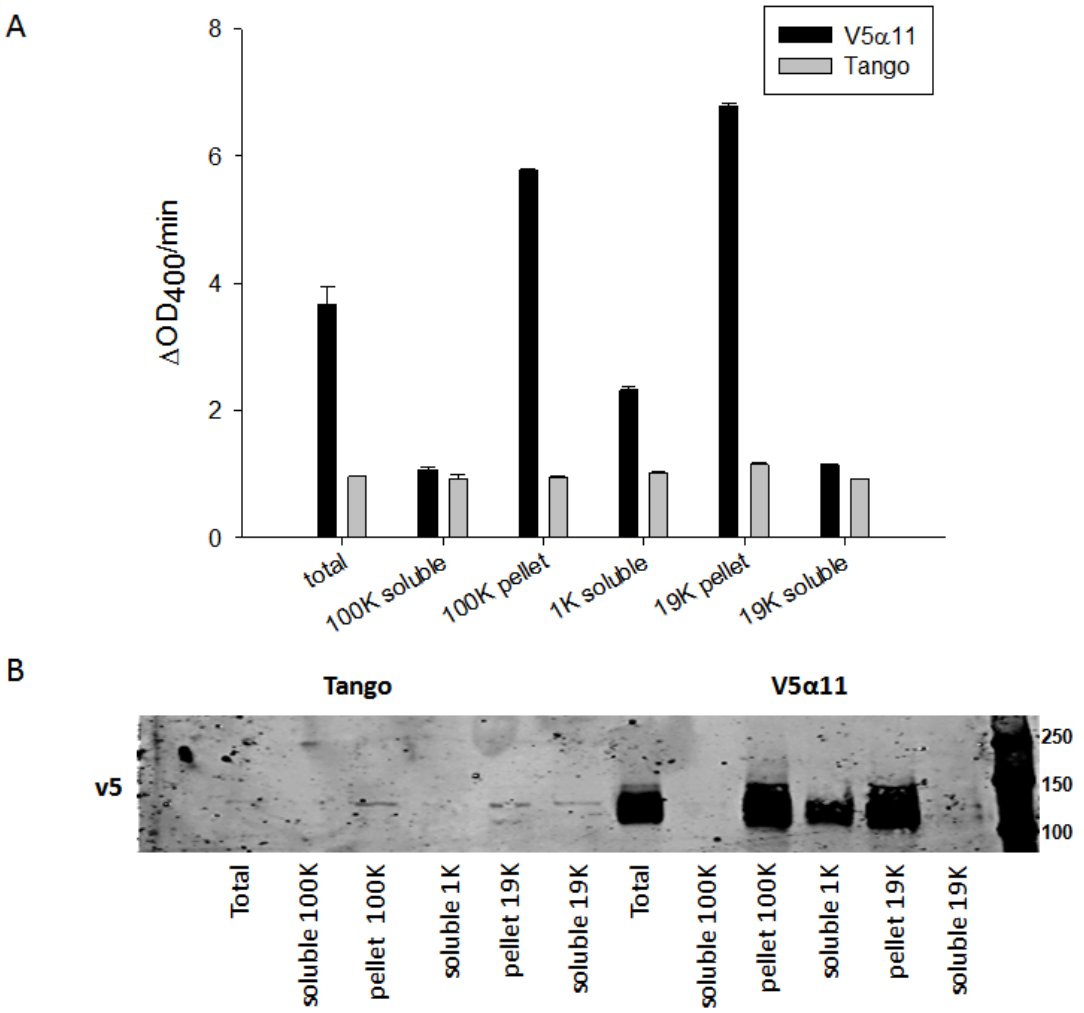

Figure 5.4. Cellular fractionation reveals high degree of specificity of PNPB as a substrate for DAGLα

V5α11 and Tango cells grown in McCoy's media supplemented with 10% FCS were homogenised and then subjected to centrifugation at different speeds (1000, 19,000 and 100,000g). Supernatants and pellets were collected, the pellets were resuspended in membrane buffer (20mM HEPES, pH 7.0, 2mM DTT), and activities of both the supernatants and pellets (12.5µg/ml) were measured using 250µM PNPB as previously described and are presented above (mean of 3 wells ±SEM) (A). DAGLα-V5 was also detected in these fractions (10µg) by Western blotting using a V5 antibody (B).

We next tested the ability of three different DAGL inhibitors to inhibit DAGL activity in the PNPB membrane assay. Membranes prepared above were pre-incubated with different concentrations of OMDM-188, RHC-80267 or THL for 5 minutes before the PNPB was added. As described above, the OD_{400} was measured over 30 minutes and the reaction rates were calculated over 10 minutes. All three inhibitors inhibited activity in the assay, albeit with different efficacies (Figure 5.5). Only a slight inhibition of activity was observed in the Tango membranes using any of the three inhibitors (~25%) suggesting that the relatively low basal activity observed in the parental Tango membranes was 'non DAGL'. Furthermore, as THL is a very general lipase inhibitor (Borgstrom, 1988; Hadvary et al., 1988), any THL insensitive activity in this assay is probably non-enzymatic. A much larger inhibition of activity was observed in the V5α11 membranes following inhibitor treatment which lowered activities to the low basal level seen with parental Tango membranes (Figure 5.5). OMDM-188 was the most potent inhibitor, showing complete inhibition at ~25 to 50nM (Figure 5.5A). THL was also relatively potent, fully inhibiting the response at 100 to 200nM (Figure 5.5A). In contrast, RHC-80267 at a concentration of 100μM was required to achieve full inhibition of the response (Figure 5.5B). The inhibitor results provided further evidence that the 6-fold higher activity observed in the V5α11 membranes was indeed DAGL activity. In further experiments, a concentration of 1μM THL was used as a control when measuring DAGLα-V5 activity.

In summary, membranes from cells that overexpressed DAGLα by ~5-fold showed a ~6 to 10-fold increase in hydrolytic activity against the PNPB substrate (Figure 5.6), this hydrolytic activity fractionated with DAGLα and was fully inhibited with three independent DAGL inhibitors. We can conclude that the assay does indeed reflect the hydrolytic activity of the DAGLα transgene.

Figure 5.5. V5α11 activity detected in the PNPB membrane assay is inhibited by three different DAGL inhibitors (OMDM-188, THL, and RHC-80267)

V5α11 and Tango membranes prepared from cells grown in McCoy's media supplemented with 10% FCS (12.5µg/ml) were incubated with different concentrations of the 3 inhibitors as indicated, for 5 minutes. Activity was then measured using 250µM PNPB as previously described and is presented above (mean of 3 wells ±SEM).

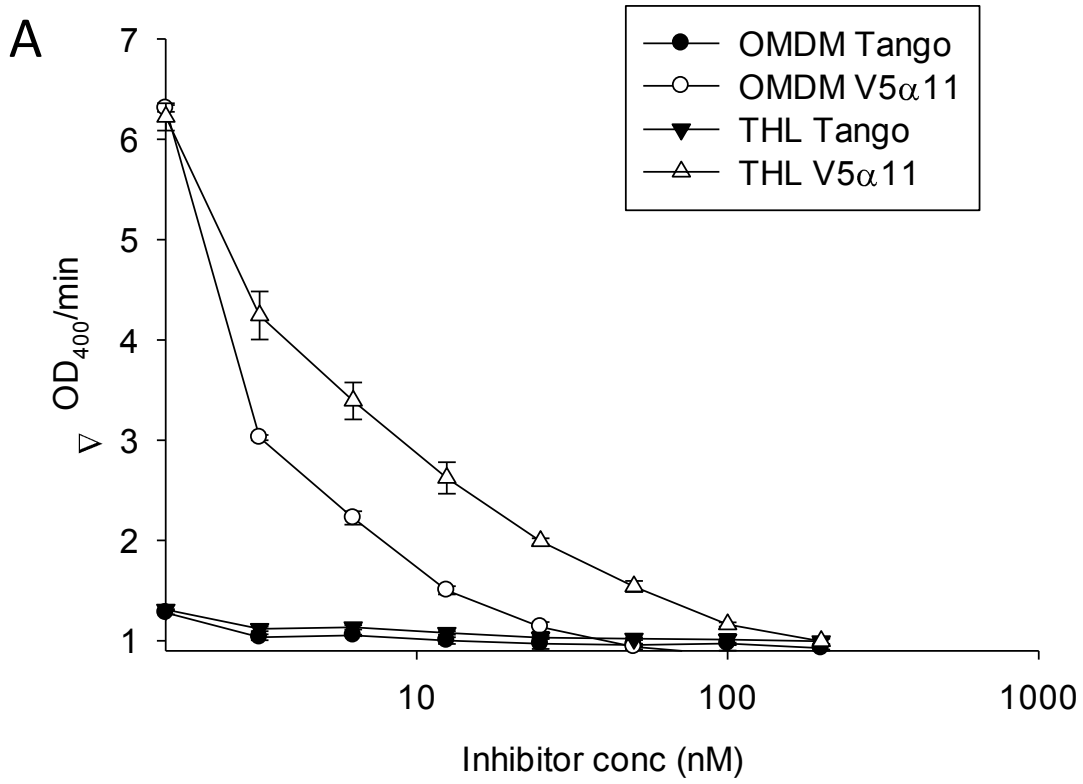
A
OMDM Tango
OMDM V5α11
THL Tango
THL V5α11
∇ OD400/min
7
6
5
4
3
2
1
10
100
1000
Inhibitor conc (nM)

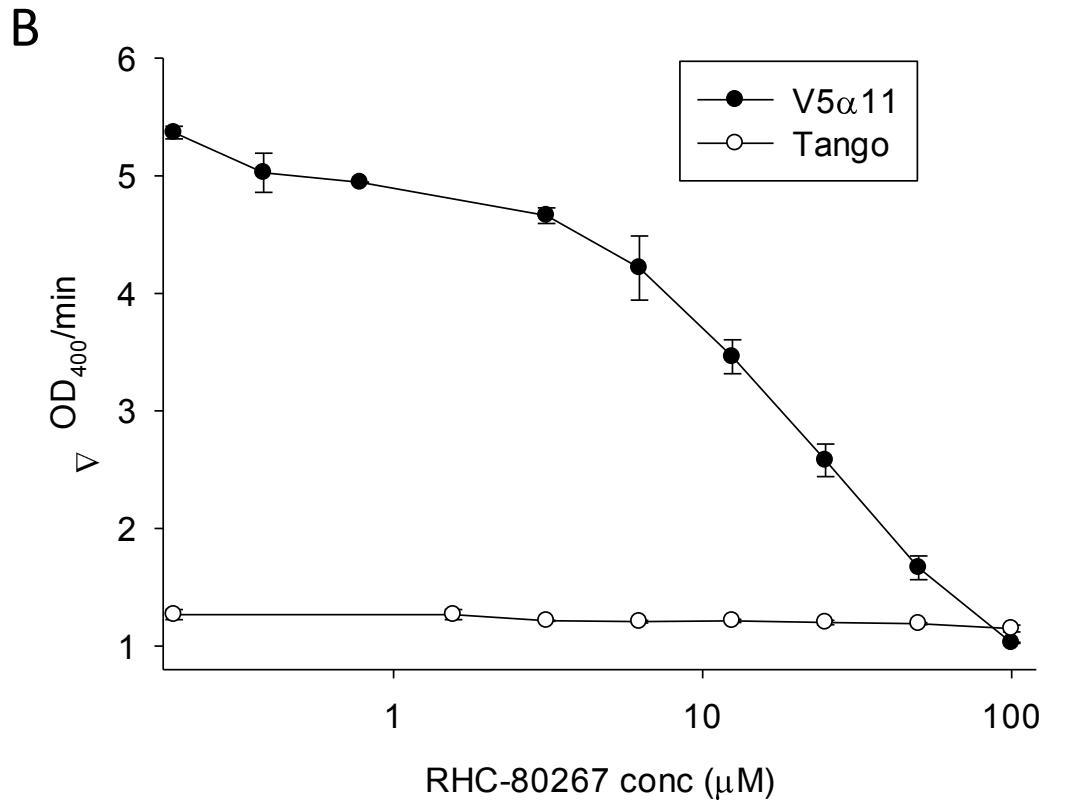
B
V5α11
Tango
∇ OD400/min
6
5
4
3
2
1
1
10
100
RHC-80267 conc (μM)

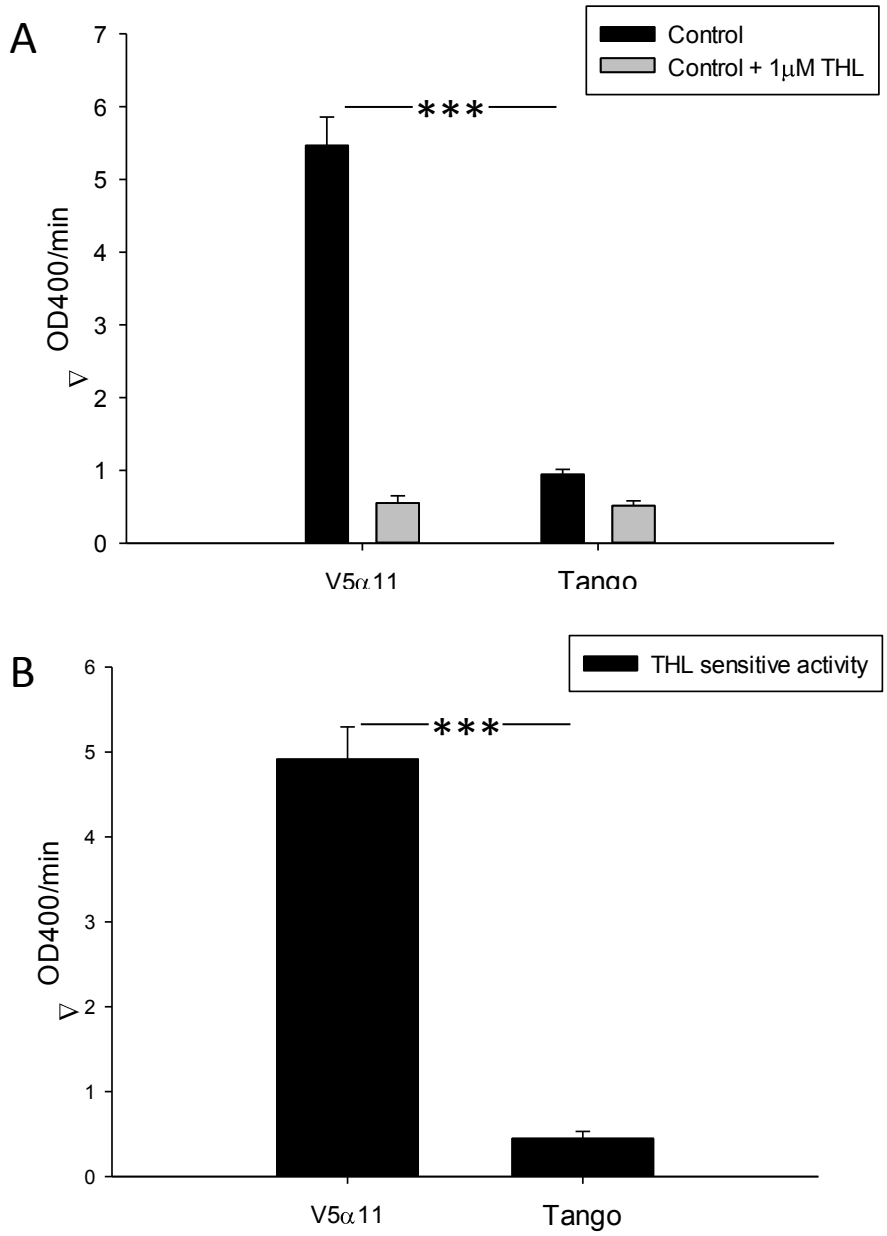

Figure 5.6. The PNPB membrane assay can be used to measure DAGLα-V5 activity

V5α11 or Tango membranes (12.5μg/ml) prepared from cells cultured in McCoy's media 10% FCS were incubated in the presence or absence of 1μM THL for 5 minutes. Activity was then measured using PNPB (250μM) as previously described (mean±SEM presented above. V5α11 n=10, Tango n=13, where n=the number of independent experiments) (A). The THL sensitive activity (total activity with THL insensitive background subtracted) is also presented (B). *** $p < 0.001$ (two tailed t-test).

5.1.3 Investigating DAGLα activation using the PNPB membrane assay

Calcium can stimulate DAGL activity in cells (Bisogno et al., 2003; Aguado et al., 2005) and we have postulated that this may occur due to phosphorylation of the DAGLs by calcium activated kinases. In order to investigate this, we tested whether calcium and serum deprivation (starvation) can affect the DAGL activity measured in the above membrane assay. To this end V5α11 cells were maintained overnight in the calcium and serum free media (Freestyle media) for 24 or 48 hours before membranes were prepared and DAGL activity determined in the presence or absence of 1μM THL. The membranes (12.5μg/ml) were pre-incubated with THL for 5 minutes after which PNPB was added (250μM). The OD_{400} was measured for 30 minute and the reaction rate was calculated over the first 10 minutes. A reduction in the total activity and THL sensitive activity (20% after 24 hours and 30% after 48 hours) was observed in the membranes prepared from starved cells when compared to membranes from cells cultured in McCoy's 10% FCS (Figure 5.7A and B). Expression levels of DAGLα-V5 in the starved and control membranes tested by Western blotting using a V5 antibody revealed a similar reduction in DAGLα-V5 levels, providing a likely explanation for the lower activity observed following starvation (Figure 5.7C and D).

As previous reports have demonstrated that $CaCl_2$ can stimulate DAGL activity *in vitro* (Bisogno et al., 2003; Pedicord et al., 2011) we decided to test this in the PNPB membrane assay. V5α11 membranes (12.5μg/ml) were pre-incubated in the absence of calcium or with increasing concentrations of $CaCl_2$ (0.25-4mM) for 5 minutes and then incubated in the presence or absence of 1μM THL for a further 5 minutes. The activity was then measured using 250μM PNPB as described above. The first important point is that DAGLα activity is maximally active in the absence of added calcium, so at least in the context of the PNPB substrate they do not require calcium for activity. Surprisingly and unexpectedly, a decrease in activity (60-80%) was observed with the increasing concentrations of $CaCl_2$ (Figure 5.8). In this particular case, $CaCl_2$ could have had a negative effect on substrate solubility which may explain the reduction in substrate hydrolysis.

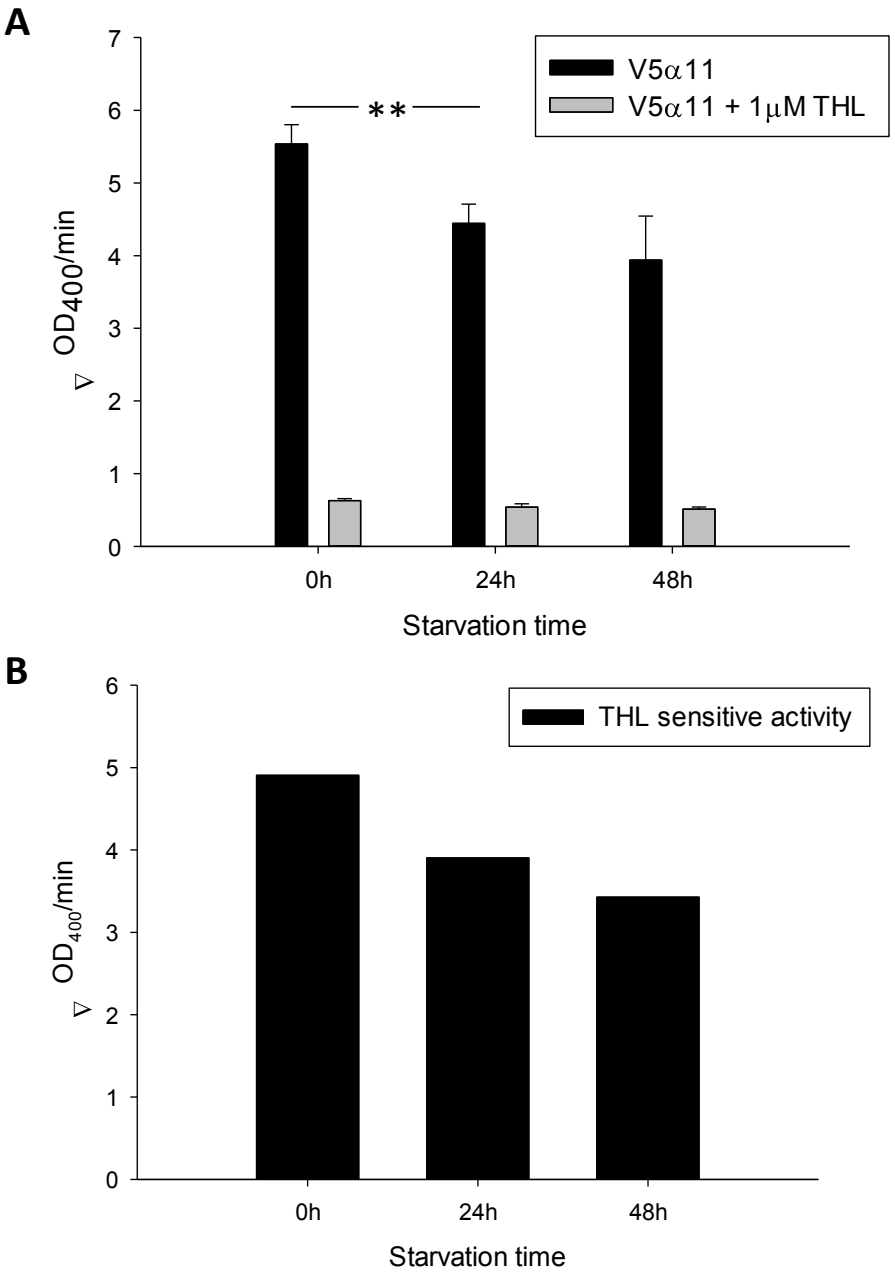
A
V5α11
V5α11 + 1μM THL
**
OD400/min
0h
24h
48h
Starvation time
B
THL sensitive activity
OD400/min
0h
24h
48h
Starvation time
C
V5α11
Tango
Starvation time
0
24
48
0
24
48
Mkr
250
150
100
V5
β-actin
n=2

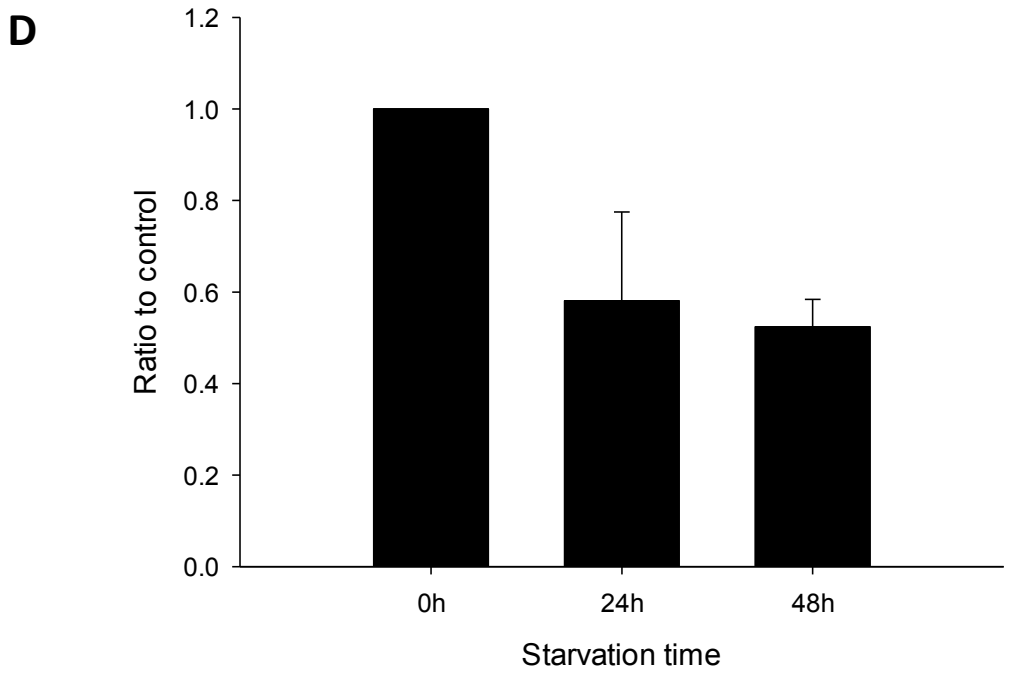

Figure 5.7. Reduction of DAGLα-V5 activity tested in the PNPB membrane assay following starvation is probably due to a reduction in DAGLα expression levels

V5α11 cells were cultured in McCoy's media supplemented with 10% FCS or maintained in Freestyle media in the absence of calcium and serum for 24 or 48 hours after which membranes were prepared as described earlier. The membranes (12.5μg/ml) were then incubated in the presence or absence of 1μM THL for 5 minutes. Hydrolytic activity was then measured using PNPB (250μM) as previously described (mean±SEM, 0h n=7, 24h n=7, 48h n=2 where n=number of independent experiments) (A). The THL sensitive activity (total activity with the THL insensitive background activity subtracted) are also presented (B). Western blotting using a V5 antibody of the control and starved membranes (10μg) was carried out; membranes prepared from parental Tango cells were included as a negative control (C). β-actin was also detected as a loading control. The DAGLα-V5 band intensities (quantified using the Odyssey software) were normalised to β-actin and are presented as a ratio to the normalised DAGLα-V5 band intensities measured in the unstarved control membranes (D) (n=2 independent experiments and results show mean±SD, n=2). ** $p<0.01$ (two tailed t-test).

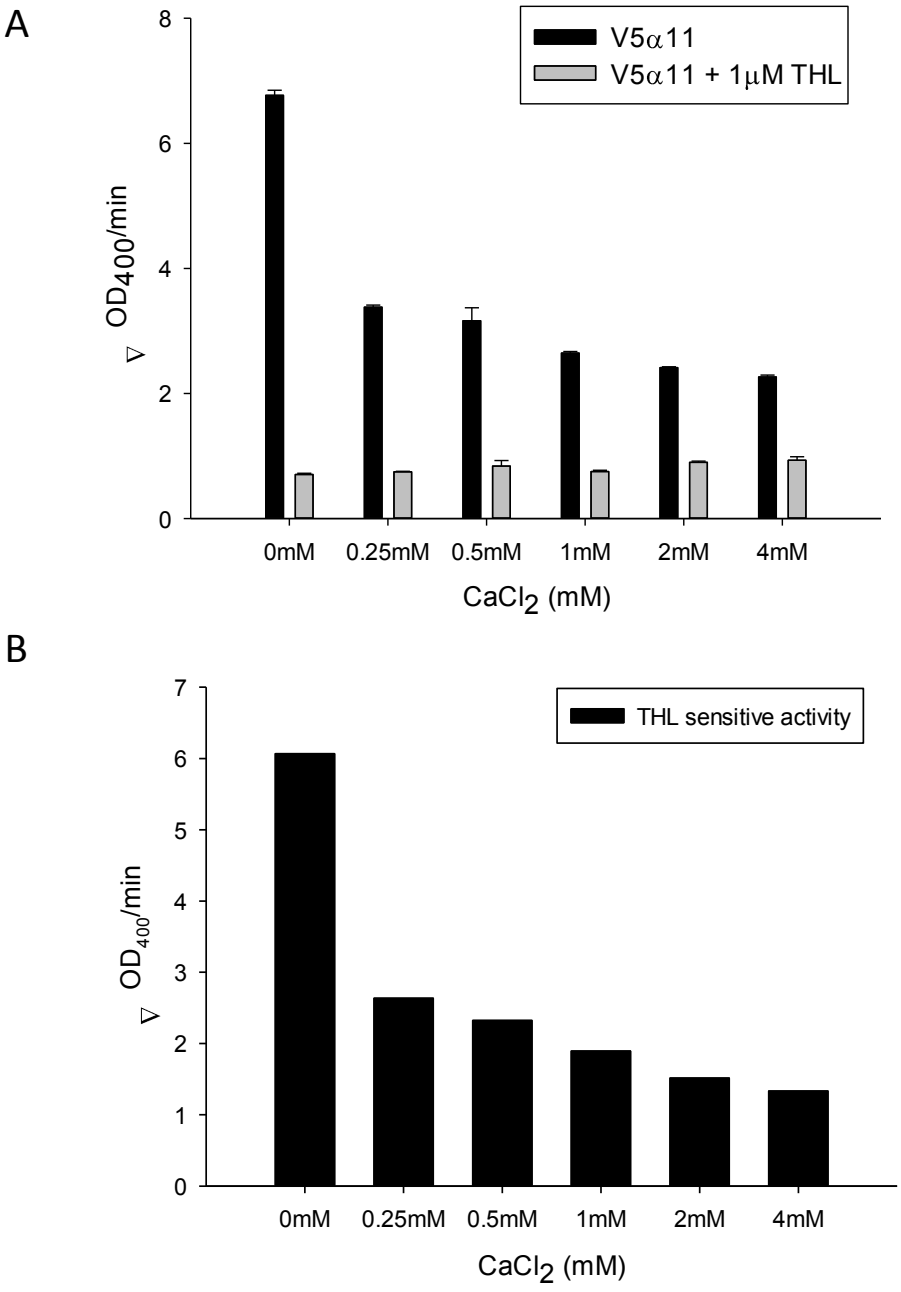

Figure 5.8. $CaCl_2$ causes a reduction in DAGLα-V5 activity tested in the PNPB membrane assay

Membranes prepared from V5α11 cells cultured in McCoy's media supplemented with 10% FCS (12.5μg/ml) were pre-incubated with different concentrations of $CaCl_2$ (0.25-4mM) for 5 minutes and then incubated in the presence or absence of 1μM THL for a further 5 minutes. The activity was then measured using 250μM PNPB as previously described (mean of 3 wells ±SEM) (A). THL sensitive activity measured in the V5α11 membranes is also presented (B).

Based on the results presented in the previous chapters that identified regulated phospho-sites in DAGLα and DAGLβ, and the observation that calcium stimulated DAGL-dependent eCB signalling in Tango cells requires PKA and PKC activity, we postulated that direct phosphorylation of the DAGLs by PKA or PKC regulates their activity. We therefore next examined whether the DAGL activity measured in the cell membranes using the PNPB substrate might differ between membranes isolated from control and PKA or PKC stimulated cells. V5α11 cells were maintained overnight in Freestyle media after which they were treated with either the PKA activator forskolin (10μM) or the PKC activator PMA (25nM) for 1 hour. Membranes were then prepared from the cells and were assayed (12.5μg/ml) as described above, in the presence or absence of 1μM THL using 250μM PNPB. No significant difference in activity was observed with membranes obtained from cells treated with forskolin or PMA (Figure 5.9). The activity of the batches of forskolin and PMA was confirmed by an increase in phosphorylation of CREB in lysates prepared from the treated cells (by Western blotting using a phospho-CREB antibody, data not shown).

The failure of the above treatments to affect DAGL activity could be due to a number of possibilities, for example PKA and/or PKC sites on DAGL might be phosphorylated in control cells. Indeed, there is reasonable evidence to think that there might be basal phosphorylation of the DAGLs (Perez Roque et al., 1998; Daub et al., 2008; Shonesy et al., 2013), and that it might be removed by a general phosphatase activity. For this reason we undertook a speculative experiment to see if phosphatase treatment could modulate activity. In this context direct treatment of the membranes with calf intestinal phosphatase (CIP) as described in the methods section had no effect on DAGL activity in the standard assay (Figure 5.10). This might be because the DAGLs are not phosphorylated, or the phosphatase might not have removed regulatory phosphates. These questions are explored later in the thesis. In summary, our experiments failed to demonstrate any changes in DAGL activity towards the PNPB substrate in a membrane assay.

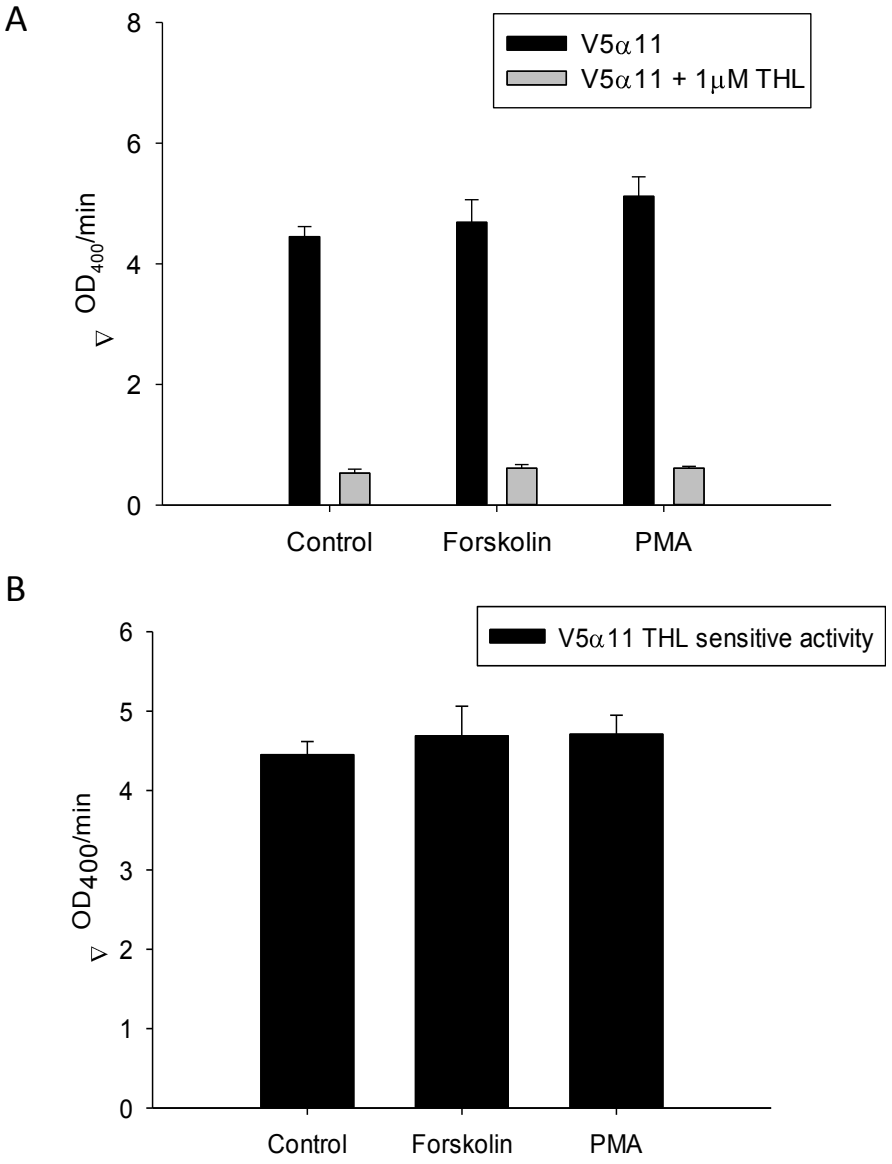

Figure 5.9. Treating V5α11 cells with PKA or PKC activators does not cause an increase in DAGLα-V5 activity, *in vitro*, in the PNPB membrane assay

V5α11 cells were maintained in Freestlye media for 24 hours and then treated with either the PKA activator forskolin (10μM) or the PKC activator PMA (25nM) for 1 hour after which membranes were prepared. The membranes (12.5μg/ml) were incubated in the presence or absence of 1μM THL for 5 minutes. Activity was then measured using PNPB (250μM) as previously described (n=3 independent experiments and shown as the mean±SEM) (A). The THL sensitive activity measured is also presented (B).

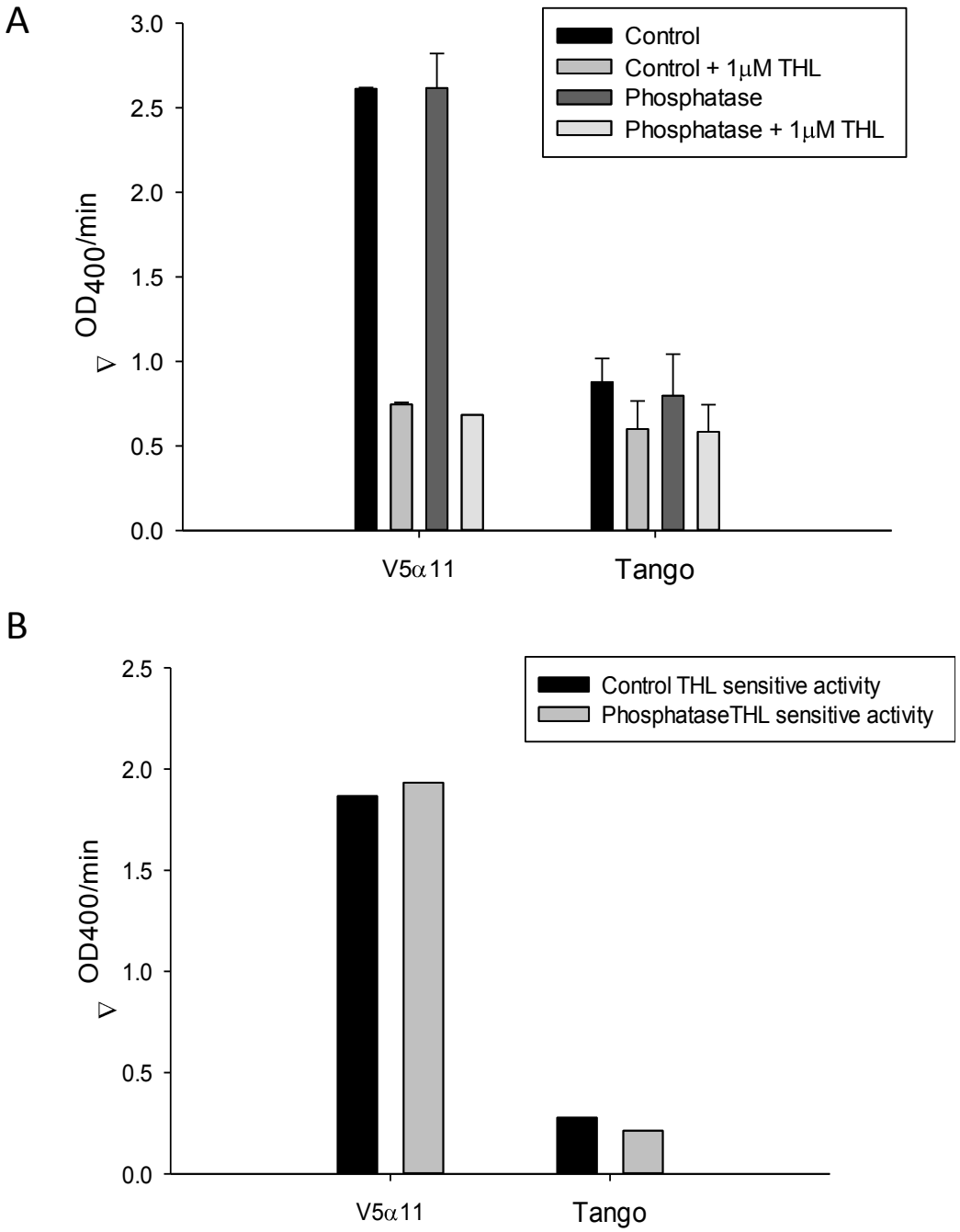

Figure 5.10. Phosphatase treatment of V5α11 (or Tango membranes) did not affect DAGLα (-V5) activity tested in the PNPB membrane assay

100μg V5α11 or Tango membranes were incubated with 50 units of calf intestinal phosphatase (37ºC for 60 minutes). The membranes (12.5μg/ml) were then incubated in the presence or absence of 1μM THL for 5 minutes. Activity was then measured using PNPB (250μM) as previously described (the mean of 3 wells ±SEM are presented above) (A). The THL sensitive activity is also presented (B).

This might be because the various treatments do not impact on DAGL structure and function, a loss of any impact as a consequence of membrane preparation, or perhaps the PNPB substrate can access the catalytic domain of both an “open” and “closed” enzyme due to its high solubility and small size.

5.1.4 Development of a DAGLα PNPB cell based assay

In order to start to address some of the above questions it was decided to see if the PNPB substrate could be used to explore DAGL activity in a live cell assay. To this end, V5α11 or Tango cells were seeded in 96-well plates in Freestyle media and maintained overnight. The media was then discarded and the cells were washed in assay buffer (50mM HEPES pH 7.4). The washed cells were incubated in the presence or absence of 25μM THL for 5 minutes and the hydrolytic activity was measured using the reaction rate calculated over the first 10 minutes. By varying cell number (20,000-40,000) and PNPB concentrations (100 to 500μM), and subtracting the background hydrolysis seen in the presence of 25μM THL (data not shown) conditions were established that showed the V5α11 cells hydrolysed the substrate at 3 to 4-fold higher rates than the parental cells (Figure 5.11A). Importantly, the enhanced activity in the DAGLα transfected cells and the basal activity in the parental Tango cells were completely inhibited by RHC-80267 and THL (Figure 5.11B and C). This assay was next used to test the effects of various treatments on the DAGL dependent hydrolysis of PNPB.

5.1.5 Investigating DAGLα activation using the PNPB cell based assay

Having established a PNPB cell based assay that could detect DAGLα (V5) activity, various treatments were next screened for their ability to modulate the DAGL dependent hydrolysis of PNPB in living cells. Following up from previous reports, (Bisogno et al., 2003; Sugiura et al., 2006) and the results observed in chapter 4 (Tango assay), we first tested whether $CaCl_2$ could stimulate PNPB hydrolysis in the assay.

Figure 5.11. DAGLα activity can be measured using the PNPB cell based assay which is inhibited by THL and RHC-80267

40,000 V5α11 or Tango cells per well were seeded in Freestyle media in 96-well plates and maintained overnight. The media was then discarded and the cells were washed in assay buffer (50mM HEPES pH 7.4). The washed cells were incubated in the presence or absence of 25μM THL for 5 minutes. Hydrolytic activity was then measured using 500μM PNPB by measuring the OD_{400} for 60 minutes. The reaction rate was calculated over the first 10 minutes and the THL sensitive activity is presented above (n=9 independent experiments and results show mean±SEM) (A). Additionally, cells that were seeded, maintained, and washed as described above were incubated with different concentrations of the DAGL inhibitors RHC-80267 or THL as indicated for 5 minutes. Activity was then measured using 500μM PNPB and the mean of 6 replicate wells ±SEM are presented above for the THL (B) and RHC-80267 (C) treated cells.

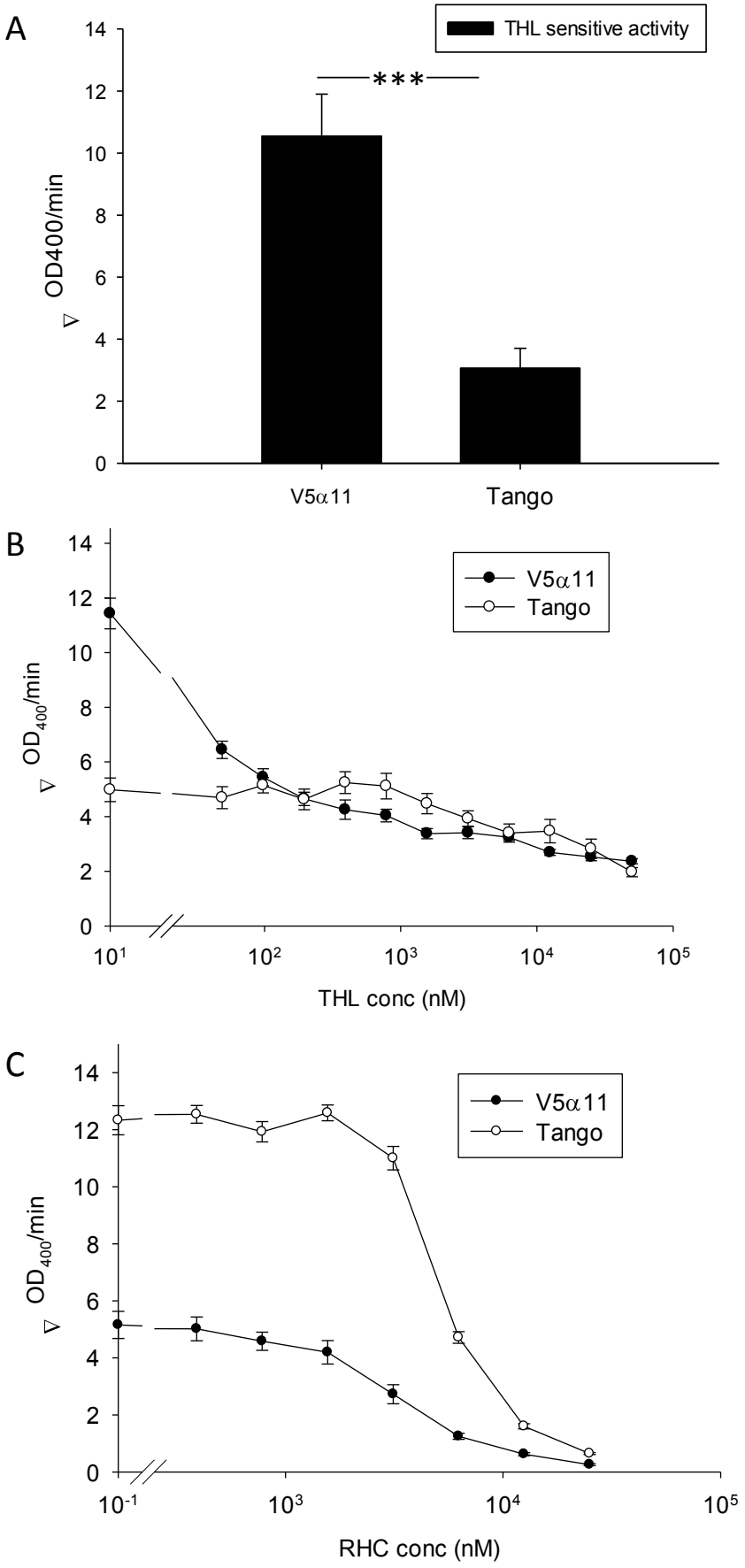
A
THL sensitive activity
***
OD400/min
14
12
10
8
6
4
2
0
V5α11
Tango
B
V5α11
Tango
OD400/min
14
12
10
8
6
4
2
0
10¹
10²
10³
10⁴
10⁵
THL conc (nM)
C
V5α11
Tango
OD400/min
14
12
10
8
6
4
2
0
10-1
10³
10⁴
10⁵
RHC conc (nM)

V5α11 or Tango cells were maintained overnight in the Freestyle media after which they were incubated in the absence or presence of 1 or 2mM $CaCl_2$ overnight as both stimulated DAGL-dependent eCB signalling under these conditions (see chapter 4). The cells were then washed in assay buffer and the activity was measured in the presence or absence of 25μM THL using 500μM PNPB. No increase in activity was observed in the V5α11 cells, furthermore, an almost 50% decrease in activity was observed in the cells treated with 2mM $CaCl_2$ (Figure 5.12A). This may have been caused by residual calcium interfering with substrate solubility or some other as of yet to be identified reason.

We next tested the effects of PKA activators on the activity of DAGLα in the PNPB cell based assay. V5α11 and Tango cells maintained in Freestyle media were treated with different concentrations of forskolin for 10 minutes or 4 hours after which the activity was measured in the presence or absence of THL as described above. No increase in activity was observed in the V5α11 cells using forskolin, following 10 minute (Figure 5.12B) or 4 hour treatments (data not shown). Similarly, no change in activity was observed when the cells were treated with the stable cAMP analogue 8-MA-cAMP. In addition to this, treating the cells with a PKA inhibitor H89 (5μM for 1 or 4 hours) did not affect PNPB hydrolysis in this assay (data not shown).

Having failed to detect a significant change in DAGL activity towards the PNPB substrate in the V5α11 cells following treatments with PKA activators or inhibitor we next tested the effects of PKC activation in the PNPB cell based assay. V5α11 cells were treated with the PKC activator PMA for 10 minutes and then activity in the cells was measured using 500μM PNPB in the presence or absence of 25μM THL as described above. Once again, no major change in activity in the V5α11 cells was observed following PMA treatment (Figure 5.12C). We have successfully developed a cell based and membrane assay to monitor DAGLα activity using PNPB as a substrate. However we were unable to demonstrate any PKA/PKC dependent activation of DAGLα activity against this substrate in these assays using the V5α11 cells.

Figure 5.12. $CaCl_2$ or PKA and PKC activators failed to stimulate DAGLα activity in the PNPB cell based assay

40,000 V5α11 or Tango cells were seeded per well of 96-well plates in Freestyle media and then maintained overnight. The cells were then incubated overnight in the absence or presence of $CaCl_2$ (1 or 2mM). The media was then discarded and the cells were washed in assay buffer (50mM HEPES pH 7.4). The washed cells were incubated in the presence or absence of 25μM THL for 5 minutes. Activity was measured using 500μM PNPB as previously described. The THL sensitive activity (mean of 6 wells ±SEM) is presented above (A). For the PKA/PKC activators, V5α11 cells were seeded, maintained, and washed as described above (in the absence of $CaCl_2$). The washed cells were then first treated with different concentrations of forskolin or PMA as indicated for 10 minutes and then incubated in the presence or absence of 25μM THL for 5 minutes. Activity was measured using 500μM PNPB as previously described. The THL sensitive activities are presented above for Forskolin (n=2 independent experiments and results show mean±SD) (B) and PMA (mean of 6 wells ±SEM) (C).

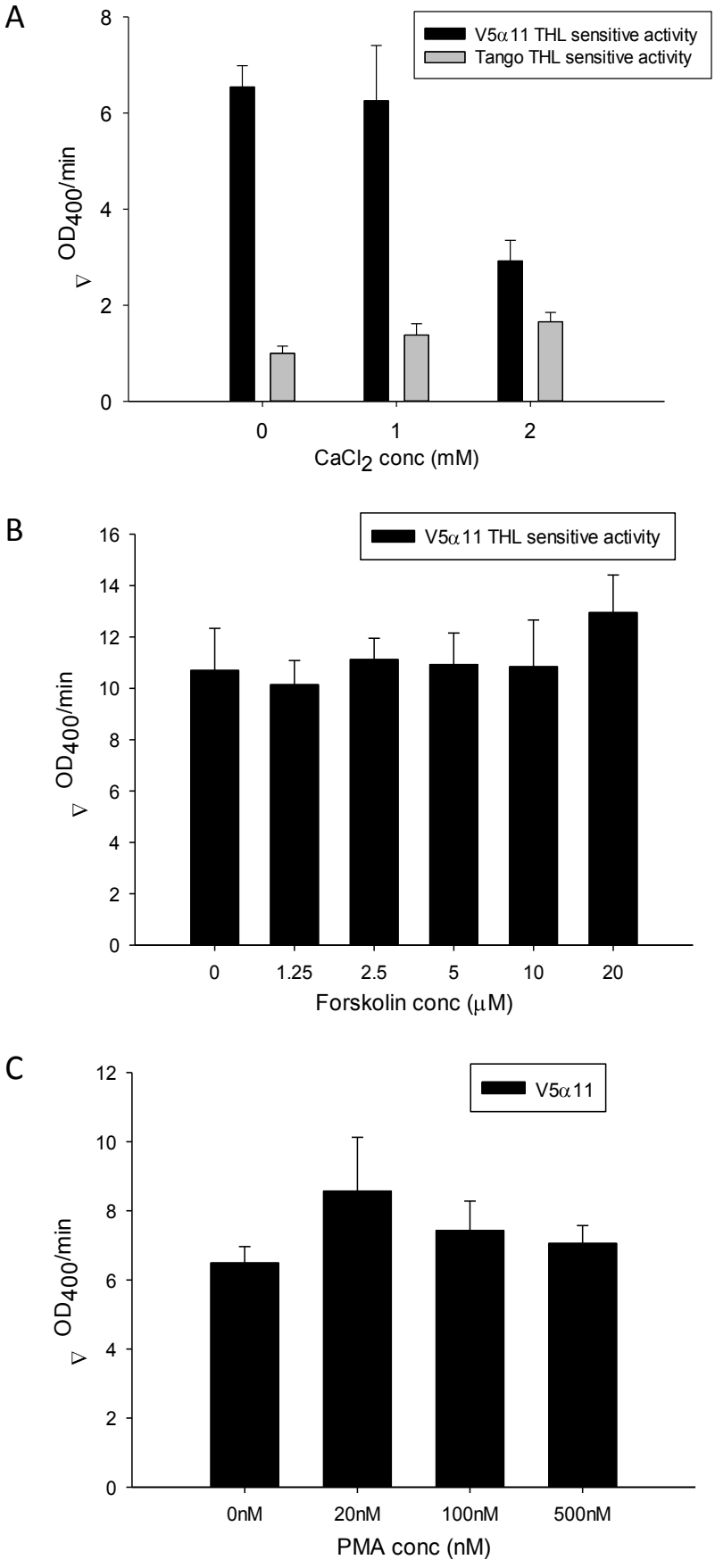
A
V5α11 THL sensitive activity
Tango THL sensitive activity
∇ OD400/min
CaCl2 conc (mM)
B
V5α11 THL sensitive activity
∇ OD400/min
Forskolin conc (μM)
C
V5α11
∇ OD400/min
PMA conc (nM)
0nM
20nM
100nM
500nM

As discussed earlier, it is possible that PKA/PKC stimulated DAGLα activity cannot be detected using a relatively small substrate like PNPB (~3 times smaller than DAG, Figure 5.1), that is also likely to access the enzyme from the cytosol and not the membrane. We therefore went on to develop DAGL assays using the fluorogenic substrate DiFMUO which is larger (338Da) than PNPB (209Da), and suggested to access the enzyme from the membrane (Pedicord et al., 2011) to study DAGL activation.

5.1.6 Development of a DAGLα-DiFMUO membrane and cell based assay

DiFMUO is a fluorogenic substrate which can be hydrolysed to DiFMU by DAGLα (Pedicord et al., 2011). DAGLα activity using this substrate can be detected by measuring the fluorescent product DiFMU (excitation 360nm, emission 450nm). In order to test whether DiFMUO could be used to measure DAGLα activity in our set up, membranes were prepared from V5α11 and Tango cells (grown in McCoy's media supplemented with 10% FCS) as described previously for the PNPB assay. The activity of different concentrations of membranes (1 to 50µg/ml) was measured in the presence or absence of 1µM THL using 10µM DiFMUO by measuring the rate of product formation (excitation 360nm, emission 450nm) over 10 minutes, when the reaction was linear. Increasing concentrations of membranes resulted in increasing activity in both sets of membranes (Figure 5.13A). The V5α11 membranes were more active than the parental Tango membranes at all the concentrations tested and this was completely inhibited by 1µM THL.

A maximum fold difference in activity between the two sets of membranes (1.6-fold) was achieved at a concentration of 12.5µg/ml which was then used to test the effects of substrate concentration in the assay (in the presence or absence of 1µM THL). Increasing substrate concentrations between 1-5µM resulted in an increase in activity, but a further increase between 5-15µM had no effect (Figure 5.13B).

Figure 5.13. Developing a DAGLα DiFMUO membrane assay

Membranes were prepared from V5α11 or Tango cells cultured in McCoy's media supplemented with 10% FCS. Different concentrations of the membranes were incubated in the presence or absence of 1μM THL for 5 minutes after which activity was measured using DiFMUO (10μM). Activity was monitored by measuring the fluorescence (excitation 360nm, emission 450nm) every 30 seconds for 30 minutes. The reaction rates were calculated over 10 minutes and are presented above (mean of 3 wells ±SEM) (A). This was repeated using membranes at a concentration of 12.5μg/ml and different concentrations of DiFMUO as indicated, the THL sensitive activity is presented above (mean of 3 wells ±SEM) (B). The optimum assay conditions were achieved using membranes at a concentration of 12.5μg/ml and DiFMUO at 10μM. The THL (1μM) sensitive activity measured using these conditions are presented above (n=7 independent experiments and results show mean±SEM) (C) *** $p < 0.001$ (two tailed t-test).

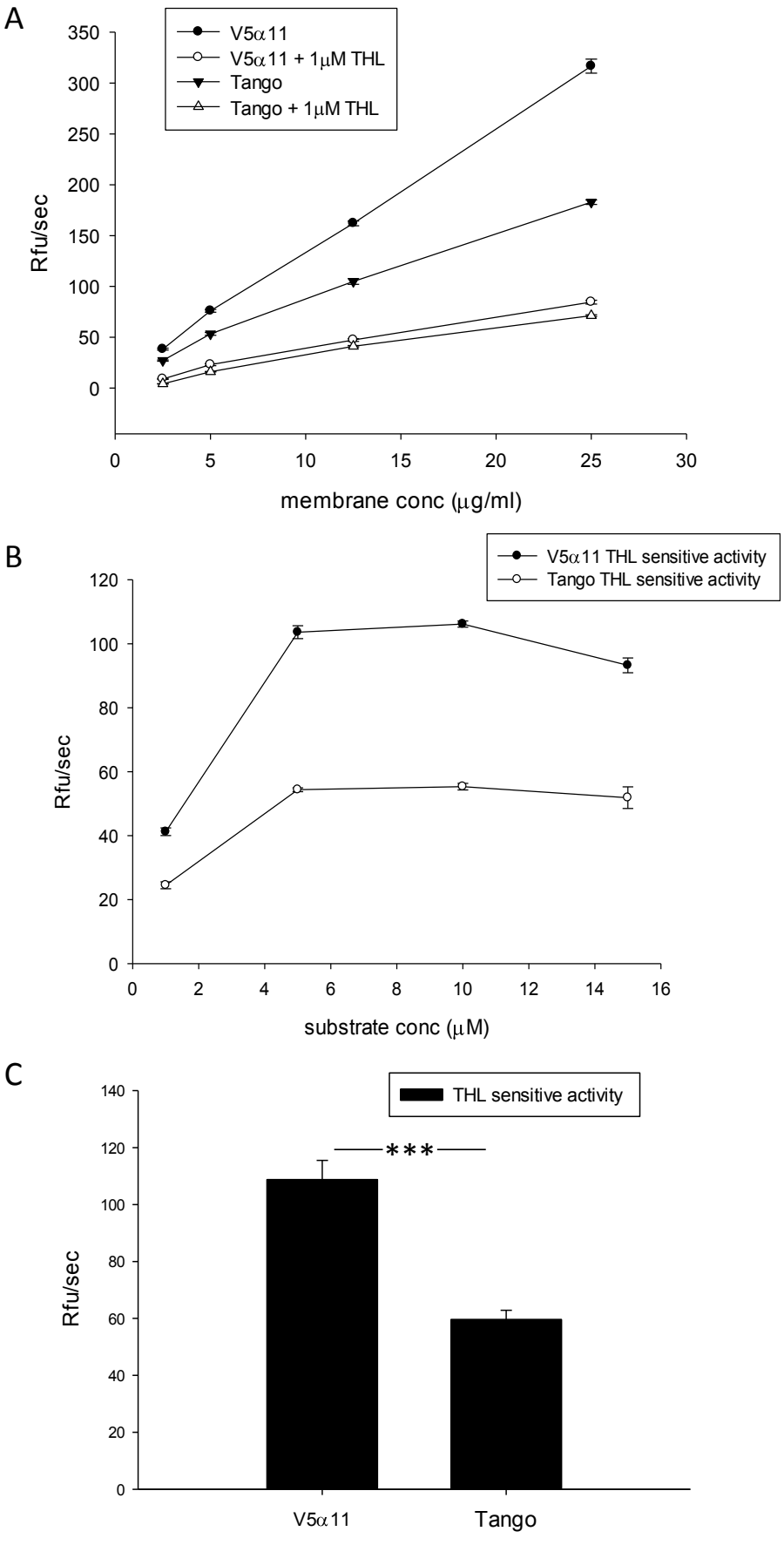
A
V5α11
V5α11 + 1μM THL
Tango
Tango + 1μM THL
Rfu/sec
membrane conc (μg/ml)
B
V5α11 THL sensitive activity
Tango THL sensitive activity
Rfu/sec
substrate conc (μM)
C
THL sensitive activity
***
Rfu/sec
V5α11
Tango

When using membranes at a concentration of 12.5µg/ml and DiFMUO at 10µM (to ensure substrate was in excess) the difference in activity between the V5α11 and Tango membranes was much less than what was observed in the PNPB membrane assay (1.6-fold versus 6-fold) (Figure 5.13C). The THL (1µM) insensitive background was higher in this assay compared to the PNPB membrane assay (30% versus 10%) possibly indicating that DiFMUO was more unstable than PNPB, or that it was hydrolysed by other THL insensitive membrane associated lipases. The difference between the THL sensitive activity of the V5α11 and Tango membranes was also lower compared to the PNPB membrane assay (2-fold versus 12-fold) (Figure 5.13C). Nevertheless we did observe a 2-fold window between the THL sensitive activities of the V5α11 and Tango membranes. This difference in activity was inhibited by two additional DAGL inhibitors RHC-80267 and OMDM-188 (data not shown). Furthermore, when comparing different cellular fractions from V5α11 and Tango cells, any enhanced activity measured in the V5α11 fractions compared to the Tango fractions correlated with the positive detection of DAGLα-V5 protein in the fraction (Western blotting) (Figure 5.14). Collectively these results confirmed that the 2-fold difference in activity between the V5α11 and Tango membranes was due to the DAGLα-V5 transgene, thereby validating the DiFMUO membrane assay as a tool to study DAGLα (V5) activity. The fact that 5-fold more enzyme increased hydrolysis by only 2-fold suggests that something other than enzyme levels (and possibly activation state) limits hydrolysis in this assay.

Nonetheless, in order to assess whether phosphorylation of DAGLα-V5 might be influencing its activity in the DiFMUO membrane assay, V5α11 and Tango membranes were treated with calf intestinal phosphatase (CIP) or PKA in speculative experiments, however no reduction in the total or THL sensitive activity was observed (data not shown).

5.1.7 Development of a DAGLα DiFMUO cell based assay

We next determined if DiFMUO might be a suitable substrate to measure DAGLα activity in live cells. To this end, 40,000 V5α11 cells were seeded per well (96-well plate) in Freestyle media and then maintained overnight.

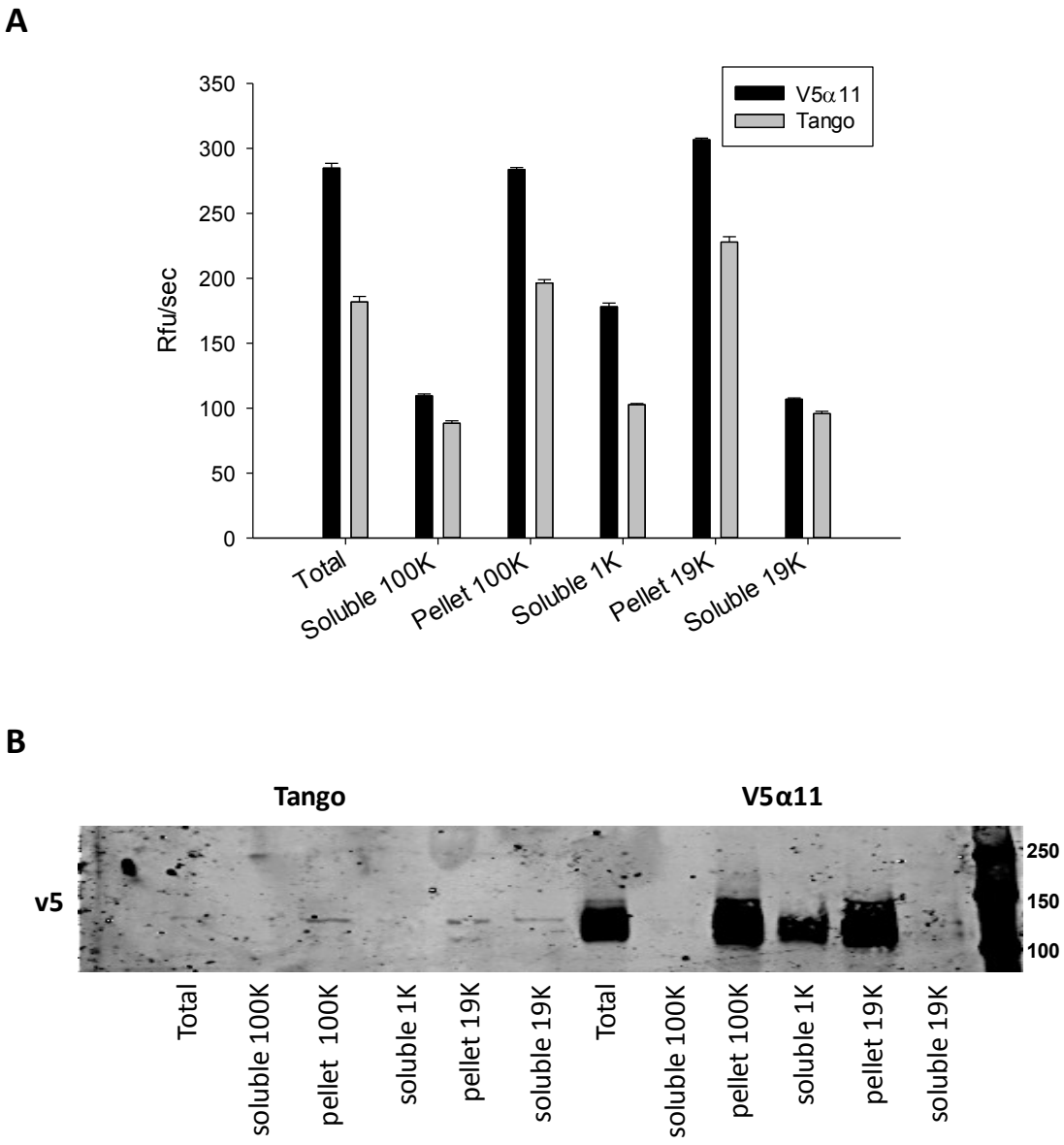

Figure 5.14. Cellular fractionation reveals DAGLα-V5 specific activity can be detected in the DiFMUO membrane assay

V5α11 and Tango cells cultured in McCoy's media supplemented with 10% FCS were homogenised and then subjected to centrifugation at different speeds (1000, 19,000 and 100,000g). Supernatants and pellets were collected, the pellets were resuspended in membrane buffer, and activities of both the supernatants and pellets (25µg/ml) were measured using DiFMUO (10µM) as previously described (mean of 3 wells ±SEM) (A). DAGLα-V5 was detected in these fractions (10µg) by Western blotting using a V5 antibody (B).

Prior to assaying, the media was discarded and the cells were washed with assay buffer (50mM MES pH 6.5).The washed cells were incubated in the presence or absence of THL (25μM) for 5 minutes and then activity was measured as the rate of DiFMUO hydrolysis over the first 10 minutes. By varying substrate concentration and subtracting the background hydrolysis seen in the presence of 25μM THL, a maximum difference in activity of 1.6-fold was observed between V5α11 and Tango cells (Figure 5.15). This was lower compared to the PNPB cell based assay (3.5-fold). Nevertheless, the difference in activity between the V5α11 and Tango cells observed in the DiFMUO cell based assay (Figure 5.15) was significant and was completely blocked by three different DAGL inhibitors (RHC-80267, OMDM-188 and THL) (data not shown). Thus we can conclude that something other than enzyme levels is rate limiting in this assay, and can speculate that this might be availability of the substrate to the enzyme, or enzyme activity towards this substrate.

5.1.8 Investigating DAGLα activation using the DiFMUO cell based assay

We proceeded to test the effects of various stimuli on DAGLα activity using the DiFMUO cell based assay. Prior to the treatments, V5α11 and Tango cells were maintained overnight in Freestyle media. In order to test whether PKA activation in cells could stimulate DAGLα activity measured in the DiFMUO cell based assay, V5α11, or parental Tango cells were treated with different concentrations of the PKA activator forskolin (0 to 20μM) for 10 minutes or 4 hours. Activity in the cells was then measured in the presence or absence of 25μM THL using 10μM DiFMUO. No significant increase in activity was observed in either the V5α11 or parental Tango cells following forskolin treatment (Figure 5.16A). We also tested the effects of a PKA inhibitor (H89 5μM) in this assay. Both cell types were treated with H89 for 1 hour and the activity was then measured as described above. A slight reduction (~10%) in the THL sensitive activity was observed in the V5α11 cells (Figure 5.16C). However, a corresponding, non-significant decrease in activity was also observed in the parental Tango cells.

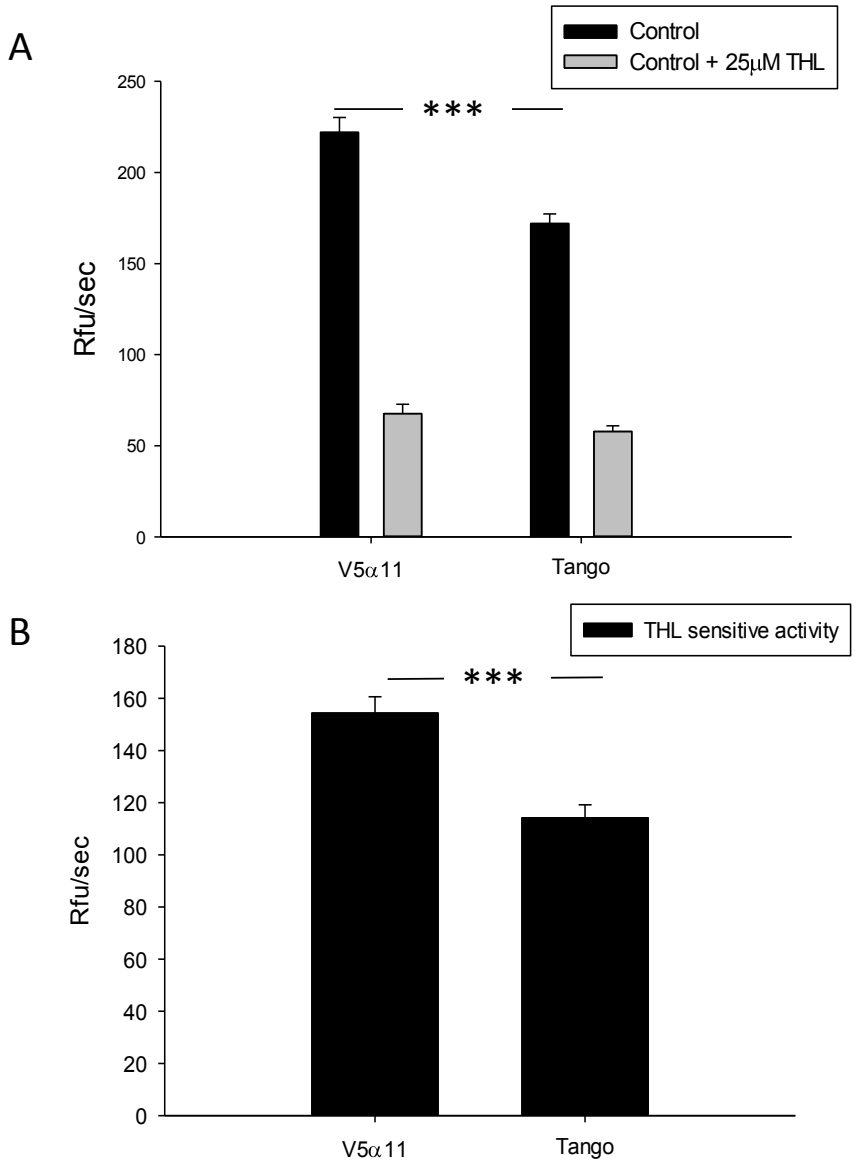

Figure 5.15.The DiFMUO cell based assay can be used to measure DAGLα-V5 activity in the V5α11 cells

40,000 V5α11 or Tango cells per well were seeded in Freestyle media in 96-well plates and cultured overnight. The media was then discarded and the cells were washed in assay buffer (50mM MES pH 6.5). The cells were incubated in the presence or absence of 25μM THL for 5 minutes and then the activity was measured using 10μM DiFMUO as previously described. The reaction rates were calculated over 10 minutes and the total activity (mean±SEM, V5α11 n=16, Tango n=22. In each instance, n= the number of independent experiments) (A) and THL sensitive activity (B) are presented above. ***$p < 0.001$ (two tailed t-test).

A

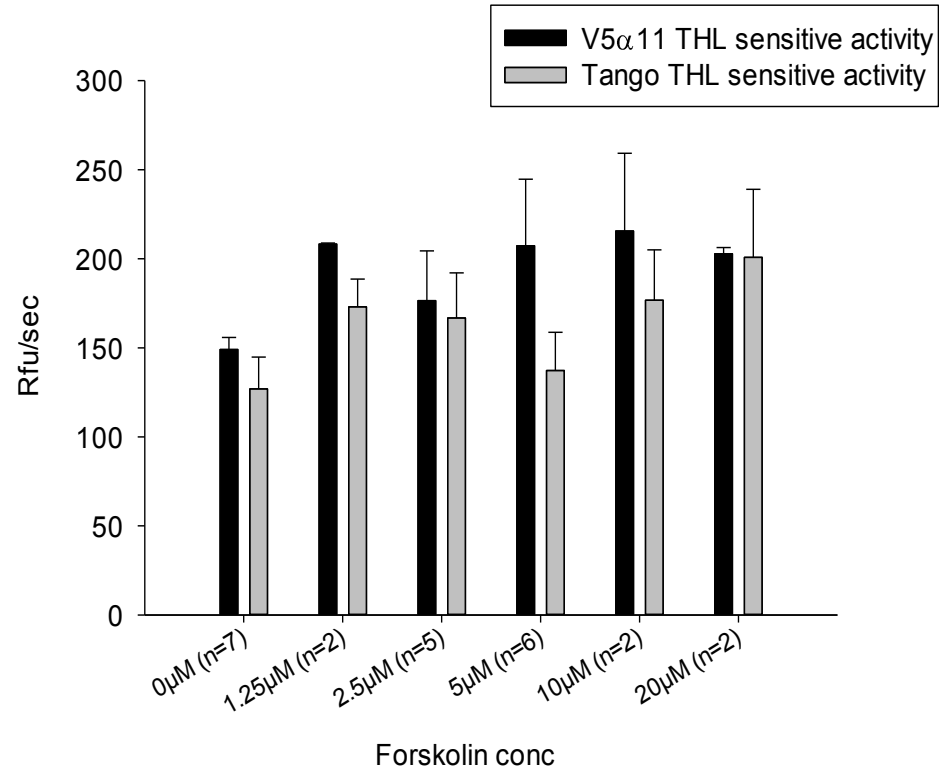
V5α11 THL sensitive activity
Tango THL sensitive activity
300
250
200
150
100
50
0
Rfu/sec
0μM (n=7)
1.25μM (n=2)
2.5μM (n=5)
5μM (n=6)
10μM (n=2)
20μM (n=2)
Forskolin conc

B

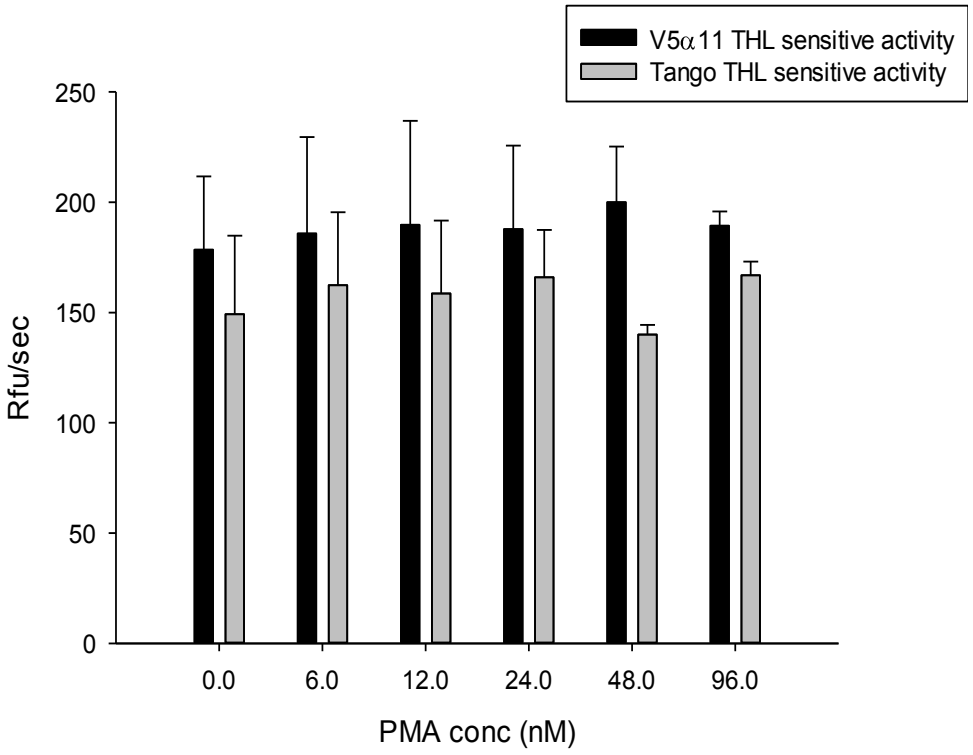
V5α11 THL sensitive activity
Tango THL sensitive activity
250
200
150
100
50
0
Rfu/sec
0.0
6.0
12.0
24.0
48.0
96.0
PMA conc (nM)

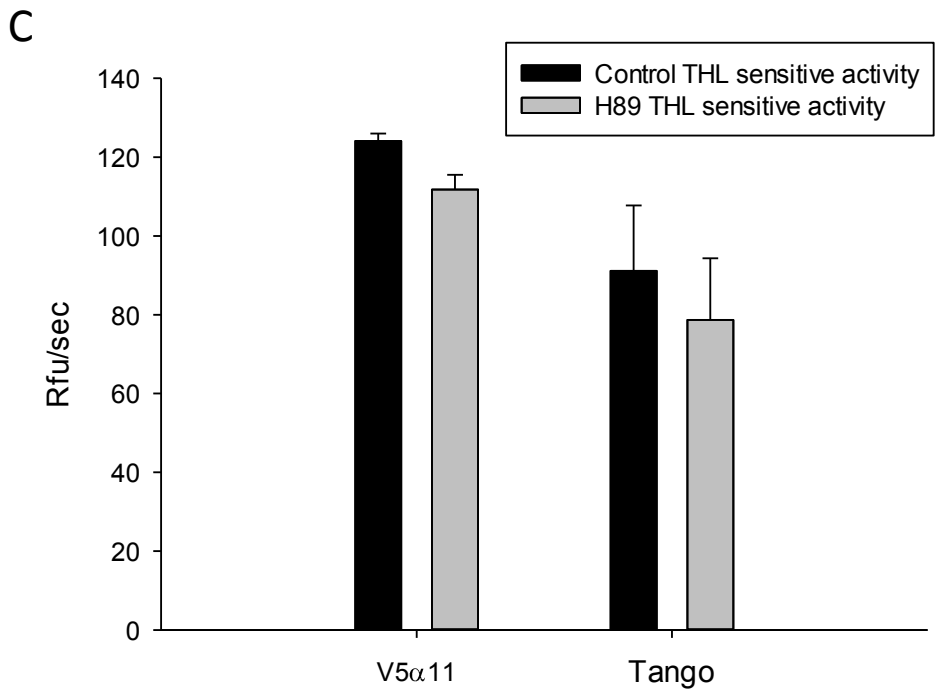

Figure 5.16. PKA or PKC modulators did not affect DAGLα activity in the DiFMUO cell based assay

40,000 V5α11 or Tango cells were seeded in Freestyle media per well of 96-well plates and maintained overnight. The media was discarded and the cells were washed in assay buffer (50mM MES pH 6.5). The washed cells were treated with different concentrations of forskolin or PMA as indicated for 10 minutes after which they were incubated in the presence or absence of 25μM THL for 5 minutes. The activity was then measured using 10μM DiFMUO as previously described. The THL sensitive activity for the forskolin treatments (mean±SD for n=2, mean±SEM for n>2, where n=the number of independent experiments) (A) and PMA treatments (mean±SEM n=3 independent experiments) (B) are presented above. For the PKA inhibitor treatment, the cells were seeded and maintained as described above but then treated for 1 hour with 5μM H89 before the activity was measured in the presence or absence of 25μM THL using 10μM DiFMUO. The THL sensitive activity is presented above. (V5α11 n=2 mean±SD, Tango n=3, mean±SEM, n=the number of independent experiments).

DAGLα-V5 was therefore unlikely to be responsible for this reduction in activity (Figure 5.16C). Finally, we tested whether PKC activation would stimulate DAGLα-V5 activity in the DiFMUO cell based assay. V5α11 and Tango cells were treated with the PKC activator PMA for 10 minutes and then activity was measured as described above. Once again, no significant change in activity was observed in either the V5α11 or the parental Tango cells following PMA treatment (Figure 5.16B).

We have developed a total of 4 different DAGLα assays (membrane and cell based) using two different substrates (PNPB and DiFMUO). However despite using a range of treatments and stimuli (phosphatase, calcium, PKA activation, PKA inhibition, and PKC activation) we failed to detect any changes in DAGLα activity using either DiFMUO or PNPB. These results failed to support our hypothesis that PKA and PKC activate the DAGLs by phosphorylation which was based on our findings in chapter 4 where we demonstrated that calcium, PKA, and PKC stimulated DAGL dependent eCB signalling in the Tango cells. However, it is possible that the DAGL-dependent eCB signalling observed in the Tango assay may have been mediated by DAGLβ rather than DAGLα. We therefore thought it prudent to conduct a similar set of experiments on DAGLβ using the V5β4 Tango cells described in chapter 4. This line overexpresses V5 tagged human DAGLβ to a similar extent that V5α11 cells over express DAGLα (Figure 4.14 and Figure 4.15).

5.1.9 DAGLβ-V5 PNPB membrane and cell based assays

All assays using the V5β4 cells were run as previously described for the V5α11 cells and membranes. A summary of the results are presented below.

Activity of membranes prepared from V5β4 cells (McCoy's media 10% FCS) were first tested in the PNPB membrane assay. A significant difference in activity between the V5β4 and parental Tango membranes was observed. However, the window of activity between the membranes was only 2-fold (Figure 5.17A) which was much smaller than what was observed between the V5α11 and Tango membranes (10-fold) (Figure 5.6).

Figure 5.17. PNPB can be used to measure DAGLβ-V5 activity

For the membrane assay, V5β4 or Tango membranes (12.5µg/ml) prepared from cells cultured in McCoy's media supplemented with 10% FCS were incubated in the presence or absence of 1µM THL for 5 minutes. Activity was then measured using PNPB (250µM) as previously described and the THL sensitive activity (mean±SEM, V5β4 n=9, Tango n=13. where n=number of independent experiments) is presented above (A). For the cell based assay 40,000 V5β4 or Tango cells were seeded per well in Freestyle media in 96-well plates and maintained overnight. The media was then discarded and the cells were washed in assay buffer (50mM HEPES pH 7.4). The cells were incubated in the presence or absence of 25µM THL for 5 minutes and then the activity was measured using 500µM PNPB as previously described. The THL sensitive activity (mean±SEM, V5β4 n=6, Tango n=9. where n=the number of independent experiments) is presented above (B) ** $p < 0.01$ (two tailed t-test).

A

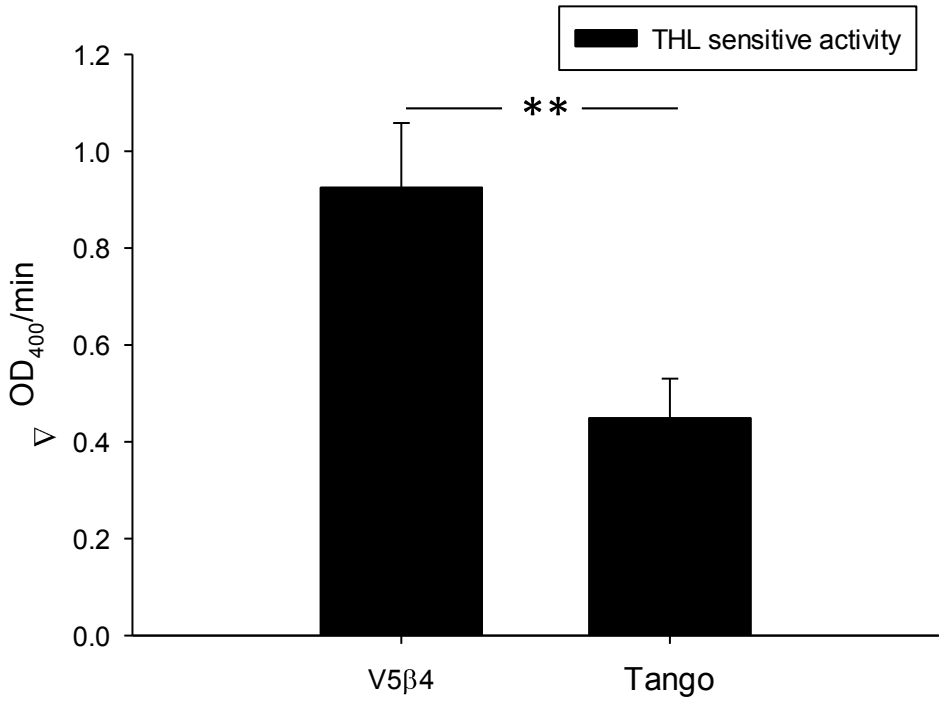
THL sensitive activity
**
1.2
1.0
0.8
0.6
0.4
0.2
0.0
∇ OD400/min
V5β4
Tango

B

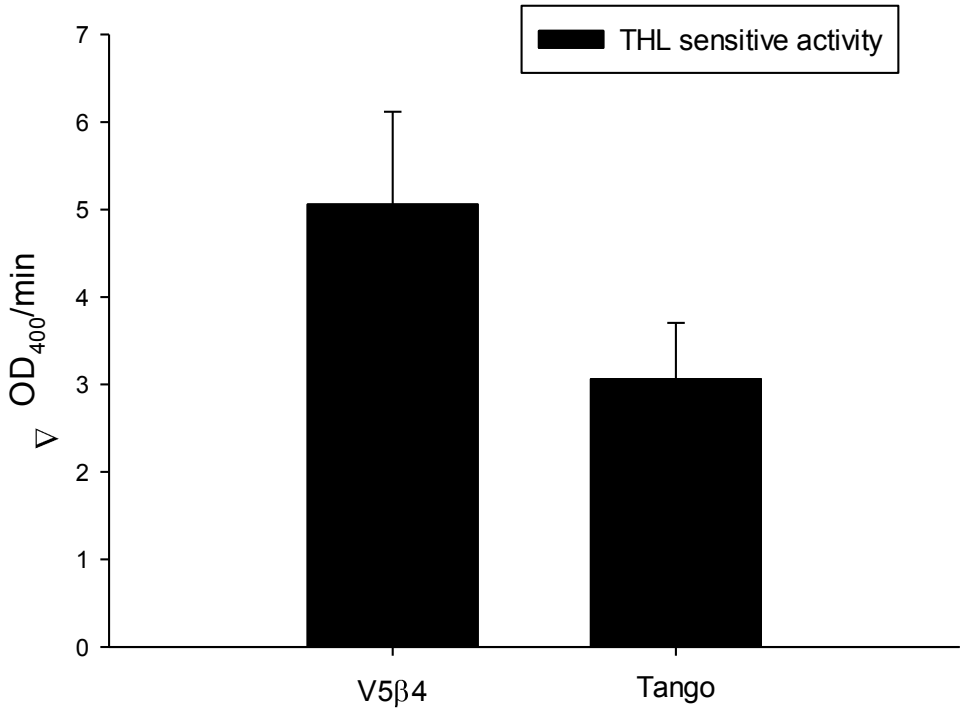
THL sensitive activity
7
6
5
4
3
2
1
0
∇ OD400/min
V5β4
Tango

We also observed greater activity in the V5β4 live cell assay compared to the Tango cells using the PNPB cell based assay. This increase in activity was however relatively small (1.7-fold) (Figure 5.17B), not significant and much lower compared to the difference between the V5α11 and Tango cells (3.5-fold) (Figure 5.11A). Despite the small difference in activity between the V5β4 and parental Tango cells we attempted to stimulate DAGLβ activity in the V5β4 cells working on the assumption that activation of DAGLβ might reveal a bigger window of activity between these cells. Activity of Vβ4 cells treated with the PKA activator forskolin (10 minutes and 4 hours), the PKA inhibitor H89 (1 hour), and the PKC activator PMA (10 minutes and 4 hours) were tested using the PNPB cell based assay. None of these stimuli were found to affect DAGLβ-V5 activity in the assay (data not shown).

5.1.10 DAGLβ DiFMUO membrane and cell based assays

Having failed to detect DAGLβ activation in the V5β4 cells using the small PNPB substrate, we next attempted to detect stimulated DAGLβ activity using the larger DiFMUO. Firstly, the activity of membranes prepared from V5β4 cells was tested in the DiFMUO membrane assay to confirm that DAGLβ could hydrolyse this substrate. Unlike the V5α11 membranes, no significant difference between V5β4 and parental Tango membranes was detected at membrane concentrations of 12.5 or 25μg/ml. However, a small but significant difference (1.4-fold) at the higher concentration of 50μg/ml was observed (Figure 5.18A). A significant difference between the activity (1.4-fold) of the V5β4 and Tango cells in the DiFMUO cell based assay was also observed (Figure 5.18B). However, once again we generally failed to detect any increase in DAGLβ-V5 activity after treating the V5β4 cells with a range of stimuli (Forskolin, H89, PMA) when using the DiFMUO cell based assay (data not shown).

As in the case of DAGLα, the DAGLβ assays using PNPB and DiFMUO did not (and possibly could not) detect PKA and PKC stimulated DAGL activity. We generally observed greater activity in the V5α11 cells and membranes compared to the V5β4 cells and membranes in the PNPB and DiFMUO assays (summarised in Table 5.1 and Table 5.2).

Figure 5.18. DiFMUO can be used to measure DAGLβ activity

For the membrane assay V5β4 or Tango membranes (12.5, 25 or 50µg/ml) prepared from cells cultured in McCoy's media supplemented with 10% FCS were incubated in the presence or absence of 1µM THL for 5 minutes. Activity was then measured using DiFMUO (10µM) as previously described and the THL sensitive activity is presented above (mean±SEM. V5β4 12.5µg/ml n=4, 25µg/ml n=4 and 50µg/ml n=3. Tango 12.5µg/ml n=8, 25µg/ml n=6 and 50µg/ml n=4. In each instance n=the number of independent experiments) (A). For the cell based assay 40,000 V5β4 or Tango cells per well were seeded in Freestyle media in 96-well plates and maintained overnight. The media was then discarded and the cells were washed in assay buffer (50mM MES pH 6.5). The washed cells were incubated in the presence or absence of 25µM THL for 5 minutes and then the activity was measured using 10µM DiFMUO as previously described. The THL sensitive activity (mean±SEM, V5β4 n=6, Tango n=22. where n=number of independent experiments) is presented above (B). *** $p < 0.001$ * $p < 0.05$ (two tailed t-test).

A

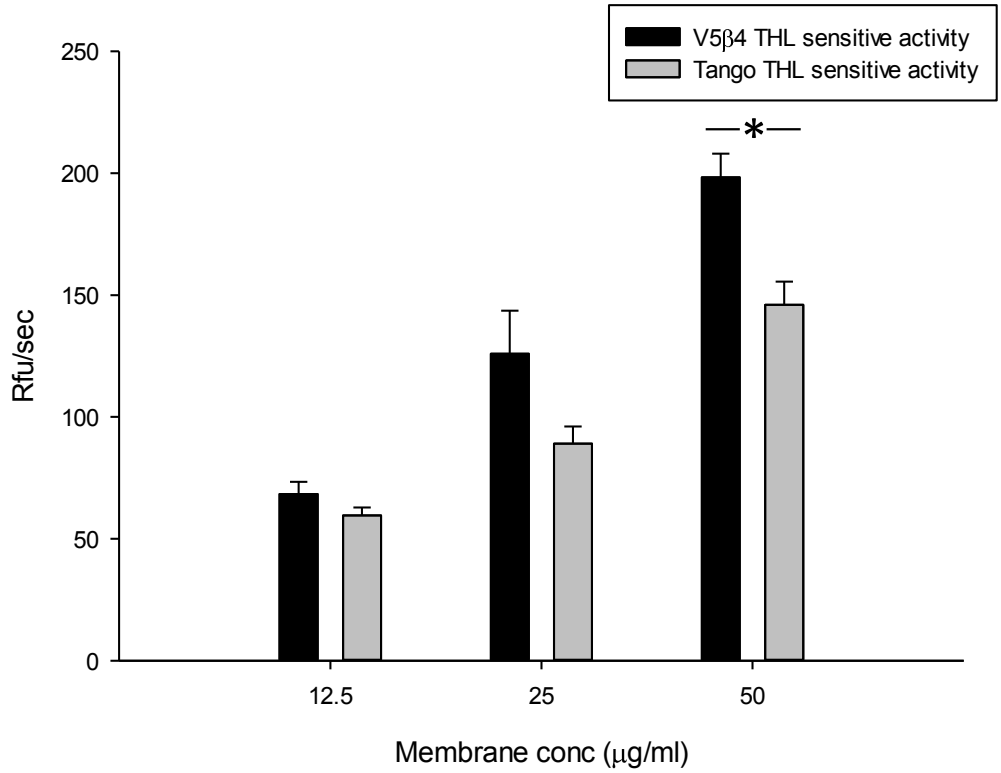
V5β4 THL sensitive activity
Tango THL sensitive activity
*
250
200
150
100
50
0
Rfu/sec
12.5
25
50
Membrane conc (μg/ml)

B

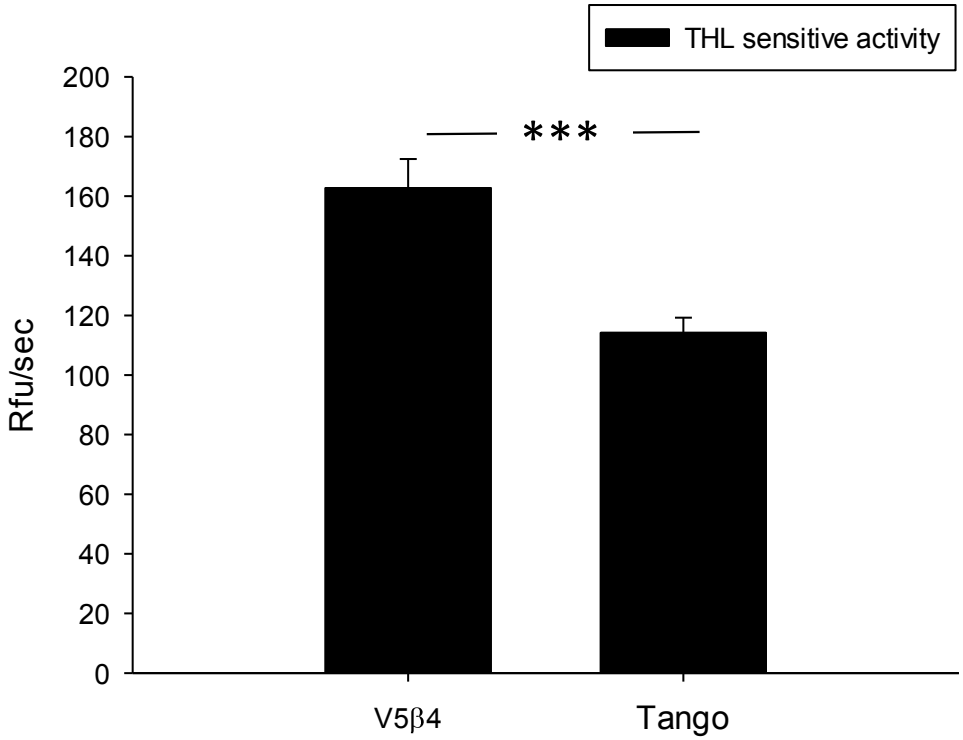
THL sensitive activity
***
200
180
160
140
120
100
80
60
40
20
0
Rfu/sec
V5β4
Tango

Table 5.1. Summary of results from the surrogate substrate membrane assays

Cell line	Substrate	THL insensitive background	THL sensitive activity versus Tango (fold difference)
V5α11	PNPB	10%	11.0
V5β4	PNPB	31%	2.1
Tango	PNPB	55%	1.0
V5α11	DiFMUO	31%	1.8
V5β4	DiFMUO	32%	1.4
Tango	DiFMUO	40%	1.0
V5α11	EnzChek	2%	1.6
V5β4	EnzChek	3%	2.5
Tango	EnzChek	3%	1.0

Table 5.2. Summary of results from the surrogate substrate live cell assays

Cell line	Substrate	THL insensitive background	THL sensitive activity versus Tango (fold difference)
V5α11	PNPB	31%	3.4
V5β4	PNPB	45%	1.7
Tango	PNPB	59%	1.0
V5α11	DiFMUO	30%	1.4
V5β4	DiFMUO	30%	1.4
Tango	DiFMUO	34%	1.0

5.1.11 DAGLα and DAGLβ demonstrate different activities towards the surrogate substrates

In order to check whether the higher activity detected in V5α11 cells compared to V5β4 cells was reflective of higher expression levels of DAGLα-V5 compared to DAGLβ-V5, 10µg of V5α11 and V5β4 membranes were analysed by Western blotting using a V5 antibody. Surprisingly, the intensity of the DAGLβ-V5 band was found to be 5 times greater than the DAGLα-V5 band (Figure 5.19). Admittedly, these are different proteins of different sizes and this can affect the efficiency of transfer and detection during the Westerns. However, based on these results it does seem unlikely that differences in expression levels could account for the 5-fold difference in the THL sensitive activity measured in V5α11 and V5β4 membranes using PNPB. The difference is even greater (9-fold) if the THL sensitive parental Tango activity is subtracted from the activity of both the membranes, in order to enable comparisons between DAGLα-V5 and DAGLβ-V5 activity.

The DAGL enzymes may instead have different activities against these substrates. In order to query this, the activity of membranes (12.5µg/ml) prepared from V5α11, V5β4, and Tango parental cells were tested using a third substrate, EnzChek, which is a commercially available fluorogenic substrate (structure presented in Figure 5.1). Lipase activity against this substrate relieves internal quenching within the substrate resulting in increased fluorescence. Interestingly, V5β4 membranes showed the highest activity against this substrate followed by the V5α11 and then the Tango membranes (Figure 5.20). Virtually all of the activity detected in this assay was found to be THL sensitive (1µM)

Based on the results in this chapter it therefore appears that PNPB is the best substrate for DAGLα-V5 relative to DiFMUO and EnzChek, whereas EnzChek is clearly the best substrate for DAGLβ-V5 (Table 5.1). These results indicate that the DAGLs can differentiate between different surrogate substrates and this is discussed later in the thesis.

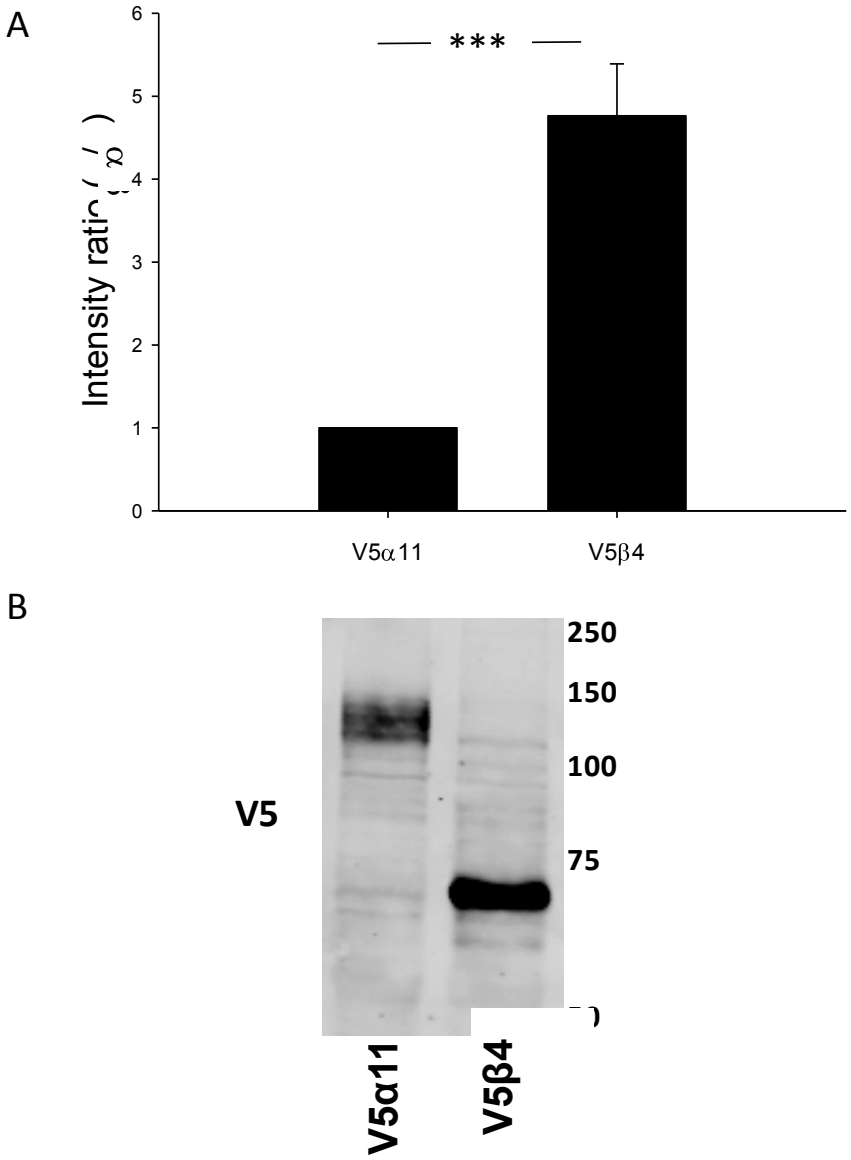

Figure 5.19. Western blotting analysis using the V5 antibody indicates that DAGLβ-V5 in the V5β4 cells are expressed at higher levels than DAGLα-V5 in the V5α11 cells

Membranes were prepared from V5α11 and V5β4 cells grown in McCoy's media supplemented with 10% FCS. Western blotting analyses of the membranes (10µg) using a V5 antibody were visualised using the Odyssey infrared imaging system. Band intensities were quantified using the Odyssey software and are presented as a ratio of the DAGLα-V5 band intensities (mean±SEM of 5 independent experiments presented above) (A). A representative Western blot is also shown (B). *** $p < 0.001$ (two tailed t-test).

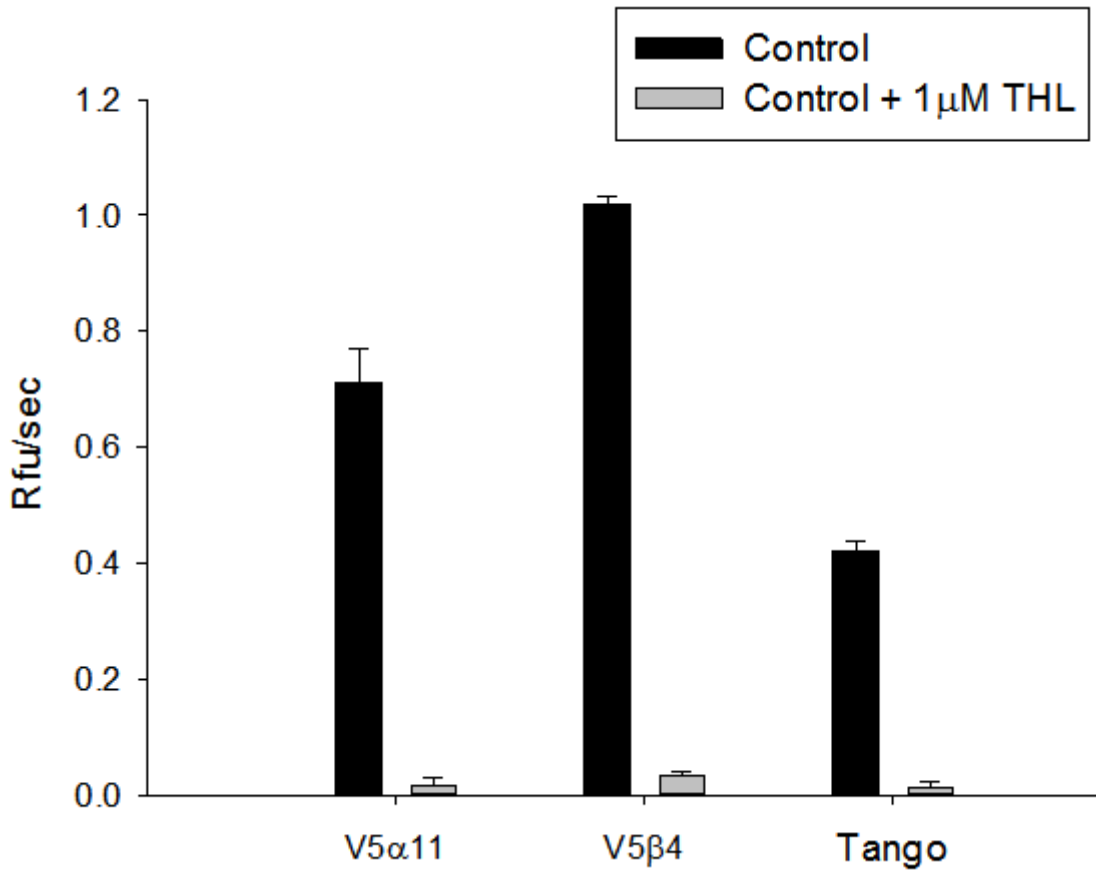

Figure 5.20. EnzChek as a tool to measure DAGLα and DAGLβ activity in membranes

Membranes were prepared from V5α11, V5β4, or Tango cells grown in McCoy's media supplemented with 10% FCS. Different concentrations of the membranes were incubated in the presence or absence of 1μM THL after which activity was measured using 2μM EnzChek by measuring the fluorescence (excitation 480nm, emission 540nm) every 48 seconds for 10 minutes. The reaction rates were calculated over 2 minutes and are presented above (mean of 3 wells ±SEM). This is a representative of two separate experiments.

5.2 Discussion and conclusions

Our results in the previous chapter showed that calcium, PKA and PKC can stimulate DAGL activity in a cellular context, as measured by CB1 activation (Tango assay). The results however did not reveal whether DAGLα, DAGLβ, or indeed both were responsible for the stimulated DAGL activity. In addition, overexpression of DAGLα (5-fold) had little if any effect on basal eCB tone in media containing 1% FCS and these cells showed only a modest (at best ~2-fold) increased response to the above stimuli (data not shown). Traditionally, DAGL activity is measured by the quantification of its product 2-AG, however this requires an expensive and elaborate laboratory set up (Balgoma et al., 2013). In this chapter, we therefore used surrogate DAGL substrates in conjunction with cell lines overexpressing DAGLα/β to investigate whether calcium, PKA or PKC could modulate the hydrolysis of these by DAGLα and/or DAGLβ.

We successfully developed a range of 96-well plate assays to study both DAGLα and DAGLβ activity, using either membranes or cells. These assays exploited affordable surrogate substrates, namely DiFMUO and PNPB that are capable of detecting and measuring DAGL catalytic activity (Pedicord et al., 2011). The larger DiFMUO is fluorogenic and by virtue of that more sensitive compared to the smaller chromogenic PNPB.

The cell lines overexpressing the DAGLs generally showed greater activity in these assays compared to the parental Tango cells (summarised in Table 5.1 and Table 5.2) and this difference in activity was inhibited by at least 2 different DAGL inhibitors. These assays can therefore undoubtedly measure DAGL catalytic activity. However, with the exception of the established enzyme inhibitors, our various attempts to modulate DAGL activity with the use of physiologically relevant stimuli using these surrogate substrates were unsuccessful. We included treatments that might be expected to reduce activity (starvation, phosphatase treatment, PKA inhibition) as well as treatments that might be expected to stimulate activity ($CaCl_2$, PKA activation, PKC activation).

At first glance, these results might indicate that PKA and PKC do not activate the DAGLs. However, before coming to that conclusion, it is important to first consider the nature of these substrates. Firstly and fore-mostly, these are surrogate substrates and therefore might be incapable of detecting certain structural features and mechanisms which influence the catalytic activity of the DAGLs against its native substrate DAG. In support of this - phosphorylation of HSL by PKA has been shown to increase its activity *in vitro* when using a triglyceride substrate but not when using PNPB as the substrate (Tsujita et al., 1989).

DAG is generally found integrated in the membrane (Goni and Alonso, 1999). The DAGLs are likely to use their transmembrane domains coupled with mechanisms like palmitoylation to sub localise them at the membranes, close to the substrate, and orient themselves in a manner facilitating DAG-catalytic site interaction. The regulatory loop (lid) is likely to be membrane and therefore substrate proximal, which would facilitate interfacial activation (potentially supported by phosphorylation). The surrogate substrate PNPB is relatively small in size (~3 times smaller than DAG) meaning that it may be able to access the catalytic site of the DAGLs through the aqueous phase (rather than membrane phase), therefore potentially by-passing any steric hindrance provided by the regulatory loop. This would explain why we observed ~10-fold difference in activity between V5α11 and Tango membranes in the PNPB assay but less than 2-fold difference in the DiFMUO assay (Table 5.1). DiFMUO is believed to access the catalytic site through the membrane (Pedicord et al., 2011). This could also explain why we did not observe any activation or inhibition of DAGL activity using the various treatment and stimuli in the PNPB assays.

If DiFMUO indeed accessed the catalytic site of the DAGLs through the membrane then one would expect mechanisms regulating the opened and closed conformation of the enzyme to affect the activity seen with the substrate. However none of the treatments affected the activity of the DAGLs in the DiFMUO assays. One possible explanation is that the smaller size (~2 times smaller than DAG) of DiFMUO coupled with other structural differences compared to DAG might once again enable this substrate to access the

catalytic site, even when the enzyme is in the 'closed' conformation. Another explanation is that the rate limiting step in DiFMUO hydrolysis is not the activity of the DAGLs but the actual rate of diffusion through the membrane (Pedicord et al., 2011). This is supported by the fact that the activity in our PNPB assays saturated at ~500μM substrate concentration and the activity measured using DAGL-DAG assays tend to saturate at a DAG concentration of 200-400μM (Pedicord et al., 2011; Shonesy et al., 2013). DiFMUO on the other hand showed saturation at a much lower concentration of ~10-20μM (differences in solubility between the substrates may also contribute to these differences between the substrates). Therefore, there are various reasons why the surrogate substrates PNPB and DiFMUO may potentially fail to differentiate between the 'open' and 'closed' state of the DAGLs. If this was the case then these substrates would also fail to detect phosphorylation events that would activate these enzymes by regulating the lid.

Rather than focussing on the negative results, it is useful to consider some of the interesting novel findings. Foremost amongst these was the observation in the differences in activity of DAGLα and DAGLβ towards the various surrogate substrates (Table 5.1 and Table 5.2). DAGLα-V5 was far more active (5-fold) than DAGLβ-V5 using PNPB as the substrate in the membrane assay. Western blotting analysis (using the V5 tag) did not indicate 5-fold higher expression levels of DAGLα-V5 (V5α11 Tango cells) compared to DAGLβ-V5 (V5β4 Tango cells). If anything the results showed higher DAGLβ-V5 expression levels. This indicated that the DAGLs probably showed different activities against this substrate. This was supported by the fact that when comparing activities of V5α11 and V5β4 cells or membranes, the difference in activity between the DAGLs appears much less pronounced using DiFMUO. Thus we can conclude that despite the very high homology, and the fact that they catalyse the same physiological reaction, there are in fact clear differences between the catalytic properties of DAGLα and DAGLβ.

In support, DAGLβ appears the more active of the two against a third substrate, EnzChek. These results indicated structural differences between the DAGLs that might indicate the possibility to develop selective inhibitors for each. Indeed, during the course of this work a report appeared that

identified a novel DAGLβ inhibitor with a 60-fold selective profile over DAGLα (Hsu et al., 2012). In the absence of a crystal structure for the DAGLs, mutagenesis studies in combination with the surrogate substrates might help further our understanding of both conserved and divergent features of the catalytic sites of these closely related enzymes. Additionally, size wise, the EnzChek substrate is ~5 times larger than PNPB, 3 times larger than DiFMUO and ~1.5 times larger than DAG. It would therefore be interesting to further study DAGL activity using this 'large' substrate, especially if steric hindrance due to the lid is a key regulatory mechanism for these enzymes. Unfortunately, it only became available for study towards the end of this thesis.

In conclusion, the surrogate substrates used here appear to be unsuitable to study DAGL activation mechanisms that govern the displacement of a regulatory lid to allow access of the physiological substrate DAG from the cell membrane to the active site of the enzymes. Although data was not obtained to support our hypothesis that PKA/PKC directly phosphorylate the DAGLs to activate them, it would be premature to discard the hypothesis as there are clear limitations to the use of surrogate substrates. In addition, time did not allow for a full evaluation of EnzChek as a substrate that possibly could reveal differences between an open and closed state of the enzymes given its relatively large size. Nevertheless, the work described in this chapter details various assays that are valuable tools to monitor DAGL activity, and would be especially useful to study and screen inhibitors targeting the catalytic site. In particular, I have developed the first living cell based assay for DAGLα using the PNPB substrate, and this has the potential to be used in high-throughput screens to identify DAGLα inhibitors that might be developed as novel pharmaceuticals.

Key questions that remained unanswered here is how do PKA/PKC stimulate the DAGLs? Do these kinases induce phosphorylation (directly/indirectly) of DAGLα/β? And if so, how do these phosphorylation events effect DAGL activity? In order to begin to address these questions we purified the DAGLs and used them in *in vitro* phosphorylation studies using purified PKA and

PKC to determine if they are indeed substrates for these kinases. This work is described in the next chapter.

Chapter 6 (Results 4): Generation of the purified active catalytic domain of the DAGLs for phosphorylation and other studies

6.1 Introduction

The structural mechanisms that govern DAGL function would be directly addressed by NMR and/or crystallography - this requires milligram quantities of highly pure catalytically active protein and although beyond the scope of the present study we reasoned that some headway might be made in related studies by embarking on this journey. For example, the phosphorylation status of the purified catalytic domain of these enzymes might be determined by mass-spec and it might be useful for direct biochemical studies with purified kinases to at least determine if the catalytic domain can serve as a kinase substrate. Identification of such sites would not only yield insights into the regulatory mechanism, it would also point the way to the generation of phospho-specific antibodies that might be able to serve as surrogate markers for the activation state of the DAGLs and also provide a means to identify the factors that function upstream of the DAGLs to regulate cell function.

In chapter 3 we discussed how phosphorylation of the DAGLs appears to be a likely mechanism to regulate their activity, especially as several phospho-sites in the DAGL sequences have been identified. In chapter 4 we demonstrated that PKA and PKC stimulated DAGL dependent eCB signalling in a cell based assay (Tango assay). We were therefore particularly interested in investigating whether PKA and PKC directly phosphorylated the DAGLs in order to activate them. We focussed on using mass spectrometry (MS) to try to identify phospho-sites as this is a highly sensitive method of choice within the field (Paradela and Albar, 2008; Macek et al., 2009; St-Denis and Gingras, 2012) and a service was available at KCL. However, success is still dependant on the abundance and ionisation properties of the phospho-peptide(s) obtained from the protein of interest and there are also complexities involved in MS based quantitation (Steen et al., 2006; Alcolea et al., 2009; Liebler and Zimmerman, 2013).

In an attempt to address this question, we decided to purify the DAGLs in order to perform *in vitro* phosphorylation studies using these kinases. The *E. coli* and baculovirus expression systems have been used for years to generate high yields of purified proteins for a range of applications including highly demanding X-ray crystallography applications which require large amounts of protein (several mgs) of high purity. The *E. coli* expression system, is the cheaper and quicker option, and relies on a plasmid-antibiotic selection system to overexpress the gene. On the other hand, the baculovirus is more expensive (not cost prohibitive) and requires the generation of a recombinant baculovirus which accounts for the longer timelines (~1 additional month) compared to *E. coli*. The biggest disadvantage of using *E. coli* is that it is a prokaryotic expression system and therefore can sometimes fail to express correctly folded, soluble mammalian proteins. The baculovirus-insect cell expression system on the other hand is a eukaryotic expression system and is therefore more amenable towards expressing complex mammalian proteins. These expression systems have been extensively reviewed (Kost et al., 2005; Francis and Page, 2010).

In this chapter I successfully expressed and purified the GST tagged catalytic domains (CD) of both DAGLs and then used a gel-shift assay to demonstrate that both PKA and PKC phosphorylated these proteins. No phospho-sites were detected within the DAGL sequence of GST-DAGLα CD and in addition to that this protein was inactive. On the other hand GST-DAGLβ CD was purified in the active form and was phosphorylated by both PKA and PKC within the RL. Details about the phospho-sites as well as the successful development of a phospho-specific antibody (pAb) against one of these sites are presented and discussed here.

6.2 Results

6.2.1 Summary of DAGL purification/phospho-mapping work

A summary of the work carried out to purify the DAGLs is described below and presented in Table 6.1 (DAGLα) and Table 6.2 (DAGLβ). We initially focussed on purifying endogenous DAGLα by immunoprecipitation (IP) from the mouse cerebellum where it is highly expressed.

Table 6.1. Summary of DAGLα purification work

Source/expression system	Construct	Purification	Comments
Mouse cerebellum	na	Immunoprecipitation	Poor MS coverage
Mammalian	DAGLα-V5	V5 Immunoprecipitation	Poor yields based on Coomassie stained gels
Insect cell	DAGLα-V5-6His	Ni-nta (His affinity)	No enrichment post purification
E. coli	DAGLα catalytic domain (6His or MBP tagged)	na	Insoluble expression, attempts to refold unsuccessful
Insect cell	6His-Tev-DAGLα catalytic domain	Ni-nta (His affinity)	No enrichment post purification suggesting tag not exposed to bind to resin
Insect cell	GST-DAGLα catalytic domain	Glutathione resin	Successful purification

Table 6.2. Summary of DAGLβ purification work

Source/expression system	Construct	Purification	Comments
Mammalian	DAGLβ-V5	V5 Immunoprecipitation	Poor yields based on Coomassie stained gels
Mammalian	DAGLβ-GFP	GFP Immunoprecipitation	Poor coverage by MS
Insect cell	DAGLβ-V5-6His	Ni-nta (His affinity)	No enrichment post purification
E. coli	DAGLβ catalytic domain (6His or MBP tagged)	na	Insoluble expression, attempts to refold unsuccessful
Insect cell	6His-DAGLβ catalytic domain	Ni-nta (His affinity)	No enrichment post purification suggesting tag not exposed to bind to resin
Insect cell	GST-DAGLβ catalytic domain	Glutathione resin	Successful purification

Various parameters in the IP protocol were optimised including the concentrations of antibody and cerebellar homogenate used. The IPs were resolved by SDS-PAGE and the area of the gel containing DAGLα (identified in parallel by Western blotting) was excised and trypsinised following which the peptides were extracted and lyophilised. The lyophilised peptides were then resuspended in 50mM ammonium bicarbonate and analysed by LC/MS/MS. Attempts to identify phospho-sites in the IP were disappointing, only a 5% of total sequence coverage was obtained following the MS analysis. The quantity of antibody required, coupled with the cost of the MS analysis, was prohibitive to pursue this approach any further. In addition to this there were no suitable antibodies available for endogenous DAGLβ IP at the time. We therefore turned our efforts towards overexpression systems, namely the mammalian, baculovirus, and *E. coli* systems.

Firstly, we focussed on DAGL (tagged) IPs from mammalian cell lines (untreated). If phospho-mapping from these IPs was successful then we intended to treat these cells with PKA/PKC activators prior to phospho-mapping in order to identify potential PKA/PKC dependent DAGL phospho-sites. At this stage we made a decision to only pursue MS (phospho-mapping) analyses on purified samples that were visible on Coomassie stained gels as this would generally ensure decent sequence coverage. DAGLα-V5 IPs using the V5 tag was successful (Western blotting) but insufficient to visualise on Coomassie stained gels so were abandoned. DAGLβ-GFP IP was also successful and the yields were sufficient enough to visualise the sample on Coomassie stained gels. However, no DAGLβ peptides were identified following mass-spectrometry, indicating the band visualised was non-specific.

Having failed to phospho-map the DAGLs from mammalian expression systems we directed our efforts towards the baculovirus-insect cell expression system, and the *E. coli* expression system. Our initial priority was to work with the full length proteins and so we successfully expressed both the full length DAGLs with a 6His tag using the baculovirus system; however our attempts to purify them using the 6His-tag were unsuccessful, possibly because the small tag (~1kDa) was not exposed.

We followed this up with attempts to purify the catalytic domain of the DAGLs using the 6His tags in both the baculovirus and *E. coli* expression systems. No soluble expression was obtained using *E. coli*, all the protein was found in inclusion bodies (aggregated, mis-folded). We successfully expressed the catalytic domains using the baculovirus system, but as with the full length, the 6His affinity purification was unsuccessful, probably because the tag was not exposed. We therefore expressed the catalytic domains with the larger (~26kDa) GST tag using the baculovirus system and using this strategy were able to successfully purify the catalytic domains. This will be described in more detail in the next section.

6.2.2 Expression of GST tagged DAGL catalytic domains using the baculovirus-insect cell expression system

Baculoviruses engineered to contain the genes expressing N-terminally GST tagged versions of the catalytic domains of either DAGLα or DAGLβ were generated as described in the methods section. The baculoviruses were then used to infect insect cells for expression studies.

In order to optimise the expression of GST-DAGLβ catalytic domain (GST-DAGLβ CD) a time course of expression was carried out. Insect cells (Sf9) were infected with recombinant baculoviruses containing the GST-DAGLβ CD gene and cell viability was monitored at different time points (0-96h). Recombinant baculoviruses not only infect but also amplify and propagate in Sf9 cells resulting in a decrease in cell viability. Cell viability is therefore a convenient way to monitor infection of Sf9 cells by the baculovirus. During the time course of this experiment a decrease in viability was observed (98% to 30%) indicating that the cells were successfully infected by the baculoviruses (data not shown). Cells were also collected at various time points and then lysed and analysed by Western blotting using a GST antibody. A band at the predicted molecular weight (~75kDa) was detected at all expression time points but not in the non-infected cells (0h) (Figure 6.1). Relative expression levels were found to be highest 48 hours post-infection (relative to 24 hours expression levels).

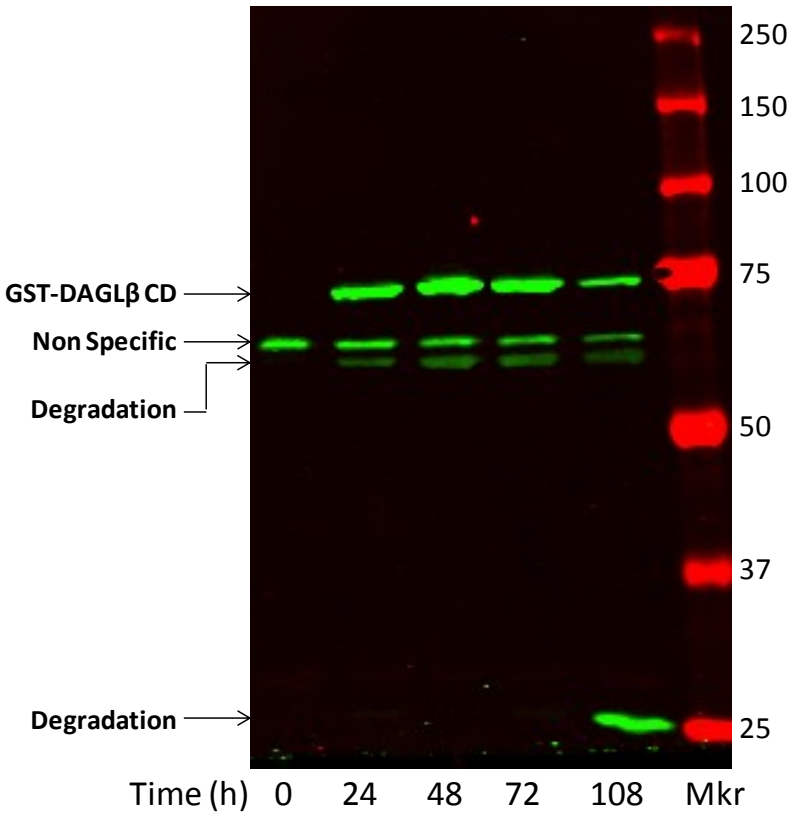

Figure 6.1. Expression time course of GST-DAGLβ CD reveals 48 hours as the optimum time point

Sf9 cells were infected with GST-DAGLβ CD baculoviruses and grown for 4 days. Cells were collected at different time points, lysed and 20µg lysates were analysed by Western blotting using a GST antibody.

An additional band at ~65kDa was detected; however this was also detected in the non-infected cells and was therefore deemed to be non-specific.

Another band ~60kDa was detected in all the samples except the non-infected cells and was deemed to be a degradation product of the full size protein. 48 hours was deemed to be an optimal time-point based on the ratio of the desired protein to the degradation products and was adopted for the follow up studies.

6.2.3 GST affinity purification of GST-DAGLβ CD

Having optimised expression of GST-DAGLβ CD the next step was to purify the protein using the GST tag. The hydrophobic regions in lipases make them prone to aggregation (Salameh and Wiegel, 2010) and to mitigate this Triton X-100 was used in the purification process (Linke, 2009). A high concentration of Triton X-100 (1%) was used to solubilise GST-DAGLβ CD during lysis and then lower concentrations (0.05%) were employed to elute and store the protein, as described in other membrane protein purification protocols (Linke, 2009; Rice et al., 2009). Cells were lysed by dounce homogenisation in the purification buffer (50mM Tris, 150mM NaCl, 2mM DTT, pH 7.8) containing 1% Triton X-100 and then incubated for 2 hours (4ºC). The lysates were then subjected to centrifugation (75,000g for 60 minutes). Following this the supernatant was collected and incubated with GST binding beads (Glutathione sepharose 4B) for 30 minutes. The beads were collected in a plastic drip column and washed with the purification buffer. Following this, 0.5ml elution fractions were collected using the elution buffer (purification buffer containing 0.05% Triton X-100 and 50mM glutathione). The GST elutions obtained were then analysed (20µl) by Coomassie stained SDS-PAGE. A prominent band at the predicted size of GST-DAGLβ CD (~75kDa) was detected in the elutions (Figure 6.2). The purity was adjudged to be ~50% with the major contaminants detected at ~25kDa. Due to the significant size difference between the contaminants and the full size protein gel filtration chromatography was used to further purify the GST-DAGLβ CD.

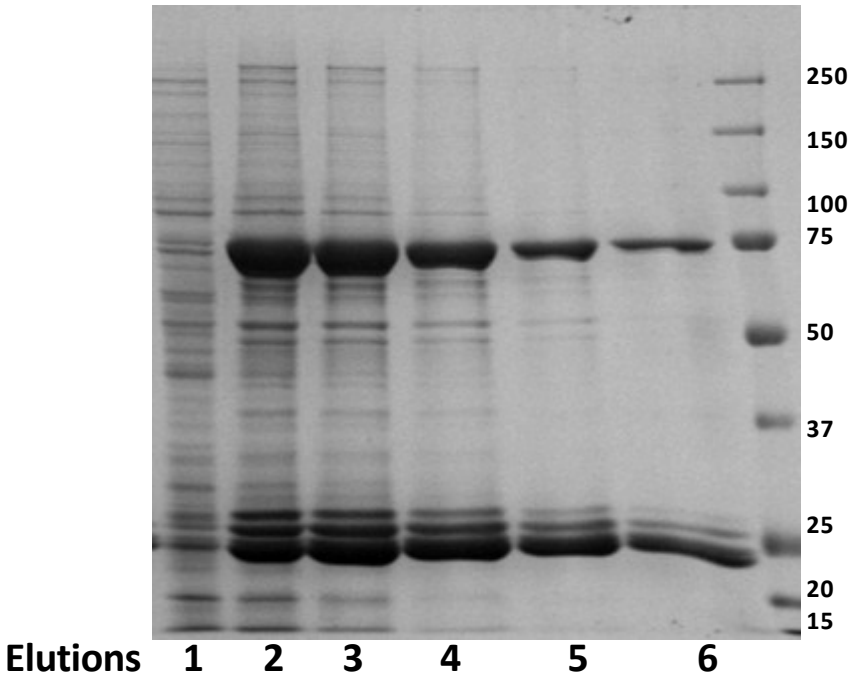

Figure 6.2. GST affinity purification of GST-DAGLβ CD

GST-DAGLβ CD (75kDa) was expressed in insect cells and then lysed (solubilised) in the purification buffer (50mM Tris, 150mM NaCl, 2mM DTT, pH 7.8) containing 1% Triton X-100. Clarified lysates obtained post solubilisation were incubated with glutathione sepharose 4B beads for 30 minutes. The beads were then collected, and washed. Bound protein was eluted using elution buffer containing 50mM glutathione and 0.05% Triton X-100. 20µl of the elutions were analysed by Coomassie stained SDS-PAGE and is presented above.

This step would also enable the measurement of the native molecular weight of the purified GST-DAGLβ CD as well as a buffer exchange of the protein to a suitable storage buffer (without high concentrations of glutathione).

6.2.4 Gel filtration purification of GST-DAGLβ CD

The GST elutions were further purified by gel filtration using a S200 column (HiLoad 13/300 Superdex 200). 0.5ml of the GST elution (2nd elution in Figure 6.2) were subjected to gel filtration chromatography in the purification buffer (50mM Tris, 150mM NaCl, 2mM DTT) containing 0.05% Triton X-100. Any fractions corresponding to peaks in the chromatogram (absorbance at 280nm - A280) (Figure 6.3A) were analysed by Coomassie stained SDS-PAGE (Figure 6.3B). A chromatogram (provided by the manufacturer) of protein standards separated using this column (not shown) was used to determine the approximate molecular weights of the fractions obtained following the gel filtration purification.

The first peak corresponded to a molecular weight of >600kDa and consisted mostly of GST-DAGLβ CD (fractions 5-10ml). This was likely to be aggregated as indicated by the high native molecular weight of this fraction and the fact that the molecular weight of GST-DAGLβ CD is 75kDa. The second peak (estimated molecular weight ~160kDa) predominantly consisted of GST-DAGLβ CD (probably dimeric, especially as GST has a propensity to dimerise (Waugh, 2005) was collected in fractions 12-13ml. The next peak (~80kDa) contained much lower levels of the protein. Subsequent peaks corresponding to the lower molecular weight impurities were also observed. GST-DAGLβ CD was therefore successfully separated from the lower molecular weight contaminants, predominantly in 'aggregated' or 'dimeric' forms.

Surprisingly the higher amounts of 'aggregated' GST-DAGLβ CD compared to the 'dimeric' form obtained (Figure 6.3B) following the purification did not correspond to a larger peak in the chromatogram (Figure 6.3A). Triton X-100 absorbs light at 280nm which probably accounts for this. Triton X-100 micelle size is ~90kDa.

Figure 6.3. Gel filtration purification of active GST-DAGLβ CD (~75kDa)

0.5mls of the elutions from the GST affinity purification (elution 2 Figure 6.2) were loaded onto a S200 column (HiLoad 13/300 Superdex 200 GL). The purification buffer (50mM Tris, 150mM NaCl, 2mM DTT) contained 0.05% Triton X-100. The chromatogram (absorbance at 280nm) of the fractions collected and the corresponding Coomassie stained SDS-PAGE analysis (20µl) of the fractions are presented above (A and B). Estimated molecular weights of the peaks are annotated above, indicating whether the purified DAGL is likely to be in the aggregated or dimeric form. Activity of these fractions was tested using EnzChek. Equal volumes of the fractions were incubated in the presence or absence of THL (1µM) for 5 min after which EnzChek (2µM) was added. Activity was monitored by measuring the fluorescence (excitation 480nm, emission 540nm) every 48 seconds for 10 minutes. The reaction rates were calculated over 2 minutes and are presented above (C) (mean of 3 wells ±SEM).

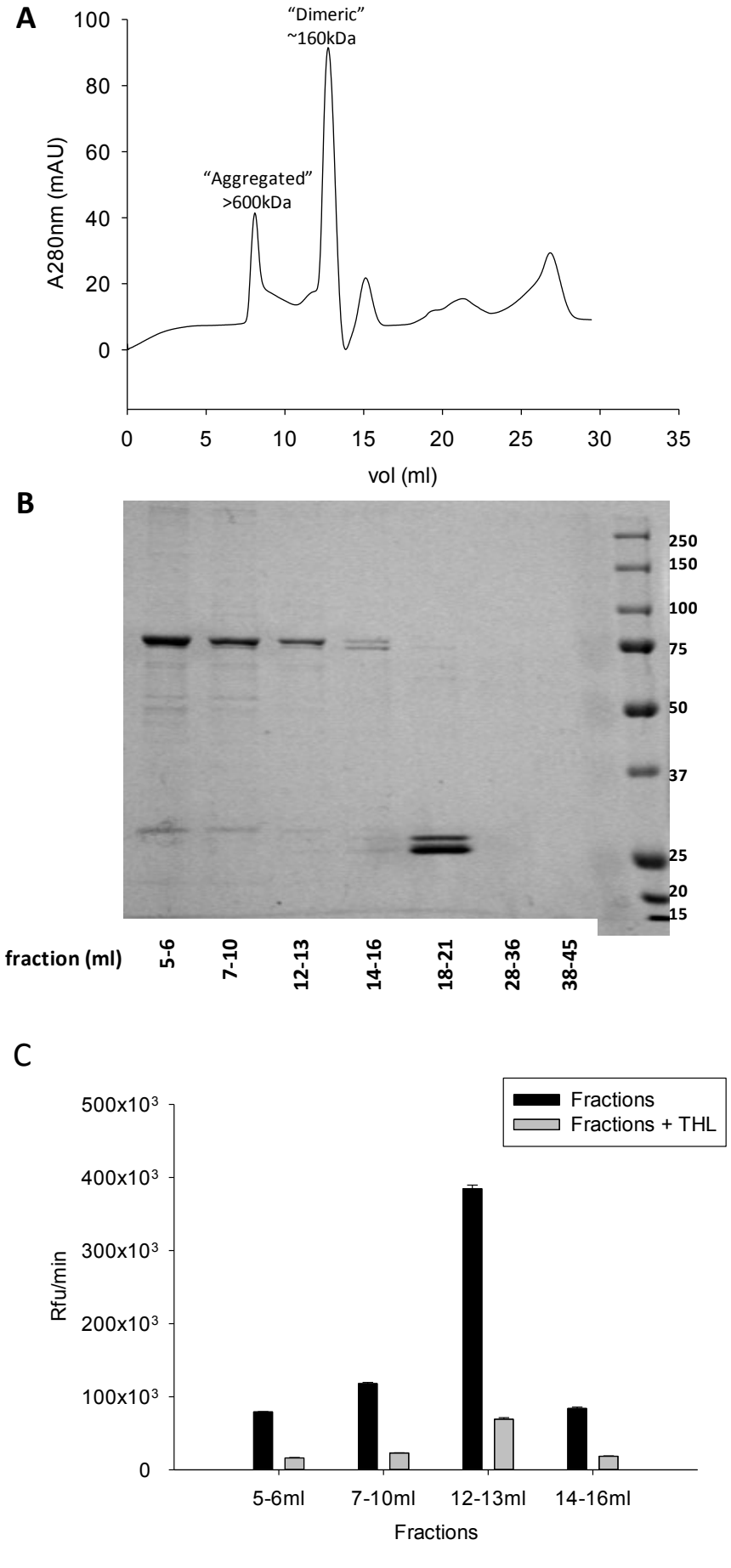
A
"Dimeric"
~160kDa
"Aggregated"
>600kDa
A280nm (mAU)
vol (ml)
B
250
150
100
75
50
37
25
20
15
fraction (ml)
5-6
7-10
12-13
14-16
18-21
28-36
38-45
C
Fractions
Fractions + THL
Rfu/min
Fractions
5-6ml
7-10ml
12-13ml
14-16ml

The peaks observed between 12-13ml could therefore correspond to either dimerised GST-DAGLβ CD (~150kDa) or a single GST-DAGLβ CD molecule associated with a Triton-X100 micelle (~165kDa) or indeed a mixture of both. We next compared the activities of the fractions.

The activity of equal volumes of the fractions was tested using the commercially available fluorogenic lipase substrate EnzChek (2μM) in the presence or absence of 1μM THL (DAGL inhibitor). THL sensitive activity was detected in both the 'aggregated' and 'dimeric' fractions but the activity was notably higher in the 'dimeric' fractions despite the fact that this fraction had relatively low amounts of protein (Figure 6.3B and C). When normalised for protein concentration, the activity of the 'dimeric fraction was ~5-fold more active than any other fraction (data not shown). These results demonstrate that the GST-DAGLβ CD fraction following gel filtration, that appeared to have a native molecular weight greater than 600kDa, was likely to be aggregated and largely inactive. On the other hand the 'dimeric' fraction was found to be active.

To summarise the results above GST affinity and gel filtration chromatography were successfully combined to purify active GST-DAGLβ CD at >80% purity. Additionally, including Triton X-100 in the purification was critical to enhancing the yield of the active protein (220μg/L insect cell culture) when compared to other detergents like DDM (90μg/L dimeric fraction but mostly inactive), Elugent (130μg/L) or LDAO (interfered with GST affinity purification) or to a detergent free purification (<10μg/L) (data not shown). We next used these conditions to purify the GST tagged catalytic domain of DAGLα (GST-DAGLα CD) as described in the next section.

6.2.5 Purification of GST-DAGLα CD

GST-DAGLα CD was expressed and purified as described for DAGLβ above. Following the GST affinity purification, GST-DAGLα CD was obtained at similar purity levels to GST-DAGLβ CD, a highly enriched band observed at ~75kDa corresponding to GST-DAGLα CD was accompanied by prominent lower molecular contaminants at ~25kDa (Figure 6.4A).

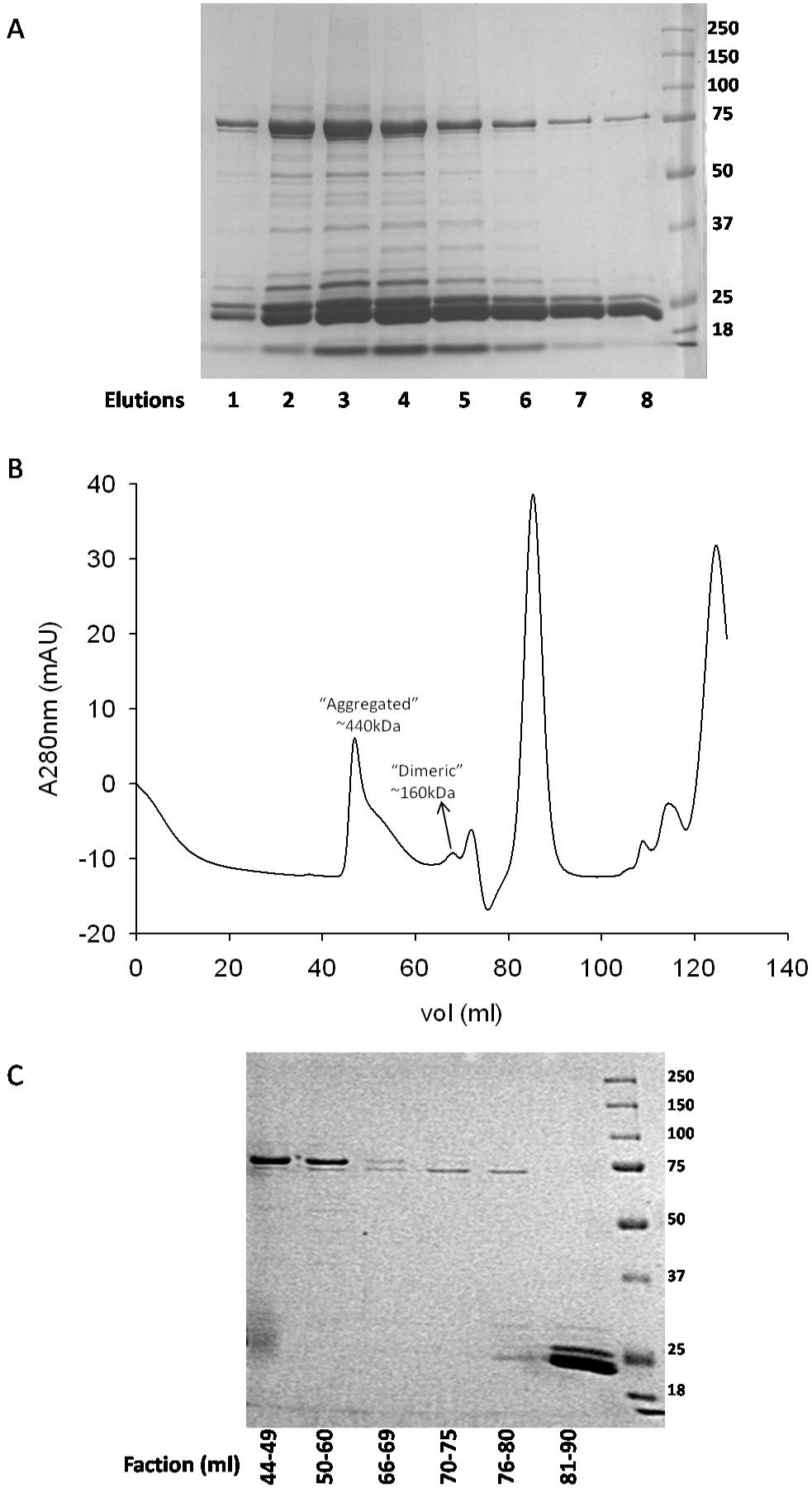
A
250
150
100
75
50
37
25
18
Elutions 1 2 3 4 5 6 7 8
B
A280nm (mAU)
40
30
20
10
0
-10
-20
"Aggregated"
~440kDa
"Dimeric"
~160kDa
0 20 40 60 80 100 120 140
vol (ml)
C
250
150
100
75
50
37
25
18
Faction (ml)
44-49
50-60
66-69
70-75
76-80
81-90

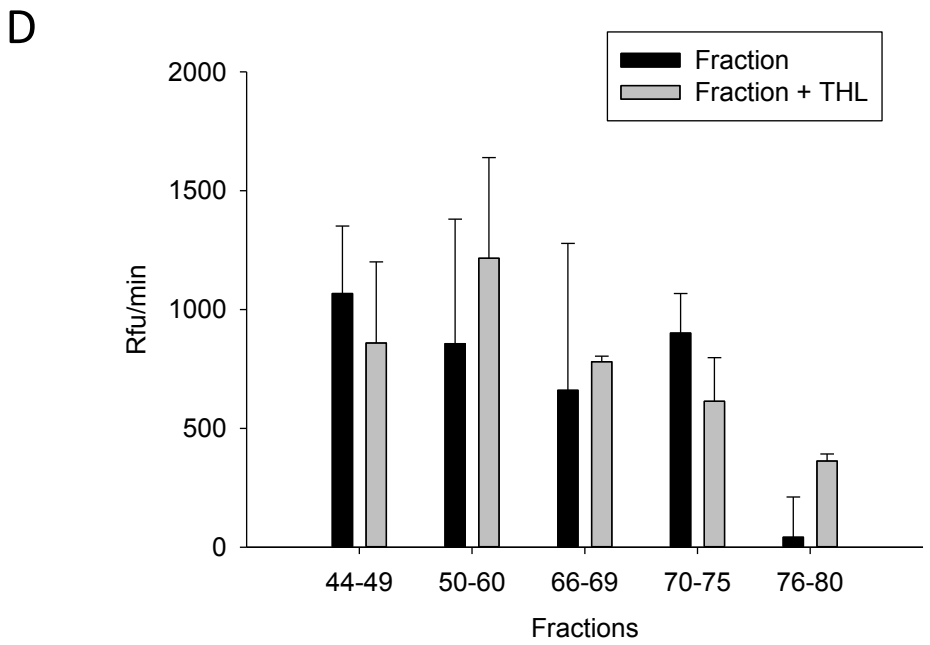

Figure 6.4. Purification of GST-DAGLα CD using GST affinity and gel filtration chromatography

Lysates obtained from Sf9 cells infected with GST-DAGLα CD (75kDa) baculoviruses were lysed in the presence of 1% Triton X-100 after which GST-DAGLα CD was captured using glutathione sepharose 4B beads and eluted in the presence of 0.05% Triton X-100 using 50mM glutathione. Equal volumes of the elutions were analysed by Coomassie stained SDS-PAGE (A). Elutions 2-7 (3mls) were loaded onto a S200 column (HiLoad 16/600 Superdex 200 prep grade) and 1ml fractions were collected. Fractions associated with the peaks observed in the A280 chromatogram (B) were analysed (20µl) by Coomassie stained SDS-PAGE (C). Estimated molecular weights of the peaks are annotated above, indicating whether the purified DAGL is likely to be in the aggregated (44-60ml) or dimeric (66-69ml) form. Activity of these fractions was tested using EnzChek. Equal volumes of the fractions were incubated in the presence or absence of THL (1µM) for 5 min after which activity was measured using EnzChek (2µM) as previously described and is presented as the mean of 3 replicate wells ±SEM (D).

The GST elutions were further purified using gel filtration (S200 column - HiLoad 16/600 Superdex 200 prep grade). As with GST-DAGLβ CD, the lower molecular weight contaminants were effectively separated from GST-DAGLα CD but most of the GST-DAGLα CD was collected in fractions (40-60ml) with a native molecular weight ~440kDa and was therefore likely to be aggregated (Figure 6.4B and C).

Smaller amounts of GST-DAGLα CD were collected in the fractions (66-69ml) corresponding to a native molecular weight of ~160kDa. This fraction consisted of a doublet at ~75kDa when analysed by Coomassie stained SDS-PAGE (Figure 6.4C). Only the upper band was found to be immuno-reactive to a GST antibody (data not shown) indicating that the lower band was an insect/baculovirus protein. This band was subsequently identified as a heat shock protein (HSP) and will be discussed further down. The GST-DAGLα CD in this fraction is therefore likely to exist as a homodimer or as a heterodimer with the HSP. Additional fractions containing mainly of what appeared to be the HSP were also collected (70-80mls).

The activity of the fractions obtained following the gel filtration purification was tested using EnzChek as the substrate. The activity detected in these fractions (Figure 6.4D) was extremely low compared to the GST-DAGLβ CD fractions (Figure 6.3C). In addition to that, no THL sensitive activity was detected indicating that the GST-DAGLα CD present in the fractions was inactive. Additionally, no THL sensitive activity was detected in the fractions using a different DAGL surrogate substrate PNPB (data not shown). However this did not necessarily preclude the use of GST-DAGLα CD as a substrate for PKA and PKC to identify phospho-sites which is discussed in the next section.

6.2.6 *In vitro* phosphorylation studies of GST-DAGLα CD

Our results in chapters 3 and 4 demonstrated that the DAGLs are phosphorylated and that both PKA and PKC can stimulate DAGL activity in a cellular context. In order to test whether PKA and PKC can directly phosphorylate DAGLα, the purified DAGLα catalytic domain was used as part of *in vitro* phosphorylation (IVP) studies. In order to monitor IVP, a

phosphate-binding molecule (Phos-tag) was used as part of a gel shift assay. Migration of phosphorylated proteins is retarded in SDS-PAGE gels containing Phos-tag as a result of which phosphorylated and non-phosphorylated forms of a protein can be resolved to a greater extent than generally seen in a standard SDS-PAGE gel (Kinoshita et al., 2006).

The ability of PKA and PKC to phosphorylate GST tagged myelin basic protein (GST-MBP) was first tested as a positive control (Kishimoto et al., 1985). GST-MBP (1μM) was incubated with either PKA (0.1μM) or PKC (0.1μM) in IVP buffer (50mM Tris, 0.05% Triton X-100, 2mM DTT pH 7.8, 2.4mM ATP and 240mM MgCl2) for 1 hour at 30ºC. The samples were then resolved by SDS-PAGE gels containing 70μM Phos-tag and detected by Western blotting using a GST antibody. A kinase dependent shift in GST-MBP incubated with either PKA or PKC confirmed that Phos-tag could be used to detect IVP and that the PKA and PKC employed were both active (Figure 6.5A). GST-DAGLα CD (0.5μM) was then incubated with either PKA or PKC (0.1μM) in IVP buffer for 1 hour at 30ºC. The samples were resolved by SDS-PAGE gels containing 70μM Phos-tag and detected by Western blotting using a GST antibody. No shift was observed in the PKA treated samples (Figure 6.5A), even when incubated for longer time periods (1-3 hours) (Figure 6.5C). On the other hand, a PKC dependent shift in the GST-DAGLα CD samples was observed indicating that PKC could directly phosphorylate GST-DAGLα CD *in vitro* (Figure 6.5A).

This shift was also found to be ATP dependent further validating the kinase dependency of this reaction (Figure 6.5B). It is worth mentioning here that GST-DAGLα CD was found to be unstable when stored at -80ºC, smaller fragments were identified on Coomassie stained SDS-PAGE when analysed after two months of storage (GST-DAGLβ CD was found to be stable) (Figure 6.5D). At least one of the fragments was found to be GST immunopositive and was also phosphorylated by PKC (Figure 6.5E).

Figure 6.5. Detection of PKC (but not PKA) mediated phosphorylation of GST-DAGLα CD *in vitro*

GST-MBP and GST-DAGLα CD were incubated in the presence or absence of PKA or PKC in IVP buffer. The samples were incubated for 1 hour at 30°C after which they were resolved using SDS-PAGE containing 70μM Phos-tag and analysed by Western blotting using a GST antibody (A) This was repeated using GST-DAGLα CD but with ATP excluded from the IVP buffer (B) or for longer incubation times (C). Stability of GST-DAGLα CD and GST-DAGLβ CD stored at -80°C was analysed by Coomassie stained SDS-PAGE (D). GST-DAGLα CD was found to be unstable, at least one of the fragments was GST immunopositive (Western blotting using Phos-tag 70μM) (E). This band was also phosphorylated by PKC (A, B, E).

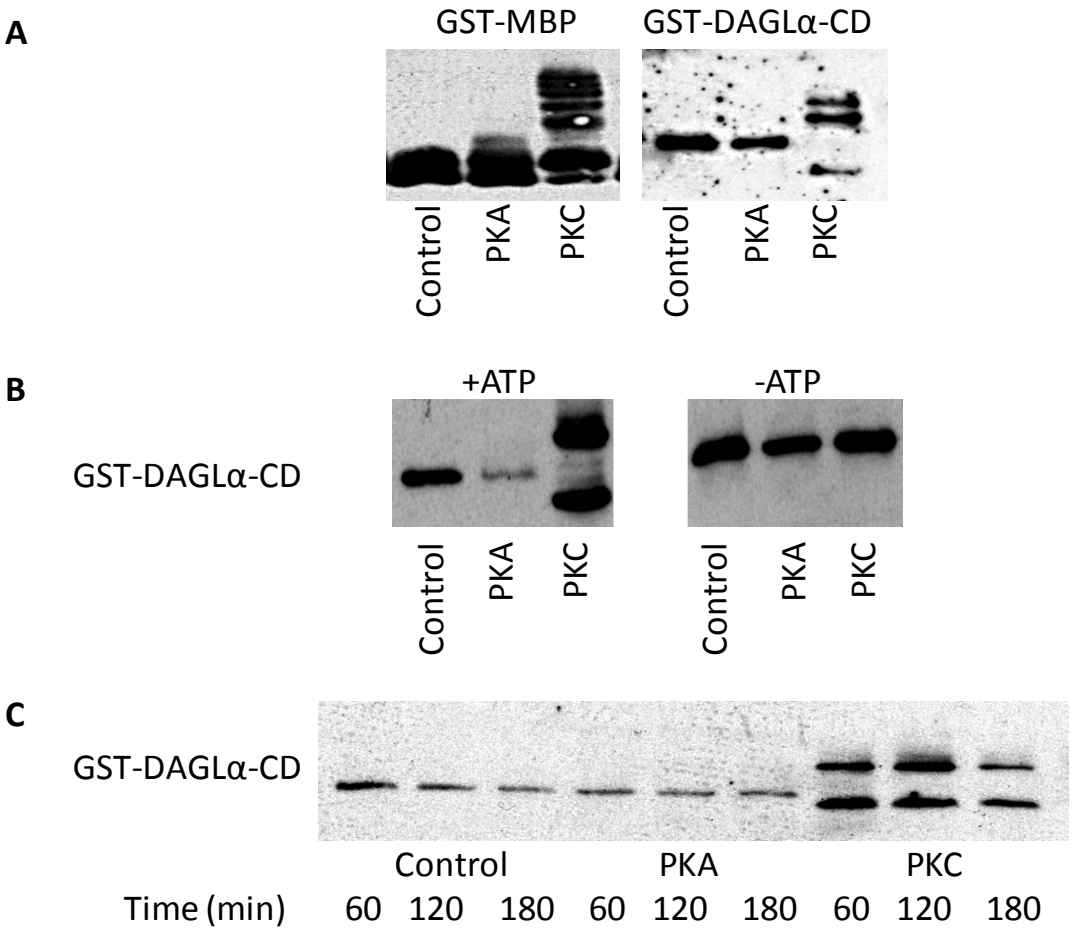
A
GST-MBP
GST-DAGLα-CD
Control
PKA
PKC
Control
PKA
PKC
B
+ATP
-ATP
GST-DAGLα-CD
Control
PKA
PKC
Control
PKA
PKC
C
GST-DAGLα-CD
Control
PKA
PKC
Time (min) 60 120 180 60 120 180 60 120 180

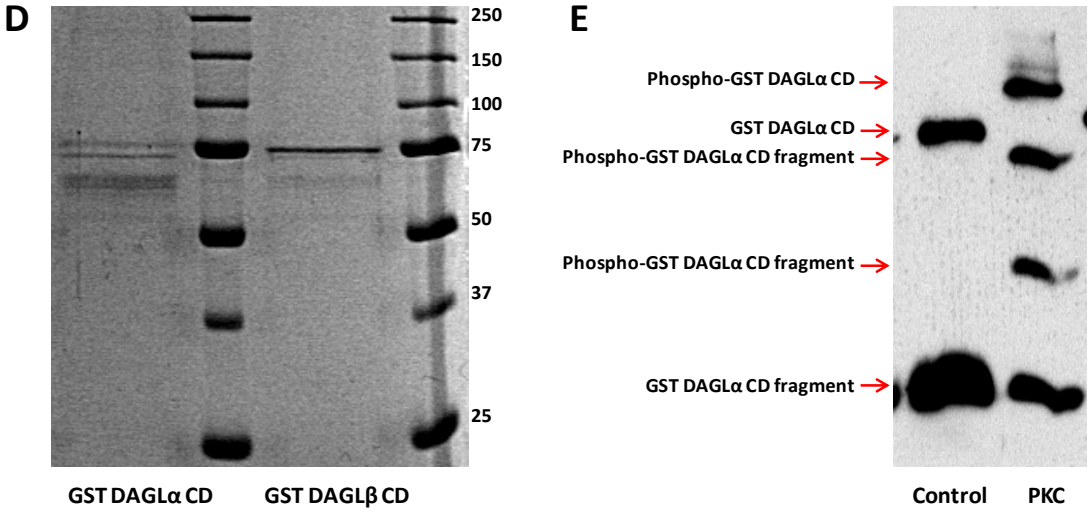
D
250
150
100
75
50
37
25
GST DAGLα CD
GST DAGLβ CD
E
Phospho-GST DAGLα CD
GST DAGLα CD
Phospho-GST DAGLα CD fragment
Phospho-GST DAGLα CD fragment
GST DAGLα CD fragment
Control
PKC

For phospho-mapping studies GST-DAGLα CD was treated with PKC using the conditions mentioned above (0.1μM PKC, 30°C, 1 hour). The samples were then analysed by Coomassie stained SDS-PAGE and the bands corresponding to GST-DAGLα CD were excised and trypsinised. The peptides obtained were subjected to MS analysis as described in the methods section.

Only 50% sequence coverage was achieved using mass spectrometry, the phospho-sites identified are shown in Table 6.3. No phospho-sites were identified in the DAGLα sequence, all the sites identified were located in a linker region between the GST tag and the DAGLα sequence in the PKC treated sample. Furthermore, the protein (~75kDa) found to co-purify with GST-DAGLα-CD following gel filtration was identified in these MS studies as a heat shock protein (HSP). HSPs are involved in protein folding and the purified GST-DAGLα CD is therefore probably an incompletely folded heterodimer (with the HSP), relying on the HSP to prevent it from aggregating. As the GST-DAGLα CD was also found to be inactive in the enzyme assay and unstable on storage we did not progress this work any further.

6.2.7 *In vitro* phosphorylation studies of GST-DAGLβ CD

In order to examine whether PKA and PKC could directly phosphorylate the catalytic domain of DAGLβ we employed IVP studies, similar to the DAGLα studies above. GST-DAGLβ CD (1μM) was incubated with either 0.1μM PKA or 0.1μM PKC in IVP buffer for 1 hour at 30ºC. The samples were then resolved by SDS-PAGE gels containing 70μM Phos-tag and detected by Western blotting using a GST antibody.

A kinase dependent shift was observed in the GST-DAGLβ CD samples indicating that both PKA and PKC could directly phosphorylate GST-DAGLβ CD *in vitro* (Figure 6.6A). This reaction was also found to be ATP dependent further validating the kinase dependency of this reaction (Figure 6.6B). A complete shift in GST-DAGLβ CD was not observed following kinase treatment; further optimisation experiments were therefore carried out to improve the IVP conditions.

Table 6.3. Phospho-sites identified in GST-DAGLα CD following PKC treatment

Phospho-sites (construct numbering)	Phospho-sites (Native sequence numbering)	GST/Linker/ CD/RL	Control	PKC
T228	na	Linker	No	Yes
S229	na	Linker	No	Yes
T241	na	Linker	No	Yes
S243	na	Linker	No	Yes

(linker - sequence between GST and DAGL, CD - catalytic domain, RL - regulatory loop)

Figure 6.6. PKA and PKC can phosphorylate GST-DAGLβ CD *in vitro*

GST-MBP and GST-DAGLβ CD were incubated in the presence or absence of PKA or PKC in IVP buffer. The samples were incubated for 1 hour at 30°C after which they were resolved using SDS-PAGE containing 70μM Phos-tag and analysed by Western blotting using a GST antibody (A) This was repeated using GST-DAGLβ CD but with ATP excluded from the IVP buffer (B) or for longer incubation times (C). The effects of a shorter 30 minute incubation time, temperature (30°C versus 37°C) and PKA/PKC concentration (0.1μM versus 1μM) were also tested (D).

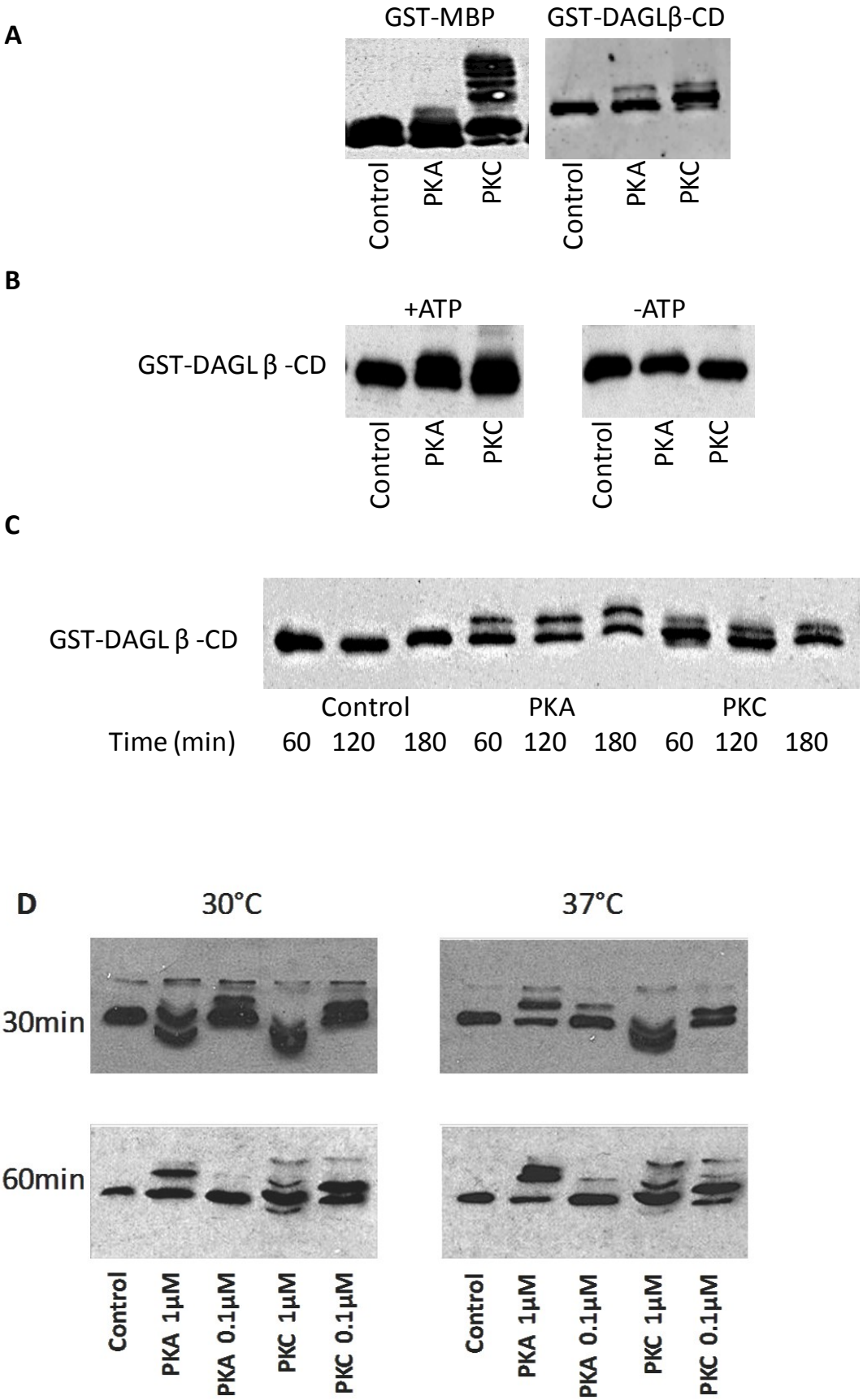
A
GST-MBP
GST-DAGLβ-CD
Control
PKA
PKC
Control
PKA
PKC
B
+ATP
-ATP
GST-DAGL β -CD
Control
PKA
PKC
Control
PKA
PKC
C
GST-DAGL β -CD
Control
PKA
PKC
Time (min)
60 120 180 60 120 180 60 120 180
D
30°C
37°C
30min
60min
Control
PKA 1μM
PKA 0.1μM
PKC 1μM
PKC 0.1μM
Control
PKA 1μM
PKA 0.1μM
PKC 1μM
PKC 0.1μM

Firstly, longer incubation times were tested, however no major time dependent increase in phosphorylation was observed when comparing 1, 2 or 3 hour incubation times (Figure 6.6C). The effects of kinase concentration (0.1 or 1μM) and temperature (30ºC versus 37ºC) along with two incubation times (30 and 60min) was also tested (Figure 6.6D). In the case of PKA, no difference in phosphorylation was observed between the 30 min and 60 min incubation times at either kinase concentrations or temperatures. Higher concentrations of PKA resulted in increased phosphorylation at both temperatures. Incubation at 37ºC resulted in phosphorylation of a greater proportion of GST-DAGLβ CD when compared to 30ºC, when using the higher concentration of PKA (1μM). In future experiments GST-DAGLβ CD was therefore incubated with 1μM PKA at 37ºC for 30 minutes. In the case of PKC, the higher concentrations of the kinase impeded the visualisation of GST-DAGLβ CD causing wavy bands. The lower concentration (0.1μM) shifted a large proportion of the GST-DAGLβ CD when incubated for 60 min at 37ºC and so these conditions were used in further experiments.

Phosphatase treatment of the GST-DAGLβ CD did not cause a shift in the Phos-tag assay indicating no background phosphorylation (data not shown). For phospho-mapping studies GST-DAGLβ CD was treated with PKA and PKC using the optimised conditions mentioned above. The samples were then analysed by Coomassie stained SDS-PAGE and the bands corresponding to GST-DAGLβ CD were excised and trypsinised. The peptides obtained were subjected to MS analysis as described in the methods section. 70% sequence coverage was achieved using mass spectrometry which also identified several phospho-sites (Table 6.4).

Surprisingly, 6 phospho-sites were identified in the control (no kinase) sample, 4 of which were within the DAGLβ CD sequence and 2 of which were within the regulatory loop. Both of the regulatory loop sites pS574 and pS584 have been previously identified as phospho-sites by others (Table 3.2, chapter 3).

Table 6.4. Phospho-sites identified in GST-DAGLβ CD following PKA and PKC treatment

Phospho-sites (construct numbering)	Phospho-sites (Native sequence numbering)	GST/Linker /CD/RL	Control	PKA	PKC
T228	**na**	Linker	**Yes**		**Yes**
S229	**na**	Linker	**Yes**		**Yes**
Y327	**Y318**	CD			**Yes**
S377	**S368**	CD	**Yes**		
S510	**S501**	CD	**Yes**		
S579	**S570***	RL		**Yes**	
S583	**S574***	RL	**Yes**		**Yes**
S593	**S584***	RL	**Yes**	**Yes**	
S614	**S605**	RL			**Yes**
S626	**S617**	CD			**Yes**

*S570 identified in 3 published and 0 CST reports
*S574 identified in 1 published and 17 CST reports
*S584 identified in 5 published and 0 CST reports
(see Table 3.2 for references)

(linker - sequence between GST and DAGL, CD - catalytic domain, RL - regulatory loop)

The relative amounts of phosphorylated GST-DAGLβ CD in the control sample could not be determined using the mass spectrometry data; however the fact that no shift in the GST-DAGLβ CD band was observed following phosphatase treatment probably indicates that only a small proportion of the sample was phosphorylated. Only 3 of the 6 sites identified in the control were also identified in the PKC treated samples (2 in the linker region and 1 in the regulatory loop). This discrepancy between the control and kinase treated sample was unexpected. Contaminating phosphatases in the purified PKC (commercial source) could provide a possible explanation for this. 3 additional sites were also identified in the PKC treated sample, one of which is a tyrosine. This was again surprising as PKC is a Serine/Threonine kinase. Once again, a contaminating kinase in the purified PKC (commercial source) could provide a possible explanation for this. Both the other phospho-sites were located with the catalytic domain (pS605, pS617), one of which was within the regulatory loop (pS605). Neither of these sites has been previously reported.

In the case of the PKA treated sample, only 1 of the 6 phospho-sites identified in the control was detected (S584). Contaminating phosphatases in the purified PKA (commercial source) could once again provide a possible explanation for this. Furthermore, the site (S584) that was identified in the control and PKA treated sample lies within a PKA consensus sequence. IVP by PKA may have out-competed the action of the contaminating phosphatases. As mentioned above, this phospho-site is located in the regulatory loop and has been identified in the literature (Table 3.2, chapter 3). The other phospho-site (S570) identified in the PKA treated sample was not identified in the control, was located within the regulatory loop, lies within a PKA consensus sequence and has been previously reported in the literature (Table 3.2 and Table 3.4, chapter 3).

The fact that both these phospho-sites have been previously reported, on more than one occasion, indicated that phosphorylation at these sites may be physiologically relevant. As the final part of this project we had pAbs against these two (S570 and S584) sites generated (Eurogentec) in order to study these phosphorylation events within cells. To date, we have been unable to

get the pS584 pAb to work in Western blotting, immunohisto/cytochemical studies or by ELISA. Work is ongoing to optimise the conditions using this pAb in those experimental formats. The last section of this thesis will focus on recent results obtained using the pS570 pAb.

6.2.8 Studying phosphorylation of DAGLβ at S570 in a cellular context

In order to establish whether the S570 pAb could be used as an analytical tool, the pAb was tested by Western blotting using membranes prepared from the V5β4 cells (cultured in McCoy's media 10% FCS). The V5β4 cells are Tango cells that stably overexpress human DAGLβ-V5 by 5-fold compared to the endogenous gene (Figure 4.15, chapter 4). Tango membranes were also included in the experiment as a negative control.

The pAb was tested at different dilutions (1/100 to 1/1000) using different blocking agents (milk versus BSA). All dilutions of antibodies and blocking agents were carried out in PBS 0.01% Tween (PBST). When both the S570 pAb and the corresponding secondary antibody (rabbit HRP conjugate) were diluted in blocking buffer containing 2% BSA, several bands were detected (Figure 6.7A). No difference was observed between the V5β4 and Tango membranes at any of the antibody dilutions. This indicated that the pAb was either extremely non-specific or that the blocking conditions were inadequate. 2% milk PBST was next used to dilute both the antibodies. This reduced the overall intensity of the bands detected (compared to BSA) although several bands were still detected in both samples (Figure 6.7B). Notably, a band was detected at ~75kDa, in the V5β4 samples when using lower dilutions of the pAb (1/100, 1/200), and this is the predicted and observed molecular weight for human DAGLβ-V5. This band was absent/less prominent in the Tango samples indicating that the pAb could recognise human DAGLβ-V5.

Furthermore, when the pAb was diluted using 2% BSA but the secondary was diluted using 2% milk, several of the non-specific bands detected using the other blocking conditions were not visualised and a prominent band at ~75kDa was detected in the V5β4 samples at all 3 dilutions using these blocking conditions (Figure 6.7C). These results demonstrated that the pAb could indeed detect DAGLβ-V5.

Figure 6.7. Optimisation of Western blotting conditions for the DAGLβ pS570 antibody

V5β4 and Tango membranes (10µg) were analysed by Western blotting using different dilutions of the DAGLβ pS570 antibody as indicated. Different blocking conditions were tested for the primary and corresponding secondary (rabbit HRP conjugate) antibody as follows. Primary and secondary diluted in 2% BSA PBST (A), primary and secondary diluted in 2% Milk PBST (B), primary diluted in 2% BSA PBST and secondary diluted in 2% Milk PBST (C). Longer exposure also presented for C (D).

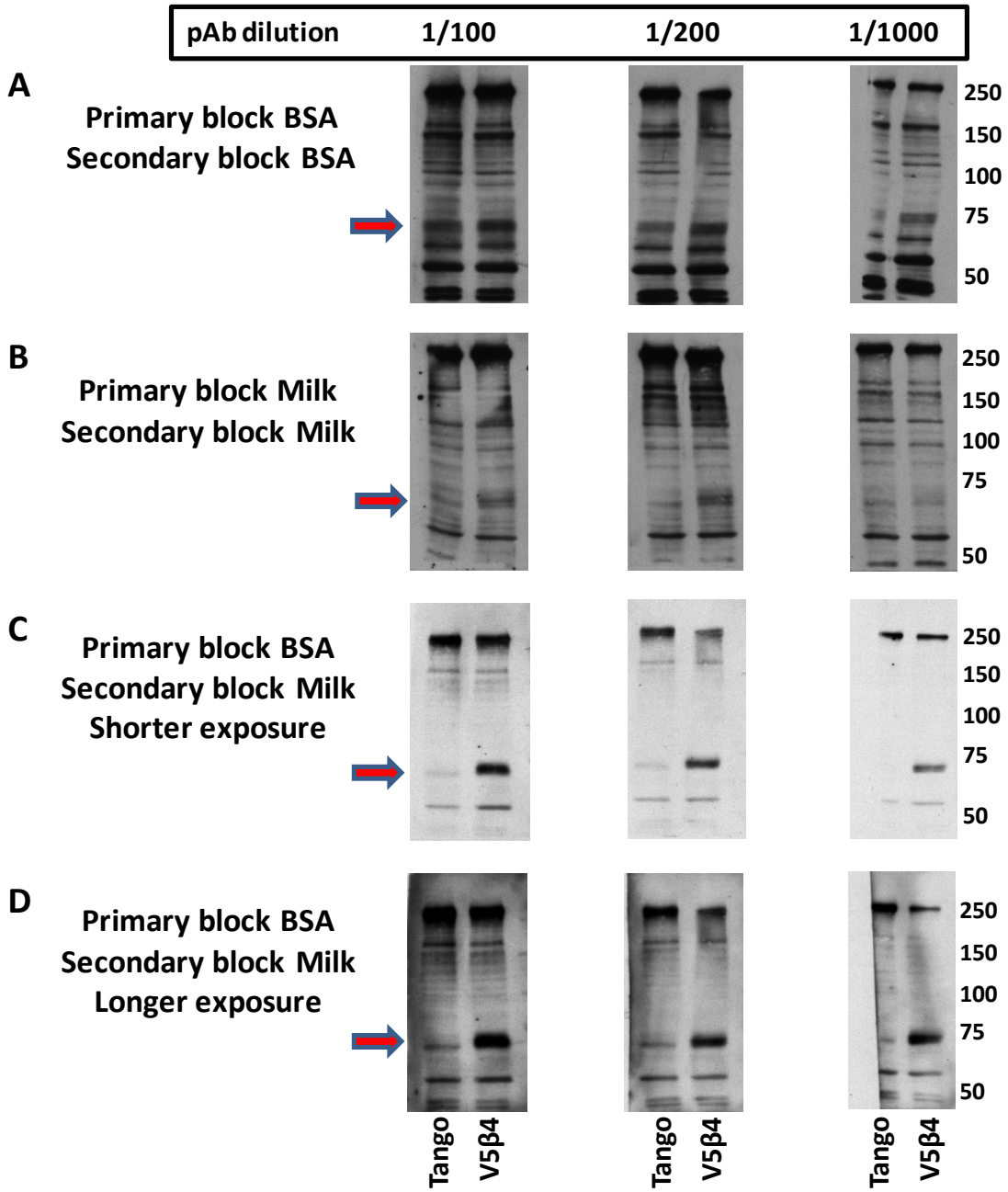
pAb dilution
1/100
1/200
1/1000
A
Primary block BSA
Secondary block BSA
B
Primary block Milk
Secondary block Milk
C
Primary block BSA
Secondary block Milk
Shorter exposure
D
Primary block BSA
Secondary block Milk
Longer exposure
250
150
100
75
50
Tango
Vβ4

Additionally, at lower dilutions of the antibody or using longer exposure times, a fainter band at a slightly lower molecular weight compared to the V5β4 75kDa band was detected (Figure 6.7C and D) which may correspond to endogenous DAGLβ.

Having confirmed that the S570 pAb can detect human DAGLβ-V5 by Western blotting, we also confirmed that this binding did not occur via the V5 epitope using membranes containing DAGLα-V5 (from V5α11 cells) as a negative control (data not shown). In order to confirm the phospho-specific nature of the antibody, V5β4 membranes were treated with phosphatase and then analysed by Western blotting using the S570 pAb. The phosphatase treatment abolished the binding of the pAb to DAGLβ-V5 confirming that the pAb was indeed recognising a phosphorylated epitope within DAGLβ-V5 (Figure 6.8). In addition to this, the site specificity of the pAb has very recently been confirmed as the antibody failed to detect the corresponding non-phosphorylatable mutant (S570A) of DAGLβ by Western blotting (recently completed experiment, data not shown). Collectively these results confirm the phospho-site specificity of the human DAGLβ S570 pAb when using Western blotting.

The final set of experiments focussed on determining whether phosphorylation at this phospho-site could be modulated in cells. In order to address this V5β4 cells were first cultured in McCoy's media supplemented with 10% FCS and then maintained in Freestyle media, in the absence of serum (starvation) for 24 or 48 hours. Membranes from the cells were then prepared and analysed by Western blotting using the S570 pAb. A highly significant decrease in phosphorylation at S570 was detected following 24 hours starvation (Figure 6.9). No further decrease was detected after 48 hours starvation (data not shown).

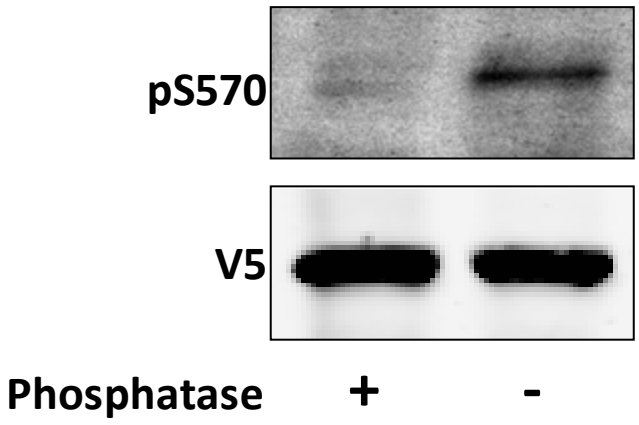

Figure 6.8.The DAGLβ S570 pAb is phospho-specific

V5β4 membranes (10µg) prepared from cells cultured in McCoy's media 10% FCS were treated in the presence or absence of calf intestinal phosphatase (50 units) for 30 minutes at 37°C. The membranes were then analysed by Western blotting and DAGLβ was detected using the S570 pAb as well as a V5 antibody.

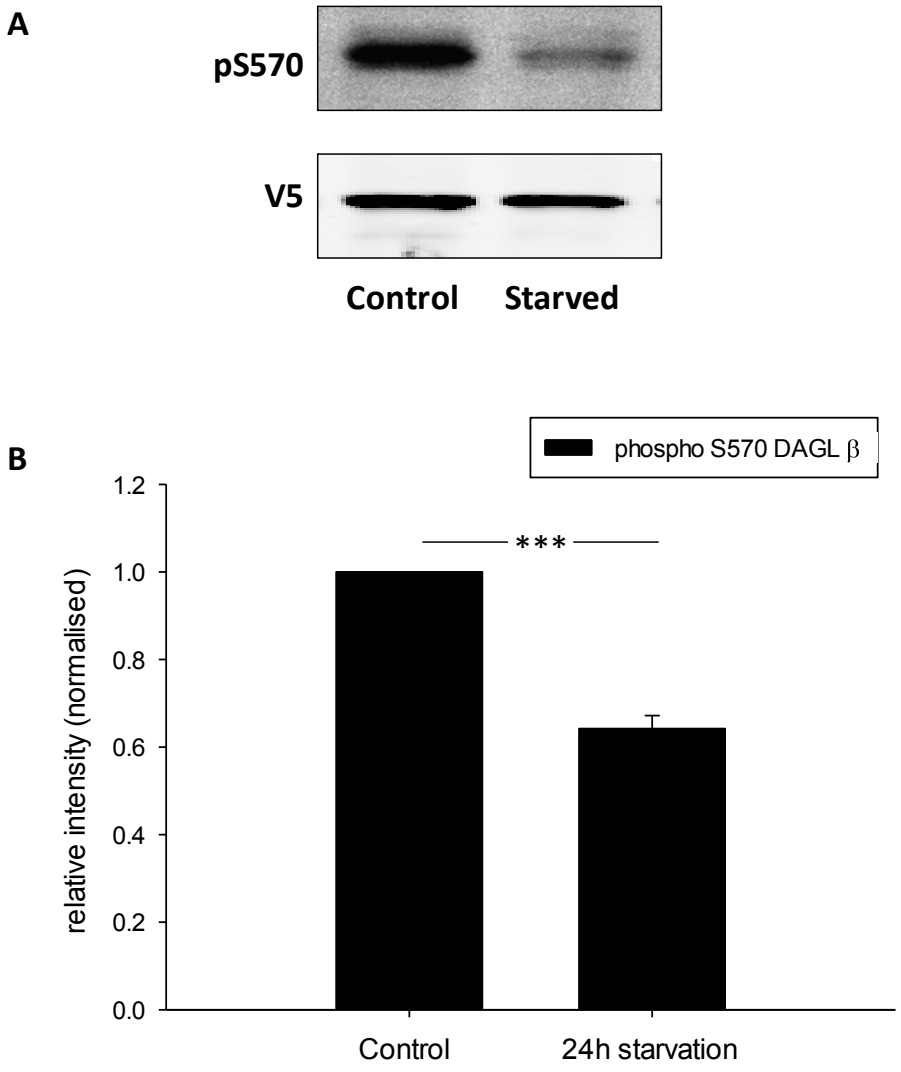

Figure 6.9. Reduction in phosphorylation at DAGLβ-V5 S570 in V5β4 cells following 24 hours starvation

V5β4 cells were maintained overnight in Freestyle media (starved) or cultured in McCoy's media 10% FCS for 24 hours. Membranes were then prepared and analysed (10µg) by Western blotting. DAGLβ was detected using the S570 pAb as well as a V5 antibody (A). The intensity of the phospho S570 band was quantified using ImageJ and the V5 band using the Odyssey software. The reduction in phosphorylation was then quantified by first normalising the DAGLβ phospho S570 band intensities to the corresponding V5 bands and then presenting them as a ratio of the control (McCoy's 10% FCS) (mean±SEM of 5 independent experiments are presented) (B).

Having established that serum deprivation can reduce DAGLβ phosphorylation at S570, we next tested whether serum treatment could increase phosphorylation at S570 following 24 hours starvation. V5β4 cells grown in Freestyle media for 24 hours were treated with different concentrations of serum (1% to 10%) for either 4 hours or 24 hours. Membranes were then prepared and analysed by Western blotting using the S570 pAb which revealed that serum treatment did indeed enhance DAGLβ phosphorylation at S570 in the starved cells (Figure 6.10). As this site lies within a PKA and PKC consensus phosphorylation motif, we finally tested the effects of PKA and PKC activators on phosphorylation at this site. V5β4 cells were maintained in Freestyle media for 24 hours and then treated with the PKA activator Forskolin (10 and 20μM) or the PKC activator PMA (25 or 50nM) for 24 hours. Membranes were then prepared from the cells which were analysed by Western blotting using the S570 pAb which indeed revealed that both PKA and PKC activators caused an increase in phosphorylation at this site (Figure 6.11).

We have therefore shown that the pAb can be used to study DAGLβ (S570) phosphorylation by Western blotting and using this tool we have detected both the up and down regulation of phosphorylation at S570 within cells.

6.3 Discussion

Results presented in the previous chapters identified regulated phospho-sites in DAGLα and DAGLβ and demonstrated that calcium stimulated DAGL-dependent eCB signalling in Tango cells requires PKA and PKC activity. We have therefore postulated that direct phosphorylation of the DAGLα/β by PKA or PKC regulates their activity. In order to investigate this further, in this chapter, we set out to test whether purified PKA and PKC could indeed phosphorylate DAGLα/β *in vitro*.

Several unsuccessful attempts to purify the full length DAGLs (at the required yields) have been made in our lab (Table 6.1 and Table 6.2). Working with full length proteins is generally more desirable, however, the N-terminus transmembrane domains of the DAGLs makes them very challenging to purify.

Figure 6.10. Serum treatment causes an increase in DAGLβ phosphorylation at S570 following 24 hours starvation

V5β4 cells were maintained overnight in Freestyle media (starved) after which they were treated with different concentrations of serum as indicated for either 4 or 24 hours. Membranes were then prepared and analysed (10μg) by Western blotting. DAGLβ was then detected using the S570 pAb as well as a V5 antibody (A). The intensity of the phospho S570 bands were quantified using ImageJ and the V5 bands using the Odyssey software. Changes in phosphorylation levels was then quantified by first normalising the DAGLβ phospho S570 band intensities to the corresponding V5 bands and then presenting them as a ratio of the control (0% Serum) (B and C).

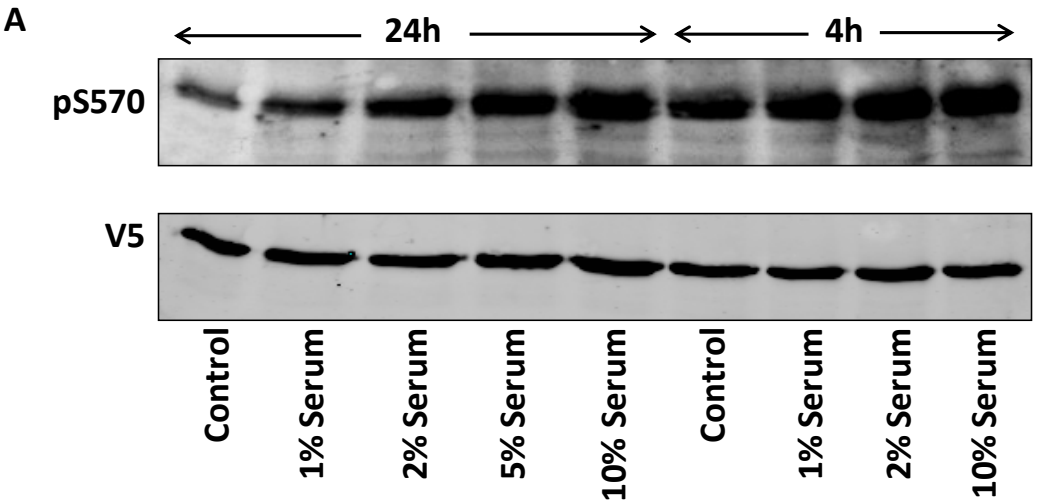
A
24h
4h
pS570
V5
Control
1% Serum
2% Serum
5% Serum
10% Serum
Control
1% Serum
2% Serum
10% Serum

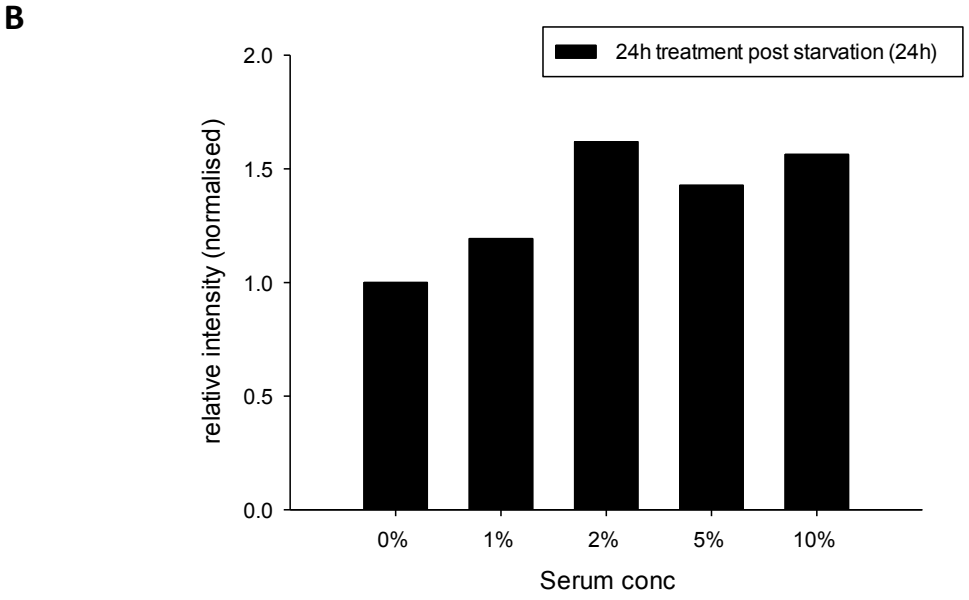
B
24h treatment post starvation (24h)
relative intensity (normalised)
2.0
1.5
1.0
0.5
0.0
0%
1%
2%
5%
10%
Serum conc

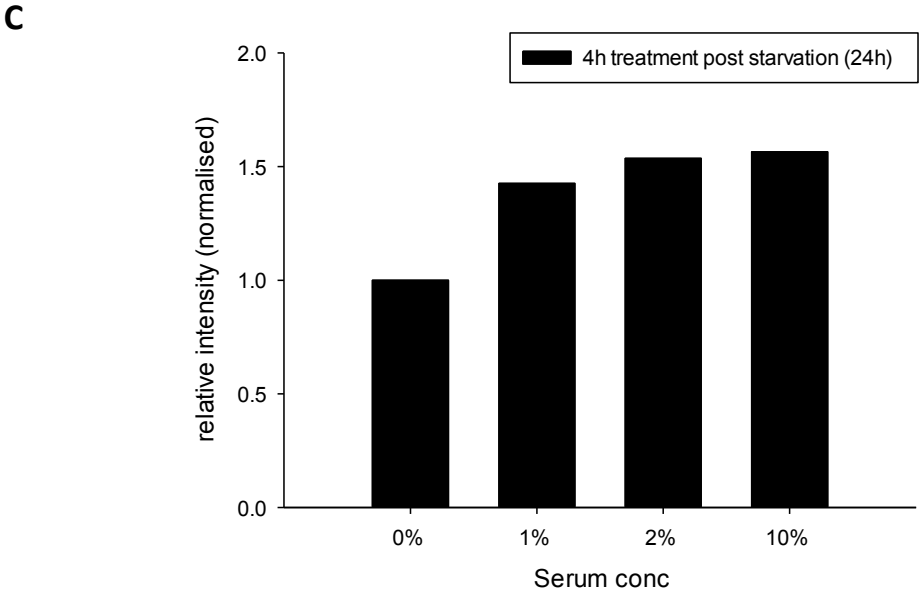
C
4h treatment post starvation (24h)
relative intensity (normalised)
2.0
1.5
1.0
0.5
0.0
0%
1%
2%
10%
Serum conc

Figure 6.11. PKA and PKC activators cause an increase in DAGLβ phosphorylation at S570

V5β4 cells were maintained overnight in Freestyle media (starved) after which they were treated with 10/20μM forskolin or 25/50nM PMA for 24 hours. Membranes were then prepared and analysed (10μg) by Western blotting. DAGLβ was detected using the S570 pAb as well as a V5 antibody and a representative blot for the 10μM forskolin and 25nM PMA treatments is presented (A). Similar results were obtained using the higher concentrations of forskolin/PMA and were also included in the quantification. The intensity of the phospho S570 bands were quantified using ImageJ and the V5 bands using the Odyssey software. Changes in phosphorylation levels was then quantified by first normalising the DAGLβ phospho S570 band intensities to the corresponding V5 bands and then presenting them as a ratio of the control (untreated) (mean±SEM of 5 independent experiments are presented) (B).

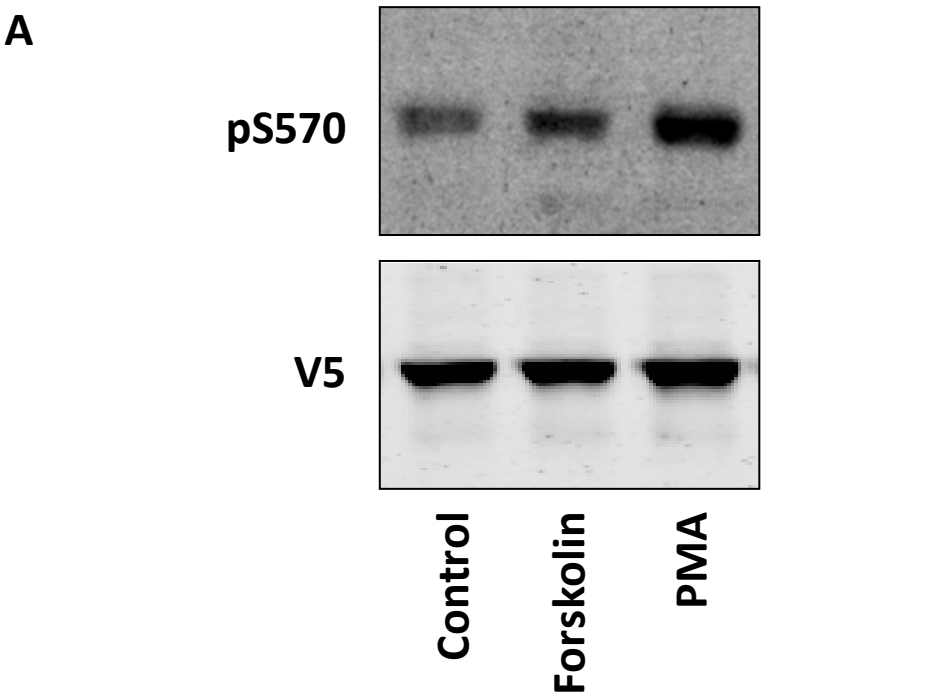
A
pS570
V5
Control
Forskolin
PMA

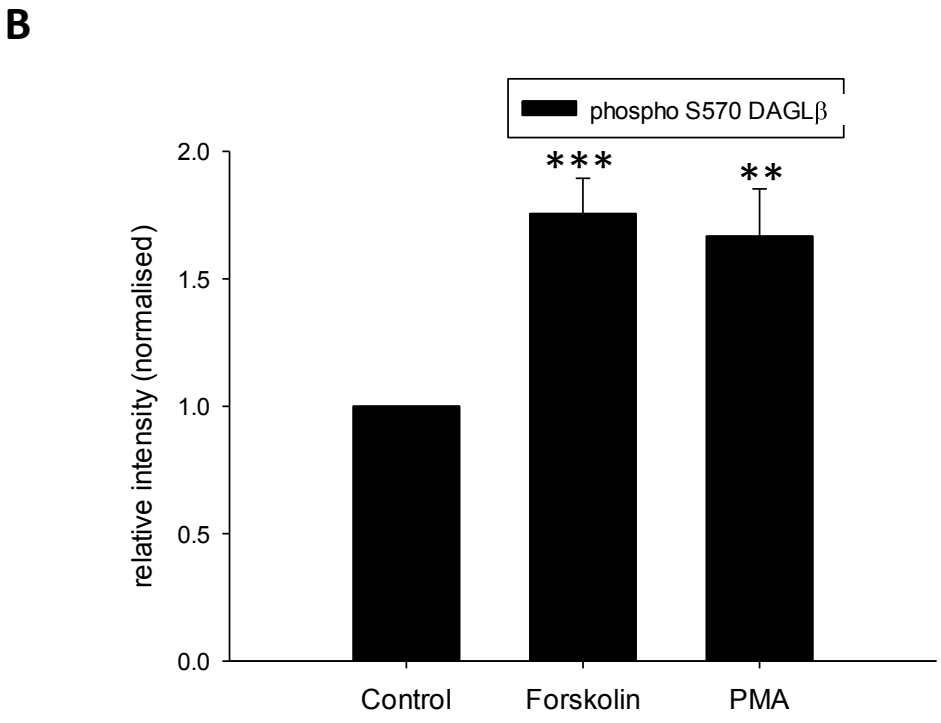
B
phospho S570 DAGLβ
relative intensity (normalised)
2.0
1.5
1.0
0.5
0.0
***
**
Control
Forskolin
PMA

Furthermore, we were particularly interested in mechanisms that regulate the 'open' and 'closed' conformation of the DAGLs and based on other lipase models (HSL) we predicted that phosphorylation within the regulatory loop (RL) is a likely mechanism to regulate this (Holm, 2003; Krintel et al., 2009; Lampidonis et al., 2011). As the active site and regulatory loop of the DAGLs is located within a well defined catalytic domain (Chapter 3) we focussed our efforts on purifying this for IVP studies.

Attempts to express the catalytic domains in the *E. coli* prokaryotic expression system were unsuccessful. We therefore employed the baculovirus expression system which is a eukaryotic expression system. The principle behind this expression system is as follows - baculoviruses engineered to contain the gene of interest are used to infect insect (Sf9) cell cultures. The baculoviruses then not only infect but also multiply within these cells as a consequence of which high levels of expression of the gene of interest are obtained (Jarvis, 2009). This expression system has been used to express and purify mammalian proteins from a wide range of target classes including kinases (McCoy et al., 2005), topoisomerases (Singh et al., 2011) and lipases (Krintel et al., 2009).

We made unsuccessful attempts to purify the catalytic domains with a small 6His tag (~1kDa), possibly due to the tag not being exposed, and therefore focussed our efforts on employing the commonly used larger GST tag (27kDa) (Waugh, 2005). We successfully purified the catalytic domains of the DAGLs using the GST tag to ~50% purity, with reasonable yields (~1 to 2mg/L) using GST affinity purification. However, further analysis using gel filtration chromatography revealed that a majority of the purified protein was aggregated and inactive. The hydrophobic regions in lipases make them prone to aggregation (Salameh and Wiegel, 2010). We therefore included detergents that are commonly used to purify membrane proteins in the purification process (Linke, 2009; Rice et al., 2009) which enabled us to purify the catalytic domain of DAGLβ in the active state, albeit at lower yields (~0.2mg/L).

GST-DAGLα CD on the other hand was found to co-purify with a HSP indicating that it was incompletely or incorrectly folded. This would explain why it was inactive and unstable. We nevertheless attempted to use this as a substrate for IVP studies. PKA did not phosphorylate this protein whereas PKC was only found to phosphorylate the protein within a linker region (incorporated as part of the molecular biology strategy) between the GST tag and the CD. Due to the misfolded/aggregated nature of the purified DAGLα CD we were unable to obtain any evidence to support the hypothesis that PKA/PKC directly phosphorylates DAGLα within the CD and RL. Previous reports have demonstrated that the DAGLα tail and transmembrane domain is dispensable for activity (Won et al., 2009; Pedicord et al., 2011). We were therefore surprised to find GST-DAGLα CD to be completely aggregated and inactive. One may attribute this to the GST tag but 6His-DAGLα CD was also found to be inactive (comparing overexpressing and control lysates using the surrogate substrates, data not shown). However, full length DAGLα expressed using the baculovirus system is active (data not shown) confirming that this expression system can be used to express active DAGLα - however attempts to purify it were unsuccessful. It was for this reason we pursued the catalytic domain strategy. The domain boundaries selected for the DAGLα CD were similar to DAGLβ which was successfully purified; therefore one would also assume these boundaries were suitable choices for DAGLα too. As this does not appear to be the case, one would need to probably screen a few different constructs to identify the most appropriate boundaries to express and purify the catalytic domain (Dyson, 2010). Our collaborator who performed the mass spectrometry studies for us has recently acquired a mass spec with greater sensitivity compared to what was used at the start of the project, thereby reducing the amount of material required for phospho-mapping analysis (Steve Lynham, personal communication). Therefore IPs from mammalian cell lines would probably be a more attractive, feasible, and rewarding approach to further investigate DAGLα phosphorylation. Unlike the GST-DAGLα CD, we were successfully able to purify active GST-DAGLβ CD. Furthermore PKA and PKC were found to phosphorylate the protein *in vitro* and we were also successful in mapping these phospho-sites as discussed below.

Firstly, we were surprised to find 6 phospho-sites in the control sample, not due to the fact that insect cell kinases could have phosphorylated the DAGL, but because we had not detected any phosphorylation in the Phos-tag gel shift assay. It is worth mentioning here that the abundance of the phospho-sites could not be estimated. This was a revelation to us as we expected this to be easily acquired from the MS analysis. However, despite our collaborators best efforts this was not possible. This meant that the phosphorylation levels at the individual sites in the control could range from very low to very high percentages, however based on our gel-shift assay the former seems more likely. For future studies, it will be worthwhile to either phosphatase treat the GST-DAGLβ CD prior to the kinase treatment in order to eliminate background phosphorylation or to include internal peptide standards (of the GST-DAGLβ CD sequence) during the MS run to enable quantitation of the post-translational modifications (Liebler and Zimmerman, 2013). Additionally, certain discrepancies were observed when comparing the control and kinase treated samples, i.e. some sites were identified in the control samples but not in the kinase treated samples. This may have occurred due to contaminating phosphatases, including phosphatase inhibitors in the future may help avoid such discrepancies. However, without an idea of the abundance of these phospho-sites it is difficult to assess what factors are truly behind this discrepancy. For example, these phospho-sites may be present at levels testing the lower limits of sensitivity of the MS and therefore discrepancies in samples would not be surprising. In the absence of the desired quantitative data we were still able to draw some clear and important conclusions from the phospho-mapping of the GST-DAGLβ samples as discussed below.

In the control, amongst the 6 sites identified, 2 were non DAGL; they were located in a linker region between the GST tag and the CD. 2 sites (S368 and S501) were located within the CD, these phospho-sites have not been reported previously, and any functional significance of these phospho-sites is unclear. Based on our catalytic model presented earlier, only one of these sites (S501) is membrane proximal, but both are predicted to be phospho-sites by NetPhos 2.0 (but not DISPHOS). Both these sites are conserved in

mouse but neither is conserved in DAGLα. Whether these phosphorylation events are simply the consequence of an irrelevant event involving a human protein and insect cell kinase or bear more significance remains to be seen.

This brings us to the last two samples identified in the control, S574 and S584. Both these samples are located in the regulatory loop. Phosphorylation at S574 has only been previously reported once in the literature, in the phosphoproteome of Jurkat cell line (T lymphocyte) (Mayya et al., 2009). However this has also been detected 17 times in the unpublished CST studies in different cancer cells/tissues (Table 3.2). Here, we have reported an additional instance of this site being phosphorylated. This site does not lie within a PKA or PKC consensus sequence; however it lies in close proximity to a PKA phospho-site (S570, discussed below). It is tempting to speculate that phosphorylation at S574 site plays a role in relation to the S570 site, i.e. phosphorylation at S574 could prevent phosphorylation at S570 (e.g. S563 and S565 in HSL (Garton et al., 1989)) or indeed enhance the effect of phosphorylation at S570, potentially towards the displacement of the lid (Salazar and Hofer, 2009). Although this site is not conserved in DAGLα, or even in mouse DAGLβ, the numerous reports of this phospho-site combined with its localisation to the regulatory loop means that this site would be an interesting candidate for mutagenesis and activity studies. The other phospho-site identified in the control sample was S584 and is discussed further down.

6 sites were identified in the PKC treated samples, once again like the control, 2 were located in the linker region between the tag and the DAGL sequence. Phosphorylation at the 574 site, located in the RL, which was identified in the control, was also detected. On the other hand 3 of the sites identified in the control were not identified in the PKC sample. One possible explanation is that contaminating phosphatases (in the purified PKC) specific for these sites but not for others may have caused this. Additionally phosphorylation at a tyrosine residue (Y318) was detected in the PKC sample but not in the control, as PKC is a serine/threonine kinase it is likely that a contaminating kinase in the purified PKC probably accounted for this. As mentioned above, we could not determine the abundance of these

phosphorylations, in theory this tyrosine phospho-site could have been present at extremely low levels (theoretically could be <<<1%), maybe at the lower detection limits of the MS in which case variation between the samples would be understandable.

This takes us to the two serine phospho-sites identified in the PKC treated sample but not in the control - S605 (RL) and S617 (6 amino acids after the RL). Both sites are located within PKC (and PKA) consensus sequences and are predicted to be phospho-sites by NetPhos 2.0 (but not DISPHOS). S605 is predicted to be membrane proximal and is conserved in mouse but not in DAGLα. On the other hand S617 is not conserved at all and is not predicted to be membrane proximal. Neither site has been reported before, whether phosphorylation at these sites is physiologically relevant remains to be seen. The fact that S605 is located within the RL and is conserved in mouse does make it an attractive candidate to regulate DAGL activity.

In the PKA treated sample, 5 of the 6 sites from the control were not detected in this sample. This was surprising and the likely explanation is that, once again a contaminating phosphatase in the purified kinase may have been responsible for this. Interestingly, the only 2 phospho-sites detected in this sample are PKA consensus sites, S570 and S584. S584 was also detected in the control. We were unable to determine the relative abundance of this phospho-site in both the samples, however the fact that this was the only site in the control sample to be detected in the PKA sample may indicate that PKA activity outweighed the activity of contaminating phosphatases to preserve or increase phosphorylation levels at this site.

The alignment of this site is ambiguous with the mouse sequence, mouse S582 could align with either S583 or S584 in the human sequence. Human S584 lies within a PKA/PKC consensus sequence whereas mouse S582 does not, but this site in both species does share other consensus motifs for kinases, e.g. CDK5. There have been 4 published reports that have identified phosphorylation at S582 (mouse) in the brain (Tweedie-Cullen et al., 2009; Huttlin et al., 2010; Wisniewski et al., 2010; Trinidad et al., 2012). In human samples, there have been no reports of phosphorylation at S583 but one for

S584 (plus this report), in HeLa cells (Dephoure et al., 2008). The fact that the S584 phospho-site lies within a PKA/PKC consensus motif does make it an interesting site to pursue, however the fact that the motif is not conserved within mouse does raise doubts as to whether this site would be a major determinant of PKA/PKC stimulated DAGLβ activity. A pAb against this site has been generated and is currently being evaluated in our lab.

This takes us to possibly, the most exciting finding of the thesis. Firstly, phosphorylation at S570 was not detected in the control but was detected in the PKA treated sample. This site is conserved in mouse (but not DAGLα) and lies within a PKA (and PKC) consensus sequence in the RL of both human and mouse DAGLβ. S570 is predicted to be a phospho-site by DISPHOS (but not NetPhos 2.0) and is also membrane proximal. This site has been reported by three published studies using HeLa (Daub et al., 2008; Olsen et al., 2010) and Jurkat cells (Mayya et al., 2009). Collectively, these data suggest that this site is a prime candidate to be phosphorylated by PKA and PKC, in order to most probably regulate DAGLβ activity.

We have successfully developed an antibody that can specifically recognise phospho S570 by Western blotting as demonstrated here using phosphatase and mutagenesis studies. This antibody was used to demonstrate that phosphorylation at this site is regulated within cells. Firstly, maintaining (starving) cells in Freestyle media (serum free) resulted in a significant decrease in phosphorylation at this site when compared to cells grown in McCoy's media supplemented with 10% serum. Furthermore, phosphorylation was then upregulated by feeding the starved cells with serum or by treating them with PKA and PKC activators, the latter two having previously been shown to stimulate DAGL-dependent eCB signalling in the CB1-Tango assay (chapter 4), thus confirming that phosphorylation at this site is regulated.

To summarise, our attempts to study *in vitro* phosphorylation of DAGLα by PKA and PKC were unsuccessful due to the misfolded/aggregated nature of the purified DAGL. On the other hand we successfully purified the catalytic domain of DAGLβ, in the active state and also identified phospho-sites in the

control as well as PKA and PKC treated samples. We successfully developed a phospho-specific antibody against the PKA phospho-site S570 and demonstrated that phosphorylation at this site is regulated in cells. As this is the only PKA or PKC consensus site in the RL that is conserved in mouse, we postulate that this site is a key mediator in the regulation of DAGLβ activity by playing a role in the displacement of the lid. As far as we are aware, this is the first report of the successful purification of active DAGLα/β as well as of a DAGL pAb tool. Both these tools will undoubtedly prove to be valuable in further understanding mechanisms behind DAGL regulation.

Chapter 7 : General Discussion

7.1 Why study DAGL regulation - the physiological, pathological and therapeutic significance of these enzymes

In the last decade - the cloning (Bisogno et al., 2003) and genetic deletion (Gao et al., 2010; Tanimura et al., 2010) of the major 2-AG synthesising enzymes, DAGLα and DAGLβ, has helped establish the importance of these enzymes in various physiological processes mediated by eCB signalling. These enzymes impact developmental processes to ensure that axons are extended in the correct manner and are directed towards their targets (Mulder et al., 2008; Keimpema et al., 2010; Wu et al., 2010). They promote the formation of new neurons in the adult brain (Goncalves et al., 2008; Gao et al., 2010) where these enzymes are also relied on to ensure synaptic signalling is appropriately regulated (Gao et al., 2010; Tanimura et al., 2010; Hashimotodani et al., 2013).

The DAGL cloning and knockout studies were also important in establishing 2-AG as the major eCB. These enzymes, individually, are responsible for virtually all the 2-AG in the brain (DAGLα) and liver (DAGLβ) (Gao et al., 2010). It was surprising that these enzymes can exert such control over this important signalling molecule, especially as knockout studies have failed to identify major synthesising pathways for the other widely studied (putative) eCB AEA (Leung et al., 2006; Simon and Cravatt, 2010). What was even more surprising was the parallel reduction of AA levels with 2-AG levels in the brain and liver in the DAGL KO mice. This coupled with dramatic increases in 2-AG and complementary decreases in AA and eicosanoids following deletion or inhibition of the major 2-AG hydrolysing enzyme MAGL, has established non-eCB roles for the DAGLs in the context of eicosanoid signalling (Schlosburg et al., 2010; Nomura et al., 2011; Piro et al., 2012).

Several studies have therefore demonstrated that the DAGLs, by virtue of their DAG hydrolysis activity, regulate 2-AG (eCB) and AA (eicosanoid) signalling pathways, but despite these important roles, very little is known about how these enzymes are regulated. Studying the regulation of these

enzymes will improve our understanding of both their physiological and pathological roles which in turn will help assess and exploit any therapeutic potential they may hold. Indeed, as key eCB signalling mediators as well as potential inflammatory mediators, they are implicated in various diseases.

For example, aberrant DAGLα localisation coupled to disrupted mGluR5 synaptic signalling in mouse Fragile X mental retardation protein (FMRP) KO models has recently been implicated in Fragile X syndrome. Fragile X syndrome is caused by the failure to express FMRP which plays an important role in the transport of various mRNA to the synapses and this has recently been extended to DAGLα (Jung et al., 2012; Sidorov et al., 2013). Blocking 2-AG hydrolysis helped overcome the dysregulated mGluR5 signalling as well as corresponding behavioural deficits in FMRP KO mice thereby indicating a potential therapeutic role for DAGLα activators towards treating certain aspects of Fragile X syndrome (Jung et al., 2012). Furthermore, such activators could potentially be exploited to enhance the stress induced antinociceptive properties of DAGLα in the context of synaptic signalling in the dlPAG (Gregg et al., 2012). Additionally, as the DAGLs play a role in adult neurogenesis (Goncalves et al., 2008; Gao et al., 2010), such activators may also hold therapeutic potential in counteracting the effects of neuronal loss in brain injury and neurodegenerative diseases.

The role of the DAGL-MAGL pathway in AA and thereby eicosanoid production in the brain has also implicated them in neurodegenerative diseases. For example, elevated brain levels of AA and eicosanoids are observed in an Alzheimer's disease mouse model. These are reduced 5 to 10-fold (coupled with an increase in 2-AG levels) following the genetic deletion of MAGL in this model which also causes a reduction in microglia and astrocyte activation, inflammatory cytokine levels, and amyloid plaques (Piro et al., 2012). Similarly, in a Parkinson's disease model, MAGL deletion or inhibition prevents MPTP induced increases in AA and eicosanoids as well as neuronal loss in the brain (Nomura et al., 2011). These studies have focussed on the disruption of MAGL activity to prevent neuroinflammation. As the DAGLs are responsible for most of the AA in the brain, DAGLα/β

inhibition is likely to have similar effects making them attractive targets to treat neuroinflammation (Gao et al., 2010).

Beyond the nervous system, in the liver of mice, increased CB1 expression, DAGLβ expression and 2-AG levels are observed following ethanol feeding which has been linked to alcohol induced hepatic steatosis (Jeong et al., 2008). In addition to this, a reduction in ethanol induced hepatic steatosis and inflammation is observed in CB1 KO mice or in wild type mice treated with a CB1 antagonist (Jeong et al., 2008; Trebicka et al., 2011). CB1 has also been linked to the pathogenesis of high fat diet induced hepatic steatosis (Osei-Hyiaman et al., 2008). Inhibiting DAGLβ in this context may prevent CB1 activation and thereby hepatic steatosis, especially as DAGLβ accounts for ~90% of 2-AG in the liver.

In general, DAGLα and DAGLβ demonstrate different tissue specific contributions towards 2-AG (and AA) levels and hence targeting them individually could prove to be therapeutically attractive and achievable (Gao et al., 2010). A DAGLβ selective inhibitor (50 times more potent against DAGLβ than DAGLα) has recently been developed (Hsu et al., 2012), this provides encouraging signs that differences in these enzymes can be exploited by medicinal chemistry.

Furthering our understanding about how DAGLα and DAGLβ are regulated, which may include both overlapping and distinct mechanisms, will help further our understanding of these enzymes and eCB signalling and support longer term studies to evaluate their therapeutic potential as drug targets. But firstly, are the DAGLs regulated?

7.2 Stimulus dependent increases in 2-AG levels indicate mechanisms regulating the DAGLs exist

Over the last 30 years, there have been numerous reports of increased 2-AG levels in response to various stimuli in a range of cells/tissues (reviewed in (Sugiura et al., 2006). Some examples of the stimuli that enhance 2-AG levels include Endothelin 1, ionomycin (5-fold) and ATP (60-fold) in astrocytes (Walter and Stella, 2003; Walter et al., 2004), ethanol (~1.7-fold),

ionomycin (~2-fold) and glutamate (~1.6-fold) in cerebellar granular neurons (CGNs) (Basavarajappa et al., 2000), ionomycin (~1.6-fold), glutamate and NMDA (~3-fold) in cortical neurons (Stella et al., 1997; Stella and Piomelli, 2001), ionomycin in neuroblastoma cells (Bisogno et al., 1997; Bisogno et al., 1999a) and Pictrotoxinin (~5-fold) and $CaCl_2$ (6-fold) in rat brains (Kondo et al., 1998; Sugiura et al., 2000a). As the major 2-AG synthesising enzymes, the DAGLs are likely candidates to mediate these increases in 2-AG levels and in some cases this has been demonstrated using a DAGL inhibitor (Stella et al., 1997; Bisogno et al., 1999a; Walter et al., 2004). These several fold increases in 2-AG in response to a range of stimuli strongly indicate that mechanisms regulating the DAGLs do exist.

7.3 DAGL post-translational modifications indicate that these enzymes are tightly regulated

As presented in this thesis, several reports of DAGL phosphorylation (30 DAGLα and 12 DAGLβ phospho-sites) have been published (see Table 3.1 and Table 3.2 for references). Phosphorylation can regulate an enzyme in multiple ways, including its activity, localisation and stability by impacting on inter and intra-molecular interactions (Johnson and Lewis, 2001; Salazar and Hofer, 2009). Furthermore, the regulatory potential of phosphorylation on a protein is increased exponentially when multiple phospho-sites exist. In other words, an enzyme that is phosphorylated at n number of sites can potentially exist in 2^n phosphorylation states, each potentially exhibiting different properties (Cohen, 2000; Salazar and Hofer, 2009). Therefore the reported DAGL phospho-sites, coupled with other reported post translational modifications of these enzymes, including palmitoylation (Kang et al., 2008; Martin and Cravatt, 2009; Yang et al., 2010) and ubiquitination (Wagner et al., 2011; Wagner et al., 2012) provide evidence that these enzymes are tightly regulated.

7.4 Mechanisms defining DAGL localisation

As a general concept, mechanisms determining the localisation and activity of an enzyme play a crucial role in their regulation. In this context, detailed anatomical studies of DAGLα have demonstrated that this enzyme is often

localised in close proximity to the CB1 receptor, thus enabling 2-AG mediated activation of the receptor in either an autocrine or paracrine manner. For example, several studies have shown that DAGLα, along with the CB1 receptor are both present in axons during development, thereby enabling eCB signalling to regulate axonal growth and guidance (Bisogno et al., 2003; Berghuis et al., 2007; Mulder et al., 2008; Watson et al., 2008; Keimpema et al., 2010). On the other hand, restricted expression of the DAGLα to dendritic spines and the CB1 receptor to pre-synaptic terminals in the adult brain plays an important role in retrograde synaptic signalling. In this case, 2-AG produced in the post synaptic cell, in response to depolarisation or receptor activation (e.g. mGluR5), activates pre-synaptic CB1 receptors to suppress synaptic signalling (Bisogno et al., 2003; Yoshida et al., 2006; Uchigashima et al., 2007; Nyilas et al., 2009).

The mechanisms determining the localisation of the DAGLs are poorly understood. A recent report has demonstrated a role for FMRP in the transport and precise localisation of DAGLα mRNA and protein at the synapse (Jung et al., 2012), thereby demonstrating localised translation as a mechanism regulating its localisation.

Reversible post-translational modifications are also likely to play a role in DAGL localisation. As discussed in this report, both the DAGLs have been shown to be palmitoylated (Kang et al., 2008; Martin and Cravatt, 2009; Yang et al., 2010), most likely in a cysteine rich insert within the catalytic domain identified here. This insert probably plays a role in targeting these enzymes to lipid rafts, in close proximity to their substrate DAG and the CB1 receptor (Canobbio et al., 2008; Rimmerman et al., 2008; Oddi et al., 2012). Furthermore, palmitoylated DAGLα has been specifically identified in rat brain synaptosomes (Kang et al., 2008) where this enzyme is specifically localised to regulate synaptic signalling.

Likewise, several DAGLα derived phospho-peptides have been identified in the brain and more specifically in synaptosomes (Table 3.1). Two independent knockout studies of the DAGLs have implicated DAGLα and not DAGLβ in eCB driven retrograde synaptic signalling (Gao et al., 2010;

Tanimura et al., 2010), despite the fact that both these enzymes are expressed in the adult brain, and more specifically in neurons (Bisogno et al., 2003; Yoshida et al., 2006; Jain et al., 2013). The most obvious structural difference between the DAGLs is the presence of a C-terminal tail region in DAGLα that is completely absent in DAGLβ (Reisenberg et al., 2012). It is therefore highly probable that this tail region (primarily but not necessarily exclusively) plays a role in regulating DAGLα in a synapse specific context.

As shown in the DAGLα phospho-map compiled in this report, a total of 20 phospho-sites have been identified in the tail region reflecting its regulatory potential (see Table 3.1 for references) and as mentioned above a large number of these phospho-sites were identified in the brain and more specifically in synaptosomes/synaptic membranes (Trinidad et al., 2006; Munton et al., 2007; Trinidad et al., 2008; Trinidad et al., 2012). These phospho-sites may therefore play a role in localising DAGLα towards the synapse, possibly by modulating protein-protein interactions. Indeed, this tail region contains a PPxxF consensus motif for binding Homer proteins (Jung et al., 2007), a family of adaptor proteins for many post-synaptic proteins, including mGluR5 (Shiraishi-Yamaguchi and Furuichi, 2007). This motif has been shown to be important for DAGLα interaction with homer proteins (Homer-1b, Homer-2) and its localisation to the plasma membrane as determined by overexpression studies in Neuro-2A cells (Jung et al., 2007).

Regulated degradation of the DAGLs is also likely to play a role in determining the localisation of these enzymes. This would facilitate the shift observed in the role of DAGLα, from autocrine CB1 activation in the axons during development, towards paracrine retrograde CB1 activation at the synapse (mediated by its dendritic localisation). In support of this, ubiquitination at three DAGLα and three DAGLβ sites have been reported in unbiased proteomic studies (Wagner et al., 2011; Wagner et al., 2012) and a putative D-box motif has also been identified within the DAGLα tail (Gareth Williams, unpublished data). The D-box (destruction box) is a consensus binding sequence for the anaphase promoting complex ubiquitin ligase which directs the ubiquitin-mediated degradation of the binding target (Min et al., 2013).

7.5 Regulating DAG levels will regulate the DAGLs

Localisation of the DAGLs close to DAG and the cannabinoid receptors is potentially a dynamic process thereby regulating eCB signalling. When in proximity of DAG and the cannabinoid receptors, further mechanisms have been implicated in regulating the activity of these enzymes. One of these is substrate availability. Detailed pharmacological studies using cerebellar neuron cultures have implicated a PLCγ-DAGL-CB1 pathway in FGFR receptor driven neurite outgrowth mechanisms (Williams et al., 1994b; Williams et al., 1994a; Saffell et al., 1997; Bisogno et al., 2003; Williams et al., 2003). In this pathway, increased PLCγ activity is likely to increase DAG levels by the hydrolysis of phospholipids and thereby increase DAGL activity, 2-AG levels, and ultimately CB1 activation. Similarly, detailed studies have also linked increased PLCβ activity to increased DAGL dependent 2-AG signalling at the synapse (Hashimotodani et al., 2007b, a; Tanimura et al., 2010). In this context, activation of certain post synaptic receptors like mGluR5 coupled with increased post synaptic calcium levels collectively activate PLCβ, which will thereby increase DAG levels and consequently DAGL activity and 2-AG levels (termed as Ca-RER - calcium assisted receptor-driven endocannabinoid release).

Therefore, palmitoylation and phosphorylation of DAGLα, coupled with its interaction with adaptor proteins like Homer, probably work cooperatively to ensure that the DAGLs are at the right place at the right time to take advantage of increased substrate levels (via FGFR/mGluR5 activation), thereby driving eCB signalling.

7.6 Phosphorylation as a mechanism to regulate DAGL catalytic activity

The processes described above (DAGL localisation and increased DAG levels) may indeed contribute towards the elevated 2-AG levels observed in various cells/tissues in response to a range of stimuli as mentioned earlier. In addition to this, further evidence also points towards intra-molecular mechanisms regulating the catalytic activity of the DAGLs. For example, glutamate elevates DAGL activity in primary mouse neuronal cultures when measured *in vitro* (Farooqui et al., 1993). Synaptosomes treated with an

mGluR5 agonist demonstrate increased DAGL activity using a synthetic substrate (Jung et al., 2012). Additionally, two CamKIIa phospho-sites (S782 and S808) in the tail region of DAGLα have been shown to exert an inhibitory effect on its catalytic activity *in vitro* (Shonesy et al., 2013).

In this context, phosphorylation is a widely used mechanism to regulate the activity of enzymes, including lipases like TGL4, PLCγ, and HSL (Kurat et al., 2009; Gresset et al., 2010; Lampidonis et al., 2011). In light of the numerous reports identifying DAGL phospho-peptides (see Table 2 and 3), phosphorylation appears to be a likely mechanism to regulate DAGL activity as well. Furthermore, some of the stimuli that drive an increase in 2-AG levels in cells/tissues also activate various kinases.

7.7 PKA and PKC dependent stimulation of DAGL activity

Two kinases implicated in stimulating 2-AG synthesis in cells are PKA and PKC. Approximately 3-fold increases in 2-AG levels were observed when treating HEK293 cells with the PKC activator PMA (blocked by a PKC inhibitor) or the PKA activator forskolin (blocked by a PKA inhibitor) (Vellani et al., 2008). Similarly, increases in 2-AG in glucocorticoid stimulated hypothalamic slices was shown to be PKA dependent (Malcher-Lopes et al., 2006). Furthermore these kinases are stimulated by calcium (Steinberg, 2008; Dunn et al., 2009) and as mentioned earlier, calcium and ionomycin (calcium ionophore) stimulated 2-AG synthesis has been widely reported using cell lines (Bisogno et al., 1999a; Bisogno et al., 2003), primary cell cultures (Stella et al., 1997; Aguado et al., 2005) and tissues (Kondo et al., 1998). In a physiological context, increased calcium levels in the post-synaptic cell drive the production of 2-AG during synaptic signalling and although in some instances (Ca-RER) this has been linked to PLCβ activation, in other instances (DSI/DSE) the mechanisms behind this are still unknown (for reviews see (Hashimotodani et al., 2007a; Castillo et al., 2012). Based on the discussion above, it is tempting to speculate that these unknown mechanisms involve phosphorylation of DAGLα, by calcium dependent kinases like PKA or PKC, thereby increasing its activity. We exploited a cell based CB1 activation assay, namely the Tango assay to test

this hypothesis, crucial to this was the fact that the Tango cells express DAGLα/β. Indeed we found that calcium stimulated DAGL dependent eCB signalling in this assay was blocked by both PKA and PKC inhibitors. Equally encouraging was the fact that PKA and PKC activators themselves stimulated DAGL dependent eCB signalling in the assay. In addition to this, an earlier report has shown that PKA treated bovine rod membranes demonstrate ~70% increase in DAGL activity *in vitro* (Perez Roque et al., 1998) and that a DAGL activity purified from bovine brain (albeit much smaller protein than DAGLα/β) is stimulated by PKA *in vitro*. These results coupled with the DAGL phospho-site analysis summarised below indicate that PKA and PKC activate the DAGLs by phosphorylating them.

7.8 Potential PKA and PKC phospho-sites within the DAGLs

As discussed in this report, several DAGL phospho-peptides have been identified by mass spectrometry analysis of a range of cell/tissue extracts. Amongst the 42 potential DAGL phospho-sites collated in this report, 11 lie within PKA and PKC consensus motifs (Amanchy et al., 2007). Phosphoproteomic analysis of complex samples can often result in the detection of false positives (and negatives) (Alcolea et al., 2009), however, a detailed probation of these sites using structure/sequence based predictions carried out as part of this project strongly indicates that several of these are genuine phospho-sites, especially as they have been reported in multiple studies. In this regard, at least 9 of the phospho-sites are likely to be genuine, 4 of which are candidate PKA/PKC phospho-sites.

2 of these sites are located within the DAGLβ RL. Indeed, using purified kinases and the purified catalytic domain of DAGLβ, we have shown that PKA can phosphorylate one of these sites (S570). We were unable to determine whether PKA phosphorylates the other site due to background phosphorylation in the control sample. Phosphatase treatment of the control sample prior to PKA treatment will help address this. The other 2 PKA/PKC 'genuine' phospho-sites are located within the tail region of DAGLα, the work in this report focussed on *in vitro* phosphorylation studies using the DAGLα

CD, it therefore remains to be seen if PKA/PKC can indeed phosphorylate these sites.

In general, the increases in 2-AG levels observed in cells/tissues in response to various stimuli (e.g. ionomycin) are likely to be mediated by DAGL activity; however the individual contribution of DAGLα and DAGLβ towards this is unclear. In this context the Tango cells express both DAGLα and DAGLβ. Therefore any of the 4 phospho-sites highlighted above may indeed be responsible for the calcium/PKA/PKC stimulated DAGL dependent eCB signalling observed in the Tango assay here, and also for the calcium stimulated 2-AG synthesis widely reported in other cells and tissues. But how would these phospho-sites affect DAGL activity?

7.9 Potential mechanisms dictating intra-molecular activation of the DAGLs

Several clues with regards to intra-molecular activation mechanisms can be gained from the architecture of the DAGLs. There is no reported crystal structure for the mammalian DAGLs. However, using homology modelling, we have identified a regulatory loop (RL) consisting of 50-60 amino acids and located as an insert within the catalytic domain of the DAGLs. The RL is likely to function as a lid, thereby restricting substrate access to the catalytic site. Related lid like structures have been reported for several lipases (Holmquist, 2000).

The lid is responsible for the 'interfacial activation' phenomenon, commonly observed with these enzymes. Interfacial activation refers to the lid displacement and increased activity of a lipase when it comes in contact with a lipid phase (Nardini and Dijkstra, 1999; Holmquist, 2000). Once membrane and substrate proximal, the displacement of the DAGL regulatory loop is likely to be triggered, thereby activating the enzymes.

In the case of hormone sensitive lipase (HSL), the lid is represented by an ~150 amino acid regulatory module and contains several PKA phospho-sites (Lampidonis et al., 2011). Furthermore, phosphorylation by PKA increases the activity and hydrophobic surface area of HSL *in vitro* (Tsujita et al., 1989;

Holm et al., 1994; Anthonsen et al., 1998; Krintel et al., 2009). This has led to a model whereby PKA dependent phosphorylation of HSL results in the displacement of the lid which exposes the hydrophobic catalytic core of the enzyme, thereby enabling substrate access to the catalytic site, resulting in increased activity. Several phospho-sites have been identified in the RL of the DAGLs. Particularly striking, is a short 15 amino acid hyper-phosphorylated region within the RL of DAGLβ containing 8 reported phospho-sites. There is only one conserved PKA/PKC consensus sequence within the RL of DAGLβ, S570. This site has been reported to be phosphorylated in cells by 3 different reports (Daub et al., 2008; Mayya et al., 2009; Olsen et al., 2010), is membrane proximal (and therefore substrate facing) and is also predicted to be a phospho-site (DISPHOS). This site is therefore a prime candidate to mediate PKA/PKC stimulatory effects within the enzyme, potentially by regulating the 'open' and closed conformation of the enzyme. Furthermore, as mentioned earlier we have used the purified catalytic domain of DAGLβ and purified PKA to demonstrate that this kinase can indeed directly phosphorylate this site *in vitro*. We have also demonstrated using a pAb, that treating cells with PKA and PKC activators upregulates phosphorylation at this site. Work is ongoing to determine the effect of phosphorylation at this site on the activity of DAGLβ.

There have been 2 reported phospho-sites located within the RL of DAGLα, however neither have been reported in published studies. It remains to be seen whether these are genuine phospho-sites and/or whether additional phospho-sites within the DAGLα RL do exist. However, the tail region of DAGLα contains numerous phospho-sites (20), 5 of which have been reported in at least 3 published studies. 2 of these phospho-sites - S743 which has been reported in 8 independent published studies and S806 which has been reported in 5 independent published studies, are located within PKA/PKC consensus sequences (see Table 3.1 and Table 3.3 for details and references). The tail region of DAGLα has been shown to be dispensable for catalytic activity (Pedicord et al., 2011). However, the recent study demonstrating the inhibitory effect of two CamKIIa phospho-sites located within the DAGLα tail, on its catalytic activity *in vitro* (Shonesy et al., 2013),

indicates that this region may interact with other regions of the protein (like the RL) to modulate DAGLα activity. Therefore the two PKA/PKC consensus sites within the tail region, that have been widely reported, may indeed be responsible for calcium/PKA/PKC stimulated DAGLα activity discussed earlier.

7.10 Phosphorylation and activity of the DAGLs

Our results in this study showed that both PKA and PKC inhibitors blocked calcium stimulated DAGL dependent activity in the Tango (cell based CB1 activation) assay. Additionally, PKA and PKC activators stimulated DAGL dependent eCB signalling in this assay. These results coupled with the fact that some of the 'genuine' DAGL phospho-sites lie within PKA/PKC consensus sequences led us to postulate that PKA and PKC directly phosphorylate and thereby activate the DAGLs.

In order to test this hypothesis we used two different DAGL surrogate substrates (PNPB and DiFMUO) (Pedicord et al., 2011) to develop membrane and live cell assays which were capable of detecting increased DAGL activity in cells overexpressing DAGLα/β. However, despite using a range of treatments (phosphatase, calcium, PKA activators, PKA inhibitors, PKC activators, starvation), some of which stimulated DAGL in the Tango assay, no change in DAGL activity was detected using these substrates. This indicated that either the treatments did not affect (phosphorylate) the DAGLs or that these substrates were incapable of detecting changes in the DAGLs induced by these treatments that may otherwise be detected using the native substrate DAG. The latter could be due to size and/or structural differences between the surrogate substrates and the native substrate DAG. In support of this - phosphorylation of HSL by PKA has been shown to increase its activity *in vitro* when using a triglyceride substrate but not when using PNPB as the substrate (Tsujita et al., 1989). In future studies, if changes in DAGL activity are indeed detected using DAG, following the treatments mentioned above, then the negative results with the surrogate substrates become all the more interesting as they might help understand specific aspects of DAGL-DAG interactions that are responsible for the treatment dependent changes

in activity. Furthermore, if these treatments do result in DAGL phosphorylation then pAbs would be particularly useful tools in these studies as they would enable one to optimise the concentration and treatment times of the stimulus to maximise its effect on the DAGLs.

7.11 DAGL phospho-antibodies as tools to investigate and monitor eCB signalling

Site specific pAbs are valuable biological tools, especially as they can be used to identify and study pathways that modulate the phosphorylation status of the site. Indeed site specific pAbs have been useful in studying down-stream signalling pathways of CB1 e.g. in granule cell precursors (phospho-AKT and phospho-GSK-3β) (Trazzi et al., 2010) and in the hippocampus (phospho-ERK) (Derkinderen et al., 2003).

Developing site specific pAbs of biological value however is no trivial task. A phospho-site first needs to be identified. If one is relying on global phosphoproteomics data then 'false positives' can prove a hindrance (Alcolea et al., 2009). If one is relying on overexpressing systems (coupled with *in vitro* phosphorylation studies) then its physiological occurrence needs to be established. Following that, the pAb itself has to be generated which can be technically challenging (Brumbaugh et al., 2011). Immunogenicity/specificity of the antigen, purification of the pAb and ultimately specificity of the pAb are issues commonly faced. If a site specific pAb is successfully generated, it also needs to be functional in the desired format(s) (e.g. Western blotting, immunohisto/cytochemistry, immunoprecipitation, ELISAs, or other antibody dependent assays). Coupled with all of this, a physiological function needs to be assigned to the phospho-site, which in itself can take years; this can actually be greatly aided by site-specific pAbs.

In this study we have successfully developed what we believe to be is the first site specific DAGL pAb (DAGLβ S570). This pAb has successfully been used in Western blotting and its phospho-site specificity has been validated by mutagenesis and phosphatase studies. Using this validated tool we found that phosphorylation at DAGLβ S570 is regulated within cells. More specifically, treating cells with PKA and PKC activators causes an

upregulation of phosphorylation at this site. This phospho-site is a prime candidate to be responsible for potential PKA/PKC dependent DAGLβ activation as it is the only conserved PKA/PKC (predicted) phospho-site located within its RL loop and as reported here, this site can be directly phosphorylated by PKA. As of yet, a function has not been assigned to this site, studies are currently ongoing to determine the effect of this phospho-site on DAGLβ activity.

Understanding the impact of the various DAGL phospho-sites on their activity coupled with the generation of other DAGL pAbs may indeed prove to be crucial in understanding how these enzymes are regulated. Furthermore, once a phospho-site has a function assigned to it, then a pAb against that site will prove to be a valuable tool to understand pathways regulating DAGL and thereby eCB signalling. A better understanding of how the DAGLs are regulated will be fundamental towards assessing and unlocking their therapeutic potential, whether it is to exploit their antinociceptive or neurogenic properties by activating them or to inhibit them in order to suppress neuroinflammation and hepatic steatosis.

7.12 Future directions

The phospho-maps of the DAGLs contain 42 phospho-sites, indicating that these enzymes are tightly regulated. However, to date, only two of these phospho-sites have a function attributed to them.

In order to assess the impact they have on the DAGLs we are currently adapting the Tango cells to use them as a platform for detailed DAGL structure/function studies. The parental Tango cells are engineered to measure CB1 activation and in this study we have adapted them to detect calcium stimulated DAGL (endogenous) dependent eCB signalling. We are currently knocking out the endogenous DAGL genes in these cells to provide us with a platform to screen various mutated version of the DAGLs. This will allow us to test the impact of the DAGL phospho-sites on their activity in a cellular context. Screening these mutants in biochemical assays using the native DAG substrate will also be imperative in establishing the effect of the various phospho-sites on DAGL activity. Of particular interest is the impact

phosphorylation at S570 has on DAGLβ activity, as we have demonstrated that PKA directly phosphorylates this site. We have also demonstrated that phosphorylation at this site is regulated in a cellular context using a pAb. Furthermore, this phospho-site, located within the RL, is well placed to regulate the 'open' and 'closed' conformation of the enzyme. Additional studies using hydrophobic probes will help test this hypothesis. We have recently also designed, generated, and successfully expressed a DAGLβ construct with the RL (lid) deleted; enzymology studies are currently underway to establish the impact this will have on the enzymes activity.

In addition to screening mutated versions of the DAGLs in the aforementioned Tango assay, we will also determine the impact of these mutations on DAGL localisation using high resolution microscopy. This work will be further supported by a panel of pAbs we have generated against some of the reported DAGL phospho-sites.

It is not feasible to generate and thoroughly test pAbs against all 42 reported DAGL phospho-sites due to which we have focussed on the catalytic domain of the DAGLs. Generating pAbs against relatively uncharacterised phospho-sites is a high risk approach because if a pAb does not work, it is difficult to assess whether that is due to issues with the pAb, issues with the detection of the pAb or due to the fact that conditions stimulating the phosphorylation event have not been determined. Furthermore, we cannot completely rule out that some of the phospho-sites these antibodies are designed against are not genuine phospho-sites. However, with high risk comes high reward. If any of these antibodies can successfully detect the DAGLs then it is relatively straight forward to validate the phospho-site specific nature of the pAb, and as discussed earlier, a validated pAb can be a powerful biological tool to study the impact of the phospho-site, not only on the enzyme but also on its related pathways.

The approaches described above will begin to validate and assign functions to the 42 DAGL phospho-sites and as a consequence of which further our understanding on the mechanisms and pathways driving DAGL dependent eCB and eicosanoid signalling.

References

Aguado T, Monory K, Palazuelos J, Stella N, Cravatt B, Lutz B, Marsicano G, Kokaia Z, Guzman M, Galve-Roperh I (2005) The endocannabinoid system drives neural progenitor proliferation. FASEB journal : official publication of the Federation of American Societies for Experimental Biology 19:1704-1706.

Aguado T, Palazuelos J, Monory K, Stella N, Cravatt B, Lutz B, Marsicano G, Kokaia Z, Guzman M, Galve-Roperh I (2006) The endocannabinoid system promotes astroglial differentiation by acting on neural progenitor cells. The Journal of neuroscience : the official journal of the Society for Neuroscience 26:1551-1561.

Aicart-Ramos C, Valero RA, Rodriguez-Crespo I (2011) Protein palmitoylation and subcellular trafficking. Biochimica et biophysica acta 1808:2981-2994.

Alcolea MP, Kleiner O, Cutillas PR (2009) Increased confidence in large-scale phosphoproteomics data by complementary mass spectrometric techniques and matching of phosphopeptide data sets. J Proteome Res 8:3808-3815.

Alger BE (2012) Endocannabinoids at the synapse a decade after the dies mirabilis (29 March 2001): what we still do not know. The Journal of physiology 590:2203-2212.

Allen AC, Gammon CM, Ousley AH, McCarthy KD, Morell P (1992) Bradykinin stimulates arachidonic acid release through the sequential actions of an sn-1 diacylglycerol lipase and a monoacylglycerol lipase. Journal of neurochemistry 58:1130-1139.

Amanchy R, Periaswamy B, Mathivanan S, Reddy R, Tattikota SG, Pandey A (2007) A curated compendium of phosphorylation motifs. Nature biotechnology 25:285-286.

Anavi-Goffer S, Baillie G, Irving AJ, Gertsch J, Greig IR, Pertwee RG, Ross RA (2012) Modulation of L-alpha-lysophosphatidylinositol/GPR55 mitogen-activated protein kinase (MAPK) signaling by cannabinoids. The Journal of biological chemistry 287:91-104.

Anthonsen MW, Ronnstrand L, Wernstedt C, Degerman E, Holm C (1998) Identification of novel phosphorylation sites in hormone-sensitive lipase that are phosphorylated in response to isoproterenol and govern activation properties in vitro. The Journal of biological chemistry 273:215-221.

Baker D, Pryce G, Davies WL, Hiley CR (2006) In silico patent searching reveals a new cannabinoid receptor. Trends in pharmacological sciences 27:1-4.

Balgoma D, Checa A, Sar DG, Snowden S, Wheelock CE (2013) Quantitative metabolic profiling of lipid mediators. Molecular nutrition & food research.

Balsinde J, Diez E, Mollinedo F (1991) Arachidonic acid release from diacylglycerol in human neutrophils. Translocation of diacylglycerol-deacylating enzyme activities from an intracellular pool to plasma membrane upon cell activation. The Journal of biological chemistry 266:15638-15643.

Bari M, Battista N, Fezza F, Finazzi-Agro A, Maccarrone M (2005) Lipid rafts control signaling of type-1 cannabinoid receptors in neuronal cells. Implications for anandamide-induced apoptosis. The Journal of biological chemistry 280:12212-12220.

Basavarajappa BS, Saito M, Cooper TB, Hungund BL (2000) Stimulation of cannabinoid receptor agonist 2-arachidonylglycerol by chronic ethanol and its modulation by specific neuromodulators in cerebellar granule neurons. Biochimica et biophysica acta 1535:78-86.

Basu D, Manjur J, Jin W (2011) Determination of lipoprotein lipase activity using a novel fluorescent lipase assay. Journal of lipid research 52:826-832.

Bataller R, Gao B (2012) Dissecting the role of CB1 receptors on chronic liver diseases. Gut.

Begbie J, Doherty P, Graham A (2004) Cannabinoid receptor, CB1, expression follows neuronal differentiation in the early chick embryo. Journal of anatomy 205:213-218.

Bell RL, Majerus PW (1980) Thrombin-induced hydrolysis of phosphatidylinositol in human platelets. The Journal of biological chemistry 255:1790-1792.

Bell RL, Kennerly DA, Stanford N, Majerus PW (1979) Diglyceride lipase: a pathway for arachidonate release from human platelets. Proceedings of the National Academy of Sciences of the United States of America 76:3238-3241.

Berghuis P, Rajnicek AM, Morozov YM, Ross RA, Mulder J, Urban GM, Monory K, Marsicano G, Matteoli M, Canty A, Irving AJ, Katona I, Yanagawa Y, Rakic P, Lutz B, Mackie K, Harkany T (2007) Hardwiring the brain: endocannabinoids shape neuronal connectivity. Science 316:1212-1216.

Bisogno T, Melck D, De Petrocellis L, Di Marzo V (1999a) Phosphatidic acid as the biosynthetic precursor of the endocannabinoid 2-arachidonoylglycerol in intact mouse neuroblastoma cells stimulated with ionomycin. Journal of neurochemistry 72:2113-2119.

Bisogno T, Sepe N, Melck D, Maurelli S, De Petrocellis L, Di Marzo V (1997) Biosynthesis, release and degradation of the novel endogenous cannabimimetic metabolite 2-arachidonoylglycerol in mouse neuroblastoma cells. The Biochemical journal 322 (Pt 2):671-677.

Bisogno T, Berrendero F, Ambrosino G, Cebeira M, Ramos JA, Fernandez-Ruiz JJ, Di Marzo V (1999b) Brain regional distribution of endocannabinoids: implications for their biosynthesis and biological function. Biochemical and biophysical research communications 256:377-380.

Bisogno T, Howell F, Williams G, Minassi A, Cascio MG, Ligresti A, Matias I, Schiano-Moriello A, Paul P, Williams EJ, Gangadharan U, Hobbs C, Di Marzo V, Doherty P (2003) Cloning of the first sn1-DAG lipases points to the spatial and temporal regulation of endocannabinoid signaling in the brain. The Journal of cell biology 163:463-468.

Blankman JL, Simon GM, Cravatt BF (2007) A comprehensive profile of brain enzymes that hydrolyze the endocannabinoid 2-arachidonoylglycerol. Chemistry & biology 14:1347-1356.

Blom N, Gammeltoft S, Brunak S (1999) Sequence and structure-based prediction of eukaryotic protein phosphorylation sites. J Mol Biol 294:1351-1362.

Borgstrom B (1988) Mode of action of tetrahydrolipstatin: a derivative of the naturally occurring lipase inhibitor lipstatin. Biochimica et biophysica acta 962:308-316.

Bosier B, Muccioli GG, Hermans E, Lambert DM (2010) Functionally selective cannabinoid receptor signalling: therapeutic implications and opportunities. Biochemical pharmacology 80:1-12.

Brasaemle DL, Levin DM, Adler-Wailes DC, Londos C (2000) The lipolytic stimulation of 3T3-L1 adipocytes promotes the translocation of hormone-sensitive lipase to the surfaces of lipid storage droplets. Biochimica et biophysica acta 1483:251-262.

Brenowitz SD, Regehr WG (2003) Calcium dependence of retrograde inhibition by endocannabinoids at synapses onto Purkinje cells. The Journal of neuroscience : the official journal of the Society for Neuroscience 23:6373-6384.

Brill LM, Xiong W, Lee KB, Ficarro SB, Crain A, Xu Y, Terskikh A, Snyder EY, Ding S (2009) Phosphoproteomic analysis of human embryonic stem cells. Cell stem cell 5:204-213.

Brittis PA, Silver J, Walsh FS, Doherty P (1996) Fibroblast growth factor receptor function is required for the orderly projection of ganglion cell axons in the developing mammalian retina. Molecular and cellular neurosciences 8:120-128.

Brumbaugh K, Johnson W, Liao WC, Lin MS, Houchins JP, Cooper J, Stoesz S, Campos-Gonzalez R (2011) Overview of the generation, validation, and application of phosphosite-specific antibodies. Methods Mol Biol 717:3-43.

Burkey TH, Quock RM, Consroe P, Ehlert FJ, Hosohata Y, Roeske WR, Yamamura HI (1997) Relative efficacies of cannabinoid CB1 receptor agonists in the mouse brain. European journal of pharmacology 336:295-298.

Cadogan AK, Alexander SP, Boyd EA, Kendall DA (1997) Influence of cannabinoids on electrically evoked dopamine release and cyclic AMP generation in the rat striatum. Journal of neurochemistry 69:1131-1137.

Canaan S, Roussel A, Verger R, Cambillau C (1999) Gastric lipase: crystal structure and activity. Biochimica et biophysica acta 1441:197-204.

Canobbio I, Trionfini P, Guidetti GF, Balduini C, Torti M (2008) Targeting of the small GTPase Rap2b, but not Rap1b, to lipid rafts is promoted by palmitoylation at Cys176 and Cys177 and is required for efficient protein activation in human platelets. Cellular signalling 20:1662-1670.

Cao Z, Mulvihill MM, Mukhopadhyay P, Xu H, Erdelyi K, Hao E, Holovac E, Hasko G, Cravatt BF, Nomura DK, Pacher P (2013) Monoacylglycerol lipase controls endocannabinoid and eicosanoid signaling and hepatic injury in mice. Gastroenterology 144:808-817 e815.

Carrier EJ, Kearn CS, Barkmeier AJ, Breese NM, Yang W, Nithipatikom K, Pfister SL, Campbell WB, Hillard CJ (2004) Cultured rat microglial cells synthesize the endocannabinoid 2-arachidonylglycerol, which increases proliferation via a CB2 receptor-dependent mechanism. Mol Pharmacol 65:999-1007.

Castagna M, Takai Y, Kaibuchi K, Sano K, Kikkawa U, Nishizuka Y (1982) Direct activation of calcium-activated, phospholipid-dependent protein kinase by tumor-promoting phorbol esters. The Journal of biological chemistry 257:7847-7851.

Castillo PE, Younts TJ, Chavez AE, Hashimotodani Y (2012) Endocannabinoid signaling and synaptic function. Neuron 76:70-81.

Cavallaro U, Niedermeyer J, Fuxa M, Christofori G (2001) N-CAM modulates tumour-cell adhesion to matrix by inducing FGF-receptor signalling. Nature cell biology 3:650-657.

Chau LY, Tai HH (1981) Release of arachidonate from diglyceride in human platelets requires the sequential action of a diglyceride lipase and a monoglyceride lipase. Biochemical and biophysical research communications 100:1688-1695.

Chen RQ, Yang QK, Lu BW, Yi W, Cantin G, Chen YL, Fearns C, Yates JR, 3rd, Lee JD (2009) CDC25B mediates rapamycin-induced oncogenic responses in cancer cells. Cancer research 69:2663-2668.

Chijiwa T, Mishima A, Hagiwara M, Sano M, Hayashi K, Inoue T, Naito K, Toshioka T, Hidaka H (1990) Inhibition of forskolin-induced neurite outgrowth and protein phosphorylation by a newly synthesized selective inhibitor of cyclic AMP-dependent protein kinase, N-[2-(p-bromocinnamylamino)ethyl]-5-

isoquinolinesulfonamide (H-89), of PC12D pheochromocytoma cells. The Journal of biological chemistry 265:5267-5272.

Cohen P (2000) The regulation of protein function by multisite phosphorylation--a 25 year update. Trends in biochemical sciences 25:596-601.

Cravatt BF, Giang DK, Mayfield SP, Boger DL, Lerner RA, Gilula NB (1996) Molecular characterization of an enzyme that degrades neuromodulatory fatty-acid amides. Nature 384:83-87.

Cravatt BF, Demarest K, Patricelli MP, Bracey MH, Giang DK, Martin BR, Lichtman AH (2001) Supersensitivity to anandamide and enhanced endogenous cannabinoid signaling in mice lacking fatty acid amide hydrolase. Proceedings of the National Academy of Sciences of the United States of America 98:9371-9376.

Daub H, Olsen JV, Bairlein M, Gnad F, Oppermann FS, Korner R, Greff Z, Keri G, Stemmann O, Mann M (2008) Kinase-selective enrichment enables quantitative phosphoproteomics of the kinome across the cell cycle. Molecular cell 31:438-448.

de Souza NJ, Dohadwalla AN, Reden J (1983) Forskolin: a labdane diterpenoid with antihypertensive, positive inotropic, platelet aggregation inhibitory, and adenylate cyclase activating properties. Medicinal research reviews 3:201-219.

Dephoure N, Zhou C, Villen J, Beausoleil SA, Bakalarski CE, Elledge SJ, Gygi SP (2008) A quantitative atlas of mitotic phosphorylation. Proceedings of the National Academy of Sciences of the United States of America 105:10762-10767.

Derewenda U, Swenson L, Green R, Wei Y, Dodson GG, Yamaguchi S, Haas MJ, Derewenda ZS (1994) An unusual buried polar cluster in a family of fungal lipases. Nature structural biology 1:36-47.

Derkinderen P, Valjent E, Toutant M, Corvol JC, Enslen H, Ledent C, Trzaskos J, Caboche J, Girault JA (2003) Regulation of extracellular signal-regulated kinase by cannabinoids in hippocampus. The Journal of neuroscience : the official journal of the Society for Neuroscience 23:2371-2382.

Deutsch DG, Ueda N, Yamamoto S (2002) The fatty acid amide hydrolase (FAAH). Prostaglandins, leukotrienes, and essential fatty acids 66:201-210.

Devane WA, Hanus L, Breuer A, Pertwee RG, Stevenson LA, Griffin G, Gibson D, Mandelbaum A, Etinger A, Mechoulam R (1992) Isolation and structure of a brain constituent that binds to the cannabinoid receptor. Science 258:1946-1949.

Di Marzo V, Bifulco M, De Petrocellis L (2004) The endocannabinoid system and its therapeutic exploitation. Nat Rev Drug Discov 3:771-784.

Di Marzo V, Fontana A, Cadas H, Schinelli S, Cimino G, Schwartz JC, Piomelli D (1994) Formation and inactivation of endogenous cannabinoid anandamide in central neurons. Nature 372:686-691.

Di Marzo V, Bisogno T, De Petrocellis L, Melck D, Orlando P, Wagner JA, Kunos G (1999) Biosynthesis and inactivation of the endocannabinoid 2-arachidonoylglycerol in circulating and tumoral macrophages. European journal of biochemistry / FEBS 264:258-267.

Dinh TP, Carpenter D, Leslie FM, Freund TF, Katona I, Sensi SL, Kathuria S, Piomelli D (2002) Brain monoglyceride lipase participating in endocannabinoid inactivation. Proceedings of the National Academy of Sciences of the United States of America 99:10819-10824.

Dunn TA, Storm DR, Feller MB (2009) Calcium-dependent increases in protein kinase-A activity in mouse retinal ganglion cells are mediated by multiple adenylate cyclases. PloS one 4:e7877.

Dyson MR (2010) Selection of soluble protein expression constructs: the experimental determination of protein domain boundaries. Biochemical Society transactions 38:908-913.

Egertova M, Giang DK, Cravatt BF, Elphick MR (1998) A new perspective on cannabinoid signalling: complementary localization of fatty acid amide hydrolase and the CB1 receptor in rat brain. Proceedings Biological sciences / The Royal Society 265:2081-2085.

Eriksson H, Ridderstrale M, Degerman E, Ekholm D, Smith CJ, Manganiello VC, Belfrage P, Tornqvist H (1995) Evidence for the key role of the adipocyte cGMP-inhibited cAMP phosphodiesterase in the antilipolytic action of insulin. Biochimica et biophysica acta 1266:101-107.

Farooqui AA, Taylor WA, Horrocks LA (1984) Separation of bovine brain mono- and diacylglycerol lipases by heparin sepharose affinity chromatography. Biochemical and biophysical research communications 122:1241-1246.

Farooqui AA, Taylor WA, Horrocks LA (1986) Characterization and solubilization of membrane bound diacylglycerol lipases from bovine brain. The International journal of biochemistry 18:991-997.

Farooqui AA, Rammohan KW, Horrocks LA (1989) Isolation, characterization, and regulation of diacylglycerol lipases from the bovine brain. Annals of the New York Academy of Sciences 559:25-36.

Farooqui AA, Anderson DK, Horrocks LA (1993) Effect of glutamate and its analogs on diacylglycerol and monoacylglycerol lipase activities of neuron-enriched cultures. Brain research 604:180-184.

Francis DM, Page R (2010) Strategies to optimize protein expression in E. coli. Current protocols in protein science / editorial board, John E Coligan [et al] Chapter 5:Unit 5 24 21-29.

Fride E, Mechoulam R (1993) Pharmacological activity of the cannabinoid receptor agonist, anandamide, a brain constituent. European journal of pharmacology 231:313-314.

Gammon CM, Allen AC, Morell P (1989) Bradykinin stimulates phosphoinositide hydrolysis and mobilization of arachidonic acid in dorsal root ganglion neurons. Journal of neurochemistry 53:95-101.

Gao Y et al. (2010) Loss of retrograde endocannabinoid signaling and reduced adult neurogenesis in diacylglycerol lipase knock-out mice. The Journal of neuroscience : the official journal of the Society for Neuroscience 30:2017-2024.

Garton AJ, Campbell DG, Carling D, Hardie DG, Colbran RJ, Yeaman SJ (1989) Phosphorylation of bovine hormone-sensitive lipase by the AMP-activated protein kinase. A possible antilipolytic mechanism. European journal of biochemistry / FEBS 179:249-254.

Gill EW, Paton WD, Pertwee RG (1970) Preliminary experiments on the chemistry and pharmacology of cannabis. Nature 228:134-136.

Gomez O, Sanchez-Rodriguez A, Le M, Sanchez-Caro C, Molina-Holgado F, Molina-Holgado E (2011) Cannabinoid receptor agonists modulate oligodendrocyte differentiation by activating PI3K/Akt and the mammalian target of rapamycin (mTOR) pathways. British journal of pharmacology 163:1520-1532.

Gomez O, Arevalo-Martin A, Garcia-Ovejero D, Ortega-Gutierrez S, Cisneros JA, Almazan G, Sanchez-Rodriguez MA, Molina-Holgado F, Molina-Holgado E (2010) The constitutive production of the endocannabinoid 2-arachidonoylglycerol participates in oligodendrocyte differentiation. Glia 58:1913-1927.

Goncalves MB, Suetterlin P, Yip P, Molina-Holgado F, Walker DJ, Oudin MJ, Zentar MP, Pollard S, Yanez-Munoz RJ, Williams G, Walsh FS, Pangalos MN, Doherty P (2008) A diacylglycerol lipase-CB2 cannabinoid pathway regulates adult subventricular zone neurogenesis in an age-dependent manner. Molecular and cellular neurosciences 38:526-536.

Goni FM, Alonso A (1999) Structure and functional properties of diacylglycerols in membranes. Progress in lipid research 38:1-48.

Goswami T, Li X, Smith AM, Luderowski EM, Vincent JJ, Rush J, Ballif BA (2012) Comparative phosphoproteomic analysis of neonatal and adult murine brain. Proteomics 12:2185-2189.

Gregg LC, Jung KM, Spradley JM, Nyilas R, Suplita RL, 2nd, Zimmer A, Watanabe M, Mackie K, Katona I, Piomelli D, Hohmann AG (2012) Activation of type 5 metabotropic glutamate receptors and diacylglycerol lipase-alpha initiates 2-arachidonoylglycerol formation and endocannabinoid-mediated

analgesia. The Journal of neuroscience : the official journal of the Society for Neuroscience 32:9457-9468.

Gresset A, Hicks SN, Harden TK, Sondek J (2010) Mechanism of phosphorylation-induced activation of phospholipase C-gamma isozymes. The Journal of biological chemistry 285:35836-35847.

Hadvary P, Lengsfeld H, Wolfer H (1988) Inhibition of pancreatic lipase in vitro by the covalent inhibitor tetrahydrolipstatin. The Biochemical journal 256:357-361.

Hanus L, Abu-Lafi S, Fride E, Breuer A, Vogel Z, Shalev DE, Kustanovich I, Mechoulam R (2001) 2-arachidonyl glyceryl ether, an endogenous agonist of the cannabinoid CB1 receptor. Proceedings of the National Academy of Sciences of the United States of America 98:3662-3665.

Harizi H, Corcuff JB, Gualde N (2008) Arachidonic-acid-derived eicosanoids: roles in biology and immunopathology. Trends in molecular medicine 14:461-469.

Hasegawa-Sasaki H (1985) Early changes in inositol lipids and their metabolites induced by platelet-derived growth factor in quiescent Swiss mouse 3T3 cells. The Biochemical journal 232:99-109.

Hashimotodani Y, Ohno-Shosaku T, Kano M (2007a) Endocannabinoids and synaptic function in the CNS. The Neuroscientist : a review journal bringing neurobiology, neurology and psychiatry 13:127-137.

Hashimotodani Y, Ohno-Shosaku T, Kano M (2007b) Ca(2+)-assisted receptor-driven endocannabinoid release: mechanisms that associate presynaptic and postsynaptic activities. Current opinion in neurobiology 17:360-365.

Hashimotodani Y, Ohno-Shosaku T, Kano M (2007c) Presynaptic monoacylglycerol lipase activity determines basal endocannabinoid tone and terminates retrograde endocannabinoid signaling in the hippocampus. The Journal of neuroscience : the official journal of the Society for Neuroscience 27:1211-1219.

Hashimotodani Y, Ohno-Shosaku T, Maejima T, Fukami K, Kano M (2008) Pharmacological evidence for the involvement of diacylglycerol lipase in depolarization-induced endocanabinoid release. Neuropharmacology 54:58-67.

Hashimotodani Y, Ohno-Shosaku T, Tanimura A, Kita Y, Sano Y, Shimizu T, Di Marzo V, Kano M (2013) Acute inhibition of diacylglycerol lipase blocks endocannabinoid-mediated retrograde synaptic suppression: evidence for on-demand biosynthesis of 2-arachidonoylglycerol. The Journal of physiology.

Herkenham M, Lynn AB, Little MD, Johnson MR, Melvin LS, de Costa BR, Rice KC (1990) Cannabinoid receptor localization in brain. Proceedings of

the National Academy of Sciences of the United States of America 87:1932-1936.

Holm C (2003) Molecular mechanisms regulating hormone-sensitive lipase and lipolysis. Biochem Soc Trans 31:1120-1124.

Holm C, Belfrage P, Osterlund T, Davis RC, Schotz MC, Langin D (1994) Hormone-sensitive lipase: structure, function, evolution and overproduction in insect cells using the baculovirus expression system. Protein engineering 7:537-541.

Holmquist M (2000) Alpha/Beta-hydrolase fold enzymes: structures, functions and mechanisms. Curr Protein Pept Sci 1:209-235.

Hoover HS, Blankman JL, Niessen S, Cravatt BF (2008) Selectivity of inhibitors of endocannabinoid biosynthesis evaluated by activity-based protein profiling. Bioorganic & medicinal chemistry letters 18:5838-5841.

Hou W, Arita Y, Morisset J (1997) Endogenous arachidonic acid release and pancreatic amylase secretion. Pancreas 14:301-308.

Houghton FJ, Bellingham SA, Hill AF, Bourges D, Ang DK, Gemetzis T, Gasnereau I, Gleeson PA (2012) Arl5b is a Golgi-localised small G protein involved in the regulation of retrograde transport. Experimental cell research 318:464-477.

Howlett AC (1995) Pharmacology of cannabinoid receptors. Annual review of pharmacology and toxicology 35:607-634.

Hsu KL, Tsuboi K, Adibekian A, Pugh H, Masuda K, Cravatt BF (2012) DAGLbeta inhibition perturbs a lipid network involved in macrophage inflammatory responses. Nature chemical biology 8:999-1007.

Hsu PP, Kang SA, Rameseder J, Zhang Y, Ottina KA, Lim D, Peterson TR, Choi Y, Gray NS, Yaffe MB, Marto JA, Sabatini DM (2011) The mTOR-regulated phosphoproteome reveals a mechanism of mTORC1-mediated inhibition of growth factor signaling. Science 332:1317-1322.

Huang SM, Strangman NM, Walker JM (1999) Liquid chromatographic-mass spectrometric measurement of the endogenous cannabinoid 2-arachidonylglycerol in the spinal cord and peripheral nervous system. Zhongguo yao li xue bao = Acta pharmacologica Sinica 20:1098-1102.

Huttlin EL, Jedrychowski MP, Elias JE, Goswami T, Rad R, Beausoleil SA, Villen J, Haas W, Sowa ME, Gygi SP (2010) A tissue-specific atlas of mouse protein phosphorylation and expression. Cell 143:1174-1189.

Iakoucheva LM, Radivojac P, Brown CJ, O'Connor TR, Sikes JG, Obradovic Z, Dunker AK (2004) The importance of intrinsic disorder for protein phosphorylation. Nucleic Acids Res 32:1037-1049.

Jain T, Wager-Miller J, Mackie K, Straiker A (2013) Diacylglycerol Lipasealpha (DAGLalpha) and DAGLbeta Cooperatively Regulate the Production of 2-Arachidonoyl Glycerol in Autaptic Hippocampal Neurons. Mol Pharmacol 84:296-302.

Jarvis DL (2009) Baculovirus-insect cell expression systems. Methods Enzymol 463:191-222.

Jeong WI, Osei-Hyiaman D, Park O, Liu J, Batkai S, Mukhopadhyay P, Horiguchi N, Harvey-White J, Marsicano G, Lutz B, Gao B, Kunos G (2008) Paracrine activation of hepatic CB1 receptors by stellate cell-derived endocannabinoids mediates alcoholic fatty liver. Cell Metab 7:227-235.

Jiang W, Zhang Y, Xiao L, Van Cleemput J, Ji SP, Bai G, Zhang X (2005) Cannabinoids promote embryonic and adult hippocampus neurogenesis and produce anxiolytic- and antidepressant-like effects. The Journal of clinical investigation 115:3104-3116.

Jin K, Xie L, Kim SH, Parmentier-Batteur S, Sun Y, Mao XO, Childs J, Greenberg DA (2004) Defective adult neurogenesis in CB1 cannabinoid receptor knockout mice. Mol Pharmacol 66:204-208.

Johnson LN, Lewis RJ (2001) Structural basis for control by phosphorylation. Chemical reviews 101:2209-2242.

Johnston M, Bhatt SR, Sikka S, Mercier RW, West JM, Makriyannis A, Gatley SJ, Duclos RI, Jr. (2012) Assay and inhibition of diacylglycerol lipase activity. Bioorganic & medicinal chemistry letters 22:4585-4592.

Jung KM, Astarita G, Thongkham D, Piomelli D (2011) Diacylglycerol lipase-alpha and -beta control neurite outgrowth in neuro-2a cells through distinct molecular mechanisms. Mol Pharmacol 80:60-67.

Jung KM, Astarita G, Zhu C, Wallace M, Mackie K, Piomelli D (2007) A key role for diacylglycerol lipase-alpha in metabotropic glutamate receptor-dependent endocannabinoid mobilization. Mol Pharmacol 72:612-621.

Jung KM, Sepers M, Henstridge CM, Lassalle O, Neuhofer D, Martin H, Ginger M, Frick A, DiPatrizio NV, Mackie K, Katona I, Piomelli D, Manzoni OJ (2012) Uncoupling of the endocannabinoid signalling complex in a mouse model of fragile X syndrome. Nature communications 3:1080.

Kang R, Wan J, Arstikaitis P, Takahashi H, Huang K, Bailey AO, Thompson JX, Roth AF, Drisdel RC, Mastro R, Green WN, Yates JR, 3rd, Davis NG, El-Husseini A (2008) Neural palmitoyl-proteomics reveals dynamic synaptic palmitoylation. Nature 456:904-909.

Katona I, Sperlagh B, Sik A, Kafalvi A, Vizi ES, Mackie K, Freund TF (1999) Presynaptically located CB1 cannabinoid receptors regulate GABA release from axon terminals of specific hippocampal interneurons. The Journal of neuroscience : the official journal of the Society for Neuroscience 19:4544-4558.

Katona I, Urban GM, Wallace M, Ledent C, Jung KM, Piomelli D, Mackie K, Freund TF (2006) Molecular composition of the endocannabinoid system at glutamatergic synapses. The Journal of neuroscience : the official journal of the Society for Neuroscience 26:5628-5637.

Katona I, Sperlagh B, Magloczky Z, Santha E, Kofalvi A, Czirjak S, Mackie K, Vizi ES, Freund TF (2000) GABAergic interneurons are the targets of cannabinoid actions in the human hippocampus. Neuroscience 100:797-804.

Kawamura Y, Fukaya M, Maejima T, Yoshida T, Miura E, Watanabe M, Ohno-Shosaku T, Kano M (2006) The CB1 cannabinoid receptor is the major cannabinoid receptor at excitatory presynaptic sites in the hippocampus and cerebellum. The Journal of neuroscience : the official journal of the Society for Neuroscience 26:2991-3001.

Keimpema E, Mackie K, Harkany T (2011) Molecular model of cannabis sensitivity in developing neuronal circuits. Trends in pharmacological sciences 32:551-561.

Keimpema E, Barabas K, Morozov YM, Tortoriello G, Torii M, Cameron G, Yanagawa Y, Watanabe M, Mackie K, Harkany T (2010) Differential subcellular recruitment of monoacylglycerol lipase generates spatial specificity of 2-arachidonoyl glycerol signaling during axonal pathfinding. The Journal of neuroscience : the official journal of the Society for Neuroscience 30:13992-14007.

Keimpema E, Tortoriello G, Alpar A, Capsoni S, Arisi I, Calvigioni D, Hu SS, Cattaneo A, Doherty P, Mackie K, Harkany T (2013) Nerve growth factor scales endocannabinoid signaling by regulating monoacylglycerol lipase turnover in developing cholinergic neurons. Proceedings of the National Academy of Sciences of the United States of America 110:1935-1940.

Kidd D, Liu Y, Cravatt BF (2001) Profiling serine hydrolase activities in complex proteomes. Biochemistry 40:4005-4015.

Kinoshita E, Kinoshita-Kikuta E, Takiyama K, Koike T (2006) Phosphate-binding tag, a new tool to visualize phosphorylated proteins. Molecular & cellular proteomics : MCP 5:749-757.

Kishimoto A, Nishiyama K, Nakanishi H, Uratsuji Y, Nomura H, Takeyama Y, Nishizuka Y (1985) Studies on the phosphorylation of myelin basic protein by protein kinase C and adenosine 3':5'-monophosphate-dependent protein kinase. The Journal of biological chemistry 260:12492-12499.

Kondo S, Kondo H, Nakane S, Kodaka T, Tokumura A, Waku K, Sugiura T (1998) 2-Arachidonoylglycerol, an endogenous cannabinoid receptor agonist: identification as one of the major species of monoacylglycerols in various rat tissues, and evidence for its generation through CA2+-dependent and -independent mechanisms. FEBS letters 429:152-156.

Kost TA, Condreay JP, Jarvis DL (2005) Baculovirus as versatile vectors for protein expression in insect and mammalian cells. Nature biotechnology 23:567-575.

Kreitzer AC, Regehr WG (2001a) Retrograde inhibition of presynaptic calcium influx by endogenous cannabinoids at excitatory synapses onto Purkinje cells. Neuron 29:717-727.

Kreitzer AC, Regehr WG (2001b) Cerebellar depolarization-induced suppression of inhibition is mediated by endogenous cannabinoids. The Journal of neuroscience : the official journal of the Society for Neuroscience 21:RC174.

Krintel C, Morgelin M, Logan DT, Holm C (2009) Phosphorylation of hormone-sensitive lipase by protein kinase A in vitro promotes an increase in its hydrophobic surface area. FEBS J 276:4752-4762.

Kurat CF, Wolinski H, Petschnigg J, Kaluarachchi S, Andrews B, Natter K, Kohlwein SD (2009) Cdk1/Cdc28-dependent activation of the major triacylglycerol lipase Tgl4 in yeast links lipolysis to cell-cycle progression. Molecular cell 33:53-63.

Lampidonis AD, Rogdakis E, Voutsinas GE, Stravopodis DJ (2011) The resurgence of Hormone-Sensitive Lipase (HSL) in mammalian lipolysis. Gene 477:1-11.

Lee MW, Severson DL (1994) Partial purification of a diacylglycerol lipase from bovine aorta. The Biochemical journal 298 (Pt 1):213-219.

Lee MW, Kraemer FB, Severson DL (1995) Characterization of a partially purified diacylglycerol lipase from bovine aorta. Biochimica et biophysica acta 1254:311-318.

Leung D, Saghatelian A, Simon GM, Cravatt BF (2006) Inactivation of N-acyl phosphatidylethanolamine phospholipase D reveals multiple mechanisms for the biosynthesis of endocannabinoids. Biochemistry 45:4720-4726.

Liebler DC, Zimmerman LJ (2013) Targeted quantitation of proteins by mass spectrometry. Biochemistry 52:3797-3806.

Ligresti A, Cascio MG, Di Marzo V (2005) Endocannabinoid metabolic pathways and enzymes. Current drug targets CNS and neurological disorders 4:615-623.

Linke D (2009) Detergents: an overview. Methods Enzymol 463:603-617.

Lister MF, Sharkey J, Sawatzky DA, Hodgkiss JP, Davidson DJ, Rossi AG, Finlayson K (2007) The role of the purinergic P2X7 receptor in inflammation. J Inflamm (Lond) 4:5.

Liu J, Wang L, Harvey-White J, Osei-Hyiaman D, Razdan R, Gong Q, Chan AC, Zhou Z, Huang BX, Kim HY, Kunos G (2006) A biosynthetic pathway for

anandamide. Proceedings of the National Academy of Sciences of the United States of America 103:13345-13350.

Liu Y, Patricelli MP, Cravatt BF (1999) Activity-based protein profiling: the serine hydrolases. Proceedings of the National Academy of Sciences of the United States of America 96:14694-14699.

Lom B, Hopker V, McFarlane S, Bixby JL, Holt CE (1998) Fibroblast growth factor receptor signaling in Xenopus retinal axon extension. J Neurobiol 37:633-641.

Long JZ, Li W, Booker L, Burston JJ, Kinsey SG, Schlosburg JE, Pavon FJ, Serrano AM, Selley DE, Parsons LH, Lichtman AH, Cravatt BF (2009) Selective blockade of 2-arachidonoylglycerol hydrolysis produces cannabinoid behavioral effects. Nature chemical biology 5:37-44.

Macek B, Mann M, Olsen JV (2009) Global and site-specific quantitative phosphoproteomics: principles and applications. Annual review of pharmacology and toxicology 49:199-221.

Maejima T, Hashimoto K, Yoshida T, Aiba A, Kano M (2001) Presynaptic inhibition caused by retrograde signal from metabotropic glutamate to cannabinoid receptors. Neuron 31:463-475.

Makara JK, Mor M, Fegley D, Szabo SI, Kathuria S, Astarita G, Duranti A, Tontini A, Tarzia G, Rivara S, Freund TF, Piomelli D (2005) Selective inhibition of 2-AG hydrolysis enhances endocannabinoid signaling in hippocampus. Nat Neurosci 8:1139-1141.

Malcher-Lopes R, Di S, Marcheselli VS, Weng FJ, Stuart CT, Bazan NG, Tasker JG (2006) Opposing crosstalk between leptin and glucocorticoids rapidly modulates synaptic excitation via endocannabinoid release. The Journal of neuroscience : the official journal of the Society for Neuroscience 26:6643-6650.

Martin BR, Cravatt BF (2009) Large-scale profiling of protein palmitoylation in mammalian cells. Nat Methods 6:135-138.

Martin BR, Compton DR, Thomas BF, Prescott WR, Little PJ, Razdan RK, Johnson MR, Melvin LS, Mechoulam R, Ward SJ (1991) Behavioral, biochemical, and molecular modeling evaluations of cannabinoid analogs. Pharmacology, biochemistry, and behavior 40:471-478.

Martiny-Baron G, Kazanietz MG, Mischak H, Blumberg PM, Kochs G, Hug H, Marme D, Schachtele C (1993) Selective inhibition of protein kinase C isozymes by the indolocarbazole Go 6976. The Journal of biological chemistry 268:9194-9197.

Matsuda LA, Lolait SJ, Brownstein MJ, Young AC, Bonner TI (1990) Structure of a cannabinoid receptor and functional expression of the cloned cDNA. Nature 346:561-564.

Mayya V, Lundgren DH, Hwang SI, Rezaul K, Wu L, Eng JK, Rodionov V, Han DK (2009) Quantitative phosphoproteomic analysis of T cell receptor signaling reveals system-wide modulation of protein-protein interactions. Science signaling 2:ra46.

McCoy CE, Campbell DG, Deak M, Bloomberg GB, Arthur JS (2005) MSK1 activity is controlled by multiple phosphorylation sites. The Biochemical journal 387:507-517.

Mechoulam R, Gaoni Y (1965) A Total Synthesis of Dl-Delta-1-Tetrahydrocannabinol, the Active Constituent of Hashish. Journal of the American Chemical Society 87:3273-3275.

Mechoulam R, Ben-Shabat S, Hanus L, Ligumsky M, Kaminski NE, Schatz AR, Gopher A, Almog S, Martin BR, Compton DR, et al. (1995) Identification of an endogenous 2-monoglyceride, present in canine gut, that binds to cannabinoid receptors. Biochemical pharmacology 50:83-90.

Miled N, Bussetta C, De caro A, Riviere M, Berti L, Canaan S (2003) Importance of the lid and cap domains for the catalytic activity of gastric lipases. Comp Biochem Physiol B Biochem Mol Biol 136:131-138.

Min M, Mayor U, Lindon C (2013) Ubiquitination site preferences in anaphase promoting complex/cyclosome (APC/C) substrates. Open biology 3:130097.

Min R, Di Marzo V, Mansvelder HD (2010a) DAG lipase involvement in depolarization-induced suppression of inhibition: does endocannabinoid biosynthesis always meet the demand? The Neuroscientist : a review journal bringing neurobiology, neurology and psychiatry 16:608-613.

Min R, Testa-Silva G, Heistek TS, Canto CB, Lodder JC, Bisogno T, Di Marzo V, Brussaard AB, Burnashev N, Mansvelder HD (2010b) Diacylglycerol lipase is not involved in depolarization-induced suppression of inhibition at unitary inhibitory connections in mouse hippocampus. The Journal of neuroscience : the official journal of the Society for Neuroscience 30:2710-2715.

Ming GL, Song H (2011) Adult neurogenesis in the mammalian brain: significant answers and significant questions. Neuron 70:687-702.

Molina-Holgado F, Rubio-Araiz A, Garcia-Ovejero D, Williams RJ, Moore JD, Arevalo-Martin A, Gomez-Torres O, Molina-Holgado E (2007) CB2 cannabinoid receptors promote mouse neural stem cell proliferation. The European journal of neuroscience 25:629-634.

Morales M, Backman C (2002) Coexistence of serotonin 3 (5-HT3) and CB1 cannabinoid receptors in interneurons of hippocampus and dentate gyrus. Hippocampus 12:756-764.

Moreira FA, Crippa JA (2009) The psychiatric side-effects of rimonabant. Rev Bras Psiquiatr 31:145-153.

Moriyama T, Urade R, Kito M (1999) Purification and characterization of diacylglycerol lipase from human platelets. Journal of biochemistry 125:1077-1085.

Mulder J, Aguado T, Keimpema E, Barabas K, Ballester Rosado CJ, Nguyen L, Monory K, Marsicano G, Di Marzo V, Hurd YL, Guillemot F, Mackie K, Lutz B, Guzman M, Lu HC, Galve-Roperh I, Harkany T (2008) Endocannabinoid signaling controls pyramidal cell specification and long-range axon patterning. Proceedings of the National Academy of Sciences of the United States of America 105:8760-8765.

Munro S, Thomas KL, Abu-Shaar M (1993) Molecular characterization of a peripheral receptor for cannabinoids. Nature 365:61-65.

Munton RP, Tweedie-Cullen R, Livingstone-Zatchej M, Weinandy F, Waidelich M, Longo D, Gehrig P, Potthast F, Rutishauser D, Gerrits B, Panse C, Schlapbach R, Mansuy IM (2007) Qualitative and quantitative analyses of protein phosphorylation in naive and stimulated mouse synaptosomal preparations. Molecular & cellular proteomics : MCP 6:283-293.

Nakane S, Oka S, Arai S, Waku K, Ishima Y, Tokumura A, Sugiura T (2002) 2-Arachidonoyl-sn-glycero-3-phosphate, an arachidonic acid-containing lysophosphatidic acid: occurrence and rapid enzymatic conversion to 2-arachidonoyl-sn-glycerol, a cannabinoid receptor ligand, in rat brain. Archives of biochemistry and biophysics 402:51-58.

Nardini M, Dijkstra BW (1999) Alpha/beta hydrolase fold enzymes: the family keeps growing. Curr Opin Struct Biol 9:732-737.

Nieman MT, Prudoff RS, Johnson KR, Wheelock MJ (1999) N-cadherin promotes motility in human breast cancer cells regardless of their E-cadherin expression. The Journal of cell biology 147:631-644.

Nomura DK, Blankman JL, Simon GM, Fujioka K, Issa RS, Ward AM, Cravatt BF, Casida JE (2008a) Activation of the endocannabinoid system by organophosphorus nerve agents. Nature chemical biology 4:373-378.

Nomura DK, Hudak CS, Ward AM, Burston JJ, Issa RS, Fisher KJ, Abood ME, Wiley JL, Lichtman AH, Casida JE (2008b) Monoacylglycerol lipase regulates 2-arachidonoylglycerol action and arachidonic acid levels. Bioorganic & medicinal chemistry letters 18:5875-5878.

Nomura DK, Morrison BE, Blankman JL, Long JZ, Kinsey SG, Marcondes MC, Ward AM, Hahn YK, Lichtman AH, Conti B, Cravatt BF (2011) Endocannabinoid hydrolysis generates brain prostaglandins that promote neuroinflammation. Science 334:809-813.

Nyilas R, Gregg LC, Mackie K, Watanabe M, Zimmer A, Hohmann AG, Katona I (2009) Molecular architecture of endocannabinoid signaling at nociceptive synapses mediating analgesia. The European journal of neuroscience 29:1964-1978.

Oddi S, Dainese E, Sandiford S, Fezza F, Lanuti M, Chiurchiu V, Totaro A, Catanzaro G, Barcaroli D, De Laurenzi V, Centonze D, Mukhopadhyay S, Selent J, Howlett AC, Maccarrone M (2012) Effects of palmitoylation of Cys(415) in helix 8 of the CB(1) cannabinoid receptor on membrane localization and signalling. British journal of pharmacology 165:2635-2651.

Oka S, Kimura S, Toshida T, Ota R, Yamashita A, Sugiura T (2010) Lysophosphatidylinositol induces rapid phosphorylation of p38 mitogen-activated protein kinase and activating transcription factor 2 in HEK293 cells expressing GPR55 and IM-9 lymphoblastoid cells. Journal of biochemistry 147:671-678.

Okamoto Y, Morishita J, Tsuboi K, Tonai T, Ueda N (2004) Molecular characterization of a phospholipase D generating anandamide and its congeners. The Journal of biological chemistry 279:5298-5305.

Okazaki T, Sagawa N, Okita JR, Bleasdale JE, MacDonald PC, Johnston JM (1981) Diacylglycerol metabolism and arachidonic acid release in human fetal membranes and decidua vera. The Journal of biological chemistry 256:7316-7321.

Olsen JV, Vermeulen M, Santamaria A, Kumar C, Miller ML, Jensen LJ, Gnad F, Cox J, Jensen TS, Nigg EA, Brunak S, Mann M (2010) Quantitative phosphoproteomics reveals widespread full phosphorylation site occupancy during mitosis. Science signaling 3:ra3.

Ortar G, Bisogno T, Ligresti A, Morera E, Nalli M, Di Marzo V (2008) Tetrahydrolipstatin analogues as modulators of endocannabinoid 2-arachidonoylglycerol metabolism. Journal of medicinal chemistry 51:6970-6979.

Osei-Hyiaman D, Liu J, Zhou L, Godlewski G, Harvey-White J, Jeong WI, Batkai S, Marsicano G, Lutz B, Buettner C, Kunos G (2008) Hepatic CB1 receptor is required for development of diet-induced steatosis, dyslipidemia, and insulin and leptin resistance in mice. The Journal of clinical investigation 118:3160-3169.

Oudin MJ, Hobbs C, Doherty P (2011a) DAGL-dependent endocannabinoid signalling: roles in axonal pathfinding, synaptic plasticity and adult neurogenesis. The European journal of neuroscience 34:1634-1646.

Oudin MJ, Gajendra S, Williams G, Hobbs C, Lalli G, Doherty P (2011b) Endocannabinoids regulate the migration of subventricular zone-derived neuroblasts in the postnatal brain. The Journal of neuroscience : the official journal of the Society for Neuroscience 31:4000-4011.

Pacher P, Mechoulam R (2011) Is lipid signaling through cannabinoid 2 receptors part of a protective system? Progress in lipid research 50:193-211.

Pacher P, Kunos G (2013) Modulating the endocannabinoid system in human health and disease--successes and failures. FEBS J 280:1918-1943.

Palazuelos J, Aguado T, Egia A, Mechoulam R, Guzman M, Galve-Roperh I (2006) Non-psychoactive CB2 cannabinoid agonists stimulate neural progenitor proliferation. FASEB journal : official publication of the Federation of American Societies for Experimental Biology 20:2405-2407.

Pan B, Wang W, Long JZ, Sun D, Hillard CJ, Cravatt BF, Liu QS (2009) Blockade of 2-arachidonoylglycerol hydrolysis by selective monoacylglycerol lipase inhibitor 4-nitrophenyl 4-(dibenzo[d][1,3]dioxol-5-yl(hydroxy)methyl)piperidine-1-carboxylate (JZL184) Enhances retrograde endocannabinoid signaling. The Journal of pharmacology and experimental therapeutics 331:591-597.

Paradela A, Albar JP (2008) Advances in the analysis of protein phosphorylation. J Proteome Res 7:1809-1818.

Patricelli MP, Giang DK, Stamp LM, Burbaum JJ (2001) Direct visualization of serine hydrolase activities in complex proteomes using fluorescent active site-directed probes. Proteomics 1:1067-1071.

Pedicord DL, Flynn MJ, Fanslau C, Miranda M, Hunihan L, Robertson BJ, Pearce BC, Yu XC, Westphal RS, Blat Y (2011) Molecular characterization and identification of surrogate substrates for diacylglycerol lipase alpha. Biochemical and biophysical research communications 411:809-814.

Perez Roque ME, Pasquare SJ, Castagnet PI, Giusto NM (1998) Can phosphorylation and dephosphorylation of rod outer segment membranes affect phosphatidate phosphohydrolase and diacylglycerol lipase activities? Comparative biochemistry and physiology Part B, Biochemistry & molecular biology 119:85-93.

Pertwee RG (2012) Targeting the endocannabinoid system with cannabinoid receptor agonists: pharmacological strategies and therapeutic possibilities. Philosophical transactions of the Royal Society of London Series B, Biological sciences 367:3353-3363.

Piro JR, Benjamin DI, Duerr JM, Pi Y, Gonzales C, Wood KM, Schwartz JW, Nomura DK, Samad TA (2012) A dysregulated endocannabinoid-eicosanoid network supports pathogenesis in a mouse model of Alzheimer's disease. Cell reports 1:617-623.

Placzek EA, Okamoto Y, Ueda N, Barker EL (2008) Membrane microdomains and metabolic pathways that define anandamide and 2-arachidonyl glycerol biosynthesis and breakdown. Neuropharmacology 55:1095-1104.

Porter AC, Sauer JM, Knierman MD, Becker GW, Berna MJ, Bao J, Nomikos GG, Carter P, Bymaster FP, Leese AB, Felder CC (2002) Characterization of a novel endocannabinoid, virodhamine, with antagonist activity at the CB1 receptor. The Journal of pharmacology and experimental therapeutics 301:1020-1024.

Prescott SM, Majerus PW (1983) Characterization of 1,2-diacylglycerol hydrolysis in human platelets. Demonstration of an arachidonoyl-monoacylglycerol intermediate. The Journal of biological chemistry 258:764-769.

Raijmakers R, Kraiczek K, de Jong AP, Mohammed S, Heck AJ (2010) Exploring the human leukocyte phosphoproteome using a microfluidic reversed-phase-TiO2-reversed-phase high-performance liquid chromatography phosphochip coupled to a quadrupole time-of-flight mass spectrometer. Anal Chem 82:824-832.

Rancz EA, Hausser M (2006) Dendritic calcium spikes are tunable triggers of cannabinoid release and short-term synaptic plasticity in cerebellar Purkinje neurons. The Journal of neuroscience : the official journal of the Society for Neuroscience 26:5428-5437.

Reisenberg M, Singh PK, Williams G, Doherty P (2012) The diacylglycerol lipases: structure, regulation and roles in and beyond endocannabinoid signalling. Philosophical transactions of the Royal Society of London Series B, Biological sciences 367:3264-3275.

Rellos P, Pike AC, Niesen FH, Salah E, Lee WH, von Delft F, Knapp S (2010) Structure of the CaMKIIdelta/calmodulin complex reveals the molecular mechanism of CaMKII kinase activation. PLoS biology 8:e1000426.

Rice AE, Mendez MJ, Hokanson CA, Rees DC, Bjorkman PJ (2009) Investigation of the biophysical and cell biological properties of ferroportin, a multipass integral membrane protein iron exporter. J Mol Biol 386:717-732.

Rikova K et al. (2007) Global survey of phosphotyrosine signaling identifies oncogenic kinases in lung cancer. Cell 131:1190-1203.

Rimmerman N, Hughes HV, Bradshaw HB, Pazos MX, Mackie K, Prieto AL, Walker JM (2008) Compartmentalization of endocannabinoids into lipid rafts in a dorsal root ganglion cell line. British journal of pharmacology 153:380-389.

Rittenhouse-Simmons S (1979) Production of diglyceride from phosphatidylinositol in activated human platelets. The Journal of clinical investigation 63:580-587.

Rosenberger TA, Farooqui AA, Horrocks LA (2007) Bovine brain diacylglycerol lipase: substrate specificity and activation by cyclic AMP-dependent protein kinase. Lipids 42:187-195.

Rosenberger TA, Villacreses NE, Contreras MA, Bonventre JV, Rapoport SI (2003) Brain lipid metabolism in the cPLA2 knockout mouse. Journal of lipid research 44:109-117.

Ross RA (2003) Anandamide and vanilloid TRPV1 receptors. British journal of pharmacology 140:790-801.

Roth SH (1978) Stereospecific presynaptic inhibitory effect of delta9-tetrahydrocannabinol on cholinergic transmission in the myenteric plexus of the guinea pig. Canadian journal of physiology and pharmacology 56:968-975.

Roussel A, Canaan S, Egloff MP, Riviere M, Dupuis L, Verger R, Cambillau C (1999) Crystal structure of human gastric lipase and model of lysosomal acid lipase, two lipolytic enzymes of medical interest. The Journal of biological chemistry 274:16995-17002.

Roussel A, Miled N, Berti-Dupuis L, Riviere M, Spinelli S, Berna P, Gruber V, Verger R, Cambillau C (2002) Crystal structure of the open form of dog gastric lipase in complex with a phosphonate inhibitor. The Journal of biological chemistry 277:2266-2274.

Rubio-Araiz A, Arevalo-Martin A, Gomez-Torres O, Navarro-Galve B, Garcia-Ovejero D, Suetterlin P, Sanchez-Heras E, Molina-Holgado E, Molina-Holgado F (2008) The endocannabinoid system modulates a transient TNF pathway that induces neural stem cell proliferation. Molecular and cellular neurosciences 38:374-380.

Russo EB, Jiang HE, Li X, Sutton A, Carboni A, del Bianco F, Mandolino G, Potter DJ, Zhao YX, Bera S, Zhang YB, Lu EG, Ferguson DK, Hueber F, Zhao LC, Liu CJ, Wang YF, Li CS (2008) Phytochemical and genetic analyses of ancient cannabis from Central Asia. Journal of experimental botany 59:4171-4182.

Ryberg E, Larsson N, Sjogren S, Hjorth S, Hermansson NO, Leonova J, Elebring T, Nilsson K, Drmota T, Greasley PJ (2007) The orphan receptor GPR55 is a novel cannabinoid receptor. British journal of pharmacology 152:1092-1101.

Saffell JL, Williams EJ, Mason IJ, Walsh FS, Doherty P (1997) Expression of a dominant negative FGF receptor inhibits axonal growth and FGF receptor phosphorylation stimulated by CAMs. Neuron 18:231-242.

Salameh MA, Wiegel J (2010) Effects of Detergents on Activity, Thermostability and Aggregation of Two Alkalithermophilic Lipases from Thermosyntropha lipolytica. The open biochemistry journal 4:22-28.

Salazar C, Hofer T (2009) Multisite protein phosphorylation--from molecular mechanisms to kinetic models. FEBS J 276:3177-3198.

Sarnataro D, Grimaldi C, Pisanti S, Gazzerro P, Laezza C, Zurzolo C, Bifulco M (2005) Plasma membrane and lysosomal localization of CB1 cannabinoid receptor are dependent on lipid rafts and regulated by anandamide in human breast cancer cells. FEBS letters 579:6343-6349.

Schlicker E, Kathmann M (2001) Modulation of transmitter release via presynaptic cannabinoid receptors. Trends in pharmacological sciences 22:565-572.

Schlosburg JE, Blankman JL, Long JZ, Nomura DK, Pan B, Kinsey SG, Nguyen PT, Ramesh D, Booker L, Burston JJ, Thomas EA, Selley DE, Sim-Selley LJ, Liu QS, Lichtman AH, Cravatt BF (2010) Chronic monoacylglycerol lipase blockade causes functional antagonism of the endocannabinoid system. Nat Neurosci 13:1113-1119.

Shiraishi-Yamaguchi Y, Furuichi T (2007) The Homer family proteins. Genome biology 8:206.

Shiromizu T, Adachi J, Watanabe S, Murakami T, Kuga T, Muraoka S, Tomonaga T (2013) Identification of missing proteins in the neXtProt database and unregistered phosphopeptides in the PhosphoSitePlus database as part of the Chromosome-centric Human Proteome Project. J Proteome Res 12:2414-2421.

Shonesy BC, Wang X, Rose KL, Ramikie TS, Cavener VS, Rentz T, Baucum AJ, 2nd, Jalan-Sakrikar N, Mackie K, Winder DG, Patel S, Colbran RJ (2013) CaMKII regulates diacylglycerol lipase-alpha and striatal endocannabinoid signaling. Nat Neurosci 16:456-463.

Sidorov MS, Auerbach BD, Bear MF (2013) Fragile X mental retardation protein and synaptic plasticity. Molecular brain 6:15.

Simon GM, Cravatt BF (2006) Endocannabinoid biosynthesis proceeding through glycerophospho-N-acyl ethanolamine and a role for alpha/beta-hydrolase 4 in this pathway. The Journal of biological chemistry 281:26465-26472.

Simon GM, Cravatt BF (2008) Anandamide biosynthesis catalyzed by the phosphodiesterase GDE1 and detection of glycerophospho-N-acyl ethanolamine precursors in mouse brain. The Journal of biological chemistry 283:9341-9349.

Simon GM, Cravatt BF (2010) Characterization of mice lacking candidate N-acyl ethanolamine biosynthetic enzymes provides evidence for multiple pathways that contribute to endocannabinoid production in vivo. Molecular bioSystems 6:1411-1418.

Singh PK, Chan PF, Hibbs MJ, Vazquez MJ, Segura DC, Thomas DA, Theobald AJ, Gallagher KT, Hassan NJ (2011) High-yield production and characterization of biologically active GST-tagged human topoisomerase IIalpha protein in insect cells for the development of a high-throughput assay. Protein expression and purification 76:165-172.

Skaper SD, Di Marzo V (2012) Endocannabinoids in nervous system health and disease: the big picture in a nutshell. Philosophical transactions of the Royal Society of London Series B, Biological sciences 367:3193-3200.

St-Denis N, Gingras AC (2012) Mass spectrometric tools for systematic analysis of protein phosphorylation. Progress in molecular biology and translational science 106:3-32.

Steen H, Jebanathirajah JA, Rush J, Morrice N, Kirschner MW (2006) Phosphorylation analysis by mass spectrometry: myths, facts, and the consequences for qualitative and quantitative measurements. Molecular & cellular proteomics : MCP 5:172-181.

Steinberg SF (2008) Structural basis of protein kinase C isoform function. Physiol Rev 88:1341-1378.

Stella N, Piomelli D (2001) Receptor-dependent formation of endogenous cannabinoids in cortical neurons. European journal of pharmacology 425:189-196.

Stella N, Schweitzer P, Piomelli D (1997) A second endogenous cannabinoid that modulates long-term potentiation. Nature 388:773-778.

Straiker A, Stella N, Piomelli D, Mackie K, Karten HJ, Maguire G (1999) Cannabinoid CB1 receptors and ligands in vertebrate retina: localization and function of an endogenous signaling system. Proceedings of the National Academy of Sciences of the United States of America 96:14565-14570.

Straiker A, Hu SS, Long JZ, Arnold A, Wager-Miller J, Cravatt BF, Mackie K (2009) Monoacylglycerol lipase limits the duration of endocannabinoid-mediated depolarization-induced suppression of excitation in autaptic hippocampal neurons. Mol Pharmacol 76:1220-1227.

Stralfors P, Honnor RC (1989) Insulin-induced dephosphorylation of hormone-sensitive lipase. Correlation with lipolysis and cAMP-dependent protein kinase activity. European journal of biochemistry / FEBS 182:379-385.

Sugiura T, Kishimoto S, Oka S, Gokoh M (2006) Biochemistry, pharmacology and physiology of 2-arachidonoylglycerol, an endogenous cannabinoid receptor ligand. Progress in lipid research 45:405-446.

Sugiura T, Yoshinaga N, Kondo S, Waku K, Ishima Y (2000a) Generation of 2-arachidonoylglycerol, an endogenous cannabinoid receptor ligand, in picrotoxinin-administered rat brain. Biochemical and biophysical research communications 271:654-658.

Sugiura T, Kondo S, Sukagawa A, Nakane S, Shinoda A, Itoh K, Yamashita A, Waku K (1995) 2-Arachidonoylglycerol: a possible endogenous cannabinoid receptor ligand in brain. Biochemical and biophysical research communications 215:89-97.

Sugiura T, Kondo S, Kishimoto S, Miyashita T, Nakane S, Kodaka T, Suhara Y, Takayama H, Waku K (2000b) Evidence that 2-arachidonoylglycerol but not N-palmitoylethanolamine or anandamide is the physiological ligand for the cannabinoid CB2 receptor. Comparison of the agonistic activities of various cannabinoid receptor ligands in HL-60 cells. The Journal of biological chemistry 275:605-612.

Sugiura T, Kodaka T, Nakane S, Miyashita T, Kondo S, Suhara Y, Takayama H, Waku K, Seki C, Baba N, Ishima Y (1999) Evidence that the cannabinoid CB1 receptor is a 2-arachidonoylglycerol receptor. Structure-activity relationship of 2-arachidonoylglycerol, ether-linked analogues, and related compounds. The Journal of biological chemistry 274:2794-2801.

Sun YX, Tsuboi K, Okamoto Y, Tonai T, Murakami M, Kudo I, Ueda N (2004) Biosynthesis of anandamide and N-palmitoylethanolamine by sequential actions of phospholipase A2 and lysophospholipase D. The Biochemical journal 380:749-756.

Sutherland CA, Amin D (1982) Relative activities of rat and dog platelet phospholipase A2 and diglyceride lipase. Selective inhibition of diglyceride lipase by RHC 80267. The Journal of biological chemistry 257:14006-14010.

Suyama K, Shapiro I, Guttman M, Hazan RB (2002) A signaling pathway leading to metastasis is controlled by N-cadherin and the FGF receptor. Cancer cell 2:301-314.

Szabo B, Urbanski MJ, Bisogno T, Di Marzo V, Mendiguren A, Baer WU, Freiman I (2006) Depolarization-induced retrograde synaptic inhibition in the mouse cerebellar cortex is mediated by 2-arachidonoylglycerol. The Journal of physiology 577:263-280.

Sztalryd C, Xu G, Dorward H, Tansey JT, Contreras JA, Kimmel AR, Londos C (2003) Perilipin A is essential for the translocation of hormone-sensitive lipase during lipolytic activation. The Journal of cell biology 161:1093-1103.

Takahashi KA, Linden DJ (2000) Cannabinoid receptor modulation of synapses received by cerebellar Purkinje cells. Journal of neurophysiology 83:1167-1180.

Tanimura A, Yamazaki M, Hashimotodani Y, Uchigashima M, Kawata S, Abe M, Kita Y, Hashimoto K, Shimizu T, Watanabe M, Sakimura K, Kano M (2010) The endocannabinoid 2-arachidonoylglycerol produced by diacylglycerol lipase alpha mediates retrograde suppression of synaptic transmission. Neuron 65:320-327.

Trazzi S, Steger M, Mitrugno VM, Bartesaghi R, Ciani E (2010) CB1 cannabinoid receptors increase neuronal precursor proliferation through AKT/glycogen synthase kinase-3beta/beta-catenin signaling. The Journal of biological chemistry 285:10098-10109.

Trebicka J, Racz I, Siegmund SV, Cara E, Granzow M, Schierwagen R, Klein S, Wojtalla A, Hennenberg M, Huss S, Fischer HP, Heller J, Zimmer A, Sauerbruch T (2011) Role of cannabinoid receptors in alcoholic hepatic injury: steatosis and fibrogenesis are increased in CB2 receptor-deficient mice and decreased in CB1 receptor knockouts. Liver international : official journal of the International Association for the Study of the Liver 31:860-870.

Trinidad JC, Specht CG, Thalhammer A, Schoepfer R, Burlingame AL (2006) Comprehensive identification of phosphorylation sites in postsynaptic density preparations. Molecular & cellular proteomics : MCP 5:914-922.

Trinidad JC, Thalhammer A, Specht CG, Lynn AJ, Baker PR, Schoepfer R, Burlingame AL (2008) Quantitative analysis of synaptic phosphorylation and protein expression. Molecular & cellular proteomics : MCP 7:684-696.

Trinidad JC, Barkan DT, Gulledge BF, Thalhammer A, Sali A, Schoepfer R, Burlingame AL (2012) Global identification and characterization of both O-GlcNAcylation and phosphorylation at the murine synapse. Molecular & cellular proteomics : MCP 11:215-229.

Tsujita T, Ninomiya H, Okuda H (1989) p-nitrophenyl butyrate hydrolyzing activity of hormone-sensitive lipase from bovine adipose tissue. Journal of lipid research 30:997-1004.

Tsutsumi T, Kobayashi T, Ueda H, Yamauchi E, Watanabe S, Okuyama H (1994) Lysophosphoinositide-specific phospholipase C in rat brain synaptic plasma membranes. Neurochemical research 19:399-406.

Tweedie-Cullen RY, Reck JM, Mansuy IM (2009) Comprehensive mapping of post-translational modifications on synaptic, nuclear, and histone proteins in the adult mouse brain. J Proteome Res 8:4966-4982.

Twitchell W, Brown S, Mackie K (1997) Cannabinoids inhibit N- and P/Q-type calcium channels in cultured rat hippocampal neurons. Journal of neurophysiology 78:43-50.

Uchigashima M, Narushima M, Fukaya M, Katona I, Kano M, Watanabe M (2007) Subcellular arrangement of molecules for 2-arachidonoyl-glycerol-mediated retrograde signaling and its physiological contribution to synaptic modulation in the striatum. The Journal of neuroscience : the official journal of the Society for Neuroscience 27:3663-3676.

Ueda H, Kobayashi T, Kishimoto M, Tsutsumi T, Okuyama H (1993) A possible pathway of phosphoinositide metabolism through EDTA-insensitive phospholipase A1 followed by lysophosphoinositide-specific phospholipase C in rat brain. Journal of neurochemistry 61:1874-1881.

van der Lee MM, Blomenrohr M, van der Doelen AA, Wat JW, Smits N, Hanson BJ, van Koppen CJ, Zaman GJ (2009) Pharmacological characterization of receptor redistribution and beta-arrestin recruitment assays for the cannabinoid receptor 1. Journal of biomolecular screening 14:811-823.

van Tilbeurgh H, Sarda L, Verger R, Cambillau C (1992) Structure of the pancreatic lipase-procolipase complex. Nature 359:159-162.

van Tilbeurgh H, Egloff MP, Martinez C, Rugani N, Verger R, Cambillau C (1993) Interfacial activation of the lipase-procolipase complex by mixed micelles revealed by X-ray crystallography. Nature 362:814-820.

Varga K, Wagner JA, Bridgen DT, Kunos G (1998) Platelet- and macrophage-derived endogenous cannabinoids are involved in endotoxin-induced hypotension. FASEB journal : official publication of the Federation of American Societies for Experimental Biology 12:1035-1044.

Varma N, Carlson GC, Ledent C, Alger BE (2001) Metabotropic glutamate receptors drive the endocannabinoid system in hippocampus. The Journal of neuroscience : the official journal of the Society for Neuroscience 21:RC188.

Vellani V, Petrosino S, De Petrocellis L, Valenti M, Prandini M, Magherini PC, McNaughton PA, Di Marzo V (2008) Functional lipidomics. Calcium-independent activation of endocannabinoid/endovanilloid lipid signalling in sensory neurons by protein kinases C and A and thrombin. Neuropharmacology 55:1274-1279.

Wagner SA, Beli P, Weinert BT, Nielsen ML, Cox J, Mann M, Choudhary C (2011) A proteome-wide, quantitative survey of in vivo ubiquitylation sites reveals widespread regulatory roles. Molecular & cellular proteomics : MCP 10:M111 013284.

Wagner SA, Beli P, Weinert BT, Scholz C, Kelstrup CD, Young C, Nielsen ML, Olsen JV, Brakebusch C, Choudhary C (2012) Proteomic analyses reveal divergent ubiquitylation site patterns in murine tissues. Molecular & cellular proteomics : MCP 11:1578-1585.

Walter L, Stella N (2003) Endothelin-1 increases 2-arachidonoyl glycerol (2-AG) production in astrocytes. Glia 44:85-90.

Walter L, Dinh T, Stella N (2004) ATP induces a rapid and pronounced increase in 2-arachidonoylglycerol production by astrocytes, a response limited by monoacylglycerol lipase. The Journal of neuroscience : the official journal of the Society for Neuroscience 24:8068-8074.

Wang H, Hu L, Dalen K, Dorward H, Marcinkiewicz A, Russell D, Gong D, Londos C, Yamaguchi T, Holm C, Rizzo MA, Brasaemle D, Sztalryd C (2009) Activation of hormone-sensitive lipase requires two steps, protein phosphorylation and binding to the PAT-1 domain of lipid droplet coat proteins. The Journal of biological chemistry 284:32116-32125.

Wang X, Dow-Edwards D, Keller E, Hurd YL (2003) Preferential limbic expression of the cannabinoid receptor mRNA in the human fetal brain. Neuroscience 118:681-694.

Wang Y, Du D, Fang L, Yang G, Zhang C, Zeng R, Ullrich A, Lottspeich F, Chen Z (2006) Tyrosine phosphorylated Par3 regulates epithelial tight junction assembly promoted by EGFR signaling. EMBO J 25:5058-5070.

Watson S, Chambers D, Hobbs C, Doherty P, Graham A (2008) The endocannabinoid receptor, CB1, is required for normal axonal growth and fasciculation. Molecular and cellular neurosciences 38:89-97.

Waugh DS (2005) Making the most of affinity tags. Trends in biotechnology 23:316-320.

Weber C, Schreiber TB, Daub H (2012) Dual phosphoproteomics and chemical proteomics analysis of erlotinib and gefitinib interference in acute myeloid leukemia cells. Journal of proteomics 75:1343-1356.

Williams EJ, Walsh FS, Doherty P (1994a) The production of arachidonic acid can account for calcium channel activation in the second messenger pathway underlying neurite outgrowth stimulated by NCAM, N-cadherin, and L1. Journal of neurochemistry 62:1231-1234.

Williams EJ, Walsh FS, Doherty P (2003) The FGF receptor uses the endocannabinoid signaling system to couple to an axonal growth response. The Journal of cell biology 160:481-486.

Williams EJ, Furness J, Walsh FS, Doherty P (1994b) Characterisation of the second messenger pathway underlying neurite outgrowth stimulated by FGF. Development 120:1685-1693.

Williams G (2012) A searchable cross-platform gene expression database reveals connections between drug treatments and disease. BMC genomics 13:12.

Wilson RI, Nicoll RA (2001) Endogenous cannabinoids mediate retrograde signalling at hippocampal synapses. Nature 410:588-592.

Winkler FK, D'Arcy A, Hunziker W (1990) Structure of human pancreatic lipase. Nature 343:771-774.

Wisniewski JR, Nagaraj N, Zougman A, Gnad F, Mann M (2010) Brain phosphoproteome obtained by a FASP-based method reveals plasma membrane protein topology. J Proteome Res 9:3280-3289.

Witting A, Walter L, Wacker J, Moller T, Stella N (2004) P2X7 receptors control 2-arachidonoylglycerol production by microglial cells. Proceedings of the National Academy of Sciences of the United States of America 101:3214-3219.

Won YJ, Puhl HL, 3rd, Ikeda SR (2009) Molecular reconstruction of mGluR5a-mediated endocannabinoid signaling cascade in single rat sympathetic neurons. The Journal of neuroscience : the official journal of the Society for Neuroscience 29:13603-13612.

Wu CS, Zhu J, Wager-Miller J, Wang S, O'Leary D, Monory K, Lutz B, Mackie K, Lu HC (2010) Requirement of cannabinoid CB(1) receptors in cortical pyramidal neurons for appropriate development of corticothalamic and thalamocortical projections. The European journal of neuroscience 32:693-706.

Xapelli S, Agasse F, Sarda-Arroyo L, Bernardino L, Santos T, Ribeiro FF, Valero J, Braganca J, Schitine C, de Melo Reis RA, Sebastiao AM, Malva JO

(2013) Activation of type 1 cannabinoid receptor (CB1R) promotes neurogenesis in murine subventricular zone cell cultures. PloS one 8:e63529.

Xie XQ, Melvin LS, Makriyannis A (1996) The conformational properties of the highly selective cannabinoid receptor ligand CP-55,940. The Journal of biological chemistry 271:10640-10647.

Yamaguchi S, Mase T, Takeuchi K (1991) Cloning and structure of the mono- and diacylglycerol lipase-encoding gene from Penicillium camembertii U-150. Gene 103:61-67.

Yang W, Di Vizio D, Kirchner M, Steen H, Freeman MR (2010) Proteome scale characterization of human S-acylated proteins in lipid raft-enriched and non-raft membranes. Molecular & cellular proteomics : MCP 9:54-70.

Yoshida T, Fukaya M, Uchigashima M, Miura E, Kamiya H, Kano M, Watanabe M (2006) Localization of diacylglycerol lipase-alpha around postsynaptic spine suggests close proximity between production site of an endocannabinoid, 2-arachidonoyl-glycerol, and presynaptic cannabinoid CB1 receptor. The Journal of neuroscience : the official journal of the Society for Neuroscience 26:4740-4751.

Zygmunt PM, Petersson J, Andersson DA, Chuang H, Sorgard M, Di Marzo V, Julius D, Hogestatt ED (1999) Vanilloid receptors on sensory nerves mediate the vasodilator action of anandamide. Nature 400:452-457.